frontiers | Research Topics

An era of personalized medicine in breast cancer: Integrating artificial intelligence into practice

Edited by
Nosheen Masood and San-Gang Wu

Published in
Frontiers in Oncology

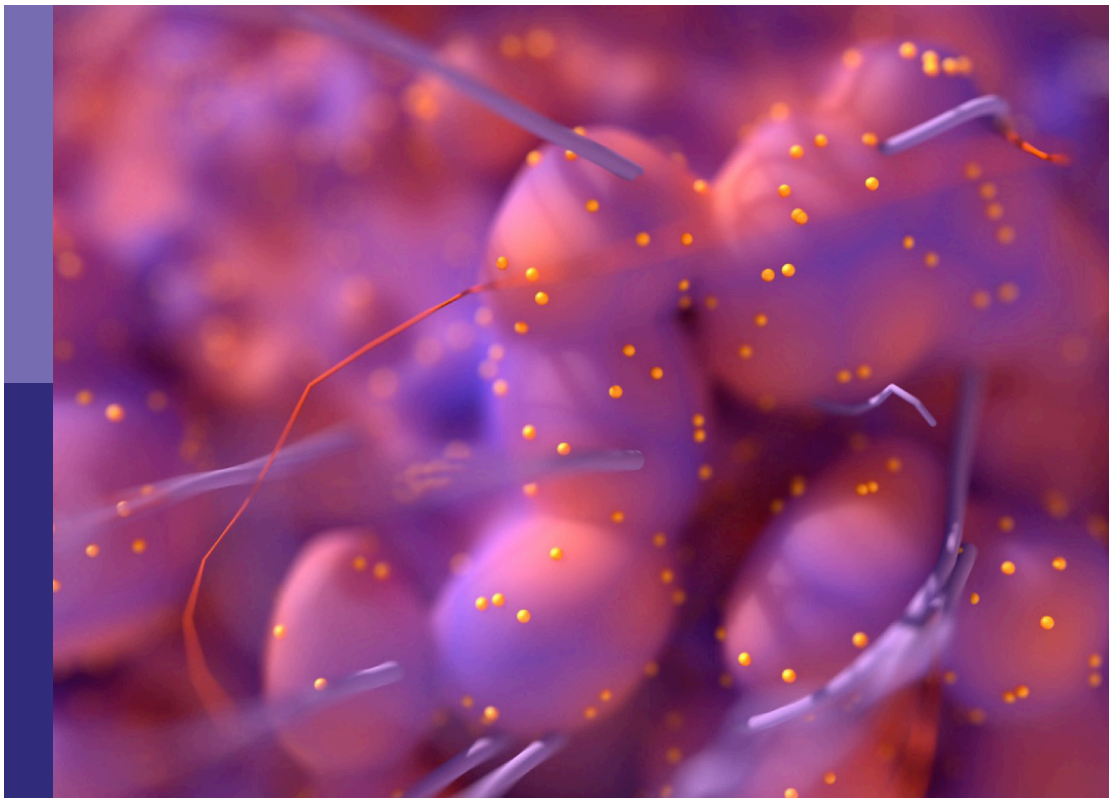

ISSN 1664-8714
ISBN 978-2-8325-2767-2
DOI 10.3389/978-2-8325-2767-2

About Frontiers

Frontiers is more than just an open access publisher of scholarly articles: it is a pioneering approach to the world of academia, radically improving the way scholarly research is managed. The grand vision of Frontiers is a world where all people have an equal opportunity to seek, share and generate knowledge. Frontiers provides immediate and permanent online open access to all its publications, but this alone is not enough to realize our grand goals.

Frontiers journal series

The Frontiers journal series is a multi-tier and interdisciplinary set of open-access, online journals, promising a paradigm shift from the current review, selection and dissemination processes in academic publishing. All Frontiers journals are driven by researchers for researchers; therefore, they constitute a service to the scholarly community. At the same time, the *Frontiers journal series* operates on a revolutionary invention, the tiered publishing system, initially addressing specific communities of scholars, and gradually climbing up to broader public understanding, thus serving the interests of the lay society, too.

Dedication to quality

Each Frontiers article is a landmark of the highest quality, thanks to genuinely collaborative interactions between authors and review editors, who include some of the world's best academicians. Research must be certified by peers before entering a stream of knowledge that may eventually reach the public - and shape society; therefore, Frontiers only applies the most rigorous and unbiased reviews. Frontiers revolutionizes research publishing by freely delivering the most outstanding research, evaluated with no bias from both the academic and social point of view. By applying the most advanced information technologies, Frontiers is catapulting scholarly publishing into a new generation.

What are Frontiers Research Topics?

Frontiers Research Topics are very popular trademarks of the *Frontiers journals series*: they are collections of at least ten articles, all centered on a particular subject. With their unique mix of varied contributions from Original Research to Review Articles, Frontiers Research Topics unify the most influential researchers, the latest key findings and historical advances in a hot research area.

Find out more on how to host your own Frontiers Research Topic or contribute to one as an author by contacting the Frontiers editorial office: frontiersin.org/about/contact

An era of personalized medicine in breast cancer: Integrating artificial intelligence into practice

Topic editors

Nosheen Masood — Fatima Jinnah Women University, Pakistan

San-Gang Wu — First Affiliated Hospital of Xiamen University, China

Topic coordinator

Saima Shakil Malik — Augusta University, United States

Citation

Masood, N., Wu, S.-G., eds. (2023). *An era of personalized medicine in breast cancer: Integrating artificial intelligence into practice*. Lausanne: Frontiers Media SA. doi: 10.3389/978-2-8325-2767-2

Table of contents

05 Editorial: An era of personalized medicine in breast cancer: integrating artificial intelligence into practice
Nosheen Masood and San-Gang Wu

07 Application of Convolution Neural Network Algorithm Based on Multicenter ABUS Images in Breast Lesion Detection
Jianxing Zhang, Xing Tao, Yanhui Jiang, Xiaoxi Wu, Dan Yan, Wen Xue, Shulian Zhuang, Ling Chen, Liangping Luo and Dong Ni

16 A machine learning model based on ultrasound image features to assess the risk of sentinel lymph node metastasis in breast cancer patients: Applications of scikit-learn and SHAP
Gaosen Zhang, Yan Shi, Peipei Yin, Feifei Liu, Yi Fang, Xiang Li, Qingyu Zhang and Zhen Zhang

31 Deep learning-based automatic segmentation for size and volumetric measurement of breast cancer on magnetic resonance imaging
Wenyi Yue, Hongtao Zhang, Juan Zhou, Guang Li, Zhe Tang, Zeyu Sun, Jianming Cai, Ning Tian, Shen Gao, Jinghui Dong, Yuan Liu, Xu Bai and Fugeng Sheng

45 Efficacy and safety of taxanes combined with chemotherapy drugs in advanced triple negative breast cancer: A meta-analysis of 26 randomized controlled trials
Qionglian Huang, Zubing Mei and Xianghui Han

57 3D-printed bolus ensures the precise postmastectomy chest wall radiation therapy for breast cancer
Xiran Wang, Jianling Zhao, Zhongzheng Xiang, Xuetao Wang, Yuanyuan Zeng, Ting Luo, Xi Yan, Zhuang Zhang, Feng Wang and Lei Liu

67 A case report of the sustained and rapid response of bevacizumab in a TP53-positive breast cancer and liver metastatic patient through personalized medicine
Mohammad Reza Eskandarion, Zahra Tizmaghz, Bahram Andalib, Nasser Parsa, Seyed Amir Hossein Emami, Reza Shahsiah, Mohammad Ali Oghabian and Reza Shirkoohi

75 Differentiating non-lactating mastitis and malignant breast tumors by deep-learning based AI automatic classification system: A preliminary study
Ying Zhou, Bo-Jian Feng, Wen-Wen Yue, Yuan Liu, Zhi-Feng Xu, Wei Xing, Zhao Xu, Jin-Cao Yao, Shu-Rong Wang and Dong Xu

85 Prediction of lymph node metastasis in patients with breast invasive micropapillary carcinoma based on machine learning and SHapley Additive exPlanations framework
Cong Jiang, Yuting Xiu, Kun Qiao, Xiao Yu, Shiyuan Zhang and Yuanxi Huang

97 Ultrasound-based radiomics analysis for differentiating benign and malignant breast lesions: From static images to CEUS video analysis
Jun-Yan Zhu, Han-Lu He, Zi-Mei Lin, Jian-Qiang Zhao, Xiao-Chun Jiang, Zhe-Hao Liang, Xiao-Ping Huang, Hai-Wei Bao, Pin-Tong Huang and Fen Chen

107 Prediction of radiation-induced acute skin toxicity in breast cancer patients using data encapsulation screening and dose-gradient-based multi-region radiomics technique: A multicenter study
Huichun Feng, Hui Wang, Lixia Xu, Yao Ren, Qianxi Ni, Zhen Yang, Shenglin Ma, Qinghua Deng, Xueqin Chen, Bing Xia, Yu Kuang and Xiadong Li

122 Biological and clinical review of IORT-induced wound fluid in breast cancer patients
Shabnam Jeibouei, Forough Shams, Fariba Mohebichamkhorami, Davood Sanooghi, Bahareh Faal, Mohammad Esmaeil Akbari and Hakimeh Zali

141 Development of a breast cancer case management information platform (BC-CMIP) module based on patient-perceived value
Yinyin Liang, Yan Gao, Guobing Yin, Wenjun Chen and Xiuni Gan

152 Hormone receptor-positive, HER2-negative, metastatic breast cancer responded well to abemaciclib and exemestane after palbociclib and fulvestrant failure: A case report and literature review
Yan Mao, Meng Lv, Yongmei Wang, Weihong Cao and Wenfeng Li

158 A nomogram based on combining clinical features and contrast enhanced ultrasound is not able to identify Her-2 over-expressing cancer from other breast cancers
Zi-mei Lin, Ting-ting Wang, Jun-Yan Zhu, Yong-yuan Xu, Fen Chen and Pin-tong Huang

frontiers | Frontiers in Oncology

TYPE Editorial
PUBLISHED 06 June 2023
DOI 10.3389/fonc.2023.1164808

OPEN ACCESS

EDITED AND REVIEWED BY
Kara Britt,
Peter MacCallum Cancer Centre, Australia

*CORRESPONDENCE
Nosheen Masood
dr.nosheen@fjwu.edu.pk

RECEIVED 13 February 2023
ACCEPTED 25 May 2023
PUBLISHED 06 June 2023

CITATION
Masood N and Wu S-G (2023) Editorial: An era of personalized medicine in breast cancer: integrating artificial intelligence into practice.
Front. Oncol. 13:1164808.
doi: 10.3389/fonc.2023.1164808

Editorial: An era of personalized medicine in breast cancer: integrating artificial intelligence into practice

Nosheen Masood[1]* and San-Gang Wu[2]

[1]Department of Biotechnology, Fatima Jinnah Women University, Rawalpindi, Pakistan, [2]Department of Radiation Oncology, First Affiliated Hospital of Xiamen University, Xiamen, China

KEYWORDS

artificial intelligence, personalized medicine, clinical tumor prediction, precision medicine, breast cancer

Editorial on the Research Topic

An era of personalized medicine in breast cancer: integrating artificial intelligence into practice

Breast cancer incidence rate is increasing rapidly despite the advancements made in this field. Hereditary, genetic, and obesity involvement, and the use of alcohol and contraceptives are a few of the main culprits for this disease. However, despite all the enormous research on this disease, cases continue to increase and the rate of recurrence and metastasis remains high. Late diagnosis, wrong diagnosis, and lack of personalized medicine make the condition much worse. For this purpose, there is a need to inculcate artificial intelligence into breast cancer diagnosis and treatment to decrease the rate of mortality and recurrence. The key to breast cancer cure lies in early detection, but there are always problems associated with early diagnosis. One of the major complications associated with a breast cancer diagnosis is to differentiate between carcinoma and other diseases. For this purpose, Zhou et al. developed a deep learning-based artificial intelligence automatic classification system to differentiate breast cancer malignancy from non-lactating mastitis. They found that the interpretations by the senior physician and AI module were consistent with postoperative pathological diagnosis whereas an intermediate aged physician's interpretations of images were not consistent with postoperative diagnosis, making this method a reliable auxiliary method to distinguish between the two types of diseases with accuracy and high specificity. Breast cancer screening is accompanied by radiological images; therefore, Zhang et al. designed a study to use artificial intelligence for the detection of breast cancer. The CNN (Convolutional Neural Network) algorithm using internal and external validation datasets was used for a total of 2,538 ABUS (automated whole-breast ultrasound) images that showed a good efficiency for BIRAD 4 and 5 compared with BIRAD 2 and 3 lesions. They also concluded that lesions greater than 10 mm were better detected. Desai et al. (2021) and Nomani et al. (2022) also reported that CNN gives higher accuracy for diagnosis and detection of breast cancer. Continuous contrast-enhanced ultrasound allows radiologists to access the dynamic vascularization of vessels and tissues in real time, and this application is exploited for differentiating benign and malignant tissues using machine learning models. The 3D-ResNet-50 model and the XGBoost

(Extreme gradient boost) model were best for classifying the tumor for the radiologists using CNN models (Zhu et al.). Lin et al. found that a CEUS-based (continuing education units) nomogram along with the evaluation of clinical features of breast cancer patients cannot differentiate HER2 higher-expressing breast cancers from others. Three models using preoperative CEUS reports that are divided into training and validation groups were analyzed for the study. A machine learning model-based study was conducted by Zhang et al. to reveal the association between ultrasound and early detection of sentinel lymph node status in breast cancer. For this purpose, 10 machine learning algorithms that are already available were used to predict the best diagnostic tool. It was found that the XGBoost model was best for SLN (sentinel lymph node) detection and for preoperative clinical guidance, and SHAP (SHapley Additive exPlanations) was the best tool for a visual picture. Prediction of lymph node metastasis can be done by different machine learning tools. A study on breast invasive micropapillary carcinoma was conducted to find the best model for the prediction of lymph node metastasis. The XGBoost model combined with SHAP was better than LR-based nomogram models. Tumor size was important for detection (Jiang et al.).

In addition to AI, laboratory experiments were conducted in case reports revealing genetic association with breast cancer. One of the case reports by Eskandarion et al. revealed that patients suffering from breast cancer had mutated p4EBP1, PTEN, and TP53 genes leading to the activation of the mTOR signaling pathway. She was given bevacizumab due to profiling and showed reduced liver metastasis followed by mastectomy. Drugs targeting CDK4/6 inhibitor in HR+/HER2− metastasized breast cancer patients need to be evaluated for their effectiveness. Another case study showed that the use of PI3K inhibitors requires more research in advanced breast stages using NGS to arrive at a conclusion (Mao et al.). Huang et al. conducted a meta-analysis to reveal the efficacy of taxane administered to triple-negative breast cancer patients. Taxane monotherapy was compared with taxane-based combination therapies, and it was found that the latter showed more promising results. Taxane-based combination therapies are more effective and well tolerated in advanced-stage triple-negative breast cancer patients. For effective treatment strategy, the size and volume of breast cancer tumors are important; time-consuming and confusing variations in radiologists' reports exist. The Res-UNet convolutional neural network was used on MRI and the results were promising as they showed that it was effective in clinical decision-making for breast cancer (Yue et al.). Most breast cancer patients undergo chemotherapy followed by radiotherapy. Radiotherapy though seems less invasive but has its consequences. A 3D printed bolus is used in postmastectomy patients undergoing radiotherapy to increase dose effectivity in radiotherapy. It was found that a 3D printed bolus is more precise and caused less acute skin toxicity (Wang et al.). Jeibouei et al. wanted to evaluate the role of seroma analysis after intraoperative radiotherapy in early breast cancer. No conclusion can be deduced from the analysis of seroma studies to decipher the effectiveness of IORT because of the variation in body reactions of patients. It seems that it is related to the immune system and probably unknown or rarely studied factors in this area, such as microbiota in the body of patients. It was suggested that the question can be answered through a trial with the clinical endpoint. Radiation-induced dermatitis of grade greater than or equal to 2 can be predicted in breast cancer patients with high accuracy using multi-region dose-gradient GBDT (gradient-boosted decision trees) with a random-based forest-based encapsulation screening method. It was proved through a study by Feng et al., where they used CT images and clinical and dosimetric details of 214 breast cancer patients.

For the facilitation of breast cancer patients, Liang et al. attempted to create a breast cancer management information platform module based on patient-perceived value. The model was comprehensive and reasonable and proved to be efficient for meeting the healthcare needs of breast cancer. The module is applicable as it provides a platform for the development of subsequent modules. To reach a conclusion, this Research Topic gives detailed information regarding the use of artificial intelligence in practice starting from screening to diagnosis to personalized treatment to management models. In short, this information is interesting, informative, and applicable for oncologists and patients.

Author contributions

NM has been involved in the write-up of the editorial. S-GW proofread the editorial sent through email. All authors contributed to the article and approved the submitted version.

Acknowledgments

We would like to acknowledge all the authors who have contributed to the Research Topic.

Conflict of interest

The authors declare that the research was conducted in the absence of any commercial or financial relationships that could be construed as a potential conflict of interest.

Publisher's note

frontiers | Frontiers in Oncology

ORIGINAL RESEARCH
published: 04 July 2022
doi: 10.3389/fonc.2022.938413

Application of Convolution Neural Network Algorithm Based on Multicenter ABUS Images in Breast Lesion Detection

Jianxing Zhang[1,2], Xing Tao[3], Yanhui Jiang[3], Xiaoxi Wu[2], Dan Yan[2], Wen Xue[2], Shulian Zhuang[2], Ling Chen[2], Liangping Luo[1*] and Dong Ni[3*]*

[1] Department of Medical Imaging Center, The First Affiliated Hospital, Jinan University, Guangzhou, China, [2] Department of Ultrasound, Remote Consultation Center of ABUS, The Second Affiliated Hospital, Guangzhou University of Chinese Medicine, Guangzhou, China, [3] Medical Ultrasound Image Computing Lab, Shenzhen University, Shenzhen, China

OPEN ACCESS

Edited by:
San-Gang Wu,
First Affiliated Hospital of Xiamen University, China

Reviewed by:
Fei Yan,
Institutes of Advanced Technology, (CAS), China
Lihua Li,
Hangzhou Dianzi University, China
Zhiyi Chen,
Third Affiliated Hospital of Guangzhou Medical University, China

***Correspondence:**
Jianxing Zhang
zhangjx@gzucm.edu.cn
Liangping Luo
tluolp@jnu.edu.cn
Dong Ni
nidong@szu.edu.cn

Specialty section:
This article was submitted to Breast Cancer, a section of the journal Frontiers in Oncology

Received: 07 May 2022
Accepted: 30 May 2022
Published: 04 July 2022

Citation:
Zhang JX, Tao X, Jiang YH, Wu XX, Yan D, Xue W, Zhuang SL, Chen L, Luo LP and Ni D (2022) Application of Convolution Neural Network Algorithm Based on Multicenter ABUS Images in Breast Lesion Detection. Front. Oncol. 12:938413. doi: 10.3389/fonc.2022.938413

Objective: This study aimed to evaluate a convolution neural network algorithm for breast lesion detection with multi-center ABUS image data developed based on ABUS image and Yolo v5.

Methods: A total of 741 cases with 2,538 volume data of ABUS examinations were analyzed, which were recruited from 7 hospitals between October 2016 and December 2020. A total of 452 volume data of 413 cases were used as internal validation data, and 2,086 volume data from 328 cases were used as external validation data. There were 1,178 breast lesions in 413 patients (161 malignant and 1,017 benign) and 1,936 lesions in 328 patients (57 malignant and 1,879 benign). The efficiency and accuracy of the algorithm were analyzed in detecting lesions with different allowable false positive values and lesion sizes, and the differences were compared and analyzed, which included the various indicators in internal validation and external validation data.

Results: The study found that the algorithm had high sensitivity for all categories of lesions, even when using internal or external validation data. The overall detection rate of the algorithm was as high as 78.1 and 71.2% in the internal and external validation sets, respectively. The algorithm could detect more lesions with increasing nodule size (87.4% in ≥10 mm lesions but less than 50% in <10 mm). The detection rate of BI-RADS 4/5 lesions was higher than that of BI-RADS 3 or 2 (96.5% vs 79.7% vs 74.7% internal, 95.8% vs 74.7% vs 88.4% external). Furthermore, the detection performance was better for malignant nodules than benign (98.1% vs 74.9% internal, 98.2% vs 70.4% external).

Conclusions: This algorithm showed good detection efficiency in the internal and external validation sets, especially for category 4/5 lesions and malignant lesions. However, there are still some deficiencies in detecting category 2 and 3 lesions and lesions smaller than 10 mm.

Keywords: automatic breast ultrasound (ABUS), convolution neural network, breast cancer, detection, validation data

INTRODUCTION

Breast cancer is the most common cancer and a leading cause of cancer death in women worldwide, but precise detection can provide an opportunity for timely treatment (1). Among the various detection methods, B-mode ultrasound screening technology is favored and recommended as a routine diagnostic tool because of its low cost and rapid imaging (2). Although breast ultrasound imaging can characterize the suspicious tumor area of the breast tissue, it has high technical dependence on the operator, poor diagnostic repeatability, long time-consuming and low accuracy, and massive daily image analysis aggravates the burden of clinical radiologists (3). Furthermore, the inconsistency of different radiologists on the same image may lead to severe false-positive problems, thereby delaying effective treatments (4).

Automatic breast ultrasound (ABUS) imaging has become an essential tool in breast cancer diagnosis. ABUS is considered to have high repeatability, low operator dependence, less time consuming by radiologists in image acquisition, automatic three-dimensional reconstruction of the whole breast, coronal information, and a relatively wide observation field. Studies have shown that mammography (MG) plus ABUS examination can increase the detection rate of breast cancer in women with dense breasts, particularly the detection rate of small lesions (5). A multi-center study on Chinese women showed that ABUS had good reliability compared with handhold ultrasound (HHUS) and MG (6). The other study conducted in the United States showed that it could help improve the detection rate of breast cancer by adding ABUS to breast cancer screening (7).

Although ABUS has many advantages, it also inevitably aggravates the workload of screening and diagnostic examiners. Different computer-aided diagnosis (CAD) systems have been developed to standardize and accelerate diagnostic procedures (8). Relevant studies suggest that computer-aided diagnosis software could effectively improve the detection of lesions and the speed of diagnosis (9). However, in breast cancer imaging research, deep learning (AI or computer-aided diagnosis CAD) has mainly focused on mammography or ultrasound 2D/3D imaging combined with deep learning (10–12). In lesion detection and diagnosis, accurate segmentation of the breast mass in a 3D ABUS image is an essential task in ABUS image analysis. It also plays a vital role in designing a computer-aided detection or diagnostic system (13–15). Recently, deep learning techniques have made significant progress in medical image segmentation (16–18). The convolution neural network (CNN) has become a promising choice in breast ultrasound image segmentation (19–22).

The diagnostic process of breast lesions includes detection, diagnosis, and treatment. Lesion detection is the premise of this diagnosis. A single ABUS volume image could have 320 frames with a layer thickness of 0.5 mm. The amount of data in ABUS images is more than that in most natural images. The cost of manually marking breast lumps is high. Direct training of large-scale segmentation networks with tens of millions of parameters may introduce potential over-fitting (23). This study aimed to evaluate a convolution neural network algorithm for breast disease detection, developed based on ABUS image and Yolo v5. The efficiency and accuracy of the algorithm were analyzed in detecting lesions with different allowable false positive values and lesion sizes, and the differences were compared and analyzed, which included the various indicators in internal validation and external validation data.

MATERIALS AND METHODS

Patients

This multi-center retrospective study was conducted following the Declaration of Helsinki and was approved by the local institutional review board (ZE2020-232). A total of 32,493 cases of ABUS examination were analyzed, which were collected from 7 hospitals (GDHCM, BHLY, CFFIC, PHHKS, YDHSZ, LKMC, and JBMH) between October 2016 and December 2020. The inclusion criteria of this study were: ① The quality control requirements of ABUS were met; ② Malignant lesions were confirmed by pathology; ③ The clinical information of the case was complete; and ④ benign lesions required a biopsy or follow-up for more than 2 years by ultrasound, mammography or MRI. The exclusion criteria in this study were: ① the quality control requirements of the image were not met; ② the patient had a history of breast trauma, surgery, mastitis, etc.; ③ suspected malignant tumor without pathological results; ④ benign lesions failed to follow up as required; and ⑤ other conditions could affect diagnosis. Finally, 30,515 cases were excluded from the study.

All training and test data were from the Guangdong Province Hospital of Chinese Medicine because each case needed a bilateral breast examination, and some lesions could be displayed in two or three-volume data. The training set collected 3,457 ABUS volume data from 936 cases (age range 18–70 years, average 41.54 ± 11.22 years), 221 malignant lesions and 3,662 benign lesions, and 791 confirmed lesions by pathology. Another 1,406 ABUS volume data of 301 cases (age range 26–69 years, average 42.37 ± 12.48 years) were used for validation, including 57 malignant lesions and 885 benign lesions, and 247 lesions were confirmed by pathology.

The other 741 cases with 2,538 volume data were included in the validation data. A total of 452 volume data of 413 cases (age range 23–67 years, average 41.21 ± 11.93 years) were used as internal validation data (IVD), including 161 malignant lesions and 1,017 benign lesions. A total of 214 lesions of BI-RADS 4 or 5 and 47 lesions of BI-RADS 3 were confirmed by pathology. The other lesions were followed up to rule out the possibility of malignancy. A total of 328 cases (age range 22–65 years, average 40.32 ± 13.44 years) with 1,086 volume data were used as external validation data (EVD), which included 57 malignant lesions and 1,879 benign lesions. A total of 96 lesions of BI-RADS 4 or 5 and 29 lesions of BI-RADS 3 were confirmed by pathology, and the other lesions were followed up as required. All cases with dense breasts were collected in this study (**Figure 1**).

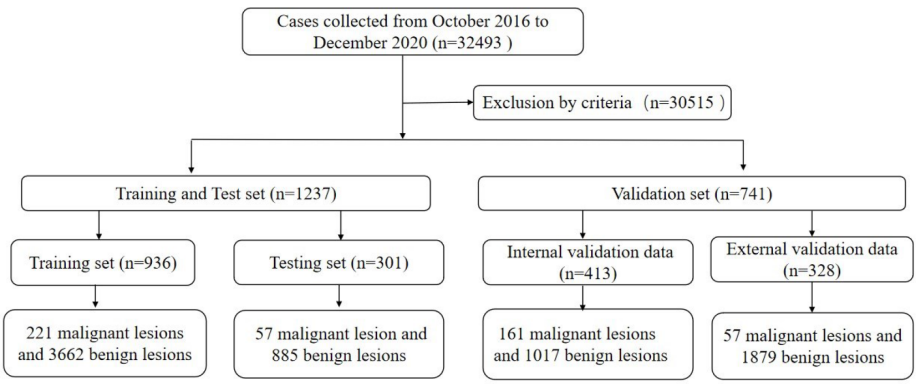

FIGURE 1 | Flowchart of the study population in the training set, testing set and validation set.

Quality Control and Reference Standard

All cases were scanned according to the scanning specifications recommended by the ABUS use manual. The standard images of unilateral breast scanning are AP, LAT, and MED. SUP and INF can be added when the breast is large. So each case had 4 to 8 volumes of data. The quality control standard recommended by the GE ABUS use manual was used for quality control, and the volume data with lesions were collected. In this study, two doctors (XW and YD) with more than 5 years of experience in ABUS were used for quality control.

Two senior radiologists (ZS and CL, with 10 and 15 years of experience in breast ultrasound diagnosis) confirmed all lesions regarding pathological or follow-up results. Cases with differences were judged by another senior radiologist (ZS, with 25 years of experience in breast ultrasound diagnosis).

Methods and Data Annotation

The algorithm (Volume-Breast Ultrasound Intelligent Lesion Detection System, V-BUILDS) was confirmed to have a data enhancement strategy of Mosaic data enhancement ratio of 0.5 and a mixed data enhancement ratio of 0, which was based on Yolo V5. It adopts WBF for model fusion, adds the detection model of the transformer encoder module method, and the algorithm obtained the 3D RESNET reducing false-positive method to detect, verify, and compare the internal and external data. The YOLOv5 classifiers were trained using the open-source Python library Image AI. In the development of the algorithm, the training and testing set were applied to the training and testing of this algorithm. The flowchart is shown in **Figure 2**.

In this study, PAIR was used to annotate ABUS images (PAIR was a multifunctional labeling software developed by the Medical Ultrasonic Image Computing Lab Music of the medical department of Shenzhen University based on C++). The pair has the advantages of supporting multiple data formats, labeling tasks, custom feature attributes, integrating deep learning semi-automatic labeling, and ensuring data security.

Equipment and Computation Platform

All images were acquired by INVENIA ABUS 1.0 (model 5500-4400-01, GE Healthcare, USA), using a C15-6 × W arc probe with a central frequency of 10 MHz. The examination depth was adjusted according to the size of the breast volume of the patient. The pixel size of the ABUS images was 0.27 × 0.27 × 0.5 mm.

The proposed method was implemented on an NVIDIA RT × 2080TiCPU, Intel(R) × eon(R) Silver 4210 CPU, PyTorch1. 7.0. The model construction of fast RCNN, Retinanet, and Fcos was carried out on the detectron2 framework.

Classification Performance Evaluation and Statistical Analysis

To evaluate the performance of the breast lesion detection model, accuracy (ACC), sensitivity (SEN), specificity (SPE), false positive (FPS), negative–positive (NPS), positive predictive value (PPV), negative predictive value (NPV), and Youden index (Yi) were evaluated by F1 score (F1). An independent sample t-test was used for inter-group comparison, and the rank-sum test (Mann–Whitney U test) was used for those who did not obey normal distribution or uneven variance. Inspection-level $\alpha = 0.05$ (normality test, $\alpha = 0.10$).

Additionally, this study also used the FROC curve to study the relationship between model sensitivity and false-positive ratio, in which vertical sitting represents sensitivity, and the abscissa represents the ratio of the number of false-positive lesions to the number of true positive lesions.

RESULTS

Pathology and Follow-Up Results of Different Data Sets

Each data set contained multiple pathological types of lesions confirmed by pathology. As shown in **Table 1**, invasive carcinoma (non-special type) is the most common breast malignant tumor, while fibroadenoma is the most common benign breast tumor. Most lesions were benign and confirmed after more than 2 years of follow-up.

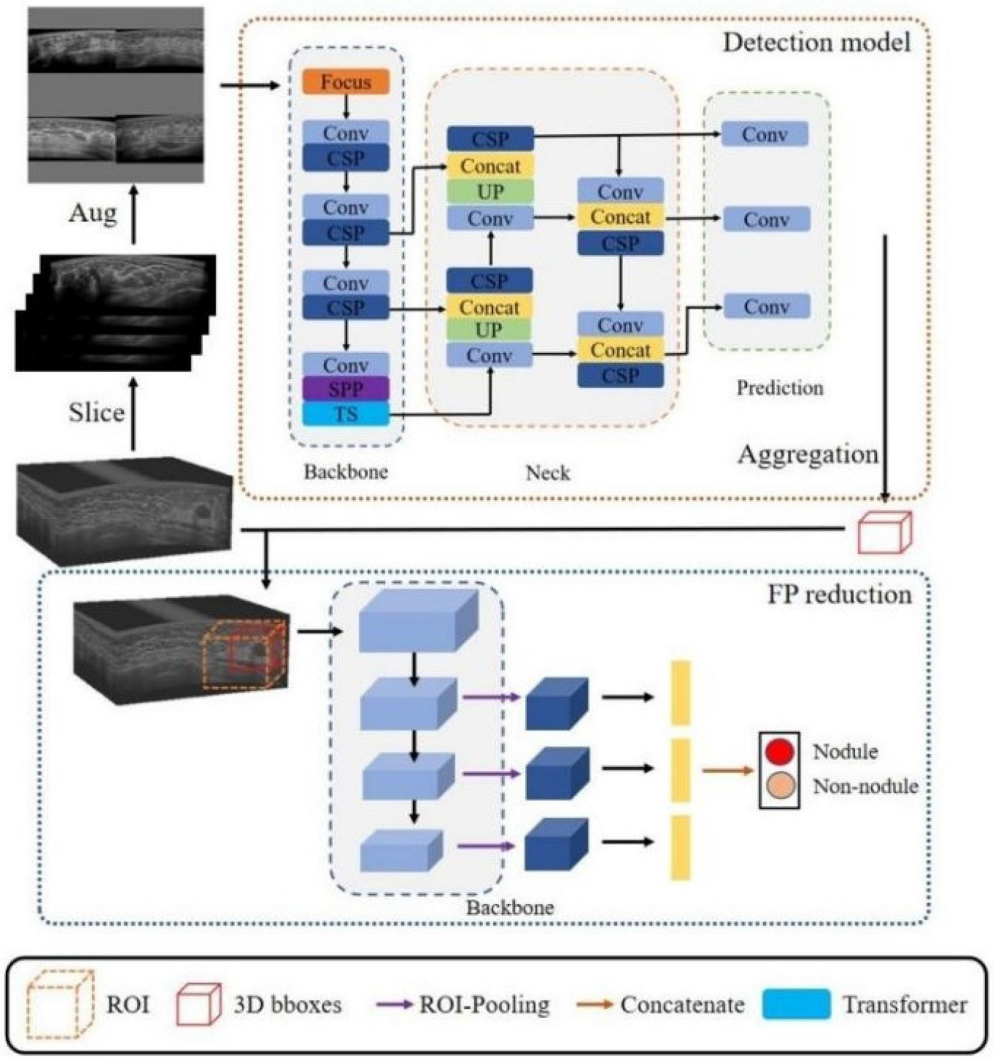

FIGURE 2 | The detection network architecture of our proposed framework. It included a detection model and a three-dimensional false positive reduction model. The ABUS volume was sliced along the cross-section in the detection model training to obtain a two-dimensional image. Four training set images were randomly selected in each study. The improved Mosaic data enhancement method was input into the network for training to develop the three-dimensional false positive reduction model. This model took the lesion as the center, cut the tumour region, inputted it into the three-dimensional classification network, and classified the multi-scale features of the classification network after ROI pooling. In the stage of network reasoning, the slice data of volume are input into the network in turn, and the detection frames of adjacent slices are combined through NMS to obtain a three-dimensional detection frame. According to the three-dimensional detection frame, the ROI area was cut from the original volume data and inputted into the false positive reduction network to obtain the probability that the location was a lesion.

Lesion Detection in Internal and External Validation Data Based on Different False Positive Values

As shown in **Table 2**, the sensitivity indicators of different categories of data to false-positive values were analyzed based on the comparison of internal and external validation data. The overall detection rate of the algorithm was as high as 78.1 and 71.2% in the internal and external validation sets. The study showed that 0.5 false-positive values per frame were susceptible to all categories of data, whether internal or external validation data. With the increase in the number of false positives allowed per frame, the detection sensitivity of each lesion also increased slightly. However, the sensitivity was 93.2% for detecting category 4/5 lesions in the internal validation set when 1.5 false positives were allowed per frame. Moreover, when 4 false positives were allowed per frame, the sensitivity was 96.5%. In the external validation set, the detection performance of category 4/5 lesions was similar. When 3 false positives were allowed per frame, it reached its highest value, and the sensitivity was 95.8%. However, the detection of category 2 and 3 lesions in the internal set and category 3 lesions in the internal and external set failed to reach 80%. With the increase in the number of the false positives

TABLE 1 | Pathology and follow-up results of different datasets.

	Pathology or follow-up	Training set (n = 3,883)	testing set (n = 912)	IVD (N = 1,178)	EVD (N = 1,936)
Malignant	invasive carcinoma (non-special type)(B5)	196	46	143	51
	invasive lobular carcinoma(B5)	9	3	3	1
	Ductal carcinoma in situ(B3)	11	7	13	4
	Other types of breast cancer	5	1	2	1
benign	papilloma	24	9	6	2
	Fibroadenoma	413	153	71	52
	hyperplasia	71	15	12	9
	cyst	57	11	7	4
	Other	5	2	4	1
	More then 2-years follow-up	3,092	695	917	1,811

allowed per frame, the detection sensitivity increased slightly. The detection rate of BI-RADS 4/5 lesions was higher than that of BI-RADS 3 or 2 (96.5% vs 79.7% vs 74.7% internal, 95.8% vs 74.7% vs 88.4% external) (P <0.001). This relationship could be more visually expressed in **Figure 3**.

Analysis of Lesion Size and Missed Diagnosis of Internal and External Validation Data

In this group of cases (**Table 3**), for the internal validation data set, the non-detection rate of lesions less than 5 mm was 55.6%, and the non-detection rate of 5–10 mm lesions was 25.3%. The non-detection rate of lesions more significant than 10 mm was 12.6%. In the external validation data set, the non-detection rate of lesions less than 5 mm in this algorithm was 61.4%, the non-detection rate of 5–10 mm lesions was 28.8%, and the non-detection rate of lesions more significant than 10 mm was 15.6%.The algorithm could detect more lesions with the increasing nodule size (87.4% in ≥10 mm lesions, but less than 50% in <10 mm). However, there was no difference between the two sets (P >0.05). **Figure 4** shows the composition of the size detection relationship of each category.

Study on the Detection Rate of Malignant Lesions by Internal and External Validation Data

As shown in **Table 4** and **Figure 3**, the detection rate of malignant lesions was higher than that of category 4/5 lesions (**Table 2**) in the internal validation set. Under the condition of allowing an average of 0.5 false positives per frame, the current detection rate reaches 91.3%. When three false positives per frame were allowed, the detection rate reached 96.9%. The current detection rate reaches 93.0% in the external verification data when the condition of allowing an average of 0.5 false positives per frame is met. When 1.5 false positives per frame were allowed, the detection rate reached 94.7%, and when 2.5 false positives per frame were allowed, the detection rate reached 98.2%.

DISCUSSION

To our knowledge, this is the first study to develop the lesion detection algorithm based on ABUS volume data and evaluate its internal and external detection efficiency. In recent years, ABUS has become a popular imaging modality in breast cancer detection and diagnosis because ABUS improves the sensitivity of dense breast detection and can be successfully applied to the visualization and characterization of breast lesions (24, 25). Therefore, the analysis of ABUS images has attracted the attention of more and more attention of radiologists and researchers (9). This study applied the deep learning algorithm (V-BUILDS) to the completed model training and 3D false positive reduction network. Based on the ABUS data, the false-positive allowable values of different frames were externally verified for the data from multiple centers. The differences between internal and external verification and the differences in various indicators such as lesion detection efficiency and accuracy were compared and analyzed.

TABLE 2 | When false positives (FPS) are allowed in different frames, the detection rates of different BI-RADS categories of lesions in different validation sets (IVD and EVD) were shown.

	Detection rate (%) of different false positives (FPS)								
	0	0.5	1	1.5	2	2.5	3	3.5	4
IVD category 2*	3	53.8	60	64.2	67.8	69.2	70.7	72.4	74.7
IVD category 3*	3.8	54.9	64.7	68.5	71.9	73.9	75.9	78.1	79.7
IVD category 4/5	13.3	85.8	90	93.2	94.4	94.7	95.3	96.2	96.5
EVD category 2#	0.2	55	68.1	74.4	78.9	82.6	85.6	87.3	88.4
EVD category 3#	0.9	47.2	57.5	61.7	66.7	69.6	71.6	73.3	74.7
EVD category 4/5	11	83.9	88.1	89.8	92.4	94.9	95.8	95.8	95.8

**IVD category 2 VS IVD category 4/5, P < 0.001, IVD category 3 VS IVD category 4/5, P < 0.001, #EVD category 2 VS EVD category 4/5, P < 0.001. # EVD category 3 VS EVD category 4/5, P < 0.001.*

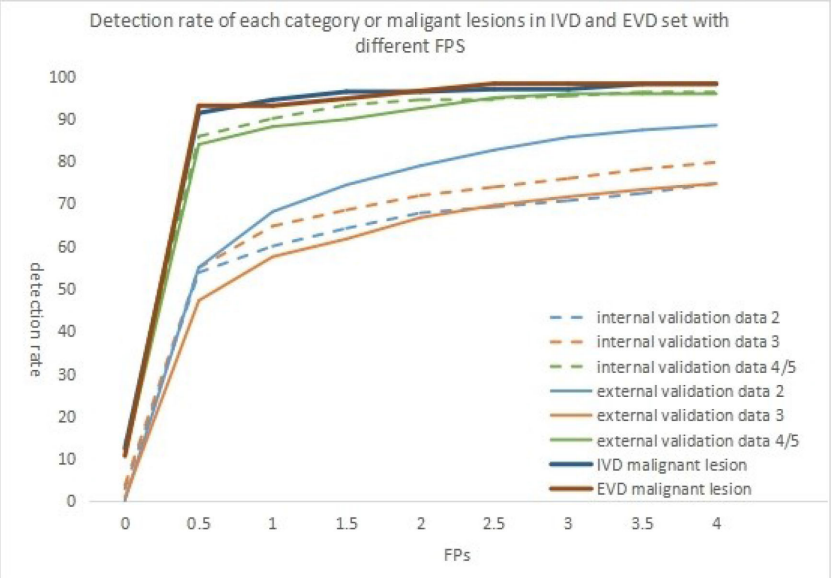

FIGURE 3 | When false positives(FPS) are allowed in different frames, the detection rates of different BI-RADS categories of lesions in different validation sets were shown in the figure. The detection rate of malignant lesion in different validation set was although shown in the figure.

The research showed that this algorithm had high detection efficiency for different categories of lesions, and the total detection efficiency for all lesions was slightly lower. However, it had a high detection efficiency for category 4 and 5 lesions, especially malignant lesions. The detection rate for category 4 and 5 lesions differed from that of category 2 or 3 in each dataset (P <0.001). The detection rate can reach 0.963 when 1.5 false positives per frame are allowed in the internal verification set.

Some cases are difficult to diagnose because of the characteristics of low signal-to-noise ratio, severe artifacts, blurred margin, and the height change of the shape (9), the small volume of the lesion, and the insufficient number of images. Such lesions may occur in different categories of lesions. However, it is difficult to compare with the surrounding tissues in the detection process, which can easily lead to missed detection or misjudgment. These conditions also occurred in lung lesions detected by CNN (26–28). In this study, when the lesion diameter was less than 10 mm, the detection rate of the lesion was low. However, when the diameter of the lesion was greater than 10 mm, the detection rate of the lesion increased significantly with the increase in the diameter of the lesion. These results were consistent with those reported in the literature (29). It is important to point out that the small lesion is usually the early stage of cancer or a benign lesion. Furthermore, it was difficult to detect with all kinds of images. There were a certain proportion of large undetected and some medium-sized lesions in the external validation data. After analyzing the causes, it was found that the edge of the lesion was blurred, the lesion (a benign lesion) was too large (almost occupying the whole breast), and the lesion scope was uneven and resembled the echo of normal gland tissue. The lesion image (pathological result: malignant lesion) was a non-mass breast lesion with an unclear boundary

TABLE 3 | In the internal (IVD) and external validation (EVD) sets, the number of possible benign (category 2 or 3) and suspicious malignant lesions (category 4 or 5) of different sizes and the number of detected lesions of different sizes.

	Number of each size										
	0-	**5-**	**10-**	**15-**	**20-**	**25-**	**30-**	**35-**	**>40**	***Z***	***P***
IVD category 2 or 3	123	406	240	99	62	24	11	8	27	0.397	0.691
EVD category 2 or 3	264	1021	382	101	36	9	1	7	3		
IDV category 4 or 5	1	28	51	39	29	12	9	1	8	0.708	0.479
EVD category 4 or 5	0	8	23	21	23	11	11	2	13		
IVD detection	55 (44.4)	325 (74.7)	238 (81.8)	123 (89.1)	86 (94.5)	34 (94.4)	19 (95)	8 (88.9)	34 (97.1)	0.177	0.860
EVD detection	102 (38.6)	733 (71.2)	323 (79.8)	108 (88.5)	55 (93.2)	20 (100)	12 (100)	9 (100)	16 (100)		
IVD no detection	69 (55.6)	110 (25.3)	53 (18.2)	15 (10.9)	5 (5.5)	2 (5.6)	1 (5)	1 (11.1)	1 (2.9)	0.489	0.625
EVD no detection	162 (61.4)	296 (28.8)	82 (20.2)	14 (11.5)	4 (6.8)	0 (0)	0 (0)	0 (0)	0 (0)		

**There is no difference between IVD and EVD. But the detection rate of different sizes is different.*

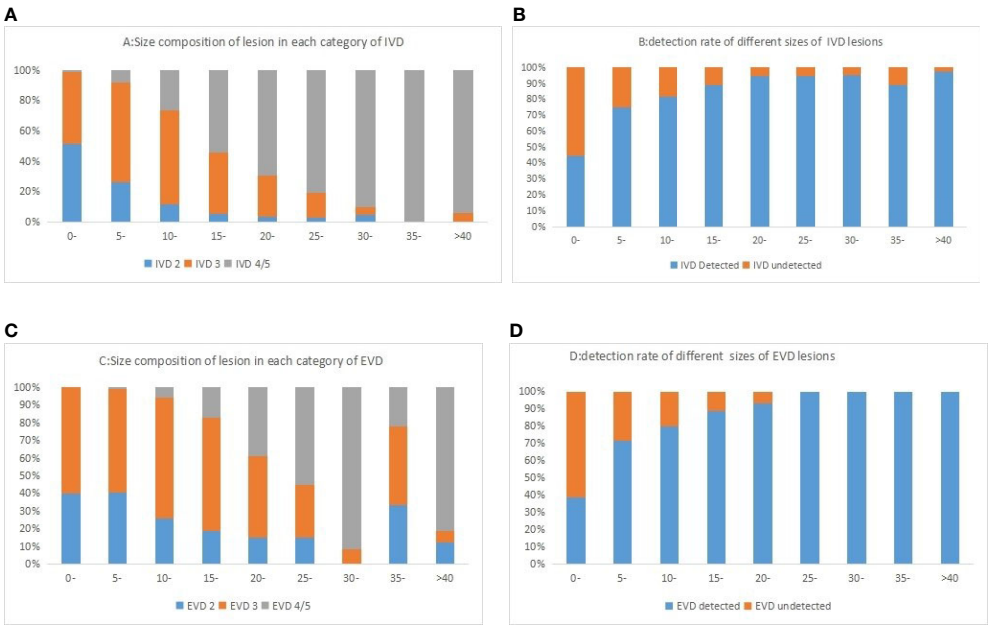

FIGURE 4 | Histogram of different categories of lesions in internal validation data **(A)** and external validation data **(C)** sets and lesions of different sizes was shown in the figure. The detection rate of different sizes of lesion in internal validation data **(B)** and external validation data **(D)** sets was shown in the figure.

between the scope and surrounding tissues, heterogeneous echo, ductal hypoechoic, or only localized hypoechoic with distortion of surrounding structures.

In the external validation, the detection of category 3 lesions was always less than that of category 2 lesions. The possible reason was that category 2 lesions were mainly manifested as breast cysts (30, 31), so they had a high detection rate. The hyperplasia lesion in category 3 belonged to uncertain lesions without a clear margin (32). The detection of this lesion needs to be determined by normal glands. When there are numerous hyperplasia lesions in the dataset, it is difficult to identify them by an artificial intelligence algorithm. In this study, there was no statistical difference in detecting malignant lesions in different data sets. The BUILDS achieved high detection sensitivity of 91.3% (IVD) and 93.0% (EVD) at 0.5 false positives per scan. The detection rate in IVD was 98.1% at 3.5 false positives per scan, and the detection rate in EVD was 98.2% at 2.5 false positives per scan. Compared to the reported performance of recently published studies on different datasets, this result was comparable to the numbers reported in a recent multi-view convolutional network study (33) and was much better than the recently published 3D CNN lung lesion detection work (34).

In this group of cases, to ensure that the training and testing set data were widely representative, the included cases were universal and often accompanied by multiple lesions. At the same time, there was the coexistence of benign and malignant lesions, which included numerous hyperplasia lesions. The detection rate of type 2 and 3 lesions in this study was lower, but it was significantly higher than that in previous studies (32, 35–37).

There were several limitations to this study. Firstly, there were some limitations in the amount of research data and some differences in image quality in this multi-center retrospective study. Secondly, the different locations of the lesion may affect the detection of the lesion. When the lesion was located at the edge of the image, it may lead to false judgment due to insufficient local pressure or incomplete display of the lesion. Moreover, if the lesion was located behind the nipple, the lesion was often unclear or incomplete because of the acoustic shadow of the nipple. Additionally, some lesions in this group were too small and lacked pixels, which will also lead to detection difficulties.

This algorithm showed good detection efficiency in internal and external validation, especially for category 4/5 lesions and malignant lesions. However, there are still some deficiencies in detecting category 2 and 3 lesions and lesions smaller than 10

TABLE 4 | The detection rate of malignant lesion in different data set was listed when different false positives (FPS) were allowed.

	Detection rate (%)									
	0	**0.5**	**1**	**1.5**	**2**	**2.5**	**3**	**3.5**	**4**	***P***
Malignant in IVD n=161	12.4	91.3	94.4	96.3	96.3	96.9	96.9	98.1	98.1	>0.05
Malignant in EVD n=57	10.7	93.0	93.0	94.7	96.5	98.2	98.2	98.2	98.2	

mm. This study showed that this algorithm could be an effective auxiliary tool for lesion detection in ABUS.

DATA AVAILABILITY STATEMENT

The raw data supporting the conclusions of this article will be made available by the authors, without undue reservation.

AUTHOR CONTRIBUTIONS

JXZ: Experimental design, organization and implementation, and thesis writing. XT: Algorithm design and verification and literature novelty search. YHJ: Image annotation and data collection. XXW: Image annotation and data collection. DY: Image annotation and data collection. WX: Image annotation and data collection. SLZ: Image annotation and statistical analysis. LC: Image annotation and experimental verification. LPL: Project acquisition and guide implementation. DN: Algorithm guidance. All authors listed have made a substantial, direct, and intellectual contribution to the work and approved it for publication.

ACKNOWLEDGMENTS

The authors thank all the hospitals that provided cases for this study, and all the radiologists and ABUS technicians of the breast remote consultation team of Guangdong Province Hospital of Chinese Medicine. This study was supported by the National Natural Science Foundation of China (No. 62171290), Shenzhen-Hong Kong Joint Research Program (No. SGDX20201103095613036) and the Shenzhen Science and Technology Research and Development Fund for Sustainable Development project (No. KCXFZ20201221173613036).

REFERENCES

1. Zhou LQ, Wu XL, Huang SY, Wu GG, Ye HR, Wei Q, et al. Lymph Node Metastasis Prediction From Primary Breast Cancer US Images Using Deep Learning. *Radiology* (2020) 294(1):19–28. doi: 10.1148/radiol.2019190372
2. Sun Q, Lin X, Zhao Y, Li L, Yan K, Liang D, et al. Deep Learning vs. Radiomics for Predicting Axillary Lymph Node Metastasis of Breast Cancer Using Ultrasound Images: Don't Forget the Peritumoral Region. *Front Oncol* (2020) 10:53. doi: 10.3389/fonc.2020.00053
3. Rajpurkar P, Irvin J, Ball RL, Zhu K, Yang B, Mehta H, et al. Deep Learning for Chest Radiograph Diagnosis: A Retrospective Comparison of the CheXNeXt Algorithm to Practicing Radiologists. *PLoS Med* (2018) 15(11): e1002686. doi: 10.1371/journal.pmed.1002686
4. Kim YG, Cho Y, Wu CJ, Park S, Jung KH, Seo JB, et al. Short-Term Reproducibility of Pulmonary Nodule and Mass Detection in Chest Radiographs: Comparison Among Radiologists and Four Different Computer-Aided Detections With Convolutional Neural Net. *Sci Rep* (2019) 9(1):18738. doi: 10.1038/s41598-019-55373-7
5. Brem RF, Tabár L, Duffy SW, Inciardi MF, Guingrich JA, Hashimoto BE, et al. Assessing Improvement in Detection of Breast Cancer With Three-Dimensional Automated Breast US in Women With Dense Breast Tissue: The SomoInsight Study. *Radiology* (2015) 274(3):663–73. doi: 10.1148/radiol.14132832
6. Hooley RJ, Greenberg KL, Stackhouse RM, Geisel JL, Butler RS, Philpotts LE. Screening US in Patients With Mammographically Dense Breasts: Initial Experience With Connecticut Public Act 09-41. *Radiology* (2012) 265(1):59–69. doi: 10.1148/radiol.12120621
7. Wilczek B, Wilczek HE, Rasouliyan L, Leifland K. Adding 3D Automated Breast Ultrasound to Mammography Screening in Women With Heterogeneously and Extremely Dense Breasts: Report From a Hospital-Based, High-Volume, Single-Center Breast Cancer Screening Program. *Eur J Radiol* (2016) 85(9):1554–63. doi: 10.1016/j.ejrad.2016.06.004
8. Hamet P, Tremblay J. Artificial Intelligence in Medicine. *Metabolism* (2017) 69s:S36–s40. doi: 10.1016/j.metabol.2017.01.011
9. Zhang X, Lin X, Zhang Z, Dong L, Sun X, Sun D, et al. Artificial Intelligence Medical Ultrasound Equipment: Application of Breast Lesions Detection. *Ultrason Imaging* (2020) 42(4-5):191–202. doi: 10.1177/0161734620928453
10. Schaefgen B, Heil J, Barr RG, Radicke M, Harcos A, Gomez C, et al. Initial Results of the FUSION-X-US Prototype Combining 3D Automated Breast Ultrasound and Digital Breast Tomosynthesis. *Eur Radiol* (2018) 28(6):2499–506. doi: 10.1007/s00330-017-5235-8
11. Venkatesh SS, Levenback BJ, Sultan LR, Bouzghar G, Sehgal CM. Going Beyond a First Reader: A Machine Learning Methodology for Optimizing Cost and Performance in Breast Ultrasound Diagnosis. *Ultrasound Med Biol* (2015) 41(12):3148–62. doi: 10.1016/j.ultrasmedbio.2015.07.020
12. Chen DR, Chien CL, Kuo YF. Computer-Aided Assessment of Tumor Grade for Breast Cancer in Ultrasound Images. *Comput Math Methods Med* (2015) 2015:914091. doi: 10.1155/2015/914091
13. Xi X, Shi H, Han L, Wang T, Ding HY, Zhang G, et al. Breast Tumor Segmentation With Prior Knowledge Learning. *Neurocomputing* (2016) 237:145–57. doi: 10.1016/j.neucom.2016.09.067
14. Cao X, Chen H, Li Y, Peng Y, Wang S, Cheng L. Dilated Densely Connected U-Net With Uncertainty Focus Loss for 3D ABUS Mass Segmentation. *Comput Methods Programs Biomed* (2021) 209:106313. doi: 10.1016/j.cmpb.2021.106313
15. Agarwal R, Diaz O, Lladó X, Gubern-Mérida A, Vilanova JC, Martí R. Lesion Segmentation in Automated 3d Breast Ultrasound: Volumetric Analysis. *Ultrason Imaging* (2018) 40(2):97–112. doi: 10.1177/0161734617737733
16. Ji Y, Zhang R, Li Z, Ren J, Luo P. UXNet: Searching Multi-Level Feature Aggregation for 3D Medical Image Segmentation. *arXiv* (2020) 32(5):2891–900. doi: 10.1007/978-3-030-59710-8_34
17. Xue Y, Xu T, Zhang H, Long LR, Huang X. SegAN: Adversarial Network With Multi-Scale L(1) Loss for Medical Image Segmentation. *Neuroinformatics* (2018) 16(3-4):383–92. doi: 10.1007/s12021-018-9377-x
18. Shen T, Gou C, Wang FY, He Z, Chen W. Learning From Adversarial Medical Images for X-Ray Breast Mass Segmentation. *Comput Methods Programs Biomed* (2019) 180:105012. doi: 10.1016/j.cmpb.2019.105012
19. Xing J, Li Z, Wang B, Qi Y, Yu B, Zanjani FG, et al. Lesion Segmentation in Ultrasound Using Semi-Pixel-Wise Cycle Generative Adversarial Nets. *IEEE/ACM Trans Comput Biol Bioinf* (2021) 18(6):2555–65. doi: 10.1109/TCBB.2020.2978470
20. Hu Y, Guo Y, Wang Y, Yu J, Li J, Zhou S, et al. Automatic Tumor Segmentation in Breast Ultrasound Images Using a Dilated Fully Convolutional Network Combined With an Active Contour Model. *Med Phys* (2019) 46(1):215–28. doi: 10.1002/mp.13268
21. Xu Y, Wang Y, Yuan J, Cheng Q, Wang X, Carson PL. Medical Breast Ultrasound Image Segmentation by Machine Learning. *Ultrasonics* (2019) 91:1–9. doi: 10.1016/j.ultras.2018.07.006
22. Wang Y, Wang N, Xu M, Yu J, Qin C, Luo X, et al. Deeply-Supervised Networks With Threshold Loss for Cancer Detection in Automated Breast Ultrasound. *IEEE Trans Med Imaging* (2020) 39(4):866–76. doi: 10.1109/TMI.2019.2936500
23. Jing L, Tian Y. Self-Supervised Visual Feature Learning With Deep Neural Networks: A Survey. *IEEE Trans Pattern Anal Mach Intell* (2021) 43 (11):4037–58. doi: 10.1109/TPAMI.2020.2992393
24. Vourtsis A, Kachulis A. The Performance of 3D ABUS Versus HHUS in the Visualisation and BI-RADS Characterisation of Breast Lesions in a Large

Cohort of 1,886 Women. *Eur Radiol* (2018) 28(2):592–601. doi: 10.1007/s00330-017-5011-9
25. van Zelst JCM, Mann RM. Automated Three-Dimensional Breast US for Screening: Technique, Artifacts, and Lesion Characterization. *Radiographics* (2018) 38(3):663–83. doi: 10.1148/rg.2018170162
26. Pezeshk A, Hamidian S, Petrick N, Sahiner B. 3-D Convolutional Neural Networks for Automatic Detection of Pulmonary Nodules in Chest Ct. *IEEE J BioMed Health Inform* (2019) 23(5):2080–90. doi: 10.1109/JBHI.2018.2879449
27. Cao H, Liu H, Song E, Ma G, Xu X, Jin R, et al. A Two-Stage Convolutional Neural Networks for Lung Nodule Detection. *IEEE J BioMed Health Inform* (2020) 24(7):2006–15. doi: 10.1109/JBHI.2019.2963720
28. Nasrullah N, Sang J, Alam MS, Mateen M, Cai B, Hu H. Automated Lung Nodule Detection and Classification Using Deep Learning Combined With Multiple Strategies. *Sensors (Basel)* (2019) 19(17):3722. doi: 10.3390/s19173722
29. Ban K, Tsunoda H, Suzuki S, Takaki R, Sasaki K, Nakagawa M. Verifification of Recall Criteria for Masses Detected on Ultrasound Breast Cancer Screening. *J Med Ultrasonics* (2018) 45:65–73. doi: 10.1007/s10396-017-0778-5
30. Mainiero MB, Goldkamp A, Lazarus E, Livingston L, Koelliker SL, Schepps B, et al. Characterization of Breast Masses With Sonography: Can Biopsy of Some Solid Masses Be Deferred? *J Ultrasound Med* (2005) 24(2):161–7. doi: 10.7863/jum.2005.24.2.161
31. Graf O, Helbich TH, Hopf G, Graf C, Sickles EA. Probably Benign Breast Masses at US: Is Follow-Up an Acceptable Alternative to Biopsy? *Radiology* (2007) 244(1):87–93. doi: 10.1148/radiol.2441060258
32. Spak DA, Plaxco JS, Santiago L, Dryden MJ, Dogan BE. BI-RADS(®) Fifth Edition: A Summary of Changes. *Diagn Interv Imaging* (2017) 98(3):179–90. doi: 10.1016/j.diii.2017.01.001
33. Setio AA, Ciompi F, Litjens G, Gerke P, Jacobs C, van Riel SJ, et al. Pulmonary Nodule Detection in CT Images: False Positive Reduction Using Multi-View Convolutional Networks. *IEEE Trans Med Imaging* (2016) 35(5):1160–9. doi: 10.1109/TMI.2016.2536809
34. Anirudh R, Thiagarajan J, Bremer T, Kim H. Lung Nodule Detection Using 3D Convolutional Neural Networks Trained on Weakly Labeled Data. *Spie* (2016) 9785:978532–6. doi: 10.1117/12.2214876
35. Magnuska ZA, Theek B, Darguzyte M, Palmowski M, Stickeler E, Schulz V, et al. Influence of the Computer-Aided Decision Support System Design on Ultrasound-Based Breast Cancer Classification. *Cancers* (2022) 14(2):277. doi: 10.3390/cancers14020277
36. Hsieh YH, Hsu FR, Dai ST, Huang HY, Chen DR , Shia WC. Incorporating the Breast Imaging Reporting and Data System Lexicon With a Fully Convolutional Network for Malignancy Detection on Breast Ultrasound. *Diagnostics (Basel, Switzerland* (2021) 12(1):66. doi: 10.3390/diagnostics12010066
37. Wang F, Liu X, Yuan N, Qian B, Ruan L, Yin C, et al. Study on Automatic Detection and Classification of Breast Nodule Using Deep Convolutional Neural Network System. *J Thorac disease* (2020) 12(9):4690–701. doi: 10.21037/jtd-19-3013

Conflict of Interest: The authors declare that the research was conducted in the absence of any commercial or financial relationships that could be construed as a potential conflict of interest.

Publisher's Note: All claims expressed in this article are solely those of the authors and do not necessarily represent those of their affiliated organizations, or those of the publisher, the editors and the reviewers. Any product that may be evaluated in this article, or claim that may be made by its manufacturer, is not guaranteed or endorsed by the publisher.

frontiers | Frontiers in Oncology

TYPE Original Research
PUBLISHED 25 July 2022
DOI 10.3389/fonc.2022.944569

OPEN ACCESS

EDITED BY
Nosheen Masood,
Fatima Jinnah Women University, Pakistan

REVIEWED BY
Prasannavenkatesan Theerthagiri, Gandhi Institute of Technology and Management (GITAM), India
Abdulhamit Subasi, University of Turku, Finland
Pawel Zyblewski, Wrocław University of Science and Technology, Poland

*CORRESPONDENCE
Zhen Zhang
2662898158@qq.com

SPECIALTY SECTION
This article was submitted to Breast Cancer, a section of the journal Frontiers in Oncology

RECEIVED 15 May 2022
ACCEPTED 01 July 2022
PUBLISHED 25 July 2022

CITATION
Zhang G, Shi Y, Yin P, Liu F, Fang Y, Li X, Zhang Q and Zhang Z (2022) A machine learning model based on ultrasound image features to assess the risk of sentinel lymph node metastasis in breast cancer patients: Applications of scikit-learn and SHAP. *Front. Oncol.* 12:944569. doi: 10.3389/fonc.2022.944569

A machine learning model based on ultrasound image features to assess the risk of sentinel lymph node metastasis in breast cancer patients: Applications of scikit-learn and SHAP

Gaosen Zhang[1], Yan Shi[2], Peipei Yin[2], Feifei Liu[3], Yi Fang[1], Xiang Li[1], Qingyu Zhang[4] and Zhen Zhang[1]*

[1]Department of Ultrasound, First Affiliated Hospital of China Medical University, Shenyang, China, [2]Department of Ultrasound, Binzhou Medical University Hospital, Binzhou, China, [3]Department of Ultrasound Medicine, Peking University People's Hospital, Beijing, China, [4]College of Information Science and Engineering, Northeastern University, Shenyang, China

Background: This study aimed to determine an optimal machine learning (ML) model for evaluating the preoperative diagnostic value of ultrasound signs of breast cancer lesions for sentinel lymph node (SLN) status.

Method: This study retrospectively analyzed the ultrasound images and postoperative pathological findings of lesions in 952 breast cancer patients. Firstly, the univariate analysis of the relationship between the ultrasonographic features of breast cancer morphological features and SLN metastasis. Then, based on the ultrasound signs of breast cancer lesions, we screened ten ML models: support vector machine (SVM), extreme gradient boosting (XGBoost), random forest (RF), linear discriminant analysis (LDA), logistic regression (LR), naive bayesian model (NB), k-nearest neighbors (KNN), multilayer perceptron (MLP), long short-term memory (LSTM), and convolutional neural network (CNN). The diagnostic performance of the model was evaluated using the area under the receiver operating characteristic (ROC) curve (AUC), Kappa value, accuracy, F1-score, sensitivity, and specificity. Then we constructed a clinical prediction model which was based on the ML algorithm with the best diagnostic performance. Finally, we used SHapley Additive exPlanation (SHAP) to visualize and analyze the diagnostic process of the ML model.

Results: Of 952 patients with breast cancer, 394 (41.4%) had SLN metastasis, and 558 (58.6%) had no metastasis. Univariate analysis found that the shape, orientation, margin, posterior features, calculations, architectural distortion,

duct changes and suspicious lymph node of breast cancer lesions in ultrasound signs were associated with SLN metastasis. Among the 10 ML algorithms, XGBoost had the best comprehensive diagnostic performance for SLN metastasis, with Average-AUC of 0.952, Average-Kappa of 0.763, and Average-Accuracy of 0.891. The AUC of the XGBoost model in the validation cohort was 0.916, the accuracy was 0.846, the sensitivity was 0.870, the specificity was 0.862, and the F1-score was 0.826. The diagnostic performance of the XGBoost model was significantly higher than that of experienced radiologists in some cases (P<0.001). Using SHAP to visualize the interpretation of the ML model screen, it was found that the ultrasonic detection of suspicious lymph nodes, microcalcifications in the primary tumor, burrs on the edge of the primary tumor, and distortion of the tissue structure around the lesion contributed greatly to the diagnostic performance of the XGBoost model.

Conclusions: The XGBoost model based on the ultrasound signs of the primary breast tumor and its surrounding tissues and lymph nodes has a high diagnostic performance for predicting SLN metastasis. Visual explanation using SHAP made it an effective tool for guiding clinical courses preoperatively.

KEYWORDS

breast cancer, ultrasound signs, sentinel lymph node metastasis, XGBoost, SHAP

Introduction

Breast cancer is the most common malignancy in women, and its incidence is increasing annually (1). Whether sentinel lymph node (SLN) metastases have important clinical significance for breast cancer staging, surgical selection, and prognosis is still being determined. Sentinel lymph node biopsy (SLNB) is the gold standard for diagnosing SLN metastasis of breast cancer. An invasive method, SLNB may cause complications such as infection at the puncture site and hematoma (2). Moreover, SLNB has a false-positive rate of 5%–10% (3), which leads to the possibility of secondary surgery. This urgently requires imaging to accurately determine the status of SLNs, to avoid extensive lymph node dissection and minimize the trauma to patients.

Ultrasonography has become the preferred method for breast diseases due to its advantages of non-invasiveness, high reproducibility, and good patient cooperation (4). Previous studies (5) showed that the morphological characteristics of the primary breast cancer have a certain relationship with the activity (biological behavior) of the tumor, and its morphology will change with the biological behavior such as lymph node metastasis. This suggests that monitoring the morphological features of breast cancer lesions is of great value in assessing SLN status. Conventional ultrasound can provide macroscopic features of lesions, but the weight of these macroscopic features in relation to SLN status is unclear.

Machine learning (ML) algorithms have been applied in the medical field for outcome prediction, diagnosis, and treatment (6). For example, ML model has been used to differentiate between benign breast nodules and breast cancer based on ultrasound images (7). But the logic and complexity of various ML algorithms are different (8), and there may also be differences in clinical application. A study (9) compared the diagnostic performance of different ML algorithms in the diagnosis of benign and malignant thyroid nodules and found that the random forest (RF) model achieved the best area under the receiver operating characteristic (ROC) curve (AUC) (0.924). Due to the complex nonlinear relationship of some ML algorithms, the model results are difficult to interpret, resulting in a "black-box" problem (10), which limits the clinical application of predictive models. Therefore, the interpretability algorithm of ML model results has become a new research focus (11). SHapley Additive exPlanation (SHAP), based on cooperative game theory, has global and local interpretability, interpreting the predicted value of the model as the sum of the contribution values of each input feature, that is, the shapley value. Compared with other explanation methods in previous literature, SHAP can visualize the prediction process of complex ML prediction models. These advantages make it

possible to solve the "black-box" problem of complex ML models with SHAP. At present, SHAP has been successfully applied to intraoperative hypoxemia risk prediction (12) and COVID-19 prognosis assessment (13). Therefore, this study aimed to develop a ML model based on the ultrasound signs of breast cancer lesions and surrounding soft tissues and lymph nodes to predict the risk of axillary lymph node metastasis in breast cancer patients. Using SHAP to visually interpret the prediction results of the ML model, so as to guide the clinical formulation of personalized diagnosis and treatment plans. The SHAP also can promote the clinical application of the prediction model.

Materials and methods

Patients

As a retrospective study, this study was approved by the Ethics Committee of the First Affiliated Hospital of China Medical University (AF-SOP-07-1.1-07), which waived the requirement for patient informed consent. All patients in this study underwent ultrasonography of breast cancer lesions and ipsilateral axillary lymph nodes in our department. The inclusion criteria were as follows: (1) patients with primary breast cancer who were first discovered and had no history of other malignancies; (2) no axillary mass was found on physical examination; (3) ultrasound examination within 2 weeks before breast cancer surgery or percutaneous biopsy of the lesion; (4) no other adjuvant therapy such as chemotherapy or radiotherapy was performed before ultrasound examination; (5) and the ultrasound image of the lesion was clear and complete. The exclusion criteria were as follows: (1) non-single lesions; and (2) absence of clinical data and pathology. Finally, we screened 902 consecutive female patients with breast cancer from June 2017 to June 2021 as a primary cohort, constructed a predictive model, and performed internal validation, with a mean age of 49.98 ± 9.81 years (range: 24–86 years). Following the same inclusion and exclusion criteria, we screened another 50 female patients with breast cancer from July 2021 to December 2021 as a validation cohort, with a mean age of 49.82 ± 10.99 years (range: 25–74 years). Pathological findings of all patients in the primary cohort and validation cohort were confirmed postoperatively or after percutaneous needle biopsy.

Ultrasound evaluation

In this study, three types of ultrasonic diagnostic instruments including Hitachi HI VISION Ascendus (Hitachi Medical Corp., Tokyo, Japan), Canon APLIO 500 (Canon Medical Systems Corp., Otawara, Japan), and SuperSonic Aixplorer (SuperSonic Imagine SA, Aix-en-Provence, France) were used for image acquisition, all of which were equipped with superficial high-frequency linear array probes with a frequency of 8–15MHz. Images were stored in the picture archiving and communication system (PACS) workstation for further analysis. Ultrasound signs of breast cancer lesions images in the PACS workstation were evaluated by two experienced radiologists without knowledge of the exact pathological findings. To assess intra- and inter-observer reproducibility, radiologist A assessed all ultrasound signs in the primary cohort and reassessed these after 1 week to test for intra-observer consistency. All ultrasound signs in the primary cohort were also assessed by radiologist B and compared with those from radiologist A to test for interobserver agreement. The evaluation of ultrasound signs mainly included the shape of the original lesion (oval, round, or irregular), orientation (parallel or not parallel), margin (circumscribed, indistinct, angular, microlobulated, or spiculated), echo pattern (hyperechoic, isoechoic, hypoechoic, anechoic, or complex cystic and solid), posterior features (no posterior features, enhancement, or shadowing), calcifications (no calcification, macrocalcification, microcalcification, or rim calcification), architectural distortion, duct changes, hyperechoic halo, and suspicious lymph nodes. Lymph node classification criteria (14) were evaluated, with categories 1–3 considered benign, and categories 4–6 considered metastatic.

Data preprocessing

Firstly, we performed univariate analysis of all data from the primary and validation cohorts to screen for ultrasound signs associated with SLN metastasis. Then, it was found by statistics that the number of samples in the SLN transfer group with a small number of samples accounted for 41.4% (394/952) of the total number of samples, which was a balanced sample. Therefore, no relevant processing to deal with data imbalance, such as over-sampled or under-sampled, is performed on the dataset. Finally, in order to speed up the training and improve the diagnostic performance of the model, we standardize and normalize the dataset. For details of data preprocessing, see Supplementary Material 1.

Screening and validation of machine learning models

The 902 samples in the primary cohort were randomly divided into ten parts, and 10-fold cross-validation were performed on 10 ML algorithms such as support vector machine (SVM), extreme gradient boosting (XGBoost), RF, linear discriminant analysis (LDA), logistic regression (LR), naive Bayesian model (NB), k-nearest neighbors (KNN), multilayer perceptron (MLP), long short-term memory

(LSTM) and convolutional neural network (CNN). The diagnostic performance of all ML algorithms was adjusted by grid search algorithm to optimize the performance of the ML model and avoid overfitting of the model. We comprehensively evaluated the diagnostic performance of 10 algorithms for predicting breast cancer SLN metastasis using the Average-AUC, Average-Kappa and Average-Accuracy derived from the 10-fold cross-validation. Then, the entire primary cohort was used for 10 ML models for training. The diagnostic performance of the ML model was verified through the validation set data, and the diagnostic performance of all models were evaluated using the ROC curve and the detection error trade-off (DET) curve. Then we used the learning curve to verify the fit of the best performing model. Finally, we compared the best performing ML algorithm with experienced radiologist.

Visualizing machine learning models

SHAP measures feature importance by calculating the contribution value, while describing whether the influence of the feature is positive or negative (15). We also utilize SHAP for the visual interpretation of the ML models both holistically and individually (16), which facilitates the clinical applications of the ML model (Figure 1).

Statistical analysis

SPSS (v. 26.0; IBM Corp., Armonk, NY, USA) statistical software was used. Continuous variables were expressed as ($\bar{x} \pm s$) using independent samples t-tests and the F-test; categorical variables were expressed as frequencies using the χ^2 test and Fisher's exact test. $P<0.05$ means the difference is statistically significant. Kappa (K) analysis was used to assess intra- and inter-observer agreement. Data analysis used 10 ML algorithms from the Scikit-learn (https://scikit-learn.org/stable/) and Pytorch (https://pytorch.org/) packages in Python (version 3.8). Among them, SVM, XGBoost, RF, LDA, LR, NB, KNN, MLP are from Scikit-learn, and LSTM and CNN are from Pytorch. SHAP (https://github.com/slundberg/shap) was performed using the SHAP Python framework (version 0.40.0).

Results

Basic clinical features of breast cancer patients

The pathological results of 902 patients in the primary cohort are shown in Table 1, of which 305 were confirmed by surgery, and 597 were confirmed by percutaneous needle biopsy. There were 372 cases in the SLN metastasis group, with an average age of 49.53 ± 9.55 years (range: 26–86 years). There were 530 patients in the SLN non-metastatic group, with an average age of 50.29 ± 9.97 years (range: 24–82 years). There was no significant difference in age between the two groups (t=1.153, P=0.249).

Ultrasound signs of breast cancer lesions

Univariate analysis of ultrasound signs in the primary cohort and validation cohort to screen for risk factors associated with breast cancer SLN metastasis (Table 2). We found that the echo pattern (P=0.613) and hyperechoic halo (P=0.855) of lesions were not significantly different between the two groups and were removed. The remaining eight key ultrasound signs, such as shape, orientation, margin, posterior features, calculations, architectural distortion, duct changes and suspicious lymph node, were used for ML algorithms screening.

Choosing a machine learning model

The intra-observer K value of radiologist A was 0.887–0.938 in the two evaluations of the ultrasound signs of lesions, and the inter-observer K value of radiologists A and B was 0.876–0.917. This shows that the evaluation of ultrasound signs was stable and reproducible. All results of this study are based on the ultrasound features of the lesion as assessed by radiologist A.

Based on the screened eight key ultrasound signs, the ROC curves of 10 ML models of SVM, XGBoost, RF, LDA, LR, NB, KNN, MLP, LSTM and CNN were compared by 10-fold cross-validation (Figure 2). And the models were screened by Average-AUC, Average-Kappa and Average-Accuracy (Table 3). We found that the XGBoost model had the best Average-AUC (0.952), Average-Kappa (0.763) and Average-accuracy (0.891). Subsequently, we used the entire data from the primary cohort to train 10 ML models. Finally, external validation of the model used validation cohort has showed that the diagnostic performance of the XGBoost model was still the best (Figure 3). The AUC of the model was 0.916, the accuracy was 0.846, the sensitivity was 0.870, the specificity was 0.862, and the F1-score was 0.826 (Table 4). This further justifies the correctness of our model selection and experimental procedures. The DET curve shows that the false rejection rate and false acceptance rate of the XGBoost model are lower than other models (Figure 4). Additionally, we verified the fit of the model using the learning curve, and the XGBoost model showed a good fit (Figure 5). The Supplementary Material 2 shows the modeling process of the XGBoost algorithm. Finally, we selected the XGBoost algorithm, with the best diagnostic performance, and compared it with the diagnoses from radiologist A.

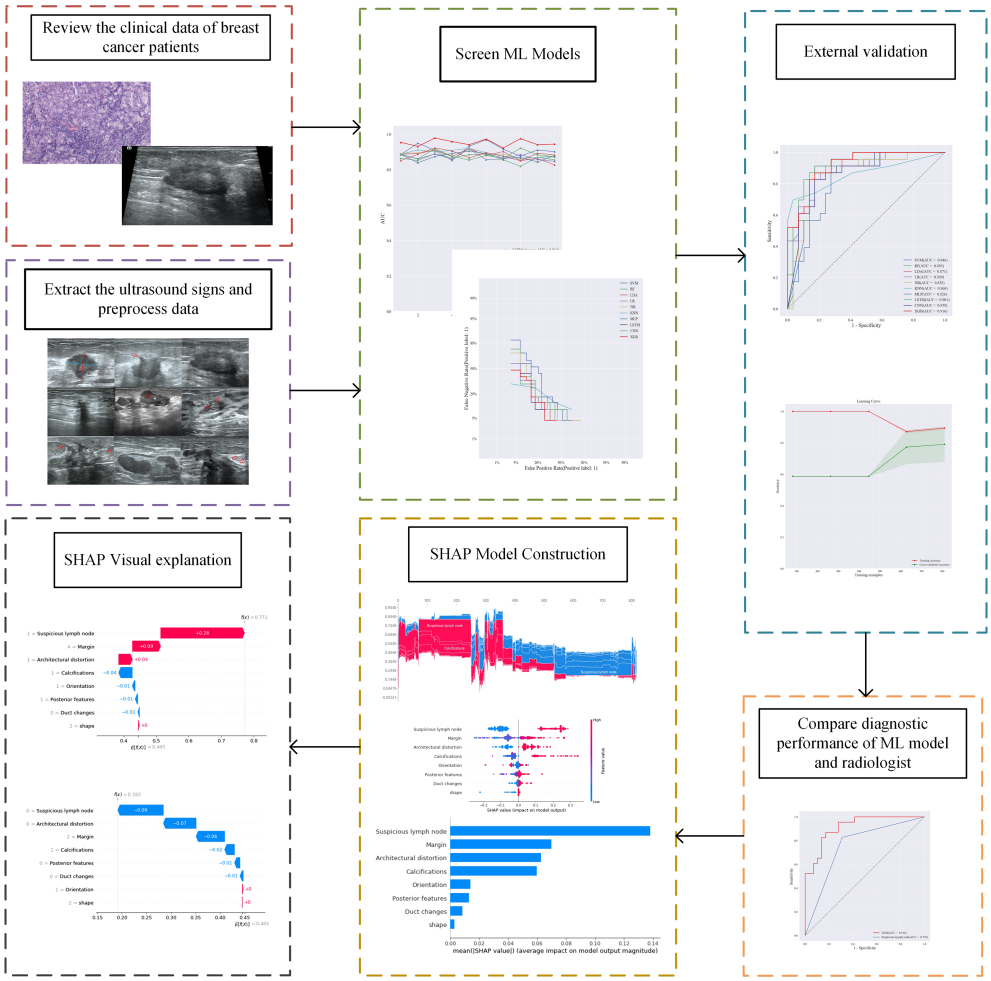

FIGURE 1
The flowchart of the study.

TABLE 1 Pathological types of breast cancer patients in the primary cohort.

Pathology	No. (%) of patients		
	SLN non-metastasis	SLN metastasis	Total
invasive ductal carcinoma	403(76.0%)	356(95.7%)	759(84.2%)
ductal carcinoma in situ	106(20.0%)	14(3.8%)	120(13.3%)
mucinous carcinoma	7(1.3%)	0	7(0.8%)
mixed breast carcinoma	6(1.1%)	1(0.3%)	7(0.8%)
intraductal papillary carcinoma	4(0.8%)	0	4(0.4%)
invasive micropapillary carcinoma	2(0.4%)	1(0.3%)	3(0.3%)
invasive lobular carcinoma	1(0.2%)	0	1(0.1%)
malignant phyllodes tumor	1(0.2%)	0	1(0.1%)
Total	530	372	902

SLN, sentinel lymph node.

10.3389/fonc.2022.944569

TABLE 2 Univariate analysis of breast cancer SLN metastasis in primary and validation cohorts.

Variable	Primary cohort (N=902)		*P*-Value	Validation cohort (N=50)		*P*-Value
	SLN metastasis (N=372)	SLN non-metastatic (N=530)		SLN metastasis (N=22)	SLN non-metastatic (N=28)	
shape			<0.001			0.277
oval	0	0		0	0	
round	4 (1.1%)	33 (6.2%)		5 (22.7%)	3 (10.7%)	
Irregular	368 (98.9%)	497 (93.8%)		17 (77.3%)	25 (89.3%)	
orientation			<0.001			0.153
parallel	201 (54.0%)	368 (69.4%)		9 (40.9%)	18 (64.3%)	
not parallel	171 (46.0%)	162 (30.6%)		13 (59.1%)	10 (35.7%)	
margin			<0.001			0.014
circumscribed	5 (1.3%)	20 (3.8%)		0	0	
indistinct	24 (6.5%)	117 (22.1%)		0	4 (14.3%)	
angular	56 (15.1%)	266 (50.2%)		2 (9.1%)	6 (21.4%)	
micro lobulated	75 (20.2%)	93 (17.5%)		4 (18.2%)	10 (35.7%)	
spiculated	212 (56.9%)	34 (6.4%)		16 (72.7%)	8 (28.6%)	
echo pattern			0.613			0.262
anechoic	0	0		0	0	
hyperechoic	0	0		0	0	
isoechoic	76 (20.4%)	111 (20.9%)		3 (13.6%)	9 (32.1%)	
complex cystic and solid	8 (2.2%)	17 (3.2%)		2 (9.1%)	1 (3.6%)	
hypoechoic	288 (77.4%)	402 (75.9%)		17 (77.3%)	18 (64.3%)	
posterior features			<0.001			0.045
enhancement	59 (15.9%)	144 (27.2%)		0	6 (21.4%)	
no posterior features	69 (18.5%)	164 (30.9%)		8 (36.4%)	11 (39.3%)	
shadowing	244 (65.6%)	222 (41.9%)		14 (63.6%)	11 (39.3%)	
calcifications			<0.001			0.004
rim calcification	10 (2.7%)	7 (1.3%)		0	1 (3.6%)	
no calcification	75 (20.2%)	275 (51.9%)		1 (4.5%)	12 (42.9%)	
macrocalcification	66 (17.7%)	231 (43.6%)		8 (36.4%)	10 (35.7%)	
microcalcification	221 (59.4%)	17 (3.2%)		13 (59.1%)	5 (17.8%)	
architectural distortion			<0.001			0.001
no	23 (6.2%)	319 (60.2%)		4 (18.2%)	19 (67.9%)	
yes	349 (93.8%)	211 (39.8%)		18 (81.8%)	9 (32.1%)	
suspicious lymph node			<0.001			0.047
no	110 (29.6%)	487 (91.9%)		6 (27.3%)	16 (57.1%)	
yes	262 (70.4%)	43 (8.1%)		16 (72.7%)	12 (42.9%)	
duct changes			0.032			0.393
no	159 (42.7%)	264 (49.8%)		10 (45.5%)	17 (60.7%)	
yes	213 (57.3%)	266 (50.2%)		12 (54.5%)	11 (39.3%)	
hyperechoic halo			0.855			1.000
no	247 (66.4%)	355 (67.0%)		16 (72.7%)	20 (71.4%)	
yes	125 (33.6%)	175 (33.0%)		6 (27.3%)	8 (28.6%)	

SLN, sentinel lymph node.

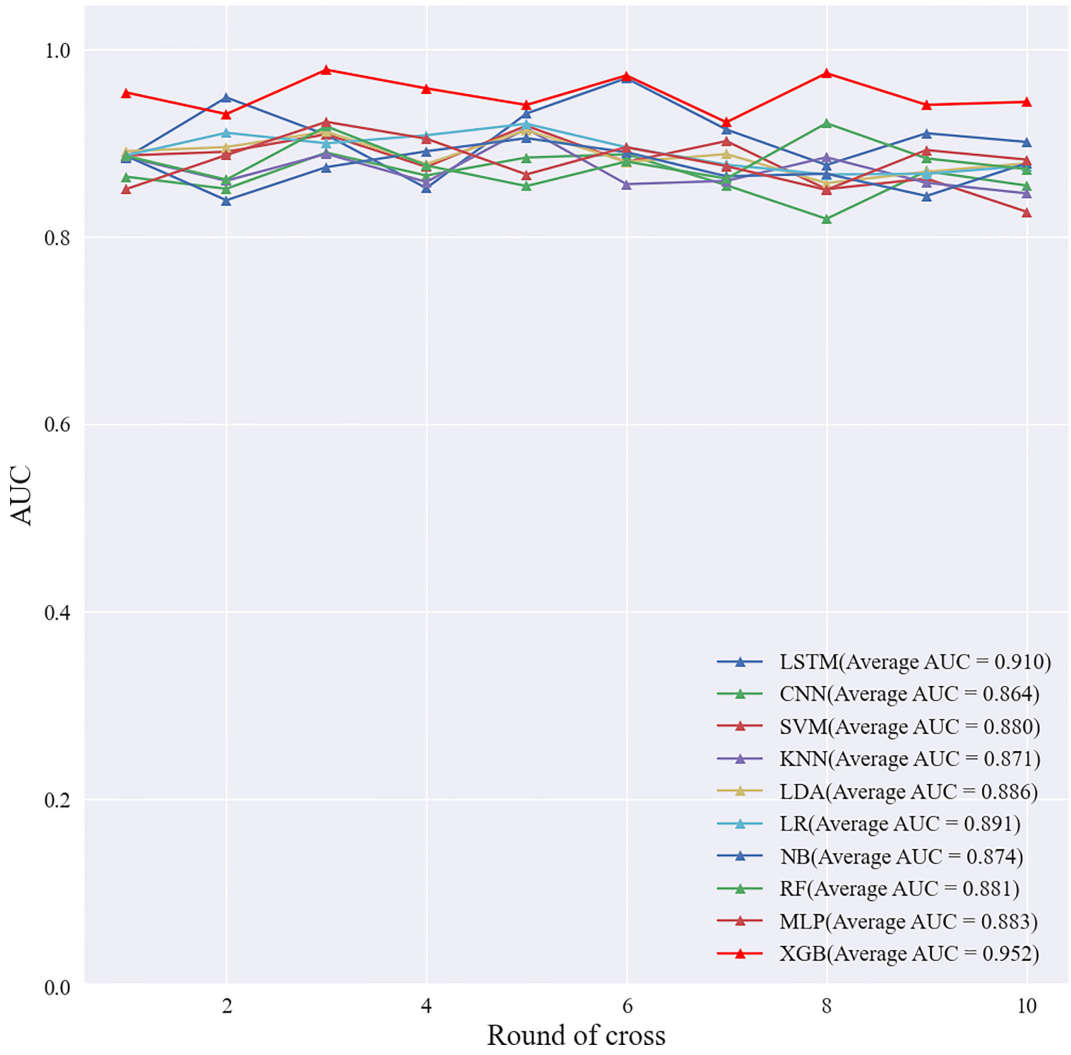

FIGURE 2
The 10-fold cross-validation of machine learning algorithms.

Factors affecting diagnostic performance of XGBoost model

We utilized SHAP to visualize the XGBoost model results. The SHAP bar graph (Figure 6) was obtained by analyzing the mean value of the absolute SHAP values of eight ultrasound signs to show the degree of influence on the final predicted probability. The SHAP scatterplot (Figure 7) shows the positive or negative impact of each ultrasound sign on the predicted probability through different colors. We found that suspicious lymph nodes, with microcalcifications, spiculation at the edge of the lesion, and distorted tissue structure around the lesion, had a

TABLE 3 Screening Evaluation Metrics for Machine Learning Algorithms Using 10-fold cross-validation.

Classifier	LSTM	CNN	SVM	KNN	LDA	LR	NB	RF	MLP	XGB
Average-AUC	0.910	0.864	0.880	0.871	0.886	0.891	0.874	0.881	0.883	0.952
Average-Kappa	0.717	0.652	0.672	0.656	0.691	0.702	0.624	0.706	0.698	0.763
Average- Accuracy	0.877	0.833	0.794	0.811	0.852	0.823	0.857	0.744	0.779	0.891

AUC, area under curve; SVM, support vector machine; XGBoost, extreme gradient boosting; RF, random forest; LDA, linear discriminant analysis; LR, logistic regression; NB, naive bayesian model; KNN, k-nearest neighbors; MLP, multilayer perceptron; LSTM, long short-term memory; CNN, convolutional neural network.

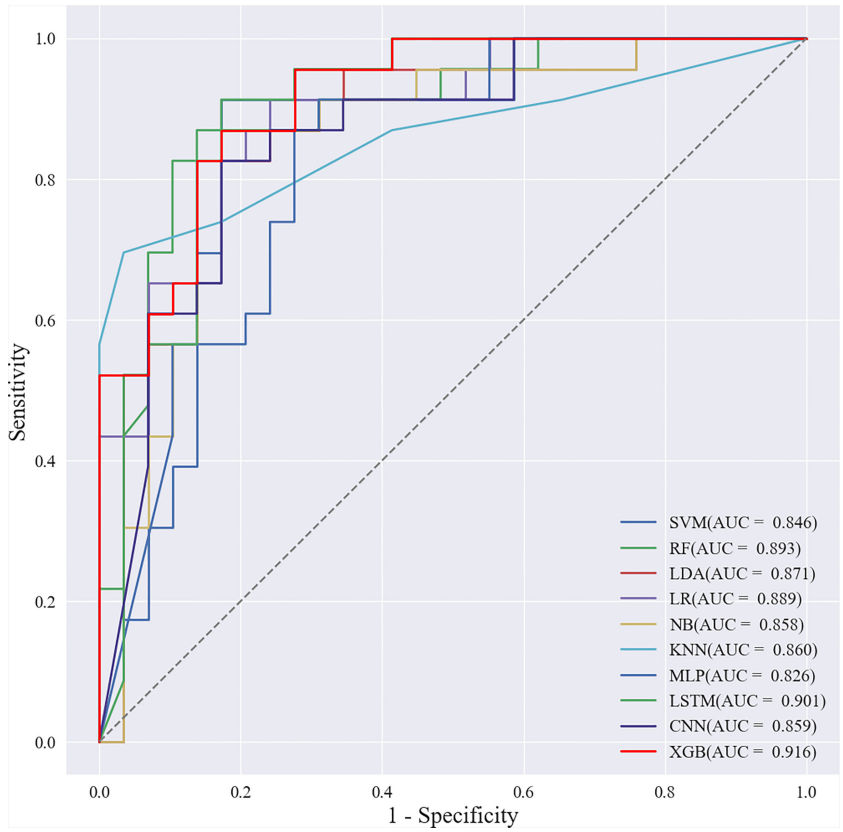

FIGURE 3
ROC curves of the validation cohort.

greater positive impact on the diagnosis of SLN metastasis in the XGBoost model. A Sankey diagram shows the distribution of key ultrasound signs in the primary cohort (Figure 8). The SHAP effort plot (Figure 9) demonstrates the cumulative effect of the contribution of each ultrasound sign in the primary cohort on the final decision. Figures 10, 11 show two examples of correctly predicted SLN transfer and no transfer, respectively. SHAP waterfall plots (Figures 10C, 11C) demonstrate the positive and negative effects of each ultrasound sign on the predicted outcome in a single case. E[f(x)] represents the basic prediction probability of the XGBoost model, and f(x) represents the final prediction probability of the model.

TABLE 4 Externally validate the performance of machine learning models.

Classifier	AUC	Accuracy	Sensitivity	Specificity	F1-score
LSTM	0.901	0.826	0.957	0.724	0.830
CNN	0.859	0.826	0.826	0.828	0.809
SVM	0.846	0.788	0.739	0.828	0.756
KNN	0.860	0.788	0.739	0.828	0.756
LDA	0.871	0.827	0.780	0.862	0.800
LR	0.889	0.800	0.826	0.759	0.800
NB	0.858	0.846	0.826	0.862	0.826
RF	0.893	0.711	0.913	0.552	0.737
MLP	0.826	0.750	0.696	0.793	0.711
XGB	0.916	0.846	0.870	0.862	0.826

AUC, area under curve; SVM, support vector machine; XGBoost, extreme gradient boosting; RF, random forest; LDA, linear discriminant analysis; LR, logistic regression; NB, naive bayesian model; KNN, k-nearest neighbors; MLP, multilayer perceptron; LSTM, long short-term memory; CNN, convolutional neural network.

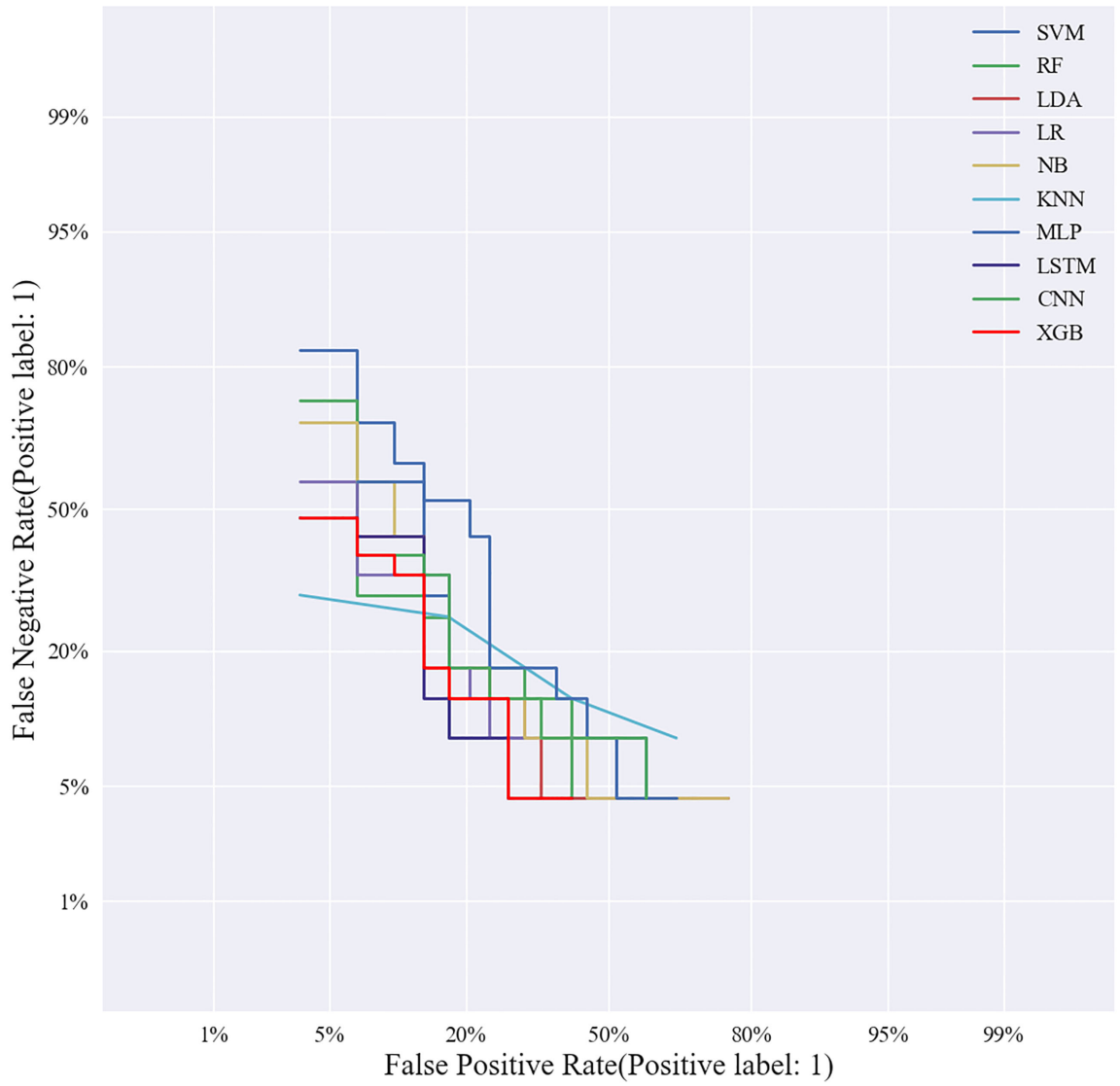

FIGURE 4
Validation cohort DET curves of 10 machine learning models.

Comparison of diagnostic performance of XGBoost model with radiologists

Radiologist A considered suspicious lymph nodes detected by ultrasound as the presence of SLN metastasis based on the lymph node ultrasound appearance and clinical experience, and we compared the diagnostic performance of the radiologists and the XGBoost model in the validation cohort. It was found that the AUC of the XGBoost model was 0.916, while the AUC of the radiologist was 0.758 (Figure 12). The difference was significant as determined by the DeLong method (P<0.001).

Discussion

This study retrospectively analyzed the ultrasound signs and pathological findings of a total of 952 breast cancer lesions in primary and validation cohorts. Using these data to screen ten common ML algorithms, it was found that the comprehensive diagnostic performance of the XGBoost model was the best and was higher than that of experienced radiologists (P<0.001). Suspicious lymph nodes, microcalcifications, spiculation signs at the edge of the lesion, and structural distortion around the lesion had a greater impact on the diagnostic performance of the

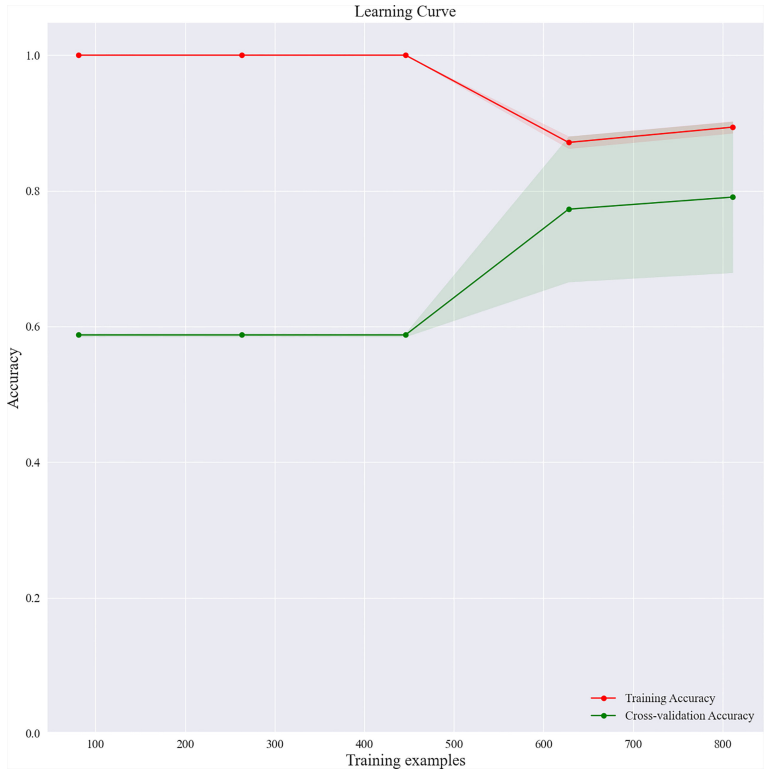

FIGURE 5
Learning curve of the XGBoost model.

XGBoost model and are the key ultrasound signs for predicting SLN status. We further used SHAP to reasonably explain the prediction results of the XGBoost model, which provides a reliable auxiliary tool for clinical decision-making.

Previous studies have mostly used logistic regression to construct nomogram clinical prediction models by extracting ultrasound image features (17). Logistic models have good interpretability, and their model coefficients represent the importance of features to prediction results. A study (18) compared the predictive ability of classification trees, random forests, artificial neural networks, and support vector machines in the ML algorithm with logistic regression and found that the predictive ability of logistic regression was equally excellent. However, this may not be statistically significant due to some

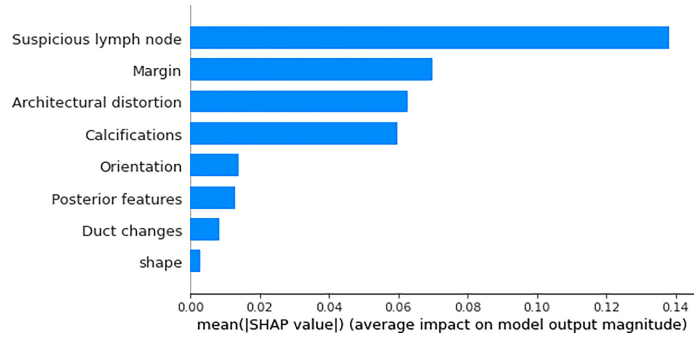

FIGURE 6
The bar graph of the SHAP summary graph shows the effect of each ultrasound sign on the XGBoost model. "Suspicious lymph node" was the factor that contributed the most to the prediction result, and margin, architectural distortion, and calculations also had a higher contribution to the prediction result.

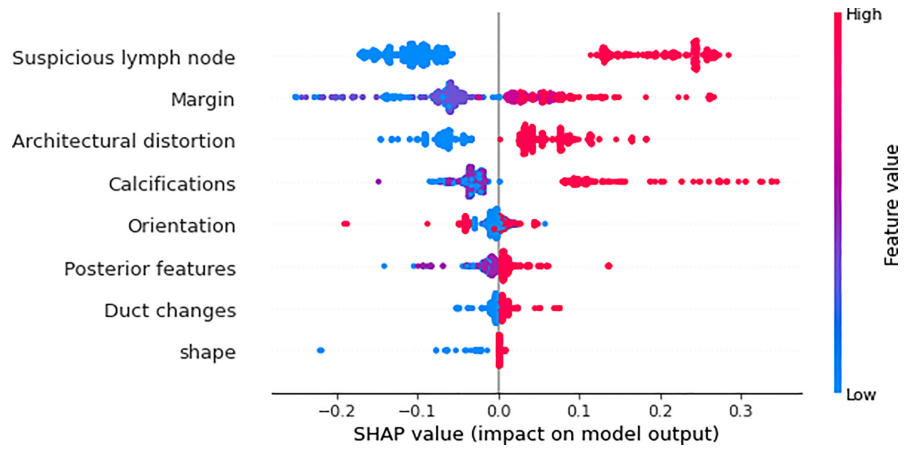

FIGURE 7
The scatter plot of the SHAP summary chart visually reflects the relationship between the feature value and the predicted probability through color, including positive and negative prediction effects. The three signs of "suspicious lymph node," "architectural distortion," and "calculations" are very clearly divided, and the margin is relatively clear. The higher the value (red), the greater the possibility of SLN transfer.

factors that have a causal relationship to the output variable (19). Excluding variables based solely on statistical assumptions reduces available information and may miss features that improve predictive power. In addition, the logistic regression model has low accuracy and is limited in practical clinical application (20). This study found that the Average-AUC (0.952), Average-Kappa (0.763) and Average-Accuracy (0.891) of the XGBoost model in the 10-fold cross-validation were higher than those of Logistic regression. The XGBoost model in the validation cohort also performed well, with AUC of 0.916,

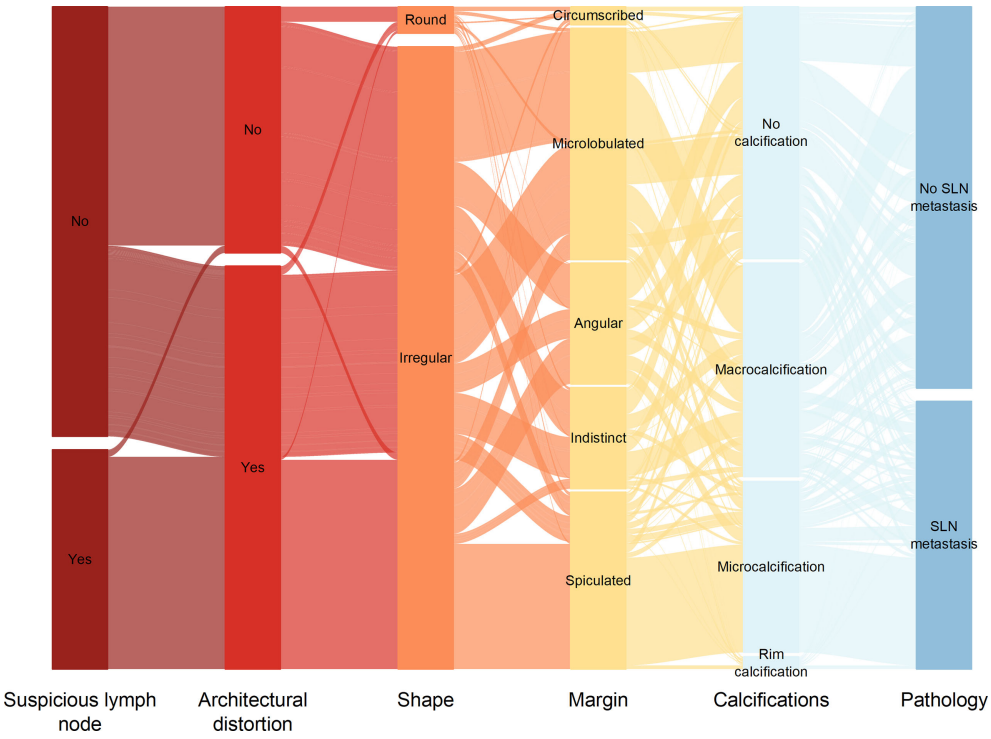

FIGURE 8
Sankey plot shows the distribution of ultrasound signs of breast cancer lesions in the primary cohort.

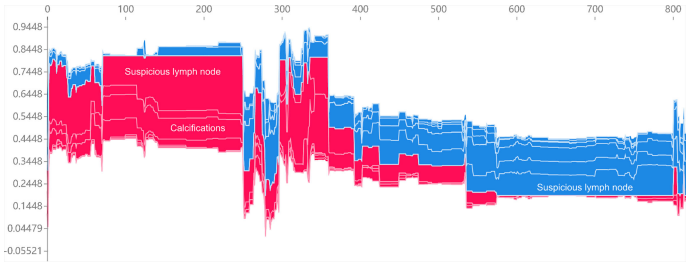

FIGURE 9
The force plot of the SHAP summary plot reflects the positive or negative impact of the eigenvalues on the diagnosis of the XGBoost model in red and blue.

accuracy of 0.846, sensitivity of 0.870, specificity of 0.862, and F1-score of 0.826. We also compared eight other ML algorithms (SVM, RF, LDA, NB, KNN, MLP, LSTM and CNN). The comprehensive diagnostic performance of the XGBoost model was still the best. Therefore, we chose to use the XGBoost algorithm to build a clinical prediction model to achieve the best diagnostic level. Next, we utilized SHAP to solve the interpretability problem of the XGBoost model. Compared with traditional ML model interpretation methods, SHAP not only considers the influence of a single variable but also considers the synergy between different variables and distinguishes the positive or negative influence of variables by color (21).

In this study, SHAP was used to find that suspicious lymph nodes detected by ultrasound had a great impact on the diagnostic performance of the XGBoost model. In addition, ultrasonographic signs such as microcalcification in the lesion, burr-like edges of the lesion, and disordered and distorted tissue structure around the lesion had a significant positive effect on the diagnosis of SLN metastasis by the XGBoost model. This may be because tumor cells infiltrate the surrounding tissues, invading the Cooper's ligament and the lymph nodes through the lymphatic vessels (22). In this study, suspicious lymph nodes were assigned the largest contribution value in the SHAP map, which is consistent with previous studies (23) in which the detection of suspicious lymph nodes by ultrasound improved the diagnostic specificity of breast cancer SLN metastases. At the same time, Drukker et al. (24, 25) also confirmed that the analysis of ultrasound images of axillary lymph nodes can effectively predict breast cancer metastasis, but the AUCs were 0.85 and 0.86, which were lower than our study (AUC=0.916). It should be considered, however, that this may be because we also included the ultrasound signs of the primary lesions of breast cancer patients to train the ML model, which further increased the diagnostic performance of the model. Li et al. (26) found that breast cancer with calcification had a higher rate of lymph node metastasis. Luo et al. (27, 28) found that the tumor pathological type, tumor burr sign, and calcification characteristics were related to axillary lymph node metastasis. These studies are consistent with the findings of the present study. The tumor edge spiculation sign is often the manifestation of the infiltration and growth of the lesion to the surrounding tissue, suggesting that the tumor is malignant, and its OR value is 14.68-10.45 (29). Compared with coarse calcification, micro calcification is usually

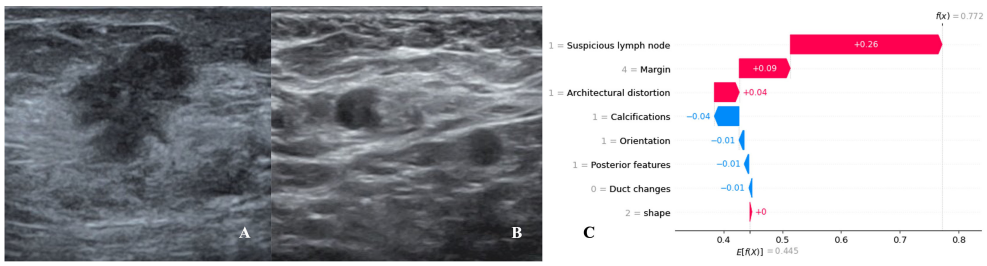

FIGURE 10
Data from a female patient, 46 years old. **(A)**. Right breast probing and hypoechoic lesions, not parallel to the skin, irregular in shape, burr-like edges, and disordered echoes of surrounding structures; **(B)**. Right axillary probing and echoes of suspicious lymph nodes. Pathological findings: invasive ductal carcinoma, metastases in sentinel lymph nodes; **(C)**. The waterfall chart of the XGBoost model predicted the process of SLN metastasis in this case. For this patient, the predicted outcome was 77.2% (baseline: 44.5%), and high-risk factors for being diagnosed with SLN metastasis included suspicious lymph nodes, spiculated lesion margins, and architectural distortion.

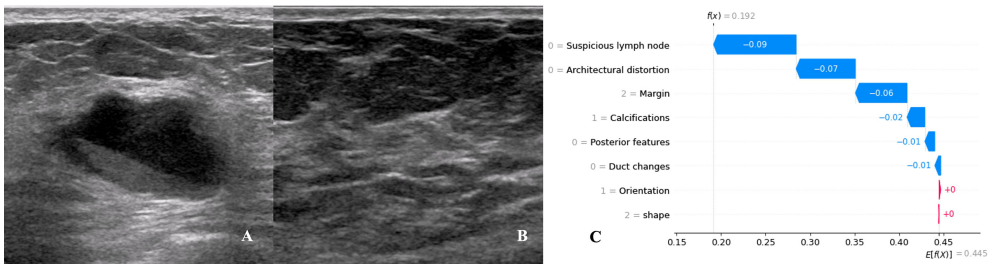

FIGURE 11
Data from a female patient, 62 years old. **(A)**. Right breast probing and mixed echogenic lesions, not parallel to the skin, irregular in shape, lobulated at the edge, and echogenic in the rear; **(B)**. No suspicious lymph node echo was detected in the right axilla. Pathological findings: invasive ductal carcinoma, no metastases in sentinel lymph nodes; **(C)**. The waterfall chart of the XGBoost model predicting the process of SLN metastasis in this case. For this patient, the predicted outcome was 19.2% (the baseline was 44.5%), and the favorable factors mainly included the margin of the lesion being lobulated, no suspicious lymph nodes being found, no obvious distortion of the tissue structure around the lesion, and no calcification in the lesion.

one of the indicators of rapid proliferation of cancer cells, and it is also a manifestation of high tumor malignancy (30), which increases the risk of SLN metastasis in breast cancer. In this study, the SHAP map also found that the contribution of architectural distortion to predicting SLN metastasis was second only to suspicious lymph nodes. Architectural distortion usually includes twisting of the ducts around the mass, shortening and straightening of Cooper's ligament, and the mass breaching the anatomical plane to invade adipose tissue (31). Paulinelli et al. (32) found that Cooper's ligament thickening is a characteristic of malignant tumors, and its odds ratio value was 15.61. The studies of Woo (33) and Lee

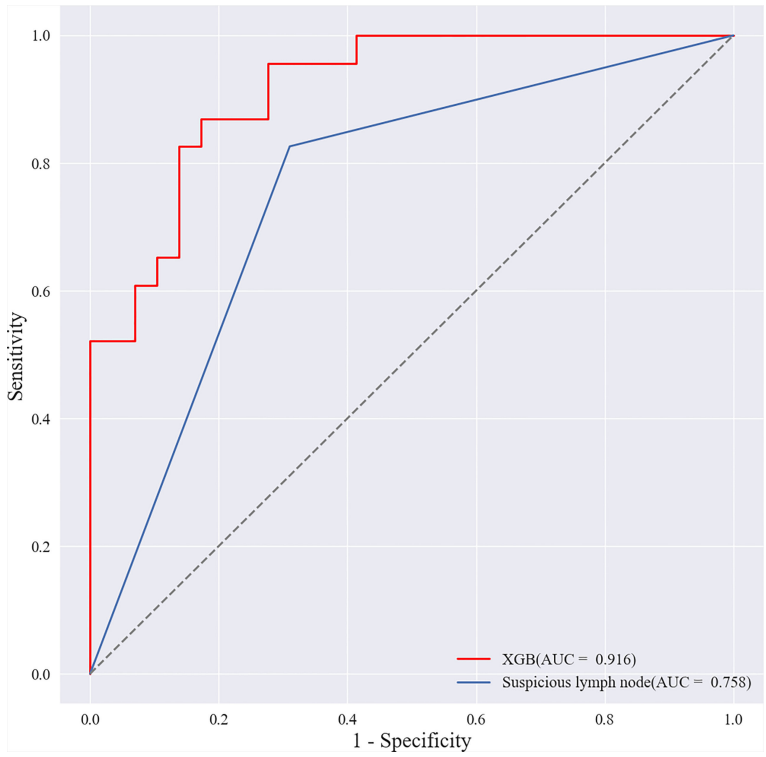

FIGURE 12
Receiver operating characteristic (ROC) curves of XGBoost models and radiologists. The areas under the curve (AUCs) of the two methods (0.916 vs. 0.758) were significantly different as determined by the DeLong method (P<0.001).

(34) also confirmed that the combination of ultrasound images of primary tumor and peritumoral tissue can more effectively predict the status of axillary lymph nodes. We believe that training the XGBoost model with the best diagnostic performance by synthesizing the ultrasound signs of breast cancer lesions, peritumoral tissues, and suspicious lymph nodes is the key to improving the accuracy of SLN metastasis prediction. At the same time, SHAP provides a personalized and reasonable explanation for prediction, breaking the "black-box" problem that has been hindering the development of complex models and significantly improving the application value of clinical models and the confidence of clinicians in the prediction model.

This study also has certain limitations. First, it was a single-center retrospective study, with limited sample size and regionality. Some cases were eliminated due to the quality of lesion images, thus reducing the sample size. Second, the pathological types of breast cancer included in the samples are not comprehensive, which may affect the results of the study. Third, a more detailed classification of the ultrasound signs of the lesion is also required. In the future, this study also needs to incorporate the relevant features of radiomics, and further analyze and study other ML algorithms involved in medicine.

In conclusion, this study more comprehensively incorporates the ultrasound signs of the primary breast cancer and its surrounding soft tissues and lymph nodes, and establishes an XGBoost model to predict the metastasis of SLN and used SHAP to solve the "black-box" problem that hinders the clinical application of ML algorithms. It provides clinicians with a non-invasive, efficient, and convenient method, assists clinicians to understand the state of SLN before surgery, and guides the selection and treatment of surgical methods.

Data availability statement

The raw data supporting the conclusions of this article will be made available by the authors, without undue reservation.

Author contributions

GZ, YS, FL participated in the conception and designed this study. ZZ provided administrative support. GZ, PY, YF, XL participated in the collection and arrangement of research data. GZ, QZ completed the analysis and interpretation of the data. GZ wrote the manuscript. All authors contributed to this article and approved the submitted version.

Funding

This research was supported by the National Natural Science Foundation of China (No.81471809; No.81971639).

Conflict of interest

The authors declare that the research was conducted in the absence of any commercial or financial relationships that could be construed as a potential conflict of interest.

Publisher's note

Supplementary material

The Supplementary Material for this article can be found online at: https://www.frontiersin.org/articles/10.3389/fonc.2022.944569/full#supplementary-material

References

1. Yardım-Akaydin S, Karahalil B, Baytas SN. New therapy strategies in the management of breast cancer. *Drug Discov Today* (2022), 2022;27(6):1755-1762. doi: 10.1016/j.drudis.2022.03.014

2. Lyman GH, Somerfield MR, Bosserman LD, Perkins CL, Weaver DL, Giuliano AE. Sentinel lymph node biopsy for patients with early-stage breast cancer: American society of clinical oncology clinical practice guideline update. *J Clin Oncol* (2017) 35(5):561–4. doi: 10.1200/JCO.2016.71.0947

3. Krag DN, Anderson SJ, Julian TB, Brown AM, Harlow SP, Constantino JP, et al. Sentinel-lymph-node resection compared with conventional axillary-lymph-node dissection in clinically node-negative patients with breast cancer: overall survival findings from the NSABP b-32 randomised phase 3 trial. *Lancet Oncol* (2010) 11(10):927–33. doi: 10.1016/S1470-2045(10)70207-2

4. Brem RF, Lenihan MJ, Lieberman J, Torrente J. Screening breast ultrasound: past, present, and future. *AJR Am J Roentgenol* (2015) 204(2):234–40. doi: 10.2214/AJR.13.12072

5. Park VY, Kim EK, Moon HJ, Yoon JH, Kim MJ. Value of ultrasound-guided fine needle aspiration in diagnosing axillary lymph node recurrence after breast cancer surgery. *Am J Surg* (2018) 216(5):969–73. doi: 10.1016/j.amjsurg.2018.04.012

6. Rajkomar A, Dean J, Kohane I. Machine learning in medicine. *Reply N Engl J Med* (2019) 380(26):2589–90. doi: 10.1056/NEJMra1814259

7. Liu H, Cui G, Luo Y, Guo Y, Zhao L, Wang Y, et al. Artificial intelligence-based breast cancer diagnosis using ultrasound images and grid-based deep feature generator. *Int J Gen Med* (2022) 15:2271–82. doi: 10.2147/IJGM.S347491

8. Bian J, Buchan I, Guo Y, Prosperi M. Statistical thinking, machine learning. *J Clin Epidemiol* (2019) 116:136–7. doi: 10.1016/j.jclinepi.2019.08.003

9. Zhang B, Tian J, Pei S, Chen Y, He X, Dong Y, et al. Machine learning-assisted system for thyroid nodule diagnosis. *Thyroid* (2019) 29(6):858–67. doi: 10.1089/thy.2018.0380

10. Castelvecchi D. Can we open the black box of AI? *Nature* (2016) 538 (7623):20–3. doi: 10.1038/538020a

11. Nyrup R, Robinson D. Explanatory pragmatism: a context-sensitive framework for explainable medical AI. *Ethics Inf Technol* (2022) 24(1):13. doi: 10.1007/s10676-022-09632-3

12. Lundberg SM, Nair B, Vavilala MS, Horibe M, Eisses MJ, Adams T, et al. Explainable machine-learning predictions for the prevention of hypoxaemia during surgery. *Nat BioMed Eng* (2018) 2(10):749–60. doi: 10.1038/s41551-018-0304-0

13. Pan P, Li Y, Xiao Y, Han B, Su L, Su M, et al. Prognostic assessment of COVID-19 in the intensive care unit by machine learning methods: Model development and validation. *J Med Internet Res* (2020) 22(11):e23128. doi: 10.2196/23128

14. Bedi DG, Krishnamurthy R, Krishnamurthy S, Edeiken BS, Le-Petross H, Fornage BD, et al. Cortical morphologic features of axillary lymph nodes as a predictor of metastasis in breast cancer: *in vitro* sonographic study. *AJR Am J Roentgenol* (2008) 191(3):646–52. doi: 10.2214/AJR.07.2460

15. Ma P, Liu R, Gu W, Dai Q, Gan Y, Cen J, et al. Construction and interpretation of prediction model of teicoplanin trough concentration via machine learning. *Front Med* (2022) 9:808969. doi: 10.3389/fmed.2022.808969

16. Goodwin NL, Nilsson SRO, Choong JJ, Golden SA. Toward the explainability, transparency, and universality of machine learning for behavioral classification in neuroscience [published online ahead of print, 2022 Apr 26]. *Curr Opin Neurobiol* (2022) 73:102544. doi: 10.1016/j.conb.2022.102544

17. Jiang T, Su W, Zhao Y, Li Q, Huang P. Non-invasive prediction of lymph node status for patients with early-stage invasive breast cancer based on a morphological feature from ultrasound images. *Quant Imaging Med Surg* (2021) 11(8):3399–407. doi: 10.21037/qims-20-1201

18. Christodoulou E, Ma J, Collins GS, Steyerberg EW, Verbakel JY, Van Calster B. A systematic review shows no performance benefit of machine learning over logistic regression for clinical prediction models. *J Clin Epidemiol* (2019) 110:12–22. doi: 10.1016/j.jclinepi.2019.02.004

19. Jonczyk MM, Fisher C, Babbitt R, Paulus JK, Freund KM, Czerniecki B, et al. Surgical predictive model for breast cancer patients assessing acute postoperative complications: The breast cancer surgery risk calculator. *Ann Surg Oncol* (2021) 28 (9):5121–31. doi: 10.1245/s10434-021-09710-8

20. Song R, Cui Y, Ren J, Zhang J, Yang Z, Li D, et al. CT-based radiomics analysis in the prediction of response to neoadjuvant chemotherapy in locally advanced gastric cancer: A dual-center study. *Radiother Oncol* (2022) 171:155–63. doi: 10.1016/j.radonc.2022.04.023

21. Dai C, Fan Y, Li Y, Bao X, Li Y, Su M, et al. Development and interpretation of multiple machine learning models for predicting postoperative delayed remission of acromegaly patients during long-term follow-up. *Front Endocrinol* (2020) 11:643. doi: 10.3389/fendo.2020.00643

22. Zong Q, Deng J, Ge W, Chen J, Xu D. Establishment of simple nomograms for predicting axillary lymph node involvement in early breast cancer. *Cancer Manag Res* (2020) 12:2025–35. doi: 10.2147/CMAR.S241641

23. Alvarez S, Añorbe E, Alcorta P, López F, Alonso I, Cortés J. Role of sonography in the diagnosis of axillary lymph node metastases in breast cancer: a systematic review. *AJR Am J Roentgenol* (2006) 186(5):1342–8. doi: 10.2214/AJR.05.0936

24. Drukker K, Giger M, Meinel LA, Starkey A, Janardanan J, Abe H. Quantitative ultrasound image analysis of axillary lymph node status in breast cancer patients. *Int J Comput Assist Radiol Surg* (2013) 8(6):895–903. doi: 10.1007/s11548-013-0829-3

25. Coronado-Gutiérrez D, Santamaría G, Ganau S, Bargallo X, Orlando S, Oliva-Branas ME, et al. Quantitative ultrasound image analysis of axillary lymph nodes to diagnose metastatic involvement in breast cancer. *Ultrasound Med Biol* (2019) 45(11):2932–41. doi: 10.1016/j.ultrasmedbio.2019.07.413

26. Li JN, Xu J, Wang J, Qing C, Zhao YM, Liu PF. Correlation between mammograghic findings and clinical/ pathologic features in women with small invasive breast carcinomas. *Asian Pac J Cancer Prev* (2014) 15(24):10643–6. doi: 10.7314/apjcp.2014.15.24.10643

27. Luo Y, Zhao C, Gao Y, Xiao M, Li W, Zhnag J, et al. Predicting axillary lymph node status with a nomogram based on breast lesion ultrasound features: Performance in N1 breast cancer patients. *Front Oncol* (2020) 10:581321. doi: 10.3389/fonc.2020.581321

28. Qiu X, Jiang Y, Zhao Q, Yan C, Huang M, Jiang T. Could ultrasound-based radiomics noninvasively predict axillary lymph node metastasis in breast cancer? *J Ultrasound Med* (2020) 39(10):1897–905. doi: 10.1002/jum.15294

29. Costantini M, Belli P, Ierardi C, Franceschini G, La Torre G, Bonomo L. Solid breast mass characterisation: use of the sonographic BI-RADS classification. *Radiol Med* (2007) 112(6):877–94. doi: 10.1007/s11547-007-0189-6

30. Logullo AF, Prigenzi KCK, Nimir CCBA, Franco AFV, Campos MSDA. Breast microcalcifications: Past, present and future (Review). *Mol Clin Oncol* (2022) 16(4):81. doi: 10.3892/mco.2022.2514

31. Mercado CL. BI-RADSupdate. *Radiol Clin North Am* (2013) 2014;52 (3):481-487. doi: 10.1016/j.rcl.2014.02.008

32. Paulinelli RR, Freitas-Júnior R, Moreira MA, de Moraes VA, Bernardes-Junior JRM, ds Silva Rocha Vidal C, et al. Risk of malignancy in solid breast nodules according to their sonographic features. *J Ultrasound Med* (2005) 24(5):635–41. doi: 10.7863/jum.2005.24.5.635

33. Moon WK, Lee YW, Huang YS, Lee SH, Bae MS, Yi A, et al. Computer-aided prediction of axillary lymph node status in breast cancer using tumor surrounding tissue features in ultrasound images. *Comput Methods Programs BioMed* (2017) 146:143–50. doi: 10.1016/j.cmpb.2017.06.001

34. Lee YW, Huang CS, Shih CC, Chang RF. Axillary lymph node metastasis status prediction of early-stage breast cancer using convolutional neural networks. *Comput Biol Med* (2021) 130:104206. doi: 10.1016/j.compbiomed.2020.104206

frontiers | Frontiers in Oncology

TYPE Original Research
PUBLISHED 11 August 2022
DOI 10.3389/fonc.2022.984626

OPEN ACCESS

EDITED BY
San-Gang Wu,
First Affiliated Hospital of Xiamen University, China

REVIEWED BY
Jan Egger,
University Hospital Essen, Germany
Jincao Yao,
University of Chinese Academy of Sciences, China

*CORRESPONDENCE
Fugeng Sheng
fugeng_sheng@163.com

SPECIALTY SECTION
This article was submitted to Breast Cancer, a section of the journal Frontiers in Oncology

RECEIVED 02 July 2022
ACCEPTED 19 July 2022
PUBLISHED 11 August 2022

CITATION
Yue W, Zhang H, Zhou J, Li G, Tang Z, Sun Z, Cai J, Tian N, Gao S, Dong J, Liu Y, Bai X and Sheng F (2022) Deep learning-based automatic segmentation for size and volumetric measurement of breast cancer on magnetic resonance imaging. *Front. Oncol.* 12:984626. doi: 10.3389/fonc.2022.984626

Deep learning-based automatic segmentation for size and volumetric measurement of breast cancer on magnetic resonance imaging

Wenyi Yue[1,2], Hongtao Zhang[1], Juan Zhou[1], Guang Li[3], Zhe Tang[3], Zeyu Sun[3], Jianming Cai[1], Ning Tian[1], Shen Gao[1], Jinghui Dong[1], Yuan Liu[1], Xu Bai[1] and Fugeng Sheng[1]*

[1]Department of Radiology, The Fifth Medical Center of Chinese PLA General Hospital, Beijing, China, [2]Chinese PLA General Medical School, Beijing, China, [3]Keya Medical Technology Co., Ltd., Beijing, China

Purpose: In clinical work, accurately measuring the volume and the size of breast cancer is significant to develop a treatment plan. However, it is time-consuming, and inter- and intra-observer variations among radiologists exist. The purpose of this study was to assess the performance of a Res-UNet convolutional neural network based on automatic segmentation for size and volumetric measurement of mass enhancement breast cancer on magnetic resonance imaging (MRI).

Materials and methods: A total of 1,000 female breast cancer patients who underwent preoperative 1.5-T dynamic contrast-enhanced MRI prior to treatment were selected from January 2015 to October 2021 and randomly divided into a training cohort (n = 800) and a testing cohort (n = 200). Compared with the masks named ground truth delineated manually by radiologists, the model performance on segmentation was evaluated with dice similarity coefficient (DSC) and intraclass correlation coefficient (ICC). The performance of tumor (T) stage classification was evaluated with accuracy, sensitivity, and specificity.

Results: In the test cohort, the DSC of automatic segmentation reached 0.89. Excellent concordance (ICC > 0.95) of the maximal and minimal diameter and good concordance (ICC > 0.80) of volumetric measurement were shown between the model and the radiologists. The trained model took approximately 10–15 s to provide automatic segmentation and classified the T stage with an overall accuracy of 0.93, sensitivity of 0.94, 0.94, and 0.75, and specificity of 0.95, 0.92, and 0.99, respectively, in T1, T2, and T3.

Conclusions: Our model demonstrated good performance and reliability for automatic segmentation for size and volumetric measurement of breast cancer, which can be time-saving and effective in clinical decision-making.

KEYWORDS

deep learning, breast cancer, magnetic resonance imaging, volumetric measurement, automatic segmentation

Introduction

Breast cancer is one of the most common malignancies afflicting women worldwide (1). Tumor size has been thought as an indispensable prognostic factor. An accurate preoperative measurement of breast cancer size is essential for surgical resection and the formulation of a chemotherapy regimen (2–4). Furthermore, monitoring the change of tumor volume during treatment is an important reference for response evaluation criteria in solid tumors (5). Thus, it is crucial to measure size and volume accurately in the clinical course.

Medical imaging, which is superior in measuring tumor size and volume, might be used to obtain anatomic information accurately and non-invasively (6–10). Among the imaging methods, magnetic resonance imaging (MRI) is a better diagnostic technique with the highest resolution and quantitative information for preoperative prediction and prognosis evaluation (11–14). However, it takes considerable time and a great deal of expertise to process images by trained radiologists. In addition, due to differences in diagnostic skills, there are inter- and intra-observer variations among radiologists and problems with decision fatigue (15, 16).

Artificial intelligence (AI) aiding medical imaging technologies exceeded the detection capabilities of radiologists in some applications, complemented clinical decision-making, and streamlined preoperative image evaluation. Automated processing by AI computational tools is a more efficient detection approach to measure the volume and the size of a tumor within a reasonable amount of time. It has great reference significance for guiding the clinical development of follow-up treatment plans and avoiding inaccurate measurement incurred by some inexperienced radiologists (17). In addition, some studies indicated that the presence of tumor necrosis correlated with tumor grade, aggressiveness, unfavorable long-term outcomes, and improved response to neoadjuvant chemotherapy (18–20). Measuring the necrosis and the cystic components manually is labor-consuming, but using AI technology improves the efficiency and provides more intuitive parameters for radiologists.

Segmentation plays a significant role in image analysis, including detection, feature extraction, classification, and treatment (21, 22). Automatic and semiautomatic segmentation can alleviate the labor-intensive problems and eliminate the high variability between intra- and inter-observers (23). Moreover, deep learning, as a subset of AI, is a promising method to make a tremendous progress in automatic segmentation by which more reproducible and effective texture features in different fields of image analysis are extracted (24–26). The convolutional neural network (CNN) is a sophisticated deep learning architecture, and it has been successfully applied in various areas of knowledge for digital image segmentation. The U-Net network is a fully CNN with high-performance in graphics processing unit (GPU) computing, requiring fewer training sets, and has higher segmentation accuracy compared with other CNNs (27). Among the U-Net network, Res-UNet is a semantic segmentation model which integrates residual module and U-Net network capable of effectively overcoming excessive parameters and gradient dispersion caused by the deepened network layer (28).

In this study, we developed a deep learning automatic segmentation model based on Res-UNet of preoperative MRI for breast cancer patients and assessed its reliability for size and volumetric measurement. To our knowledge, no reported research has applied deep learning to automatically segment breast cancer and quantify the volume as well as the size on MRI.

Materials and methods

The institutional review board approved this retrospective study and waived the need for written informed consent.

Study design

The workflow of the process is illustrated in Figure 1, including the following three steps: (1) acquisition of MRI, data annotation, automatic segmentation, image pre-processing, augmentation, and post-processing, (2) designing and building the algorithm, and (3) training and inference.

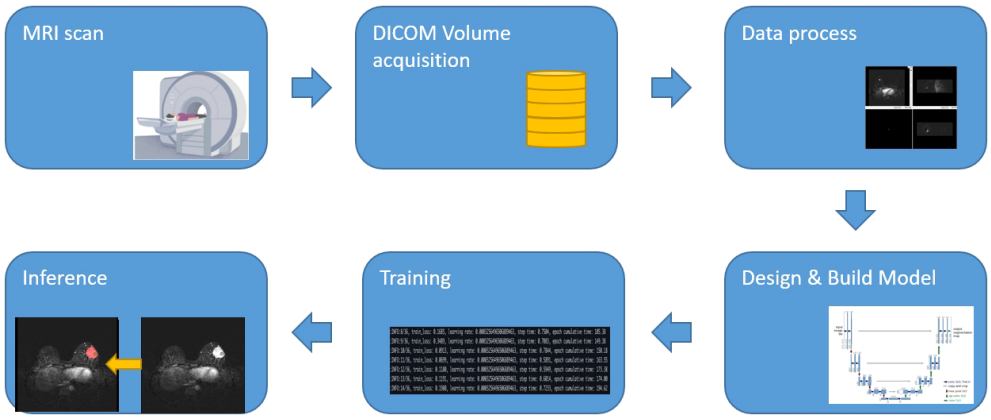

FIGURE 1
Workflow diagram.

Patient selection and data annotation

All selected female patients were diagnosed with breast cancer who underwent preoperative breast MRI prior to treatment from January 2015 to October 2021. The inclusion criteria were as follows: (1) diagnosed with breast carcinoma pathologically, (2) underwent MRI prior to treatment, (3) with complete clinical and pathological data, and (4) whose digital imaging and communications in medicine pixel data had no corruption and which were scanned under the same MR protocol. The exclusion criteria were as follows: (1) received any therapy before MRI and (2) non-mass enhancement breast cancer or normal in MRI.

According to the Cancer Staging Manual of the American Joint Committee on Cancer, the system clarified that the tumor (T) stage is based on the size of the invasive components of the longest tumor dimension (in the setting of multiple masses). Our study classified the tumor into three T categories: the size of T1 is not greater than or equal to 20 mm, the size of T2 is larger than 20 mm and not greater than 50 mm, and the size of T3 is equal or greater than 50 mm. A total of 1,000 patients were randomly divided into group 1 (n = 230), group 2 (n = 720), and group 3 (n = 50). The following ratios were used: 80% training cohort and 20% testing cohort to balance the test samples. Thus, we selected 45, 143, and 12 cases relatively for three T categories as testing cohort. In addition, 31 cases with cystic or necrotic changes were enrolled in our study.

MRI acquisition

All patients were scanned using a 1.5-T system (Magnetom Espree Pink; Siemens, Erlangen, Germany), which is equipped with an eight-channel phased-array surface coil for the breast. The patients were examined in the prone position with both breasts positioned in the coil cavity. Axial T1WI [repetition time/echo time (TR/TE), 8.7/4.7 ms; slice thickness, 1.1 mm]. Dynamic contrast-enhanced MRI (DCE-MRI) used a fast, small-angle excitation, three-dimensional imaging (3D-FLASH) sequence and fat-saturated axial T1WI: TR/TE, 4.53/1.66 ms; slice thickness, 1.1 mm. Before the contrast agent was injected, it needed to be scanned one time. After that, the contrast agent, gadopentetate dimeglumine, was injected with a high-pressure syringe at a speed of 2.0 ml/s, and then 30 ml normal saline was injected at the same speed to flush the catheter. Images of each phase were subtracted automatically at the same time.

Delineation of ROIs by iterative workflow

A radiologist used the ITK-SNAP software (www.itksnap.org) to review the first DCE-MRI subtraction images, this being the most critical and the clearest phase of breast cancer evaluation for further analysis. An iterative-label workflow was used to delineate the regions of interest (ROIs) in the early stage to get the ideal labels. It included an initial network model which was trained on our in-house dataset from 100 patients' ROIs and the pre-trained model which was applied to the remaining patients' ROIs and achieved coarse labels. After that, two radiologists checked and refined the manual revision. The iterative workflow is shown in Figure 2.

Image processing

We designed a fully automatic CNN-based segmentation network and built an end-to-end workflow based on Medical Open Network for AI[1] platform, including pre-processing, data

1 https://monai.io/

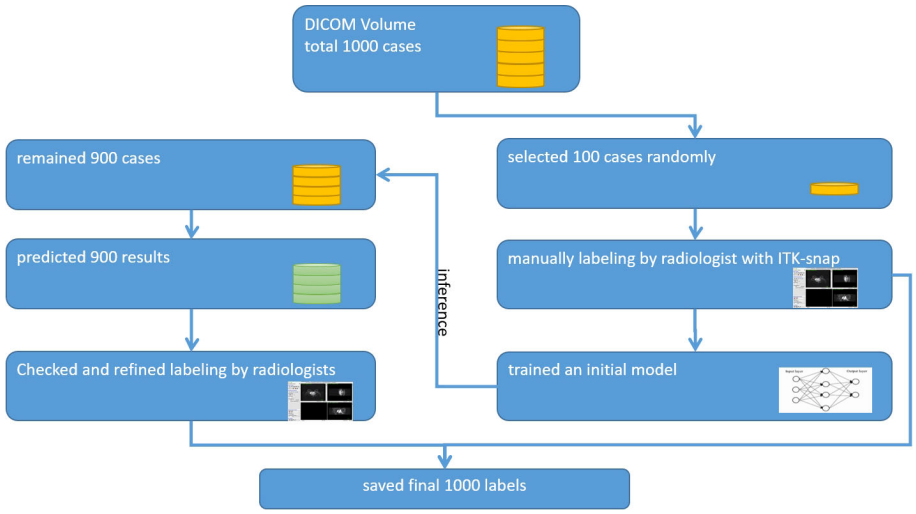

FIGURE 2
Iterative labeling workflow.

loader, augmentation, network building, post-processing, and quantification.

Pre-processing

Three steps including intensity normalization, respacing, and crop patches were performed before the training model. *Z*-score normalization was suitable for variable intensity ranges. We calculated the intensity ranges, clamped the voxels from 0.5 to 99.5%, calculated the mean and standard deviation (SD) of each case, and used the equation to normalize the images. It is defined as shown in Equation (1):

$$\text{images} = \frac{\text{images} - \text{mean}}{\text{SD}} \quad (1)$$

To automatically adapt to any new dataset, we calculated the mean spacing of all training cohorts to define the standard target. Any data needed to be resized to the target before training and inference. Most cases had the dimension of the width and the height as 384 and the depth from 128 to 320. Due to the limitation of the GPU memory size, it was challenging to send the whole image to the network. In this situation, we first calculated the average area of the lesions and set a minimum cropping patch size which can include the central regions. The cropping patch size must also be a multiple of 2 to be suitable for most regular models. According to the statistics, a patch with a 96*96*96 size was the best choice for our algorithm.

To ensure the balance of positive and negative samples for network training, we randomly selected the cropping patches with the center point at the foreground or background area with half-to-half probability. According to our experiments, crop patches with the likelihood of 2:1 between positive and negative areas can also get a similar performance.

Augmentation

Our algorithm implemented data augmentation to make the model more robust during training steps: random zoom, random scale intensity value, random shift intensity range, random Gaussian noise, random crop fore/background, random rotation with 90°, and random elastic transformation (Figure 3).

Res-UNet network building

U-Net is an overall architecture for 2D and 3D images in medical image processing. Our study designed a robust U-Net-based network called Res-UNet with the residual blocks in the encoder part. Figure 4 shows the architecture of our designed model. In the encoder part, we used residual blocks to extract features. Skip connection was a classical operation from U-Net and might focus on the extracted features from different layer levels. It was well suited for medical images since lesion targets from different scale levels included different features. Figure 5 illustrates the residual blocks. The solid line carrying the layer input to the addition operator was a residual connection. The residual connection might effectively avoid gradient disappearance, especially in deeper layers. We combined the residual connection blocks with the U-Net skip connection to

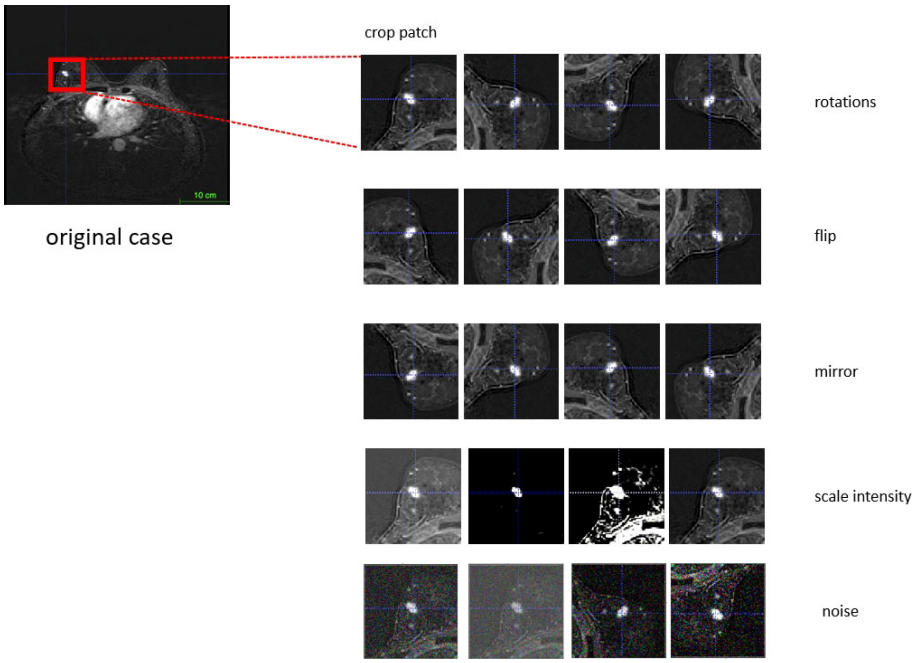

FIGURE 3
Workflow of data augmentation.

design an efficient network, which might help us obtain the accurate prediction results of lesion segmentation.

Optimizer and loss function

In our algorithm, we used Adam optimizer, dice similarity coefficient (DSC), and cross-entropy loss. The equations are shown in Equations (2)–(4):

$$loss = DSC\_loss * 0.5 + cross\_entropy\_loss * 0.5 \quad (2)$$

$$DSC\_loss = 1 - \frac{2*|X \cap Y|}{|X| + |Y|} \quad (3)$$

$$cross\_entropy\_loss = -\sum_{m=0}^{N} y_m \ln(\sigma(x_i)) \quad (4)$$

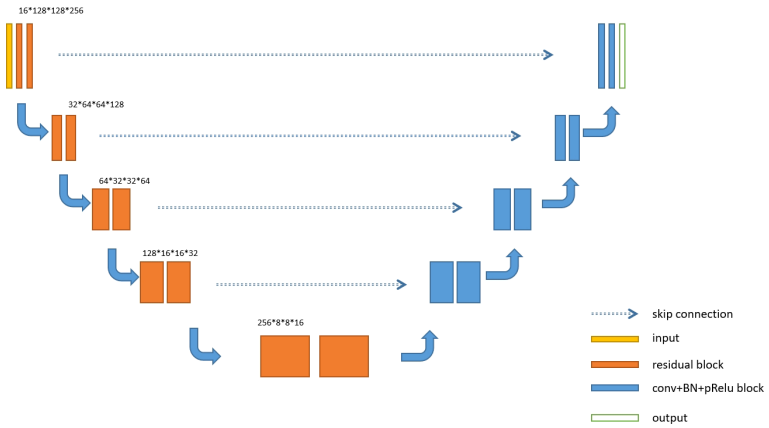

FIGURE 4
Res-UNet architecture.

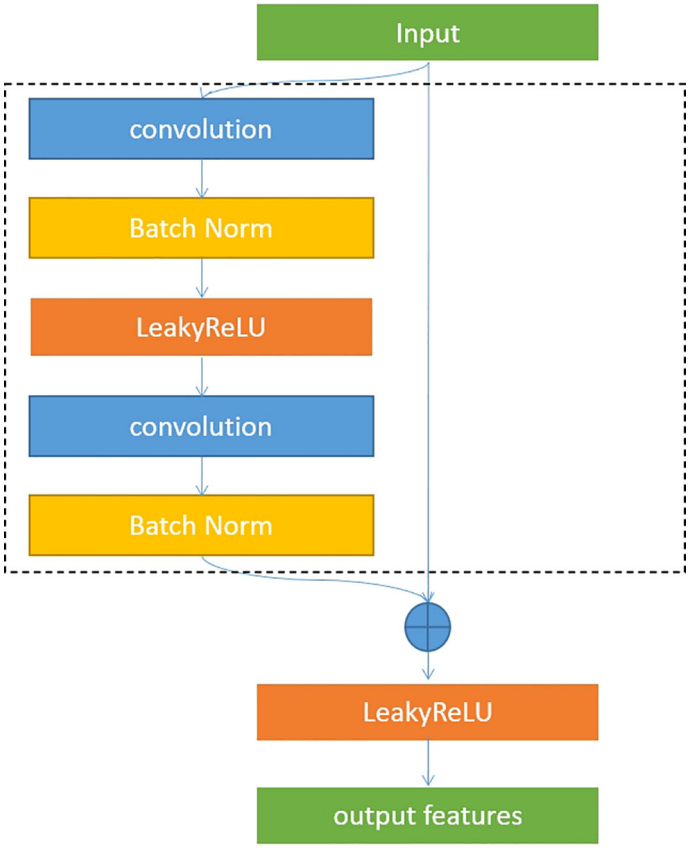

FIGURE 5
Residual blocks.

Post-processing

Usually, the tumor is an agglomerate region. We removed the outliers with less than 30 voxels in a connected region to avoid the noise of predicted results for the accuracy. Testing time augmentation is an effective way to improve accuracy in the inference step. We only applied rotation with 90°, 180°, and 270° to repeat the inference in one case to save time. It might improve the DSC of the testing cohort with 1 to 2%. We also tried a multi-model ensemble and trained the same Res-UNet network with different epochs. The ensemble also improved the accuracy by around 1%.

Measurement of pixel level

DSC and intersection over union (IOU) are commonly used metrics in segmentation algorithms. We use these two coefficients to evaluate our segmentation performance. These coefficients are spatial overlap indexes utilizing segmentation in MRI as reproducibility validation metrics. The definition of DSC and IOU are shown as Equation (5) and Equation (6). Figures 6, 7 show the DSC and IOU performance of our segmentation.

$$DSC = \frac{2*|X \cap Y|}{|X| + |Y|} \quad (5)$$

$$IOU = \frac{|X \cap Y|}{|X \cup Y|} \quad (6)$$

Figure 8 shows the ground truth and our predicted results. The comparison indicated that case 01 to case 05 get the accurate results with DSC of around 0.9 and IOU of around 0.85. In case 06, a small lesion region was not segmented by the model; thus, the DSC and IOU are 0.0. We thought that the lesion was too small and quite similar to fat. This will be solved with the more various training cohorts.

Measurement of size and volume

We used quantification indexes to calculate shape-based features such as "maximum 3D diameter, 3D mesh volume,

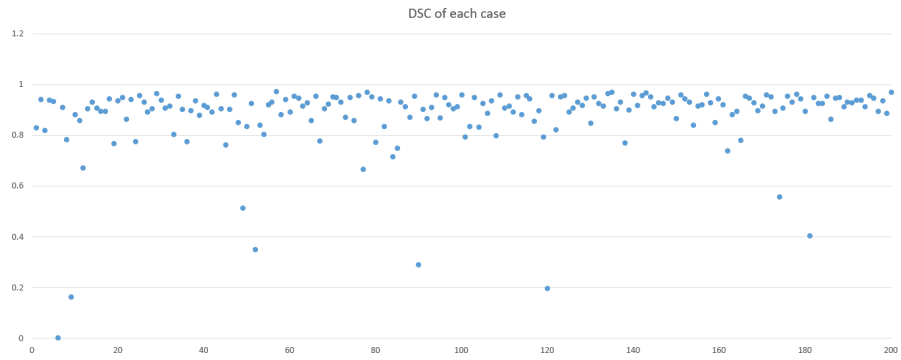

FIGURE 6
Dice similarity coefficient and intersection over union performance.

minimal diameter, maximal diameter, volume". The method firstly extracted the largest tumor area, found the maximum connected components, cropped a 3D region with its solid components fitting as an ellipsoid, and then calculated the factors which might influence shape information. These were all based on the pyradiomics library (Figure 9). We also used the Otsu's method, which is a classical intensity-based method, to divide the cystic degeneration or necrosis region manifested as hypointense in the central or paracentral area on DCE-MRI (Figure 10). It iteratively searched for the threshold that minimizes the within-class variance from the histogram. Figure 11 shows the histogram of the tumor areas calculated by Otsu's method. Moreover, the maximum value is the threshold to find the interclass variance. After that, we used the threshold as pixel intensity value to segment cystic or necrotic change areas. So far, the central part of the cystic or necrotic areas could be extracted. The outliers, a number of voxels less than 30, were removed in each connected component area.

Statistical analysis

The automatic segmentation performance was evaluated with DSC. The method performance of classifying the size according to T stage was assessed with accuracy, sensitivity, and specificity. Intraclass correlation coefficient (ICC) was adopted to measure the agreement between the size and the volumetric parameters of the predicted results and the GT results. All statistical analyses were conducted using Python version 3.8 (www.python.org) and SPSS 25.0 software package.

Results

Our improved Res-UNet got the best DSC of 0.89 among different networks. The DSCs of different networks are shown in Table 1. The details of DSC and IOU are presented in Table 2. The final metrics of the predicted outcomes in the standard-alone test cohort were accuracy = 0.93, sensitivity (T1, T2, and

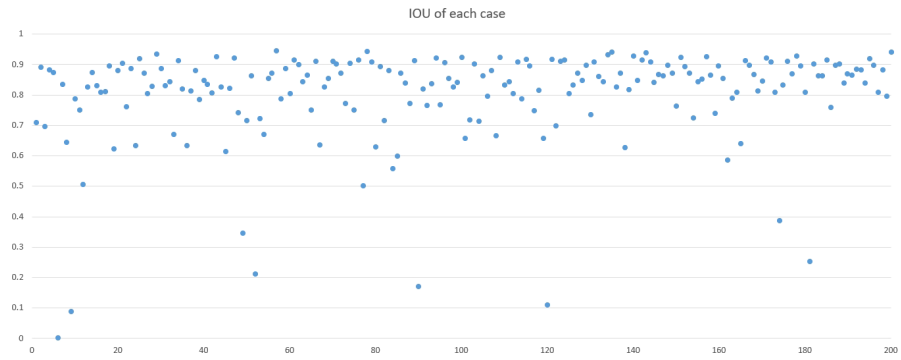

FIGURE 7
Dice similarity coefficient and intersection over union performance.

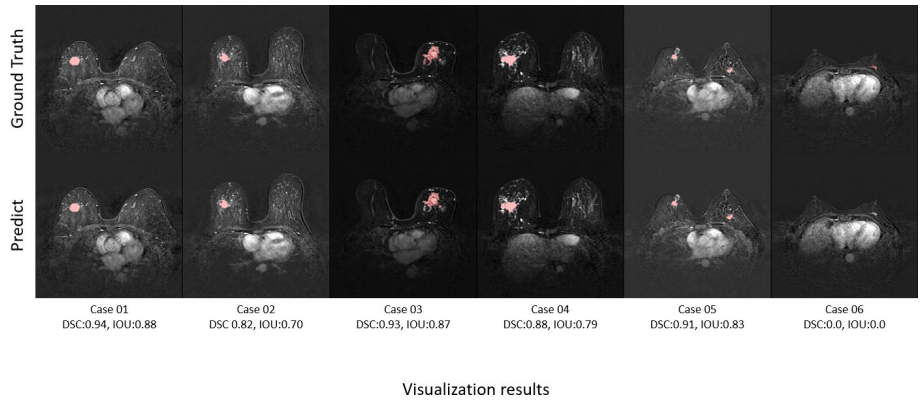

FIGURE 8
Six cases showing comparisons between the ground truth and our predicted results.

T3 = 0.94, 0.94, and 0.75, respectively), and specificity (T1, T2, and T3 = 0.95, 0.92, and 0.99, respectively. The detailed metrics are shown in Tables 3–5, while Figures 12–14 show the details of maximal diameter, minimal diameter, and volume. Table 6 shows the metrics of cystic or necrotic components including volume and mean intensity. A high concordance of size and volumetric parameters was shown between the deep learning segmentation-based prediction results and the GT segmentation results. For the minimal and maximal diameters, the ICC was greater than 0.95, and for volumetric measurement of mass enhancement breast cancer, the ICC was greater than 0.80 (Table 7). The trained model took approximately 10–15 s to provide automatic segmentation and volume analysis for each patient, while the average manual segmentation time was at least 15 min.

Discussion

Our study established a deep learning model based on the Res-UNet network architecture with DSC of 0.89 for the automatic segmentation to improve recognition efficiency

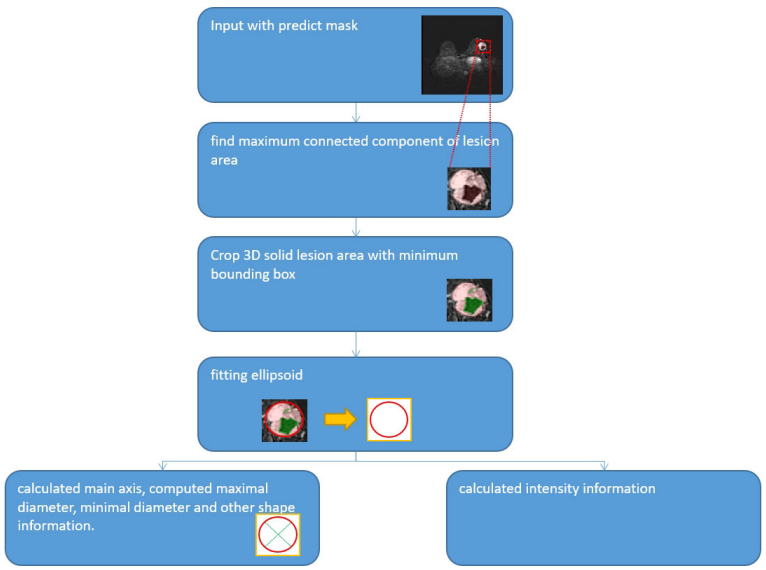

FIGURE 9
Workflow of measurement.

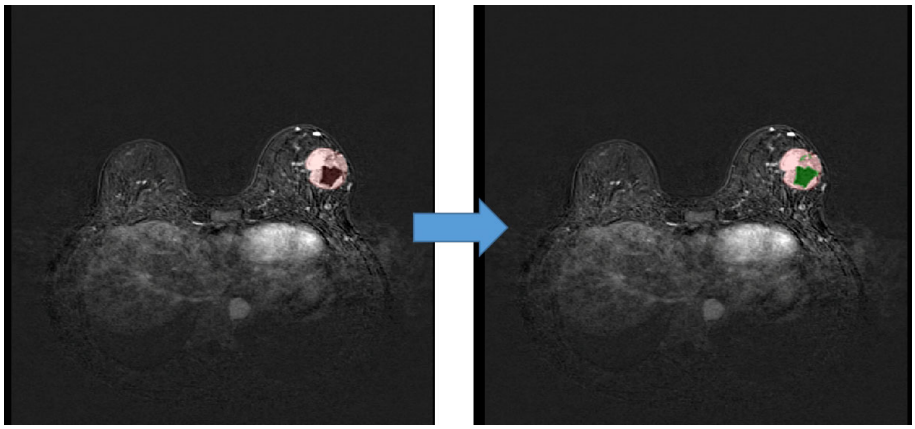

FIGURE 10
Regions of interest of the areas with cystic or necrotic changes. The green part shows the classification from the Otsu's method.

and productivity with the speed of 10–15 s for one patient, eliminate inter- and intra-observer variations among breast radiologists as much as possible, and reduce information overload. Our model achieved a good performance with an overall accuracy of 0.93, sensitivity of 0.94, 0.94, and 0.75, and specificity of 0.95, 0.92, and 0.99, respectively, for three T categories in classifying the size of mass enhancement breast cancer. In addition, the model corresponded well with the GT

TABLE 1 Different networks' dice similarity coefficient (DSC).

Metrics	UNet	nnUNet	Res-UNet
DSC	0.82	0.887	0.894
GPU memory usage in training	6 GB (batch = 8)	8 GB for normal model 32 GB for very big model	11 GB (batch = 8)

GPU, graphics processing unit.

TABLE 2 Details of dice similarity coefficient (DSC) and intersection over union (IOU).

Metrics	DSC	IOU
Average	0.88	0.80
Standard deviation	0.13	0.15

TABLE 3 Summary of geometric parameters between the prediction results and GT results.

Geometric parameters	Predict	GT
Maximum 3D diameter(mm)	33.25	34.02
3D mesh volume (mm^3)	9,335.38	10,370.29
Minimal diameter (mm)	21.17	21.57
Maximal diameter (mm)	27.41	27.77
Volume (mm^3)	9333.08	10416.14

GT, ground truth.

TABLE 4 Final predicted metrics of the classification.

Classification	Precision	Recall	F1-score	support
Small (<20 mm)	0.85	0.94	0.90	50
Medium (20–50 mm)	0.96	0.94	0.95	138
Large (>50 mm)	0.90	0.75	0.82	12

TABLE 5 Final predicted results of the classification.

Metrics	Small	Medium	Large
Macro average	0.91	0.88	0.89
Weighted average	0.93	0.93	0.93
Accuracy		0.93	

TABLE 6 Comparison of the volume and mean intensity between cystic or necrotic components and lesions.

Quantitative parameters	Mean of lesion	Mean of cystic component	Minimum of lesion	Minimum of cystic component	Maximum of lesion	Maximum of cystic component
Volume (mm^3)	23,858.41	7,816.06	2,625.14	12.92	253,526.11	128,501.66
Mean intensity	362.29	198.70	204.31	105.69	582.45	321.625

TABLE 7 Agreement of size and volumetric parameters between deep learning segmentation-based prediction results and GT segmentation results.

	Prediction	GT	Intraclass correlation coefficient
Volume (mm^3)	9,333.08 ± 13,409.19	10,416.14 ± 21,928.01	0.840
Maximal diameter (mm)	27.41 ± 13.47	27.77 ± 12.55	0.952
Minimal diameter (mm)	21.17 ± 8.63	21.57 ± 9.06	0.964

GT, ground truth.

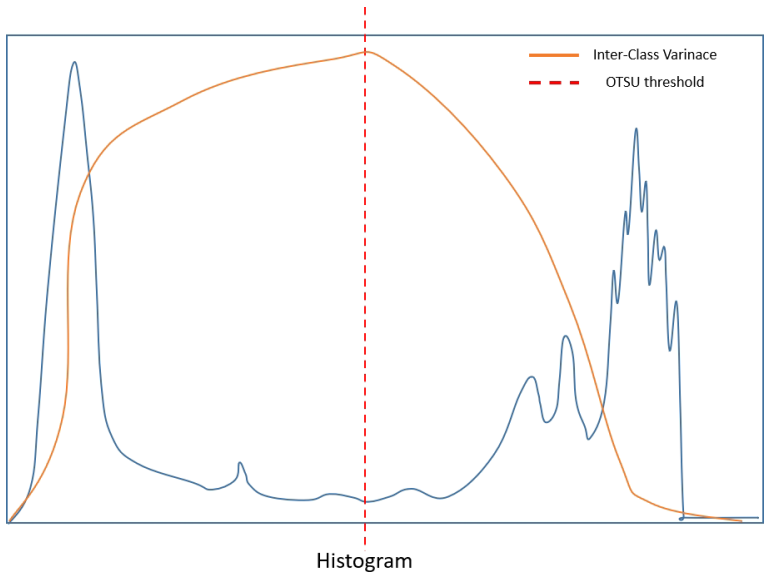

FIGURE 11
Histogram of the lesion areas.

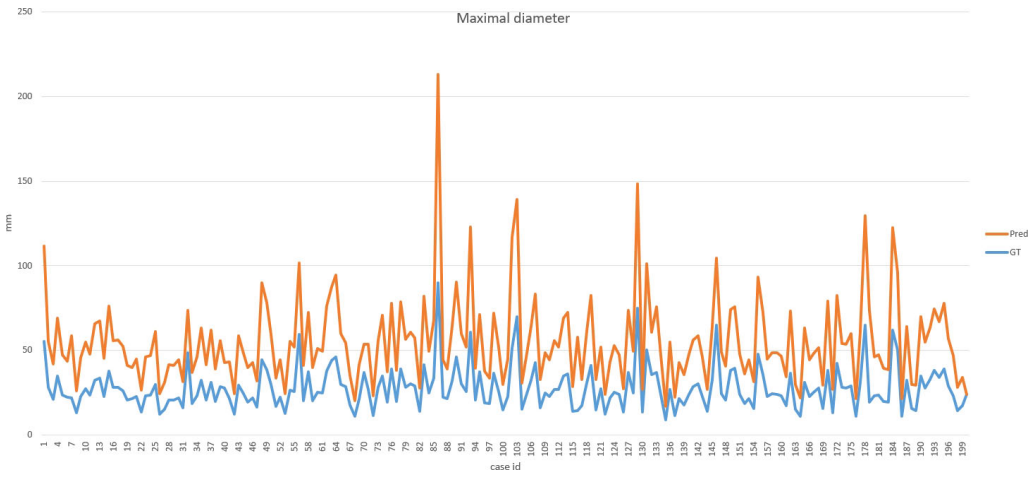

FIGURE 12
Final metrics of the predicted results.

results derived manually by radiologists in terms of size and volumetric parameters. These results implied that our framework might automate certain procedures of the preoperative evaluation for breast cancer. Although the classification capability of our model is powerful and significant, future advances which will be considered through external validation in other institutions or with larger data sets will make it more persuasive for clinical application.

Preoperative breast MRI, for its highest resolution and abundant information, becomes the most promising imaging modality for different AI applications, mainly for lesion detection and classification (12, 29). Automatically detecting and classifying (limited to benign *versus* malignant) breast lesions on MRI are relatively well-established techniques (30–33). Nevertheless, measuring the volume and the size of mass enhancement breast cancer accurately has important guidance for follow-up therapeutic decisions. In previous studies, some researchers have compared the accuracy of computer-aided detection (CAD) systems and radiologists in measuring the tumor size. The results are mostly reported such that the manual measurement of MRI is better than MRI with CAD (3, 16). However, CAD systems have limited capabilities; they also enable radiologists to process large images efficiently. Therefore, using large sample image data and more intelligent deep learning

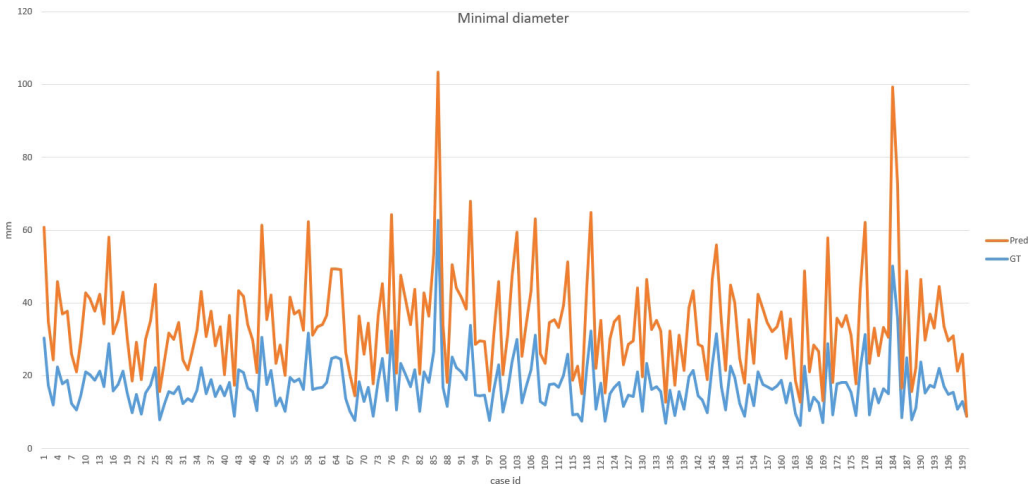

FIGURE 13
Final metrics of the predicted results.

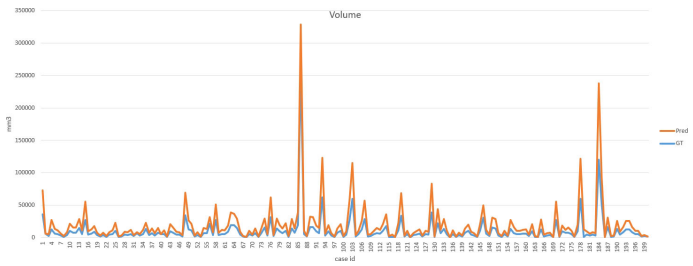

FIGURE 14
Final metrics of the predicted results.

models based on neural network structures to measure the maximum diameter and solid component volume of tumors can undoubtedly improve the efficiency.

We reported an excellent performance of the model in segmentation, which is in accordance with the previous studies on breast cancer segmentation (34–37). This observation can not only provide precise segmentation and quantitative assessments of breast cancer but also assist in image analysis including detection, feature extraction, classification, and treatment. In most previous studies, tumors were segmented manually, which are prone to inter- and intra-observer variabilities (34, 38, 39). Furthermore, for the 3D medical imaging process, it is difficult and time-consuming for radiologists to measure lesions manually. Automatic segmentation and semi-automatic segmentation will reduce the time as well as improve the reliability. We used automatic segmentation which produced results consistently and reproducibly. What is more, automatically extracting an entire 3D lesion with an irregular shape only takes a few minutes, and the region in the 3D dimension by manual drawing may be discontinuous or not smooth and time-consuming.

Although several prior studies used deep learning to segment breast cancer, they did not measure the volume and the size. To the best of our knowledge, this is the first deep learning study to automatically segment mass enhancement breast cancer and measure the volume and the size on MRI. Our model also analyzed the areas with cystic or necrotic changes. Tumor necrosis has been proposed as a negative prognostic factor in some studies and could be evaluated on MRI comprehensively (40, 41). Differing from prior studies of necrosis as a predictive reference in TNBC, our study aims to automatically delineate and measure the volume of cystic and necrosis areas through our algorithm so that radiologists can intuitively find the changes in tumor components, and this would help them predict the patients' prognosis (19, 42).

Our study had several limitations. Firstly, although this is a unicentric study with a relatively large sample size, external validation datasets from multiple centers should be set up to test the rationality of the model. Secondly, we did not simultaneously count multifocal or multicentric cancers. Non-mass enhancement breast cancer should also be tried to be divided into regions. Further research is possible in the future to expand the application scope of this model for improvement. Thirdly, from the perspective of methods, the performance of our model can still be improved. Some cases still contain false-positive regions similar to lesions with hyperintensity. We think that a false-positive-remove algorithm may suppress these error regions.

Conclusions

Utilizing a deep learning-based algorithm based on automatic segmentation to measure the volume and the size of mass enhancement breast cancer on MRI is feasible with high accuracy and reliability, thereby reducing the effort and variabilities. Further development will be added in our study for such to be implemented into future clinical practice efficiently.

Data availability statement

The raw data supporting the conclusions of this article will be made available by the authors, without undue reservation.

Ethics statement

Ethical review and approval was not required for the study on human participants in accordance with the local legislation and institutional requirements. Written informed consent for participation was not required for this study in accordance with the national legislation and the institutional requirements.

Author contributions

WY: conception, design of the study, acquisition of data, analysis and interpretation of data, and drafting the article. FS: critical revision for important intellectual content. ZS, ZT, and GL: establish the automatic segmentation with size and volumetric measurement of breast cancer. HZ, JZ, NT, SG, JD, YL, XB, and JC: acquisition of data. WY and FS: final approval of the version to be submitted. All authors contributed to the article and approved the submitted version.

Funding

This project is supported by the National Natural Science Foundation of China (no. 21575161).

Conflict of interest

Author GL, ZT and ZS were employed by Keya Medical Technology Co., Ltd.

The remaining authors declare that the research was conducted in the absence of any commercial or financial relationships that could be construed as a potential conflict of interest.

Publisher's note

References

1. Siegel RL, Miller KD, Fuchs HE, Jemal A. Cancer statistics. *CA: Cancer J Clin* (2022) 72(1):7–33. doi: 10.3322/caac.21708

2. Pop C, Stanciu-Pop C, Drisis S, Radermeker M, Vandemerckt C, Noterman D, et al. The impact of breast MRI workup on tumor size assessment and surgical planning in patients with early breast cancer. *Breast J* (2018) 24(6):927–33. doi: 10.1111/tbj.13104

3. Park JY. Evaluation of breast cancer size measurement by computer-aided diagnosis (CAD) and a radiologist on breast MRI. *J Clin Med* (2022) 11(5):1172. doi: 10.3390/jcm11051172

4. Foulkes WD, Reis-Filho JS, Narod SA. Tumor size and survival in breast cancer–a reappraisal. *Nat Rev Clin Oncol* (2010) 7(6):348–53. doi: 10.1038/nrclinonc.2010.39

5. Ding J, Xiao H, Deng W, Liu F, Zhu R, Ha R. Feasibility of quantitative and volumetric enhancement measurement to assess tumor response in patients with breast cancer after early neoadjuvant chemotherapy. *J Int Med Res* (2021) 49 (3):1410669245. doi: 10.1177/0300060521991017

6. Teichgraeber DC, Guirguis MS, Whitman GJ. Breast cancer staging: Updates in the AJCC cancer staging manual, 8th edition, and current challenges for radiologists, from the AJR special series on cancer staging. *Am J Roentgenol* (2021) 217(2):278–90. doi: 10.2214/AJR.20.25223

7. Subhas G, Shah AJ, Gupta A, Cook J, Dubay L, Silapaswan S, et al. Review of third and fourth re-excision for narrow or positive margins of invasive and intraductal carcinoma. *Int Surg* (2011) 96(1):18. doi: 10.9738/1340.1

8. Marcotte-Bloch C, Balu-Maestro C, Chamorey E, Ettore F, Raoust I, Flipo B, et al. MRI For the size assessment of pure ductal carcinoma *in situ* (DCIS): A prospective study of 33 patients. *Eur J Radiol* (2011) 77(3):462–7. doi: 10.1016/j.ejrad.2009.09.003

9. Mann RM, Veltman J, Barentsz JO, Wobbes T, Blickman JG, Boetes C. The value of MRI compared to mammography in the assessment of tumour extent in invasive lobular carcinoma of the breast. *Eur J Surg Oncol (EJSO)* (2008) 34(2):135–42. doi: 10.1016/j.ejso.2007.04.020

10. Daniel OK, Lim SM, Kim JH, Park HS, Park S, Kim SI. Preoperative prediction of the size of pure ductal carcinoma *in situ* using three imaging modalities as compared to histopathological size: does magnetic resonance imaging add value? *Breast Cancer Res Tr* (2017) 164(2):437–44. doi: 10.1007/s10549-017-4252-2

11. Chen H, Zhou J, Chen Q, Deng Y. Comparison of the sensitivity of mammography, ultrasound, magnetic resonance imaging and combinations of these imaging modalities for the detection of small (≤2 cm) breast cancer. *Medicine* (2021) 100(26):e26531. doi: 10.1097/MD.0000000000026531

12. Meyer-Bäse A, Morra L, Meyer-Bäse U, Pinker K. Current status and future perspectives of artificial intelligence in magnetic resonance breast imaging. *Contrast Media Mol I* (2020) 2020:1–18. doi: 10.1155/2020/6805710

13. Ha R, Mutasa S, Karcich J, Gupta N, Pascual Van Sant E, Nemer J, et al. Predicting breast cancer molecular subtype with MRI dataset utilizing convolutional neural network algorithm. *J Digit Imaging* (2019) 32(2):276–82. doi: 10.1007/s10278-019-00179-2

14. Mann RM, Cho N, Moy L. Breast MRI: State of the art. *Radiology* (2019) 292 (3):520–36. doi: 10.1148/radiol.2019182947

15. Song SE, Seo BK, Cho KR, Woo OH, Park EK, Cha J, et al. Preoperative tumor size measurement in breast cancer patients: which threshold is appropriate on computer-aided detection for breast MRI? *Cancer Imaging* (2020) 20(1):32. doi: 10.1186/s40644-020-00307-0

16. Song SE, Seo BK, Cho KR, Woo OH, Son GS, Kim C, et al. Computer-aided detection (CAD) system for breast MRI in assessment of local tumor extent, nodal status, and multifocality of invasive breast cancers: preliminary study. *Cancer Imaging* (2015) 15(1):1. doi: 10.1186/s40644-015-0036-2

17. Meeuwis C, van de Ven SM, Stapper G, Fernandez Gallardo AM, van den Bosch MAAJ, Mali WPTM, et al. Computer-aided detection (CAD) for breast MRI: evaluation of efficacy at 3.0 T. *Eur Radiol* (2010) 20(3):522–8. doi: 10.1007/s00330-009-1573-5

18. Ryu DW, Jung MJ, Choi WS, Lee CH. Clinical significance of morphologic characteristics in triple negative breast cancer. *J Korean Surg Soc* (2011) 80(5):301. doi: 10.4174/jkss.2011.80.5.301

19. Abdelhafez AH, Musall BC, Adrada BE, Hess K, Son JB, Hwang K, et al. Tumor necrosis by pretreatment breast MRI: association with neoadjuvant systemic therapy (NAST) response in triple-negative breast cancer (TNBC). *Breast Cancer Res Tr* (2021) 185(1):1–12. doi: 10.1007/s10549-020-05917-7

20. Masood S. Neoadjuvant chemotherapy in breast cancers. *Women's Health* (2016) 12(5):480–91. doi: 10.1177/1745505716677139

21. Siu ALU.S. Preventive Services Task Force. Screening for breast cancer: U.S. preventive services task force recommendation statement. *Ann Intern Med* (2016) 164(4):279–96. doi: 10.7326/M15-2886

22. Chan H, Samala RK, Hadjiiski LM. CAD And AI for breast cancer–recent development and challenges. *Br J Radiol* (2020) 93(1108):20190580. doi: 10.1259/bjr.20190580

23. Michael E, Ma H, Li H, Kulwa F, Li J. Breast cancer segmentation methods: Current status and future potentials. *BioMed Res Int* (2021) 2021:9962109. doi: 10.1155/2021/9962109

24. Kickingereder P, Isensee F, Tursunova I, Petersen J, Neuberger U, Bonekamp D, et al. Automated quantitative tumour response assessment of MRI in neuro-oncology with artificial neural networks: a multicentre, retrospective study. *Lancet Oncol* (2019) 20(5):728–40. doi: 10.1016/S1470-2045(19)30098-1

25. Brugnara G, Isensee F, Neuberger U, Bonekamp D, Petersen J, Diem R, et al. Automated volumetric assessment with artificial neural networks might enable a more accurate assessment of disease burden in patients with multiple sclerosis. *Eur Radiol* (2020) 30(4):2356–64. doi: 10.1007/s00330-019-06593-y

26. Zhao X, Chen K, Wu G, Zhang G, Zhou X, Lv C, et al. Deep learning shows good reliability for automatic segmentation and volume measurement of brain

hemorrhage, intraventricular extension, and peripheral edema. *Eur Radiol* (2021) 31(7):5012–20. doi: 10.1007/s00330-020-07558-2

27. Shelhamer E, Long J, Darrell T. Fully convolutional networks for semantic segmentation. *IEEE T Pattern Anal* (2017) 39(4):640–51. doi: 10.1109/TPAMI.2016.2572683

28. Liu X, Zhang Y, Jing H, Wang L, Zhao S. Ore image segmentation method using U-net and Res_Unet convolutional networks. *Rsc Adv* (2020) 10(16):9396–406. doi: 10.1039/c9ra05877j

29. Bitencourt A, Daimiel Naranjo I, Lo Gullo R, Rossi Saccarelli C, Pinker K. AI-Enhanced breast imaging: Where are we and where are we heading? *Eur J Radiol* (2021) 142:109882. doi: 10.1016/j.ejrad.2021.109882

30. Truhn D, Schrading S, Haarburger C, Schneider H, Merhof D, Kuhl C. Radiomic versus convolutional neural networks analysis for classification of contrast-enhancing lesions at multiparametric breast MRI. *Radiology* (2019) 290 (2):290–7. doi: 10.1148/radiol.2018181352

31. Dalmiş MU, Gubern-Mérida A, Vreemann S, Bult P, Karssemeijer N, Mann R, et al. Artificial intelligence–based classification of breast lesions imaged with a multiparametric breast MRI protocol with ultrafast DCE-MRI, T2, and DWI. *Invest Radiol* (2019) 54(6):325–32. doi: 10.1097/RLI.0000000000000544

32. Ji Y, Li H, Edwards AV, Papaioannou J, Ma W, Liu P, et al. Independent validation of machine learning in diagnosing breast cancer on magnetic resonance imaging within a single institution. *Cancer Imaging* (2019) 19(1):64. doi: 10.1186/s40644-019-0252-2

33. Herent P, Schmauch B, Jehanno P, Dehaene O, Saillard C, Balleyguier C, et al. Detection and characterization of MRI breast lesions using deep learning. *Diagn Interv Imag* (2019) 100(4):219–25. doi: 10.1016/j.diii.2019.02.008

34. Jiao H, Jiang X, Pang Z, Lin X, Huang Y, Li L. Deep convolutional neural networks-based automatic breast segmentation and mass detection in DCE-MRI. *Comput Math Method M* (2020) 2020:1–12. doi: 10.1155/2020/2413706

35. Xu X, Fu L, Chen Y, Larsson R, Zhang D, Suo S, et al. (2018). Breast region segmentation being convolutional neural network in dynamic contrast enhanced MRI. *Annu Int Conf IEEE Eng Med Biol Soc* (2018) 2018:750–3. doi: 10.1109/EMBC.2018.8512422

36. Chen X, Men K, Chen B, Tang Y, Zhang T, Wang S, et al. CNN-Based quality assurance for automatic segmentation of breast cancer in radiotherapy. *Front Oncol* (2020) 10:524. doi: 10.3389/fonc.2020.00524

37. Tsochatzidis L, Koutla P, Costaridou L, Pratikakis I. Integrating segmentation information into CNN for breast cancer diagnosis of mammographic masses. *Comput Meth Prog Bio* (2021) 200:105913. doi: 10.1016/j.cmpb.2020.105913

38. Leithner D, Horvat JV, Marino MA, Bernard-Davila B, Jochelson MS, Ochoa-Albiztegui RE, et al. Radiomic signatures with contrast-enhanced magnetic resonance imaging for the assessment of breast cancer receptor status and molecular subtypes: initial results. *Breast Cancer Res* (2019) 21(1):106. doi: 10.1186/s13058-019-1187-z

39. Khaled R, Vidal J, Vilanova JC, Martí R. A U-net ensemble for breast lesion segmentation in DCE MRI. *Comput Biol Med* (2022) 140:105093. doi: 10.1016/j.compbiomed.2021.105093

40. Zhang L, Zha Z, Qu W, Zhao H, Yuan J, Feng Y, et al. Tumor necrosis as a prognostic variable for the clinical outcome in patients with renal cell carcinoma: a systematic review and meta-analysis. *BMC Cancer* (2018) 18(1):870. doi: 10.1186/s12885-018-4773-z

41. Fujisaki A, Aoki T, Kasai T, Kinoshita S, Tomoda Y, Tanaka F, et al. Pleomorphic carcinoma of the lung: Relationship between CT findings and prognosis. *Am J Roentgenol* (1976) 207(2):289. doi: 10.2214/AJR.15.15542

42. Liu Y, Wang K, Xing H, Zhai X, Wang L, Wang W. Attempt towards a novel classification of triple-negative breast cancer using immunohistochemical markers. *Oncol Lett* (2016) 12(2):1240–56. doi: 10.3892/ol.2016.4778

frontiers | Frontiers in Oncology

TYPE Systematic Review
PUBLISHED 31 August 2022
DOI 10.3389/fonc.2022.972767

OPEN ACCESS

EDITED BY
San-Gang Wu,
First Affiliated Hospital of Xiamen University, China

REVIEWED BY
Takahiro Kogawa,
Cancer Institute Hospital of Japanese Foundation for Cancer Research, Japan
Kevin Thompson,
Mayo Clinic, United States

*CORRESPONDENCE
Xianghui Han
Hanxianghui1106@163.com

SPECIALTY SECTION
This article was submitted to Breast Cancer, a section of the journal Frontiers in Oncology

RECEIVED 19 June 2022
ACCEPTED 08 August 2022
PUBLISHED 31 August 2022

CITATION
Huang Q, Mei Z and Han X (2022) Efficacy and safety of taxanes combined with chemotherapy drugs in advanced triple negative breast cancer: A meta-analysis of 26 randomized controlled trials. *Front. Oncol.* 12:972767. doi: 10.3389/fonc.2022.972767

Efficacy and safety of taxanes combined with chemotherapy drugs in advanced triple negative breast cancer: A meta-analysis of 26 randomized controlled trials

Qionglian Huang[1], Zubing Mei[2] and Xianghui Han[1]*

[1]Institute of Chinese Traditional Surgery, Longhua Hospital Affiliated to Shanghai University of Traditional Chinese Medicine, Shanghai, China, [2]Department of Anorectal Surgery, Shuguang Hospital Affiliated to Shanghai University of Traditional Chinese Medicine, Shanghai, China

Background: Researchers have demonstrated that the combined use of taxanes and chemotherapy drugs, especially paclitaxel-based treatment, appeared to clinically benefit on advanced triple negative breast cancer (TNBC). This meta-analysis aims to obtain the existent evidence on efficacy and safety for taxanes-based combination therapy to treat advanced TNBC.

Methods: From 1991 to June 2022, seven databases (PubMed, Web of Science, Cochrane Library, Embase VIP, Wanfang, and CNKI databases) were comprehensively searched with no restricted language and region. The included randomized controlled trials (RCTs) compared taxanes-based combination therapy versus taxanes or other chemotherapy drugs. Statistical analysis was conducted using random-effect model, and the quality of RCTs was assessed using the tool of Cochrane Collaboration risk of bias.

Results: Twenty-six RCTs with a total of 8,236 advanced TNBC patients were included. Compared with taxanes monotherapy, taxanes-based combination therapy significantly prolonged progression-free survival (HR=0.79, 95% CI=0.74–0.83, I^2 = 0.0%, p=0.000) and overall survival (HR=0.88, 95% CI=0.82–0.94, I^2 = 9.3%, p=0.000) and increased the risk of vomiting (RR=1.26, 95%CI=1.07–1.48) and diarrhea (RR=1.82, 95%CI=1.22–2.70, I^2 = 90.3%, p=0.003). No statistical differences were observed in complete response rate (CRR), objective response rate (ORR), disease control rate (DCR), and progressive disease (PD) indexes (CRR: RR=1.38, 95%CI=0.96–1.99; ORR: RR=1.20, 95%CI=0.73–1.98; DCR: RR=1.09, 95%CI=1.00–1.19; PD: RR=0.70, 95%CI=0.47–1.04). Compared with other chemotherapy drugs, taxanes *plus*

Abbreviations: TNBC, triple negative breast cancer; PFS, progression-free survival; OS, overall survival, CRR: complete response rate; ORR, objective response rate; DCR, disease control rate; PD, progressive disease; HR, hazard ratio; RR, risk ratio; Cis, confidence intervals; RCTs, randomized controlled trials; RECIST, Response Evaluation Criteria in Solid Tumors.

other chemotherapy drugs significantly reduced the incidence of vomiting (RR=0.60, 95%CI=0.44–0.84, I^2 = 12.3%, p=0.002) and neutropenia (RR=0.58, 95%CI=0.35–0.96, I^2 = 73.0%, p=0.036) during the treatment period.

Conclusions: Taxanes-based combination therapy is evidently effective and well-tolerated in advanced TNBC, indicating that it might be a recommended option for treating advanced TNBC patients to some extent.

Systematic Review Registration: https://www.crd.york.ac.uk/PROSPERO/, identifier CRD42022337802.

KEYWORDS

triple negative breast cancer, taxane, combination therapy, efficacy, safety, meta-analysis

Introduction

Female breast cancer, with an assessed 2.3 million new cases and 0.68 million mortalities, has become the most common malignant tumor of global cancers in 2020 (1). Triple negative breast cancer (TNBC), regarded as a heterogeneous and aggressive breast cancer subtype and characterized by impaired expression of estrogen receptors, progesterone receptors, and human epidermal growth factor receptor 2, represents 10%–25% of breast cancers types and thus is strongly associated with poorer prognosis (2, 3). Furthermore, advanced TNBC usually leads to higher incidence of distant metastases such as bone, visceral, and central nervous system metastases within 5 years of diagnosis and causes high mortality afflicting on patients (4, 5). To date, there is no standard treatments for advanced TNBC, while chemotherapy was a recommended choice of treating TNBC (6–8).

Taxanes (i.e., nab-paclitaxel, paclitaxel, and docetaxel), are diterpenoid alkaloid compound with prominent antineoplastic activities. As the first-line chemotherapy drugs, taxanes were widely used in the treatment of advanced lung cancer, endometrial cancer, breast cancer, and ovarian cancer (9). US FDA approved taxanes for treating advanced or metastatic breast cancer in 2005 (10). Recently, the combination use of taxanes and other chemotherapy drugs, especially paclitaxel-based treatment, appears to be significantly beneficial on advanced TNBC patients (11, 12). A randomized clinical trial (RCT) reported that paclitaxel plus capivasertib therapy showed an improvement in progression-free survival and overall survival compared to paclitaxel monotherapy (13). Another RCT found that there were longer progression-free survival (PFS) and higher objective response rate (ORR) in advanced TNBC patients treated with nab–paclitaxel–carboplatin than gemcitabine–carboplatin (14). Paclitaxel combined with either bevacizumab or capecitabine also was set as therapy regimens for advanced TNBC, and the latter appeared to have better superiority in terms of progressive disease (15). Additionally, paclitaxel plus gemcitabine appeared less toxic than cisplatin plus gemcitabine totally when treating advanced TNBC (16). Thus, taxanes combined with other chemotherapy drugs were considered as the potential effective treatment choice based on the results of these studies.

However, to date, there is no clear evidence that taxanes plus other chemotherapy drugs benefits the advanced TNBC patients due to the limitation of small sample size included in these studies. Therefore, we summarize the date and relevant data for a comprehensive meta-analysis of all RCTs aiming to better elucidate the efficacy and safety of taxanes combined with chemotherapy drugs in advanced TNBC.

Materials and methods

This meta-analysis was conducted in accordance with the Preferred Reporting Items for Systematic Reviews and Meta-analyses (17, 18) and registered at the International Prospective Register of Systematic Reviews (PROSPERO, CRD42022337802).

Data sources and search strategy

Of no language or region restrictions, we searched PubMed, Cochrane Library, Web of Science, and Embase databases and three databases of China (CNKI, Wanfang, and VIP) from inception to February 20, 2022 systematically to recognize the full-text articles related to RCTs. We performed the following methodology to search the databases: using MeSH terms of "triple negative breast cancer" AND ("paclitaxel" OR "docetaxel") AND ("metastasis" OR

"advanced") and free terms of them *plus* randomized controlled trials. A more detailed search strategy is available at Supplementary Table S1. Assessment to the eligible articles was performed by two reviewers (QH and XH) independently after reading the titles and abstracts of all articles.

Inclusion and exclusion criteria

The identification for eligible literatures was carried out by using EndNote X9 software. Selection and assessment to the studies through different databases were conducted by two reviewers (QH and XH) independently according to PICOS criteria. The studies were included if they met the following criteria (18):

Participant: patients with age of more than 18 years and histologically confirmed advanced or metastatic TNBC (Eastern Cooperative Oncology Group performance status of 0–2).

Intervention: taxanes combined with other chemotherapy drugs (i.e., platinum, tabines, bevacizumab, and atezolizumab).

Comparator: taxanes or other chemotherapy drugs.

Outcomes: PFS, overall survival (OS), complete response rate (CRR), ORR, disease control rate (DCR), progressive disease (PD), and adverse events provided any analyzable data.

Study design: RCTs with either double-blind or multicenter design.

Exclusion criteria were the following: only abstract (19, 20), review (21), experimental research (22), case reports (23), non-RCTs (24), non-advanced TNBC (25), phase I trials (26), trials with improper control drugs (27), and no available data or duplicates (28, 29).

Data extraction and quality assessment

Two reviewers (QH and XH) independently extracted data from eligible essays in terms of the following information according to the Cochrane Handbook guidelines: first author, study design, number of participants, median age, inclusion criteria, treatment duration, primary outcomes, and secondary outcomes. The participation of a third reviewer became a necessity when discrepancies occurred during the extraction of the data and information until consensus was realized.

The efficacy and safety of taxanes combination chemotherapy on advanced TNBC were appraised by PFS, OS, CRR, ORR, DCR, and PD, and the adverse events of taxanes combination chemotherapy were evaluated according to Response Evaluation Criteria in Solid Tumors (RECIST)1.1 and WHO grading criteria (30, 31). To fulfill credible conclusions for the reviewers, the Cochrane Collaboration risk of bias tool was used to analyze the data of random sequence generation, allocated concealment, detailed information of participants blinding, completion of outcome reporting, and selective publication for assessment to methodological quality of RCTs. Grading of Recommendations, Assessment, Development and Evaluations system (GRADE) was used to assess the quality of evidence for each outcomes (32).

Definition of outcomes

PFS, OS, ORR, and total adverse events were selected as primary outcomes in this meta-analysis. Based on WHO general objective efficacy indicators of solid tumors or RECIST1.0 criteria (33), CRR, DCR, and PD were selected as secondary outcomes. PFS, the most common primary endpoint in cancer trials, is defined as the time from the date of initial treatment to the date of the first objective documentation of disease progression or the date of the last follow-up for patients who are still alive without disease progression or death without disease progression (34). OS, considered as the best therapeutic endpoint in tumor clinical trials, is interpreted as the time between randomization and death from any cause in a clinical trial (35). CRR is defined as the proportion of patients who achieved best overall response of confirmed complete responses (31). ORR is defined as the proportion of patients who achieved best overall response of confirmed complete responses and partial responses (31, 36). DCR, including cases of complete responses partial responses and stable disease, is the ratio of patients whose tumors shrink or remain stable for a certain period of time (31). PD means the sum diameter of lesions of patients increasing the sum of the largest diameter of lesions to at least 20% or greater or the emergence of a new lesion, which is often used to evaluate the aggravation of anti-tumor therapy in clinical trials (37). Adverse events from intervention and comparator drugs assessed in this article include total adverse events, anemia, vomiting, diarrhea, neutropenia, alopecia, and fatigue.

Statistical synthesis and analysis

Statistical analysis was executed using Stata software (Version 12.0.) and random-effect model along with 95% confidence intervals (CIs) were used to analyze all quantitative data. For dichotomous variables, hazard ratio (HR) was used to appraise the indexes of PFS and OS. For effect variables, risk ratio (RR) was used to evaluate the indexes of ORR, DCR, PD, and adverse events. Data of each index were analyzed and presented by Forest plots; $p<0.05$ was considered as statistical significance. To explore potential resources, the clinical benefit indexes including PFS, OS, CRR, ORR, DCR, PD, and adverse events were highlighted by the conduction of subgroup analyses. Subgroup analysis was planned according to the types of control groups including other chemotherapy drugs or taxanes.

The between-study heterogeneity was assessed using Cochrane's Q and I^2 statistic as follows: 0%–40%, might not be important; 30%–60%, might represent moderate

heterogeneity; 50%–90%, might represent substantial heterogeneity; and 75%–100%, considerable heterogeneity (38, 39). Publication bias was investigated visually according to the results of funnel plots and Egger's test. When outcomes met more than 10 RCTs, the standard error of log (HR) and HR or log (RR) and RR were used to generate funnel plots. It is classified as publication bias if the results of Egger's test are $p< 0.05$ and funnel plots are asymmetric.

Results

Search and selection of studies

A flow diagram (Figure 1) presented the procedure on how we identified the articles in this meta-analysis. First, we collected 5,559 records by searching seven databases (PubMed, Web of Science, Cochrane Library, Embase VIP, Wanfang, and CNKI databases). Next, 5,370 records were excluded for some reasons (i.e., duplicates, non-breast cancer articles, only abstract, reviews, experimental research, case reports, non-RCTs, non-advanced TNBC, and phase I trials), and 189 full-text articles were considered as prospective eligibility. After further identification, 163 studies were excluded due to erroneous control agents and no available data or duplicates. Finally, 26 full-text RCTs were included in this meta-analysis (13–16, 40–61).

Study characteristics

The fundamental characteristics of the 26 final included articles published in Chinese and English journals from 2011 to 2021 are summarized in Supplementary Table S2. These phase II or phase III trials involved 8,236 patients and were conducted in America, Europe, Asia, and Oceania. All patients histologically confirmed unresectable advanced or metastatic TNBC, ranging from 40.1 to 59.0 years of age.

Among these 26 RCTs, 12 were designed as double-blind or placebo-controlled (13, 42–44, 46, 50, 51, 53, 55–57, 60), 5 were designed as open-label or multicenter (14, 16, 40, 52, 61), and 9 were not described further in detail (15, 41, 45, 47–49, 54, 58, 59). The intervention arms in all trials were taxanes (nab-paclitaxel, 100 mg/m^2; paclitaxel, 80–175 mg/m^2; docetaxel, 75 mg/m^2) plus other chemotherapy drugs (atezolizumab, 7 trials; carboplatin, 3 trials; bevacizumab, 3 trials; gemcitabine, 2 trials; cisplatinum, 2 trials; oxaliplatin, 2 trials; ipatasertib, 2 trials; capecitabine, 1 trial; tigatuzumab, 1 trial; capivasertib, 1 trial; reparixin, 1 trial; cobimetinib, 1 trial), while the control arms were taxanes (17 trials) or other chemotherapy drugs (9 trials). For primary outcomes, 19 trials assessed PFS and OS indexes of patients, 22 studies investigated ORR index of patients, and 12 trials observed the safety of drugs. For secondary outcomes, 6 trials reported CRR, 12 trials reported DC, and 14 trials reported PD were evaluated.

Quality assessment and risk of bias

The evaluation result of risk of bias is shown in Figures 2A, B. Of 26 eligible RCTs, 25 reported adequate random sequence generation, 9 covered allocation concealment, 12 performed double-blind way, 21 avoided incomplete outcome data, and 25 averted selective reporting bias.

The high-quality evidence with heterogeneity I^2 was used as judgement of outcomes of clinical efficacy, including PFS,

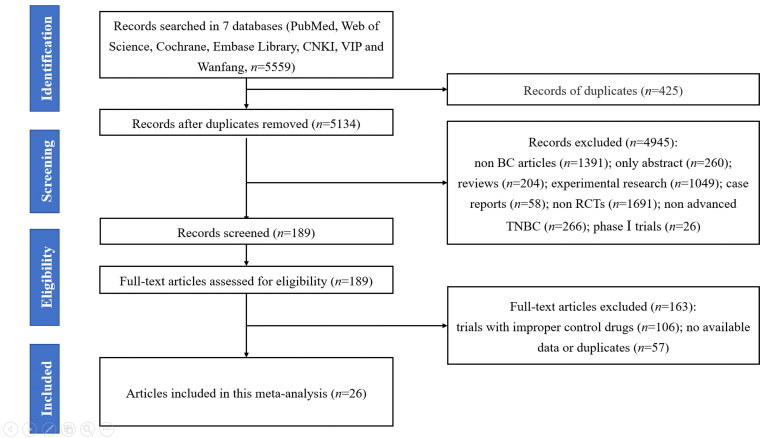

FIGURE 1
The PRISMA flowchart summarizing the process to identify randomized controlled trials for inclusion.

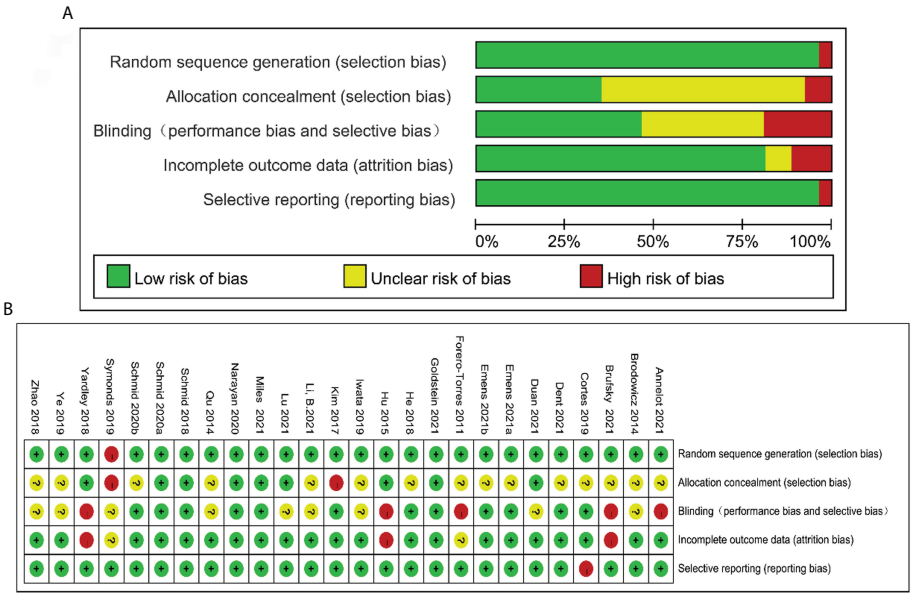

FIGURE 2
Risk of bias graph: reviewers' judgments about each risk of bias item presented as percentages across all included studies **(A)**. Risk of bias summary: reviewers' judgments about each risk of bias item for each included study according to the Cochrane Collaboration's "Risk of Bias" tool, the green circle with "plus" sign low risk of bias information, the yellow circle with "question mark" sign representing unclear risk of bias information, and the red circle with "minus" sign representing high risk of bias information **(B)**.

OS, and PD indexes, which ranged from 6.2% to 67.5%. CRR, ORR, and DCR indexes were judged as moderate-quality evidence with heterogeneity I^2 ranging from 0% to 98.6%. Adverse effects such as diarrhea and alopecia were judged as high quality with heterogeneity I^2 ranging from 6.2% to 87.8%, whereas total adverse events, vomiting, neutropenia, and fatigue were judged as moderate-quality evidence (heterogeneity I^2 = 14.0%–89.8%, Supplementary Table S3).

Publication bias

The publication bias of the outcomes (≥10 RCTs) was evaluated by the performance of funnel plot and Egger's test. The funnel plots revealed almost symmetric in 11 outcomes including PFS, OS, DCR, PD, total adverse events, anemia, vomiting, diarrhea, neutropenia, alopecia, and fatigue. The results of Egger's test showed no statistical significance in the above indexes (PFS, p=0.492; OS, p=0.608; total adverse events, p=0.554; anemia, p=0.283; vomiting, p=0.629; diarrhea, p=0.174; neutropenia, p=0.315; alopecia, p=0.217; fatigue, p=0.435), which indicates no distinct publication bias in this meta-analysis. Notably, ORR and CRR indexes appeared potential publication bias (ORR, p=0.004; CRR, p=0.030, Figures 3A–M).

Results of meta-analysis

Primary outcomes

Progression-free survival

Sixteen RCTs reported about PFS index of taxanes plus other chemotherapy agents vs. taxanes or other chemotherapy agents (platinum, bevacizumab, and tabines). A total of 3,711 patients were included in taxanes combination groups and 3,494 patients in control groups. The overall results showed significant differences between the intervention groups and control groups (HR=0.78, 95%CI=0.73–0.84, I^2 = 23.6%, p=0.000). Subgroup analysis indicated that taxanes combination therapy was superior to taxanes monotherapy in terms of PFS (HR=0.79, 95%CI=0.74–0.83, I^2 = 0.0%, p=0.000), while no difference was observed between taxanes plus other chemotherapy agents and other chemotherapy agents (HR=0.82, 95%CI=0.51–1.33, I^2 = 80.0%, p=0.421, Figure 4A).

Overall survival

With respect to OS, 16 RCTs included 3,758 patients who received taxanes plus other chemotherapy drugs and 3,541 patients who received taxanes or other chemotherapy drugs. The findings of

10.3389/fonc.2022.972767

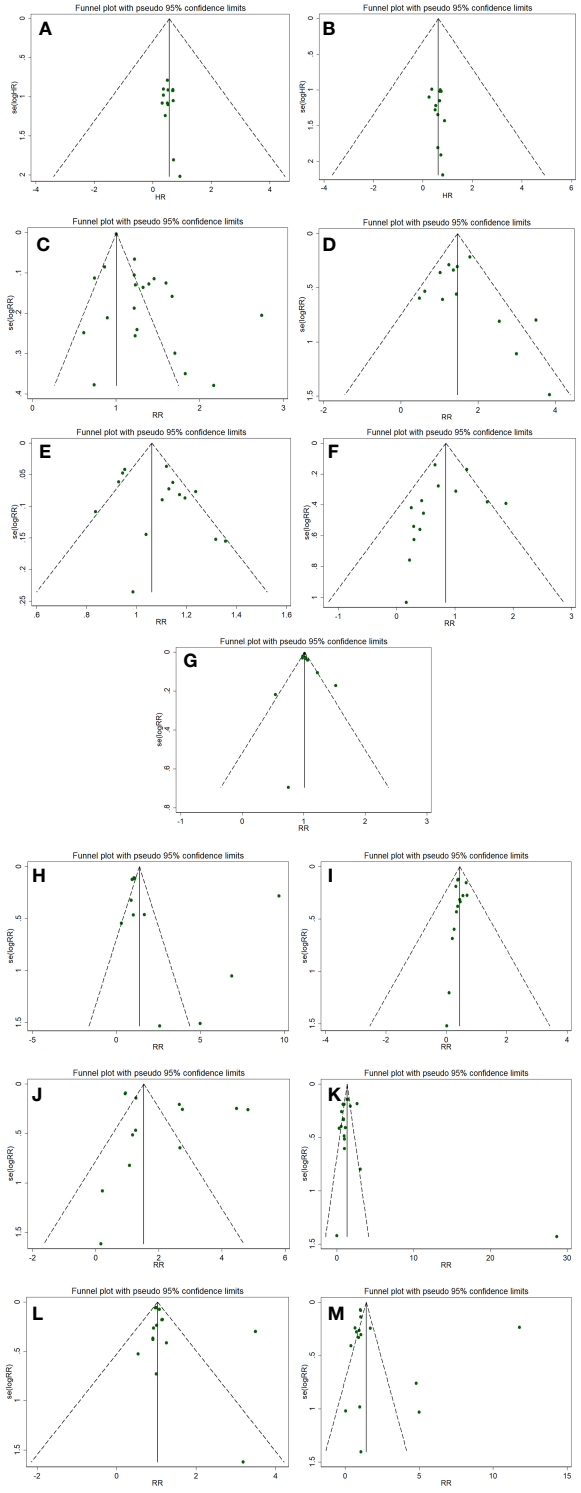

FIGURE 3
Funnel plots evaluating publication bias for following outcomes: PFS **(A)**, OS **(B)** OS, ORR **(C)**, CRR **(D)**, DCR **(E)**, PD **(F)**, total adverse events **(G)**, anemia **(H)**, vomiting **(I)**, diarrhea **(J)**, neutropenia **(K)**, alopecia **(L)**, and fatigue **(M)**.

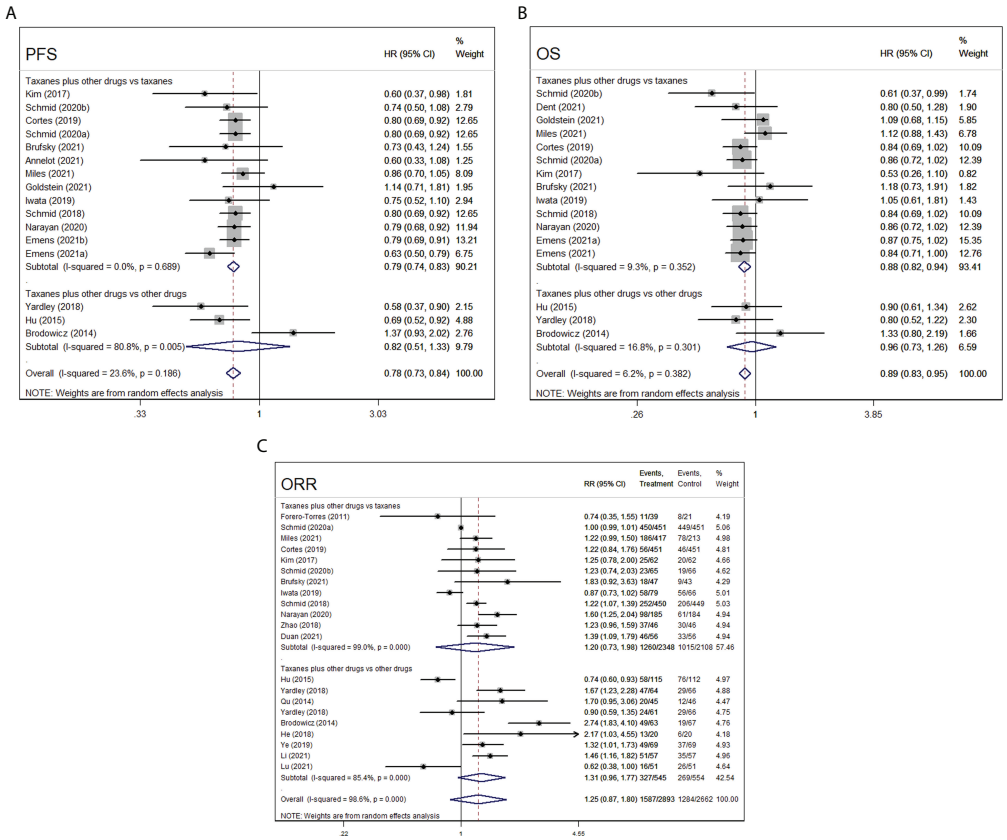

FIGURE 4
Forest plot of randomized controlled trials on taxanes combination therapy for primary outcomes: PFS **(A)**, OS **(B)**, and ORR **(C)**.

the pooled data revealed that taxanes-combination therapy significantly prolonged OS of patients when comparing to taxanes monotherapy (HR=0.88, 95%CI=0.82–0.94, I^2 = 9.3%, p=0.000), whereas no significances were observed between taxanes combination groups and other agents combination groups (HR=0.96, 95%CI=0.73–1.26, I^2 = 16.8%, p=0.763, Figure 4B).

Objective response rate

In the 21 RCTs, 1,587 of 2,893 patients achieved an ORR in taxanes-based chemotherapy groups (intervention groups), and 1,284 of 2,662 patients achieved an ORR after the treatment of taxanes monotherapy or non-taxanes chemotherapy (control groups). The pooled 12 eligible studies reported taxanes alone, and the pooled nine eligible studies reported other chemotherapy drugs. Both pooled and subgroup analysis found that the intervention groups relatively have no distinct advantage to comparators (overall, RR=1.25, 95%CI=0.87–1.80, I^2 = 98.6%, p=0.227; taxanes plus other drugs vs. taxanes, RR=1.20, 95% CI=0.73–1.98, I^2 = 99.0%, p=0.474; taxanes plus other drugs vs. other drugs, RR=1.31, 95%CI=0.96–1.77, I^2 = 85.4%, p=0.084, Figure 4C)

Adverse events

All 26 RCTs reported the total adverse events and six mainly common adverse events (anemia, vomiting, diarrhea, neutropenia, alopecia, and fatigue) caused by different drugs, in which 1,566 of 1,673 patients in intervention groups and 1,489 of 1,620 patients in control groups suffered from adverse events.

Overall and subgroup analyses of other chemotherapy drugs in control groups confirmed no statistical differences in the incidence risk of total adverse events between intervention groups (taxanes-based combination chemotherapy) and control groups (other chemotherapy drugs) (RR=1.02, 95% CI=0.99–1.04, I^2 = 55.7%, p=0.196; RR=1.02, 95%CI=0.79–1.33, I^2 = 79.2%, p=0.877). Nonetheless, the number of patients who accepted taxanes-based combination chemotherapy was obviously more than those who accepted taxanes monotherapy (RR=1.02, 95%CI=1–1.03, I^2 = 0.0%, p=0.004, Figure 5A).

Compared with taxanes monotherapy, taxanes-based combination therapy evidently increased the occurrence of vomiting (RR=1.26, 95%CI=1.07–1.48, I^2 = 0.0%, p=0.005) and diarrhea (RR=1.82, 95%CI=1.22–2.70, I^2 = 90.3%, p=0.003),

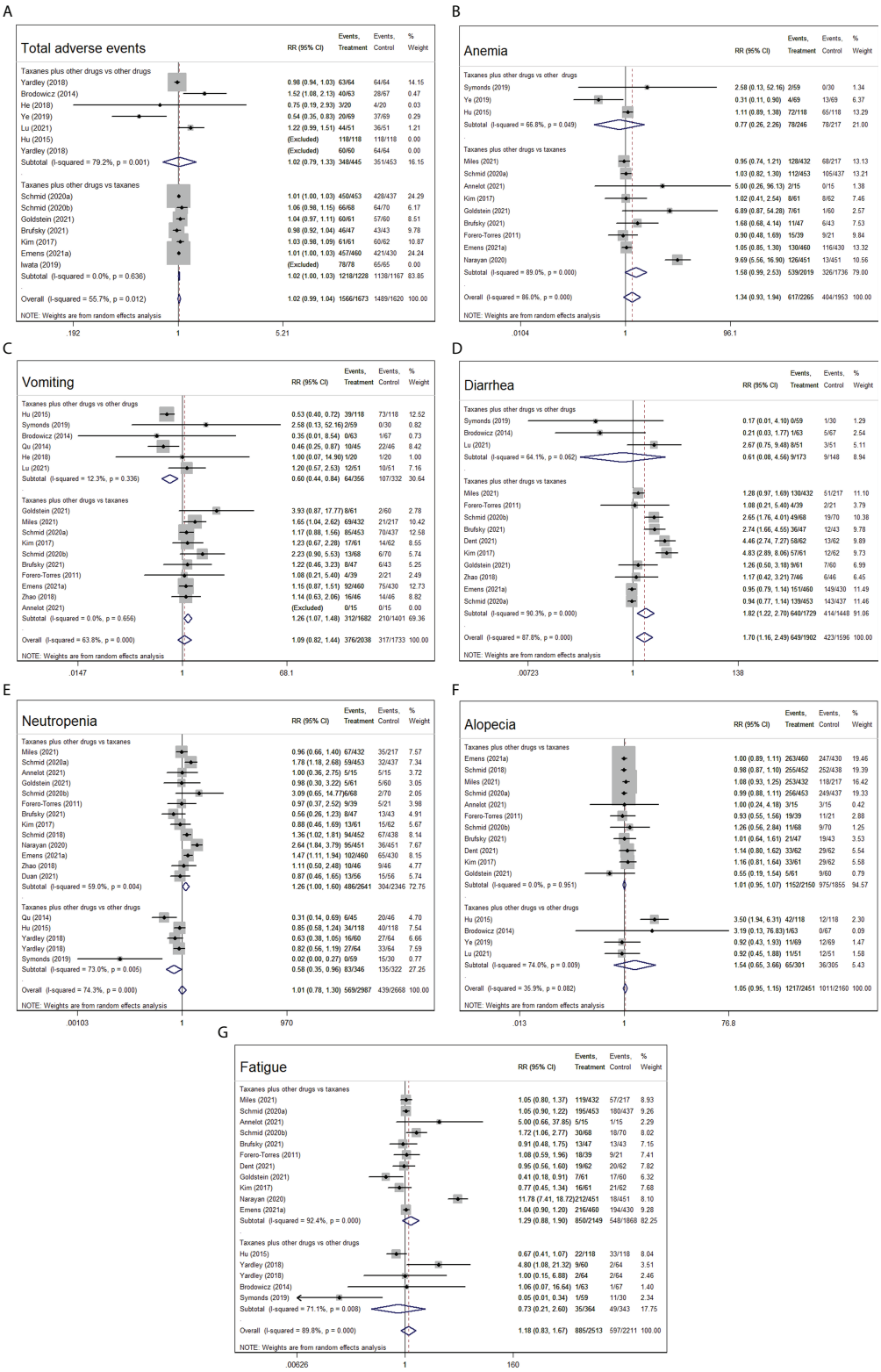

FIGURE 5
Forest plot of randomized controlled trials on taxanes combination therapy for adverse event: total adverse events **(A)**, anemia **(B)**, vomiting **(C)**, diarrhea **(D)**, neutropenia **(E)**, alopecia **(F)**, and fatigue **(G)**.

whereas no differences were seen in the rest of the four adverse events. Compared with other chemotherapy drugs, taxanes plus other chemotherapy drugs obviously reduced the occurrence of vomiting (RR=0.60, 95%CI=0.44–0.84, I^2 = 12.3%, p=0.002) and neutropenia (RR=0.58, 95%CI=0.35–0.96, I^2 = 73.0%, p=0.036), whereas no significantly differences were observed in the other five adverse events (p>0.05, Figures 5B–G).

Secondary outcomes

Complete response rate

Of 14 RCTs concerning CRR index, 6 RCTs (1,886 patients) with taxanes plus other chemotherapy drugs vs. taxanes only and 8 RCTs (969 patients) with taxanes plus other chemotherapy drugs vs. other chemotherapy drugs provided available data for CRR. In primary analysis, the taxanes-based combination treatment distinctly benefited the patients more in respect of CRR compared with the control arms (RR=1.38, 95%CI=1.10–1.72, I^2 = 0.0%, p=0.005). In secondary analysis, the number of patients in interventional arms who had complete response did not have any advantage over that in control arms (taxanes combination vs. taxanes, RR=1.38, 95%CI=0.96–1.99, I^2 = 0.0%, p=0.079; taxanes combination vs. non-taxanes drugs, RR=1.31, 95%CI=0.94–1.83, I^2 = 14.0%, p=0.110, Figure 6A).

Disease control rate

The included 15 RCTs in this meta-analysis covered DCR. The results from intervention groups showed superiority to stopping the deterioration of advanced TNBC in patients compared to control groups (RR=1.08, 95%CI=1.01–1.05, I^2 = 63.8%, p=0.027). The results of subgroup analysis suggested that there was insignificant superiority for taxanes combination therapy to increase the DCR in patients compared to taxanes monotherapy (RR=1.09, 95%CI=1.00-1.19, I^2 = 55.1%, p=0.053) or other chemotherapy drugs (RR=1.06 95%CI=0.96–1.18, I^2 = 63.8%, p=0.219, Figure 6B).

Progressive disease

In 14 RCTs, 257 of 1,531 (16.8%) patients accepting taxanes plus other chemotherapy drugs (intervention) and 295 of 1,313 (19.7%) patients accepting taxanes or other chemotherapy drugs (control) have undergone PD. The overall findings revealed that a lesser incidence of PD was seen in intervention groups than that in control groups (RR=0.63, 95%CI=0.46–0.88, I^2 = 67.5%, p=0.007). In further subgroup analysis, the results showed that there were

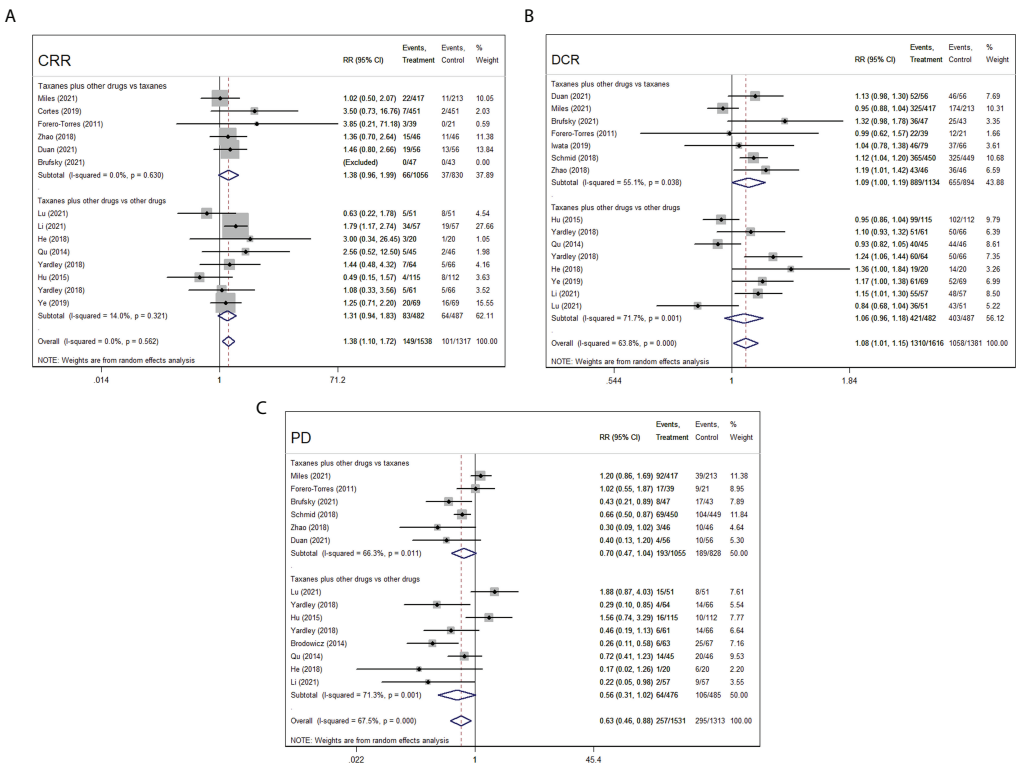

FIGURE 6
Forest plots of randomized controlled trials on taxanes combination therapy for secondary outcomes: CRR **(A)**, DCR **(B)**, and PD **(C)**.

insignificant differences in the number of patients in terms of PD between the medication regimens of taxanes plus other chemotherapy drugs and taxanes alone (RR=0.70, 95%CI=0.47–1.04, I^2 = 66.3%, p=0.075), and the same results were observed in the two groups of taxanes plus other chemotherapy drugs and other chemotherapy drugs (RR=0.56, 95%CI=0.31–1.02, I^2 = 71.3%, p=0.059, Figure 6C).

Discussion

Findings and interpretations

In this meta-analysis, we pooled the data of 26 RCTs, enrolling a total of 8,236 patients with advanced TNBC and compared taxanes-based combination therapies vs. taxanes or other chemotherapy drugs. Taken together, our results indicated that taxanes-based combination therapies had a significant beneficial effect on prolonging PFS and OS index of advanced TNBC patients compared with taxanes monotherapy. In clinics, taxanes plus other chemotherapy drugs (i.e., platinum, tabines, bevacizumab, and atezolizumab) was broadly applied in the treatment of advanced TNBC (15, 16, 61). Our results of meta-analysis found that taxanes plus bevacizumab could evidently improve ORR index and decrease PD index in patients compared to bevacizumab plus other drugs (p<0.05), but taxanes plus tabines or platinum revealed no statistical significance in therapeutic benefits compared to tabines or platinum plus other drugs (p>0.05). Additionally, taxanes *plus* other chemotherapy drugs showed more safe and well-tolerated by patients with advanced TNBC relative to other chemotherapy drugs. For example, taxanes plus other chemotherapy drugs and other chemotherapy drugs led to anemia in 31.7% and 35.9% of patients (16, 48, 49), vomiting in 18.0% and 32.2% of patients (15, 16, 41, 43, 49, 59), diarrhea in 5.2% and 6.1% of patients (15, 49, 59), neutropenia in 23.9% and 41.9% of patients (14–16, 41, 48), alopecia in 21.6% and 11.8% of patients (15, 16, 49, 59), and sfatigue in 35.2% and 27.0% of patients during the treatment period, respectively (14–16, 48). Simultaneously, indirectness of evidence, study design, publication bias, inconsistency in results, or data analysis objectively resulted in the potentially degradation of outcomes from included trials.

Strengths and limitations

Strengths can be found in this meta-analysis as follows: first, to the best of our knowledge, this review is the first systematic investigation to explore the efficacy and safety of taxanes-based combination therapy for advanced or metastatic TNBC. Second, a large sample size including 8,236 patients in 26 RCTs published from 1991 to 2022 was assessed, with no restriction to language or region. Third, our meta-analysis summarized the existed recommendation to potential effect of taxanes on advanced TNBC, providing robustness for the results of studies. Fourth, subgroup analyses were made for the key outcomes basing on the combination of taxanes and other chemotherapy drugs versus taxanes alone or other chemotherapy drugs to minimize the possible selection bias and made the findings have great credibility. Fifth, our results became more reliable due to the execution of evaluating the quality of evidence for each individual outcome.

Nevertheless, several limitations in this meta-analysis should be taken into consideration. First, only 9 of 26 RCTs reported allocation concealment and 12 of 26 RCTs performed blinding to the measurement of the outcomes in our analysis, which might affect the accuracy of the results. Second, the choice to a random-effect model for all quantitative data in this meta-analysis might bring about more weight to smaller studies and wider confidence intervals, concealing potentially expanded effects of bias in these studies. Third, funnel plots and Egger's test were not conducted to assess publication bias if the outcome was <10 RCTs included.

Conclusion

In summary, the findings of this meta-analysis demonstrated that taxanes-based combination therapy is evidently effective to treat advance TNBC than taxanes monotherapy. Moreover, taxanes-based combination had a similar efficacy and fewer adverse reactions in comparison to other chemotherapy combination. Recent studies reported that the combination therapy of taxanes and new chemotherapy drugs (tigatuzumab, atezolizumab, and bevacizumab) was widely applied in clinical practice and presented more excellent therapeutical effects. Therefore, taxanes-based combination therapy, especially taxanes *plus* chemotherapy drugs, might become a recommended option to treat advance TNBC.

Data availability statement

The raw data supporting the conclusions of this article will be made available by the authors, without undue reservation.

Author contributions

XH and QH designed the study, collected and interpreted the data, and revised the article. QH performed the systematic literature search, analyzed the data, and wrote the original draft. XH, QH, and ZM contributed to the critical revision of the manuscript for important intellectual content. All authors contributed to the article and approved the submitted version.

Acknowledgments

The authors thank all the authors of the original studies included in this meta-analysis. The research, authorship, and publication of this article were funded by the Natural Science Foundation of Shanghai, China (grant number: 20ZR1458600) and National Natural Science Foundation of China (grant number: 82174016).

Conflict of interest

The authors declare that the research was conducted in the absence of any commercial or financial relationships that could be construed as a potential conflict of interest.

Publisher's note

Supplementary material

The Supplementary Material for this article can be found online at: https://www.frontiersin.org/articles/10.3389/fonc.2022.972767/full#supplementary-material

References

1. Sung H, Ferlay J, Siegel RL, Laversanne M, Soerjomataram I, Jemal A, et al. Global cancer statistics 2020: GLOBOCAN estimates of incidence and mortality worldwide for 36 cancers in 185 countries. *CA Cancer J Clin* (2021) 71(3):209–49. doi: 10.3322/caac.21660

2. Almansour NM. Triple-negative breast cancer: A brief review about epidemiology, risk factors, signaling pathways, treatment and role of artificial intelligence. *Front Mol Biosci* (2022) 9:836417. doi: 10.3389/fmolb.2022.836417

3. Qiu X, Zhao T, Luo R, Qiu R, Li Z. Tumor-associated macrophages: Key players in triple-negative breast cancer. *Front Oncol* (2022) 12:772615. doi: 10.3389/fonc.2022.772615

4. Liedtke C, Mazouni C, Hess KR, Andre F, Tordai A, Mejia JA, et al. Response to neoadjuvant therapy and long-term survival in patients with triple-negative breast cancer. *J Clin Oncol* (2008) 26(8):1275–81. doi: 10.1200/JCO.2007.14.4147

5. Doepker Mp Fau-Holt SD, Holt Sd Fau-Durkin MW, Durkin Mw Fau-Chu CH, Chu Ch Fau-Nottingham JM, Nottingham JM. Triple-negative breast cancer: A comparison of race and survival. *Am Surg* (2018) 84(6):881–8. doi: 10.1177/000313481808400636

6. Cortazar P, Zhang L, Untch M, Mehta K, Costantino JP, Wolmark N, et al. Pathological complete response and long-term clinical benefit in breast cancer: The CTNeoBC pooled analysis. *Lancet* (2014) 384(9938):164–72. doi: 10.1016/s0140-6736(13)62422-8

7. Ou KP, Li Q, Luo Y, Lyu JJ, Zhou H, Yang Y, et al. Efficacy and safety of neoadjuvant apatinib in combination with dose-dense paclitaxel and carboplatin in locally advanced triple negative breast cancer patients. *Zhonghua Zhong Liu Za Zhi* (2020) 42(11):966–71. doi: 10.3760/cma.j.cn112152-20200224-00122

8. Tan A, Wang H, Nong L, Jia Y, Liu Y, Zhong W, et al. Efficacy and safety of continuous infusion of Rh-endostatin combined with platinum-based chemotherapy for advanced triple-negative breast cancer. *Ann Palliat Med* (2021) 10(12):12101–12. doi: 10.21037/apm-21-2624

9. Mosca L, Ilari A, Fazi F, Assaraf YG, Colotti G. Taxanes in cancer treatment: Activity, chemoresistance and its overcoming. *Drug Resist Update* (2021) 54:100742. doi: 10.1016/j.drup.2020.100742

10. Cortazar P, Justice R, Johnson J, Sridhara R, Keegan P, Pazdur R, et al. And drug administration approval overview in metastatic breast cancer. *J Clin Oncol* (2012) 30(14):1705–11. doi: 10.1200/JCO.2011.39.2613

11. Mustacchi G, De Laurentiis M. The role of taxanes in triple-negative breast cancer: Literature review. *Drug Des Devel Ther* (2015) 9:4303–18. doi: 10.2147/DDDT.S86105

12. Ogata H, Kikuchi Y, Natori K, Shiraga N, Kobayashi M, Magoshi S, et al. Liver metastasis of a triple-negative breast cancer and complete remission for 5 years after treatment with combined Bevacizumab/Paclitaxel/Carboplatin: Case report and review of the literature. *Med (Baltimore)* (2015) 94(42):e1756. doi: 10.1097/MD.0000000000001756

13. Schmid P, Abraham J, Chan S, Wheatley D, Brunt AM, Nemsadze G, et al. Capivasertib plus paclitaxel versus placebo plus paclitaxel as first-line therapy for metastatic triple-negative breast cancer: The PAKT trial. *J Clin Oncol* (2020) 38 (5):423–33. doi: 10.1200/JCO.19.00368

14. Yardley DA, Coleman R, Conte P, Cortes J, Brufsky A, Shtivelband M, et al. Nab-paclitaxel plus carboplatin or gemcitabine versus gemcitabine plus carboplatin as first-line treatment of patients with triple-negative metastatic breast cancer: Results from the TnAcity trial. *Ann Oncol* (2018) 29(8):1763–70. doi: 10.1093/annonc/mdy201

15. Brodowicz T, Lang I, Kahan Z, Greil R, Beslija S, Stemmer SM, et al. Selecting first-line bevacizumab-containing therapy for advanced breast cancer: TURANDOT risk factor analyses. *Br J Cancer* (2014) 111(11):2051–57. doi: 10.1038/bjc.2014.504

16. Hu X-C, Zhang J, Xu B-H, Cai L, Ragaz J, Wang Z-H, et al. Cisplatin plus gemcitabine versus paclitaxel plus gemcitabine as first-line therapy for metastatic triple-negative breast cancer (CBCSG006): A randomised, open-label, multicentre, phase 3 trial. *Lancet Oncol* (2015) 16(4):436–46. doi: 10.1016/s1470-2045(15)70064-1

17. Page MJ, McKenzie JE, Bossuyt PM, Boutron I, Hoffmann TC, Mulrow CD, et al. The PRISMA 2020 statement: An updated guideline for reporting systematic reviews. *Syst Rev* (2021) 10(1):89. doi: 10.1186/s13643-021-01626-4

18. Zhang F, Liu L, Zhang C, Ji S, Mei Z, Li TO. Association of metabolic syndrome and its components with risk of stroke recurrence and mortality: A meta-analysis. *Neurology* (2021) 97(7):e695–705. doi: 10.1212/WNL.0000000000012415

19. Emens LA, Adams S, Loi S, Schneeweiss A, Rugo HS, Winer EP, et al. IMpassion130: A phase III randomized trial of atezolizumab with nab-paclitaxel for first-line treatment of patients with metastatic triple-negative breast cancer (mTNBC). *J Clin Oncol* (2016) 34(15):TPS1104. doi: 10.1200/JCO.2016.34.15_suppl.TPS1104

20. Brufsky A, Miles D, Zvirbule Z, Eniu A, Lopez-Miranda E, Seo JH, et al. Cobimetinib combined with paclitaxel as first-line treatment for patients with advanced triple-negative breast cancer (COLET study): Primary analysis of cohort I. *Cancer Res* (2018) 78(4). doi: 10.1158/15387445.SABCS17-P5-21-01

21. Kang C, Syed YY. Atezolizumab (in combination with nab-paclitaxel): A review in advanced triple-negative breast cancer. *Drugs* (2020) 80(6):601–07. doi: 10.1007/s40265-020-01295-y

22. Yamamoto J, Murata T, Sugisawa N, Higuchi T, Tashiro Y, Nishino H, et al. Eribulin regresses a cisplatinum-resistant rare-type triple-negative matrix-producing breast carcinoma patient-derived orthotopic xenograft mouse model. *Anticancer Res* (2020) 40(5):2475–79. doi: 10.21873/anticanres.14217

23. Badora-Rybicka A, Kaleta B, Zarudzki L, Sikora-Jopek M, Nowara E. Bevacizumab in the 1st line treatment of triple negative metastatic breast cancer patient-case report and review of the literature. *Nowotwory* (2014) 64(4):321–26. doi: 10.5603/NJO.2014.0053

24. Sharma P, López-Tarruella S, García-Saenz JA, Ward C, Connor CS, Gómez HL, et al. Efficacy of neoadjuvant carboplatin plus docetaxel in triple-negative breast cancer: Combined analysis of two cohorts. *Clin Cancer Res* (2017) 23 (3):649–57. doi: 10.1158/1078-0432.CCR-16-0162

25. Yardley DA, Arrowsmith ER, Daniel BR, Eakle J, Brufsky A, Drosick DR, et al. TITAN: Phase III study of Doxorubicin/Cyclophosphamide followed by ixabepilone or paclitaxel in early-stage triple-negative breast cancer. *Breast Cancer Res Treat* (2017) 164(3):649–58. doi: 10.1007/s10549-017-4285-6

26. Yamamoto N, Boku N, Minami H. Phase I study of larotaxel administered as a 1-h intravenous infusion every 3 weeks to Japanese patients with advanced solid tumours. *Cancer Chemother Pharmacol* (2009) 65(1):129–36. doi: 10.1007/s00280-009-1014-9

27. Yu KD, Ye FG, He M, Fan L, Ma D, Mo M, et al. Effect of adjuvant paclitaxel and carboplatin on survival in women with triple-negative breast cancer: A phase 3 randomized clinical trial. *JAMA Oncol* (2020) 6(9):1390–96. doi: 10.1001/jamaoncol.2020.2965

28. Yardley DA, Brufsky A, Coleman RE, Conte PF, Cortes J, Glück S, et al. Erratum to: 'Phase II/III weekly nab-paclitaxel plus gemcitabine or carboplatin versus Gemcitabine/Carboplatin as first-line treatment of patients with metastatic triple-negative breast cancer (The TnAcity study): Study protocol for a randomized controlled trial. *Trials* (2016) 17:63. doi: 10.1186/s13063-016-1195-6

29. Schmid P, Adams S, Rugo HS, Schneeweiss A, Barrios CH, Iwata H, et al. Atezolizumab and nab-paclitaxel in advanced triple-negative breast cancer. *New Engl J Med* (2018) 379(22):2108–21. doi: 10.1056/NEJMoa1809615

30. Park JO, Lee S, Song SY, Kim K, Kim WS, Jung CW, et al. Measuring response in solid tumors: Comparison of RECIST and WHO response criteria. *Jpn J Clin Oncol* (2003) 33(10):533–37. doi: 10.1093/jjco/hyg093

31. Schwartz LH, Litière S, de Vries E, Ford R, Gwyther S, Mandrekar S, et al. RECIST 1.1-update and clarification: From the RECIST committee. *Eur J Cancer* (2016) 62:132–37. doi: 10.1016/j.ejca.2016.03.081

32. Guyatt GH, Oxman AD, Vist GE, Kunz R, Falck-Ytter Y, Alonso-Coello P, et al. GRADE: An emerging consensus on rating quality of evidence and strength of recommendations. *BMJ* (2008) 336(7650):924–26. doi: 10.1136/bmj.39489.470347.AD

33. Therasse P, Arbuck SG, Eisenhauer EA, Wanders J, Kaplan RS, Rubinstein L, et al. New guidelines to evaluate the response to treatment in solid tumors. European organization for research and treatment of cancer, national cancer institute of the united states, national cancer institute of Canada. *J Natl Cancer Inst* (2000) 92(3):205–16. doi: 10.1093/jnci/92.3.205

34. Bramati A, Girelli S, Torri V, Farina G, Galfrascoli E, Piva S, et al. Efficacy of biological agents in metastatic triple-negative breast cancer. *Cancer Treat Rev* (2014) 40(5):605–13. doi: 10.1016/j.ctrv.2014.01.003

35. Driscoll JJ, Rixe O. Overall survival: Still the gold standard: Why overall sSurvival remains the definitive end point in cancer clinical trials. *Cancer J* (2009) 15(5):401–05. doi: 10.1097/PPO.0b013e3181bdc2e0

36. Oxnard GR, Wilcox KH, Gonen M, Polotsky M, Hirsch BR, Schwartz LH. Response rate as a regulatory end point in single-arm studies of advanced solid tumors. *JAMA Oncol* (2016) 2(6):772–79. doi: 10.1001/jamaoncol.2015.6315

37. Lamm D, Persad R, Brausi M, Buckley R, Witjes JA, Palou J, et al. Defining progression in nonmuscle invasive bladder cancer: It is time for a new, standard definition. *J Urol* (2014) 191(1):20–7. doi: 10.1016/j.juro.2013.07.102

38. Cumpston M, Li T, Page MJ, Chandler J, Welch VA, Higgins JP, et al. Updated guidance for trusted systematic reviews: A new edition of the cochrane handbook for systematic reviews of interventions. *Cochrane Database Syst Rev* (2019) 10:ED000142. doi: 10.1002/14651858.ED000142

39. Cumpston MA-O, McKenzie JE, Welch VA, Brennan SE. Strengthening systematic reviews in public health: Guidance in the cochrane handbook for systematic reviews of interventions, 2nd edition. *J Public Health (Oxf)* (2022), 1741–3850. doi: 10.1093/pubmed/fdac036

40. Forero-Torres A, Lin NU, Liu MC, Rugo HS, Puhalla S, Nanda R, et al. TBCRC 019: An open-label, randomized, phase II trial of nanoparticle albumin-bound paclitaxel with or without the anti-death receptor 5 (DR5) monoclonal antibody tigatuzumab in patients with metastatic, triple-negative (ER, PR, and HER2-negative) breast cancer. *Clin Cancer Res* (2011) 21(12):2722–29. doi: 10.1158/1078-0432.CCR-14-2780

41. Qu H, ZHJ, XL L. Reseach of paclitaxel liposome combined with carboplatin in the treating metastatic triple negative breast cancer. *Med Innovation China* (2014) 15(19):15–8. doi: 10.13558/j.cnki.issn1672-3686.2014.06.007

42. Kim SB, Dent R, Im SA, Espié M, Blau S, Tan AR, et al. Ipatasertib plus paclitaxel versus placebo plus paclitaxel as first-line therapy for metastatic triple-negative breast cancer (LOTUS): A multicentre, randomised, double-blind, placebo-controlled, phase 2 trial. *Lancet Oncol* (2017) 18(10):1360–72. doi: 10.1016/S1470-2045(17)30450-3

43. He JT, Wang W, Zhong HM, Wu YZ, Chen JS, Mo SF. Clinical study on vinorelbine combined with cisplatin vs docetaxel combined with cisplatin in first-line treatment of advanced triple negative breast cancer. *Clin Med Eng* (2018) 25 (12):1613–14. doi: 10.3969/j.issn.1674-4659.2018.12.1613

44. Schmid P, Adams S, Rugo HS, Schneeweiss A, Barrios CH, Iwata H, et al. IMpassion130: Results from a global, randomised, double-blind, phase III study of atezolizumab (atezo) plus nab-paclitaxel (Pab-p) vs placebo plus nab-p in treatment-naive, locally advanced or metastatic triple-negative breast cancer (mTNBC). *Ann Oncol* (2018) 30(3):397–404. doi: 10.1093/annonc/mdy517

45. Zhao SH. Analysis of efficacy of paclitaxel combined with carboplatin in treatment of advanced triple negative breast cancer. *Med Innovation China* (2018) 15(19):15–8.

46. Cortes J, Andre F, Goncalves A, Kummel S, Martin M, Schmid P, et al. IMpassion132 phase III trial: Atezolizumab and chemotherapy in early relapsing metastatic triple-negative breast cancer. *Future Oncol* (2019) 15(17):1951–61. doi: 10.2217/fon-2019-0059

47. Iwata H, Im SA, Sohn J, Jung KH, Im YH, Lee KS, et al. Subgroup analysis of IMpassion1 30: Atezolizumab+Nab-paclitaxel (nab-p) in patients (pts) with advanced triple-negative breast cancer (TNBC) in Asian countries. *Ann Oncol* (2019) 30:ix13–ix4. doi: 10.1093/annonc/mdz418

48. Symonds L, Linden H, Gadi V, Korde L, Rodler E, Gralow J, et al. Combined targeted therapies for first-line treatment of metastatic triple negative breast cancer-a phase II trial of weekly nab-paclitaxel and bevacizumab followed by maintenance targeted therapy with bevacizumab and erlotinib. *Clin Breast Cancer* (2019) 19(2):e283–e96. doi: 10.1016/j.clbc.2018.12.008

49. Ye MR. Study on the effect of gemcitabine combined with cisplatin in the treatment of patients with triple negative advanced breast cancer. *Chin Community Doctors* (2019) 35(35):30–1. doi: 10.3969/j.issn.1007-614x.2019.35.015

50. Narayan P, Wahby S, Gao JJ, Amiri-Kordestani L, Ibrahim A, Bloomquist E, et al. FDA Approval summary: Atezolizumab plus paclitaxel protein-bound for the treatment of patients with advanced or metastatic TNBC whose tumors express PD-L1. *Clin Cancer Res* (2020) 26(10):2284–89. doi: 10.1158/1078-0432.CCR-19-3545

51. Schmid P, Rugo HS, Adams S, Schneeweiss A, Barrios CH, Iwata H, et al. Atezolizumab plus nab-paclitaxel as first-line treatment for unresectable, locally advanced or metastatic triple-negative breast cancer (IMpassion130): Updated efficacy results from a randomised, double-blind, placebo-controlled, phase 3 trial. *Lancet Oncol* (2020) 21(1):44–59. doi: 10.1016/S1470-2045(19)30689-8

52. Brufsky A, Kim SB, Zvirbule Ž, Eniu A, Mebis J, Sohn JH, et al. A phase II randomized trial of cobimetinib plus chemotherapy, with or without atezolizumab, as first-line treatment for patients with locally advanced or metastatic triple-negative breast cancer (COLET): Primary analysis. *Ann Oncol: Off J Eur Soc Med Oncol* (2021) 32(5):652–60. doi: 10.1016/j.annonc.2021.01.065

53. Dent R, Oliveira M, Isakoff SJ, Im SA, Espié M, Blau S, et al. Final results of the double-blind placebo-controlled randomized phase 2 LOTUS trial of first-line ipatasertib plus paclitaxel for inoperable locally Advanced/Metastatic triple-negative breast cancer. *Breast Cancer Res Treat* (2021) 189(2):377–86. doi: 10.1007/s10549-021-06143-45

54. Duan SJ. Efficacy of the combination of abraxane and oxaliplatin in patients with advanced breast cancer and its effects on serum MUC1, CD44v6 and VEGF. *J Clin Exp Med* (2021) 20(22):2416–19.

55. Emens LA, Adams S, Barrios CH, Diéras V, Iwata H, Loi S, et al. First-line atezolizumab plus nab-paclitaxel for unresectable, locally advanced, or metastatic triple-negative breast cancer: IMpassion130 final overall survival analysis. *Ann Oncol: Off J Eur Soc Med Oncol* (2021) 32(8):983–93. doi: 10.1016/j.annonc.2021.05.355

56. Emens LA, Molinero L, Loi S, Rugo HS, Schneeweiss A, Dieras V, et al. Atezolizumab and nab-paclitaxel in advanced triple-negative breast cancer: Biomarker evaluation of the IMpassion130 study. *Jnci-Journal Natl Cancer Inst* (2021) 113(8):1005–16. doi: 10.1093/jnci/djab004

57. Goldstein LJ, Mansutti M, Levy C, Chang JC, Henry S, Fernandez-Perez I, et al. A randomized, placebo-controlled phase 2 study of paclitaxel in combination with reparixin compared to paclitaxel alone as front-line therapy for metastatic triple-negative breast cancer (fRida). *Breast Cancer Res Treat* (2021) 190(2):265–75. doi: 10.1007/s10549-021-06367-5

58. Li B. The value of paclitaxel combined with capecitabine regimen in patients with advanced triple negative breast cancer. *Self Care* (2021) 4):7–8.

59. Lu Y. Clinic effect and safety of SOX regimen in the treatment of advanced triple negative breast cancer. *China Modern Med* (2021) 28(12):105–07. doi: 10.3969/j.issn.1674-4721.2021.12.029

60. Miles D, Gligorov J, André F, Cameron D, Schneeweiss A, Barrios C, et al. Primary results from IMpassion131, a double-blind, placebo-controlled, randomised phase III trial of first-line paclitaxel with or without atezolizumab for unresectable locally Advanced/Metastatic triple-negative breast cancer. *Ann Oncol Off J Eur Soc Med Oncol* (2021) 32(8):994–1004. doi: 10.1016/j.annonc.2021.05.801

61. van Rossum AGJ, Mandjes IAM, van Werkhoven E, van Tinteren H, van Leeuwen-Stok AE, Nederlof P, et al. Carboplatin-cyclophosphamide or paclitaxel without or with bevacizumab as first-line treatment for metastatic triple-negative breast cancer (BOOG 2013-01). *Breast Care (Basel)* (2021) 16(6):598–606. doi: 10.1159/000512200

frontiers | Frontiers in Oncology

TYPE Original Research
PUBLISHED 02 September 2022
DOI 10.3389/fonc.2022.964455

OPEN ACCESS

EDITED BY
San-Gang Wu,
First Affiliated Hospital of Xiamen University, China

REVIEWED BY
Luo Yuhao,
Southwest Medical University, China
Lu Cao,
Shanghai Jiao Tong University, China

*CORRESPONDENCE
Lei Liu
liuleihx@gmail.com

†These authors have contributed equally to this work

SPECIALTY SECTION
This article was submitted to Breast Cancer, a section of the journal Frontiers in Oncology

RECEIVED 08 June 2022
ACCEPTED 15 August 2022
PUBLISHED 02 September 2022

CITATION
Wang X, Zhao J, Xiang Z, Wang X, Zeng Y, Luo T, Yan X, Zhang Z, Wang F and Liu L (2022) 3D-printed bolus ensures the precise postmastectomy chest wall radiation therapy for breast cancer.
Front. Oncol. 12:964455.
doi: 10.3389/fonc.2022.964455

3D-printed bolus ensures the precise postmastectomy chest wall radiation therapy for breast cancer

Xiran Wang[1†], Jianling Zhao[2†], Zhongzheng Xiang[1†], Xuetao Wang[2], Yuanyuan Zeng[1], Ting Luo[1,3], Xi Yan[1,3], Zhuang Zhang[4], Feng Wang[1,3] and Lei Liu[1,3*]

[1]Department of Head and Neck and Mammary Oncology, West China Hospital, Sichuan University, Chengdu, China, [2]Department of Radiotherapy, West China Hospital, Sichuan University, Chengdu, China, [3]Clinical Research Center for Breast, West China Hospital, Sichuan University, Chengdu, China, [4]State Key Laboratory of Oral Diseases, West China Hospital of Stomatology, Sichuan University, Chengdu, China

Purpose: To investigate the values of a 3D-printed bolus ensuring the precise postmastectomy chest wall radiation therapy for breast cancer.

Methods and materials: In the preclinical study on the anthropomorphic phantom, the 3D-printed bolus was used for dosimetry and fitness evaluation. The dosimetric parameters of planning target volume (PTV) were assessed, including D_{min}, D_{max}, D_{mean}, $D_{95\%}$, homogeneity index (HI), conformity index (CI), and organs at risk (OARs). The absolute percentage differences (|%diff|) between the theory and fact skin dose were also estimated, and the follow-up was conducted for potential skin side effects.

Results: In preclinical studies, a 3D-printed bolus can better ensure the radiation coverage of PTV (HI 0.05, CI 99.91%), the dose accuracy (|%diff| 0.99%), and skin fitness (mean air gap 1.01 mm). Of the 27 eligible patients, we evaluated the radiation dose parameter (median(min–max): D_{min} 4967(4789–5099) cGy, D_{max} 5447(5369–5589) cGy, D_{mean} 5236(5171–5323) cGy, $D_{95\%}$ 5053(4936–5156) cGy, HI 0.07 (0.06–0.17), and CI 99.94% (97.41%–100%)) and assessed the dose of OARs (ipsilateral lung: D_{mean} 1341(1208–1385) cGy, V_5 48.06%(39.75%–48.97%), V_{20} 24.55%(21.58%–26.93%), V_{30} 18.40%(15.96%–19.16%); heart: D_{mean} 339(138–640) cGy, V_{30} 1.10%(0%–6.14%), V_{40} 0.38% (0%–4.39%); spinal cord PRV: D_{max} 639(389–898) cGy). The skin doses *in vivo* were D_{theory} 208.85(203.16–212.53) cGy, D_{fact} 209.53(204.14–214.42) cGy, and |%diff| 1.77% (0.89–2.94%). Of the 360 patients enrolled in the skin side effect follow-up study (including the above 27 patients), grade 1 was the most common toxicity (321, 89.2%), some of which progressing to grade 2 or grade 3 (32, 8.9% or 7, 1.9%); the radiotherapy interruption rate was 1.1%.

Conclusion: A 3D-printed bolus can guarantee the precise radiation dose on skin surface, good fitness to skin, and controllable acute skin toxicity, which possesses a great clinical application value in postmastectomy chest call radiation therapy for breast cancer.

KEYWORDS

3D-printed bolus, breast cancer, PMRT, dosimetry, radiation dermatitis

Introduction

Breast cancer is the most common carcinoma that accounts for 30% of female cancers according to the latest statistics conducted by the International Agency for Research on Cancer, with approximately 2.3 million new cases in 2020 (1, 2). Comprehensive treatments including surgery, chemotherapy, radiotherapy, endocrine therapy, and biotherapy are the main therapeutic modalities for breast cancer. Previous studies have shown the mastectomy rates remaining between 30% and 40% (3). Post-mastectomy radiotherapy (PMRT) is associated with a better local control and overall survival benefit in patients with unfavorable pathologic features (4–8).

During the process of radiotherapy, the maximum radiation dose of high-energy X-ray beams can be reached only after they enter the human tissue with a certain depth, which is named built-up effect or skin sparing effect (9–12). Thus, a tissue-equivalent bolus needs to be placed on the skin's surface, aiming to reduce the risk of local recurrence and improve the long-term survival rate in PMRT, such as wet gauze, paraffin wax, thermoplastic board, and so on (13). Although the use of a bolus was controversial due to skin toxicity, a worldwide e-mail survey showed that 82% of Americans and 65% of Australasians were likely to always use a bolus when delivering PMRT. Europeans were significantly more likely to use a bolus for specific indications ($p < 0.0001$) (14–21). Meanwhile, the bolus thickness and frequency of use also vary considerably between centers and are closely related to the incidence and severity of radiation dermatitis. Vu et al. found that 35% of respondents used a <10 mm bolus, most of which (89%) used a thickness of 5 mm (with responses varying from 3 to 8 mm), and the occurrence rate of severe skin reactions was 5%–30% (22). Spierer et al. found that 63.6% developed grade 3–4 skin toxicity in a follow-up study of 118 patients with the daily use of a bolus (the radiotherapy interruption rate was 28%) (23). Pignol et al. recorded acute skin toxicities of 257 patients who received PMRT; the rate of grade 3 toxicity was as high as 47% for the daily use of a 5–10 mm bolus versus only 26% for once every other day use ($p < 0.001$) (16). Another study showed that there was no observed adverse effect by adding a 5 mm bolus on alternate days in the median follow-up of 3.7 years (range 1–6.6 years) (24). In addition to the effect of cumulative dose on the skin surface, smoking history ($p = 0.03$), radiation energy ($p = 0.04$), human race ($p = 0.031$), BMI ($p = 0.043$), and postmenopausal status ($p = 0.004$) were all correlated (14, 16, 25). Thus, the National Comprehensive Cancer Network Guidelines (NCCN, version 4.2022) and the European Society for Radiotherapy & Oncology (ESTRO) recommend that special consideration should be given to the daily use of a 3–5 mm bolus in the setting of PMRT to select cases, especially for inflammatory breast cancer, skin involvement ($T_{4b\text{-}d}$), and positive anterior margin (20, 24, 25).

However, due to the irregular chest wall shape and surgical scar, it is difficult to make the commercial bolus conform perfectively with the skin; in addition, it is also easy to be deformed during radiotherapy, which usually causes air gaps between the bolus and skin (26–29). Some studies have shown that these gaps can lead to inadequate or inhomogeneous radiation doses to the skin, which may further reduce the effect of PMRT (30–34). The emerging three-dimensional (3D) printing technology offers alternative fabrication ways for an ideal patient-specific bolus, which can further optimize the effectiveness of radiotherapy (35–40). Previous studies have revealed that the patient-specific bolus reduces unnecessary irradiation to the healthy normal tissues and improves the conformity of radiation distribution for patients with irregular surface contours and varying target depths (35, 41–46). Even though a 3D-printed bolus has been gradually applied in superficial tumor radiotherapy, the clinical application of PMRT still remains spare (26, 28). This study used the patient-specific 3D-printed bolus for PMRT and evaluated the dosimetric characteristics, skin fitness, and skin adverse effects of the 3D-printed bolus, hoping to achieve improved results by ensuring a more precise radiotherapy for breast cancer patients.

Material and methods

3D-printed bolus design and fabrication

The desired bolus area for radiotherapy was marked on the anthropomorphic phantom or patient. The chest contour was created based on the computed tomography (CT) scan, which is

then expanded by the desired thickness of the bolus and subtracted from the expansion. CT images in the general digital imaging and communications in medicine (DICOM) format were exported as a stereolithography (STL) file, which was loaded into a 3D-modeling software (Mimics 10.01) to create a patient-specific bolus (Supplementary Table 1 and Figure 1). It should be noted that in order to reduce the positioning error, we developed the positioning fixator connecting the vacuum bag and the bolus; the manufacturing process of the 3D-printed bolus (thickness: 5 mm) is shown in Supplementary Figure 2.

In order to ensure that the 3D-printed bolus highly fits with the skin to further assure the radiotherapy quality, the following aspects were noted: first, a connecting fixing device was designed between the axillary side of the bolus and the vacuum bag to prevent the bolus from shifting; second, cone beam computed tomography (CBCT) was daily used to verify the reproducibility of bolus placement; third, the 3D-printed bolus was remade if necessary.

Participant population

We selected patients according to the following criteria: women aged 18–70 years who underwent radical mastectomy and primary chest wall radiotherapy, patients with $_pT_{3-4}$ or $_pN_{2-3}$ stage, one to three axillary lymph nodes positive at the $_pT_{1-2}$ stage with high-risk factors (age ≤40 years, estrogen receptor and progesterone receptor negative (ER-/PR-), human epidermal growth factor receptor 2 overexpression (HER2+++), histologic grade III (G3), lymphovascular invasion (LVI), etc.). Patients receiving radiotherapy with a commercially available bolus or without a bolus, with recurrent or metastatic disease, or previously treated, were excluded.

Dosimetric evaluation

A radiotherapist delineated the clinical target volume (CTV): the upper border was the clinically visible/palpable one and not exceeding the sternoclavicular joint (~2nd rib), the lower border was the inferior margin of the contralateral breast on CT, the anterior border extended to the skin, the posterior border included the pectoralis muscles and ribs, and the medial and lateral borders were sternum and mid-axillary line (excluding latissimus dorsi) and the organs at risk (OARs) in the RayStation treatment planning system (TPS) (version4.7.5; RaySearch Laboratories AB, Stockholm, Sweden) (47, 48). The intensity modulated radiation therapy (IMRT) within six-field irradiations was used in PMRT. The inner and outer tangential field was used in the chest wall, and the angle of increasing field was within ±15° based on the spatial relationship between the target area and the organs at risk. Pairs of penetrating field were added in the locking segment based on the radiating field of the chest wall. The angles of the radiating field of the left and right breasts were 340° and 160°, respectively, and 20° and 200°, respectively. Number of segments: 48. The maximum field area is 4 mm^2, and the maximum field hop number is 4 MU. All treatment plans are designed in the RayStation TPS (Figure 1), with a 6 MV photon beam and a collapsed cone algorithm. The dose grid size is 0.3 * 0.3 * 0.3 cm. The prescribed doses were PCTVsc (the supra- and infra-clavicular regions) and PCTVcw (the ipsilateral chest wall) 50 Gy/25 f, and doses were normalized to at least 95% target volume meeting the prescribed dose requirements (49–51). The dosimetric parameters of the planning target volume (PTV: defined as the CTVs with a 5 mm margin) were evaluated as follows: D_{min}, D_{max}, D_{mean}, $D_{95\%}$, homogeneity index (HI = $(D_{2\%}-D_{98\%})/D_{50\%}$), conformity index (CI), absolute percentage differences ($|\%diff|=|100x\ (D_{fact}- D_{theory})/D_{theory}|$) for single fraction; OARs: ipsilateral lung (D_{mean}, V_5, V_{20}, V_{30}), heart (D_{mean}, V_{30}, V_{40}), and spinal cord PRV(D_{max}) (31, 49, 52).

In vivo skin dose measurement

GafChromic EBT3 (International Specialty Products, Wayne, NJ, USA) had been proven to be suitable for absorbed dose measurement in radiotherapy (53), which was used in our study due to its thin structures, easily cutting to small size and near-tissue equivalence. To accurately position the EBT3 films, beam's eye view (BEV) at a gantry angle of 0 degree with PTV and body contours on show was printed on a paper with a scale of 1:1 to a real patient. The PTV contour was divided into eight sub-regions by four rows and two columns, with rows toward left–right and columns toward cranial–caudal directions. Eight 3 × 2 cm^2 rectangles were drawn and marked with numbers 1, 2,…, 8 in the center of each sub-region, respectively (Supplementary Figure 3). EBT3 film pieces with a fixed size of 3 × 2 cm^2 were cut from the same batch. For each patient, eight film pieces coded with numbers 1, 2,…, 8 were taped on the chest wall at the positions corresponding to the eight rectangles and covered by the 3D-printed bolus. For the sub-region where the patient's surface was very unsmooth, particularly in the region near the axilla, the 3 × 2 cm^2 film piece was replaced by a smaller one with a size of 2 × 1.5 cm^2.

Every patient's irradiated films with two reference films together were scanned by an Epson 11000XL scanner 24 h after irradiation. The two reference films—one was unexposed and the other was exposed to a known dose immediately after *in vivo* measurement—were used to rescale the calibration function to fit the responses of that specific scan. Software FilmQA Pro 2016 was used to analyze the measurement results. The film absorbed dose was achieved by averaging the reading of a region of interest (ROI) with 1 × 1 cm^2 at the center of each film piece.

The calculated surface doses were obtained in TPS. For every patient, eight ROIs in the center of each sub-region with a size of

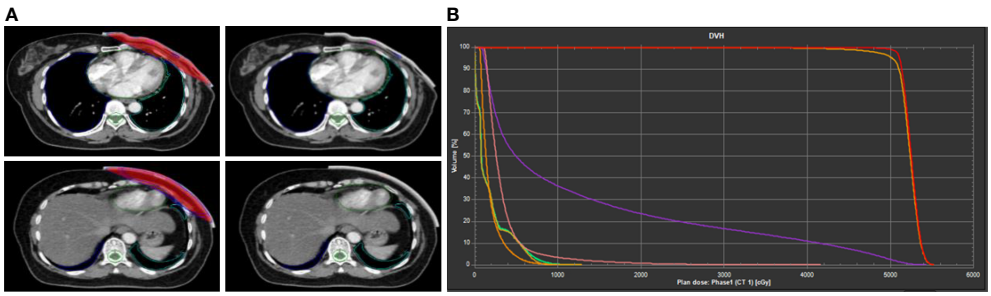

FIGURE 1
Example of dose distribution of 3D-printed bolus in treatment planning system (TPS). **(A)** Delineation of radiotherapy target area. **(B)** The dose–volume histogram (DVH) curve.

1 × 0.1 cm between the 3D-printed bolus and the patient skin across three-slice CT images were contoured (an example of the ROI contour is shown in Figure 2). The average dose of each ROI was recorded and compared with the measurement dose.

Skin toxicity

All patients referred for PMRT were visited weekly during and after 2–4 weeks of radiotherapy to assess and record skin toxicities. To ensure consistency and accuracy in the classification of acute skin side effect, the follow-up photographs of the skin (Supplementary Figure 4) were evaluated by two or three radiotherapists to determine the grading (according to the Radiation Therapy Oncology Group (RTOG)) (54). For cases with uncertain grading results, a dermatological consultation with the patient might be requested. The occurring time of skin side effect including dry or moist desquamation and the degree of erythema were evaluated. Based on the RTOG classification, the main difference between grades 2 and 3 was the presence of moist desquamation and tenderness, while grade 4 was defined as necrosis, ulceration, or bleeding.

During radiotherapy, skin care includes the following: keeping the irradiated chest wall dry, avoiding skin scratching, medical ray protection sprays, and corticosteroids or topical dressings used for excessive inflammation; antibiotics were used when necessary.

Result

Preclinical evaluation

The theoretical radiation dose of the chest wall reached the targeted values (mean value): D_{min} 4932 cGy, D_{max} 5259 cGy,

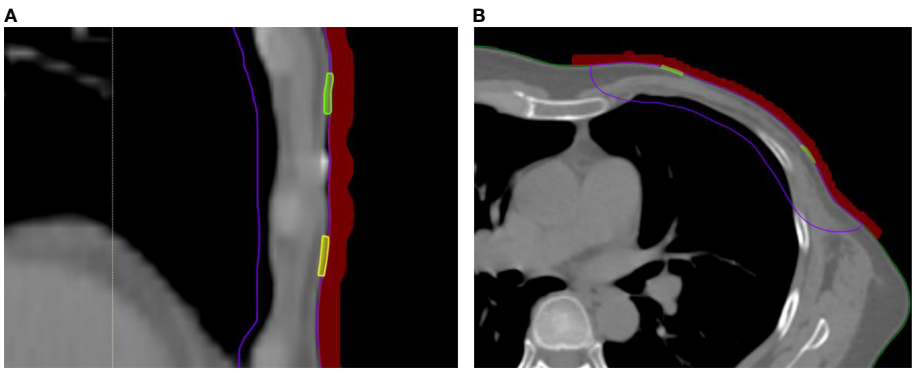

FIGURE 2
In-vivo skin doses measurement in RayStation TPS. **(A)** Coronal scan with bolus covering small film. **(B)** Cross-sectional scan with bolus covering small film.

D_{mean} 5131 cGy, $D_{95\%}$ 5021 cGy, HI 0.05, CI 99.91%. Meanwhile, there was a strict limit on the OARs in TPS: the D_{mean} values of the ipsilateral lung and heart were 1017 and 438 cGy, respectively, the D_{max} value of the spinal cord PRV was 88 cGy (Table 1). The mean D_{fact} and D_{theory} of the skin surface were 204.59 and 204.73 cGy, respectively, and the mean |%diff| was 0.99%. In addition, we also observed that the 3D-printed bolus was highly attached to the skin, and the mean air gap at the dosimetry point on the skin surface was only 1.01 mm (Supplementary Table 2).

Clinical evaluation

Patient population

Finally, we totally involved 360 patients in this study from October 2019 to July 2021 (Table 2), in which 27 patients were selected to study dosimetric parameters; the median age was 49 (24–70) years old. The lesions were mostly in the left breast (199 of 360, 55.3%). There were 24.7% (89 of 360) or 50.3% (181 of 360) of the patients with advanced pathologic stages $T_{3\text{-}4}$ or $N_{2\text{-}3}$. In addition, 39.4% (142 of 360) of the patients with early $pT_{1\text{-}2}N_1$ had at least one (85 of 142, 59.9%) and up to four (1 of 142, 0.7%) risk factors, including age ≤40 years (20 patients), ER-/PR- (42 patients), HER2+++ (59 patients), G3 (70 patients), and LVI (22 patients), in which 42 patients had two risk factors and 14 patients had three risk factors. In the tumor-node-metastasis (TNM)-based staging (8th Edition of the American Joint Committee on Cancer (AJCC) publications), patients with stage III disease accounted for the majority (217 of 360, 60.3%), in which 27.5% (99 of 360), 8.9% (32 of 360), and 23.9% (86 of 360) of the patients had stage A, B, and C, respectively. The next largest number of patients belonging to IIB was 29.6% (107 of 360). Postoperative breast reconstruction was rare, only 11.4% (41 of 360) of the patients; the rest of the patients did not undergo breast reconstruction (319 of 360, 88.6%).

Dosimetric parameters evaluation in 27 patients

The dose coverage in the target area met the prescription dose requirements in TPS: median dose(range): D_{min} 4967 (4789–5099) cGy, D_{max} 5447(5369–5589) cGy, and D_{mean} 5236 (5171–5323) cGy; $D_{95\%}$ of the target volume ranged from 4936 to 5156 cGy. The CI and HI were 99.94% (97.41%–100%) and 0.07(0.06–0.17), respectively (Supplementary Table 3). The actual radiation dose on the skin surface was very close to the theory value; the median theoretical and actual radiation doses were 208.85(203.16–212.53) cGy and 209.53(204.14–214.42) cGy, respectively, and the |%diff| ranged between 0.89% and 2.94%, with median 1.77% (Table 3). In addition, the dose of OARs is illustrated in Supplementary Table 4. The median D_{mean} of the ipsilateral lung was 1341(1208–1385) cGy; the $V_{5\%}$, $V_{20\%}$ and $V_{30\%}$ of the target volume were 48.06% (39.75%–48.97%), 24.55% (21.58%–26.93%), and 18.40% (15.96%–19.16%), respectively. The D_{mean} of the heart was 339 (138–640) cGy, with V_{30} 1.10% (0%–6.14%) and V_{40} 0.38% (0%–4.39%). The median D_{max} of the spinal cord PRV was 639(389–898) cGy.

Skin toxicity

All the 360 patients were followed up for skin toxicity study during the radiotherapy (Table 4). The most common skin toxicity was grade 1 (321 of 360, 89.2%), presenting as faint erythema (229 of 321,71.4%) or dry desquamation (54 of 321, 16.8%) or both (38 of 321, 11.8%). With the accumulation of radiation dose (especially during 21–25 fractions), the number of

TABLE 1 Dosimetry evaluation of anthropomorphic phantom with 3D-printed bolus .

PTV	Mean value	OARs		Mean value
*D_{min}, cGy	4932	Ipsilateral lung	D_{mean}, cGy	1017
D_{max}, cGy	5259		V_5	38.80%
$D_{mean,}$ cGy	5131		V_{20}	19.56%
$D_{95\%}$, cGy	5021		V_{30}	12.54%
$D_{2\%}$, cGy	5251	Heart	D_{mean}, cGy	438
$D_{98\%}$, cGy	4977		V_{30}	1.42%
$D_{50\%}$, cGy	5134		V40	0.30%
HI	0.05	Spinal Cord	D_{max}, cGy	81
CI	99.91%	Spinal Cord PRV	D_{max}, cGy	88

3D, three-dimensional; PTV, planning target volume; HI, homogeneity index (($D_{2\%}$-$D_{98\%}$)/$D_{50\%}$); CI, conformity index; PRV, planning organs at risk volume.
*D_{min}, minimum dose of the target volume; D_{max}, maximum dose of the target volume; D_{mean}, mean dose of the target volume; $D_{95\%}$, the dose that covers 95% of the target volume.

TABLE 2 Patient characteristics.

	Skin follow-up (n = 360)
Age (years)	
Median (range)	49 (24–70)
Lesion sites	
Left, n (%)	199 (55.3%)
Right, n (%)	161 (44.7%)
pT_{3-4}-stage	
T_3, n (%)	41 (11.4%)
T_4, n (%)	48 (13.3%)
pN_{2-3}-stage	
N_2, n (%)	95 (26.4%)
N_3, n (%)	86 (23.9%)
$pT_{1-2}N_1$, n (%)	142 (39.4%)
age ≤40 y, n	20
ER-/PR-, n	42
HER2+++, n	59
G3, n	70
LVI, n	22
Tumor stage	
IIA, n (%)	36 (10.0%)
IIB, n (%)	107 (29.7%)
IIIA, n (%)	99 (27.5%)
IIIB, n (%)	32 (8.9%)
IIIC, n (%)	86 (23.9%)
Breast Reconstruction	
With, n (%)	41 (11.4%)
Without, n (%)	319 (88.6%)

pT-stage, pathologic tumor stages; pN-stage, pathologic node stages; G3, histologic grade III; LVI, lymphovascular invasion; ER-,estrogen receptor negative; PR-, progesterone receptor negative; HER2+++, human epidermal growth factor receptor 2 overexpression.

patients with the above symptoms was also gradually increasing (84 of 229, 36.7%; 24 of 54, 44.5%; 21 of 38, 55.3%). With a small number of patients progressing to grade 2 (32 of 360, 8.9%), all patients presented moderate erythema (MER), in which 56.2% or 28.2% of the patients had accompanied patchy moist desquamation (PMD) (18 of 32) or moderate edema (MED) (9 of 32) that occurred after 21 fractions (14 of 18, 77.8%; 7 of 9, 77.8%); others presented large areas of MER and MED, with PMD at the folds of the skin, but the number of patients was relatively small (5 of 32, 15.6%). The incidence of grade 3 was relatively low (7 of 360, 1.9%); most patients present confluent moist desquamation (CMD) and pitting edema (PE) (5 of 7, 71.4%); treatment was discontinued in four patients because they developed during radiotherapy (1.1%). There was no grade 4 occurrence (0 of 360). The most severe reactions usually occur in the 2–4 weeks after completion of radiotherapy treatment (Table 5). The incidence of grades 2–4 acute radiation dermatitis was 41.67%, of which 64.7% were grade 2 that presented as complex lesions (moderate erythema with edema, patchy moist desquamation at the skin fold). Grade 4 events (mainly ulcers) occurred in 4.4% of the patients, and all got well again after topical corticosteroids and dressing therapy combined with antibiotics.

Discussion

In this study, the largest of its kind, we illustrated that the use of the 3D-printed bolus brought many advantages in postmastectomy chest wall radiation therapy for breast cancer, such as reducing the air gaps between the bolus and the skin, improving the dose uniformity, and ensuring the skin surface radiation dose, which might further guarantee the precise PMRT for breast cancer.

Generally speaking, unwanted air gaps lead to an inadequate or inhomogeneous radiation dose, which causes a considerable difficulty for the precise postmastectomy chest wall radiation therapy for breast cancer (30). Butson and Khan et al. reported that the dose for high-energy X-ray beam was decreased by up to 4% and 10% because of 4 and 10 mm air gaps, respectively (33, 55). Zhao et al. reported that 11 mm air gap under the commercial bolus obviously decreased the skin surface dose by about 2% (56). Similarly, James L. Robar et al. found that the air gaps of more than 5 mm were decreased from 30% (commercial bolus) to 13% (3D-printed bolus) ($p < 0.0003$), and the maximum air gaps diminished from 5 ± 3 to 3 ± 3 mm (26). Our study showed that the unwanted air gaps were reduced to as low as 1.01 mm contacting better with the patient's irregular skin surface. Accurate fitting of the bolus to the patient skin is important, and thus, our study pointed out that customized 3D-printed boluses with better fitting are suitable for clinical applications.

Furthermore, our personalized 3D-printed bolus provided an optimal dose distribution, with HI lower than 0.07 and CI >99.9%. However, the HI of the commercial bolus was 0.15 in the study of Zhang et al., which greatly reduced the effectiveness of radiotherapy (26). Hou and Park et al. also found that the 3D-printed bolus improved dose uniformity by 45% and improved the precision of the dose absorbed by the chest wall to 3% (28, 57). However, the HI and CI in their studies still did not reach a lower value. In our study, we used IMRT technology and a positioning fixation device to reduce positioning error, improve the dose uniformity, ensure skin surface radiation dose, and maximize precision radiotherapy. In addition, the actual radiotherapy dose of the skin was almost close to the theoretical dose (D_{theory} 208.85 (203.16-212.53) cGy, D_{fact} 209.53 (204.14-214.42) cGy, |%diff| 1.77% (0.89-2.94%)). This result was obviously better than the traditional bolus in the study of Park et al. whose |%diff| was 4.43% (28).

It is worthy to note that although the 3D-printed chest wall bolus has obvious dosimetric advantages, radiodermatitis is one of the distressing side effects that manifested as erythema or moist desquamation even. Although most radiodermatitis is

TABLE 3 Dose accuracy verification on skin surface of the 27 patients.

	*D_{fact} (cGy)	D_{theory} (cGy)	|%diff| (%)
P1	213.30	211.31	0.94
P2	209.53	208.52	0.48
P3	206.37	203.16	1.58
P4	208.40	205.86	1.23
P5	211.01	209.38	0.78
P6	207.71	208.41	0.34
P7	209.57	210.86	0.61
P8	205.29	204.55	0.36
P9	210.66	212.53	0.88
P10	212.18	209.03	1.51
P11	211.63	209.92	0.81
P12	210.70	211.09	0.18
P13	208.51	207.75	0.37
P14	204.44	204.83	0.19
P15	204.99	206.63	0.79
P16	209.53	207.75	0.86
P17	208.46	208.80	0.16
P18	207.51	206.73	0.38
P19	214.11	211.01	1.47
P20	212.51	208.42	1.96
P21	209.61	208.92	0.33
P22	212.90	208.59	2.07
P23	204.14	206.03	0.92
P24	211.46	211.59	0.06
P25	205.04	209.14	1.96
P26	208.94	210.67	0.82
P27	214.42	211.36	1.45
Median (min-max)	209.53 (204.14-214.42)	208.85 (203.16-212.53)	1.77 (0.89-2.94)

*D_{theory}, theoretical radiation dose for chest wall skin; D_{fact}, fact radiation dose for chest wall skin; |%diff| (the absolute percentage difference=|100x (D_{fact}- D_{theory})/D_{theory}|), the absolute differences between theoretical and fact doses at the skin surface.

TABLE 4 Skin toxicity during radiotherapy.

	≤10f	11-15f	16-20f	21-25f	Total patient
Grade 1, n (%)					321(89.2%)
Faint erythema, n (%)	32 (13.9%)	48 (20.9%)	65 (28.5%)	84 (36.7%)	229 (71.4%)
Dry desquamation, n (%)	6 (11.1%)	7 (12.9%)	17 (31.5%)	24 (44.5%)	54 (16.8%)
Both, n (%)	1 (2.6%)	4 (10.5%)	12 (31.6%)	21 (55.3%)	38 (11.8%)
Grade 2, n (%)					32(8.9%)
PMD+MER, n (%)	0	0	4 (22.2%)	14 (77.8%)	18 (56.2%)
MER+MED, n (%)	0	0	2 (22.2%)	7 (77.8%)	9 (28.2%)
PMD+MER+MED, n (%)	0	0	0	5 (100%)	5 (15.6%)
Grade 3, n (%)					7 (1.9%)
PE, n (%)	0	0	1 (50%)	1 (50%)	2 (28.6%)
PE+CMD, n (%)	0	0	0	5 (100%)	5 (71.4%)
Grade 4, n (%)	0	0	0	0	0
Treatment interruption, n (%)	0	0	2 (50%)	2 (50%)	4 (1.1%)

PMD, patchy moist desquamation; MER, moderate erythema; MED, moderate edema; CMD, confluent moist desquamation; PE, pitting edema.

TABLE 5 Skin toxicity during and after 2–4 weeks of radiotherapy.

	During the radiotherapy	2–4 weeks after radiotherapy
Grade 1	321 (89.12%)	210 (58.33%)
Grade 2	32 (8.89%)	97 (26.94%)
Grade 3	7 (1.94%)	37 (10.28%)
Grade 4	0	16 (4.4%)

reversible, it commonly causes discomfort and may bring about treatment interruption. Therefore, we have taken some measures to further reduce the incidence of radioactive dermatitis, such as skin care education for patients before radiotherapy, including keeping the irradiated chest wall dry; avoiding skin scratching; and using medical ray protection sprays, corticosteroids, or topical dressings appropriately; antibiotics were used when necessary, and so on. In this current study, the skin side effect incidences of grade 1 (321 of 360, 89.2%), grade 2 (32 of 360, 8.9%), and grade 3 (7 of 360, 1.9%) were controllable during the radiotherapy, which was similar to the incidence of radiation dermatitis caused by a traditional bolus reported by Anderson and Tieu et al. whose ≥2 grade dermatitis was 9%–24% (15, 58). However, in our study, fewer patients (4 of 360, 1.1%) had to discontinue treatment because of more unacceptable skin toxicity than Tieu's (20 of 254, 7.9%) (15). We speculated that it was the patient skin care education before radiotherapy and strict follow-up that, to a certain extent, guaranteed the patient's compliance to the whole treatment.

However, our study presents several limitations. Firstly, the study was a single-arm, single-center clinical study; the results need to be further verified in a multicenter study in the future. Secondly, since this study paid more attention to the 3D-printed bolus ensuring the precise postmastectomy chest wall radiation therapy for breast cancer, quality of patient life assessments may have been overlooked. Thirdly, the follow-up time was only limited in the radiation period, and there needs to be longer follow-up time for the 3D-printed bolus' effect on locoregional control and patient survival.

Conclusion

The new 3D-printed chest wall bolus owns a high degree of personalization, good radiation dosimetric advantages, and controllable skin toxicity, which has a relatively high clinical application value. In the future, long-term follow-up will be continued to evaluate the patient's local recurrence and survival so as to comprehensively evaluate the efficacy of the 3D-printed bolus in PMRT. Meanwhile, we will explore new 3D-printed bolus materials with higher quality and lower price, and seek the best application times to ensure the curative effect of radiotherapy.

Data availability statement

The original contributions presented in the study are included in the article/supplementary material. Further inquiries can be directed to the corresponding author.

Ethics statement

Written informed consent was obtained from the individual(s) for the publication of any potentially identifiable images or data included in this article.

Author contributions

XRW, JLZ and ZZX who write the manuscript and are responsible for statistical analysis have contributed equally to this work. XTW and YYZ are responsible for guiding the writing the paper. TL, XY, ZZ and FW take charge of recruiting patients. Liu Lei is responsible for the overall revision. All authors contribute to the article and approve the submitted version.

Funding

This research was supported by Ministry of Science and Technology of Sichuan Province (Grant No. 2019YFS0362).

Acknowledgments

We thank our colleagues for the critical reading of the manuscript.

Conflict of interest

The authors declare that the research was conducted in the absence of any commercial or financial relationships that could be construed as a potential conflict of interest.

Publisher's note

References

1. Siegel RL, Miller KD, Jemal A. Cancer statistics, 2020. *CA Cancer J Clin* (2020) 70(1):7–30. doi: 10.3322/caac.21590

2. Sung H, Ferlay J, Siegel RL, Laversanne M, Soerjomataram I, Jemal A, et al. Global cancer statistics 2020: GLOBOCAN estimates of incidence and mortality worldwide for 36 cancers in 185 countries. *CA Cancer J Clin* (2021) 71(3):209–49. doi: 10.3322/caac.21660

3. McGuire KP, Santillan AA, Kaur P, Meade T, Parbhoo J, Mathias M, et al. Are mastectomies on the rise? a 13-year trend analysis of the selection of mastectomy versus breast conservation therapy in 5865 patients. *Ann Surg Oncol* (2009) 16 (10):2682–90. doi: 10.1245/s10434-009-0635-x

4. Overgaard M, Jensen MB, Overgaard J, Hansen PS, Rose C, Andersson M, et al. Postoperative radiotherapy in high-risk postmenopausal breast-cancer patients given adjuvant tamoxifen: Danish breast cancer cooperative group DBCG 82c randomised trial. *Lancet* (1999) 353(9165):1641–8. doi: 10.1016/S0140-6736(98)09201-0

5. Boulle G, Saint-Martin C, de la Lande B, Laki F, Bidoz NF, Berger F, et al. Photons without bolus versus electrons with bolus after upfront mastectomy without immediate reconstruction in breast cancer patients. *Int J Radiat Oncol Biol Phys* (2019) 104(4):877–84. doi: 10.1016/j.ijrobp.2019.03.029

6. Recht A, Edge SB, Solin LJ, Robinson DS, Estabrook A, Fine RE, et al. Postmastectomy radiotherapy: clinical practice guidelines of the American society of clinical oncology. *J Clin Oncol Off J Am Soc Clin Oncol* (2001) 19(5):1539–69. doi: 10.1200/JCO.2001.19.5.1539

7. Damast S, Ho AY, Montgomery L, Fornier MN, Ishill N, Elkin E, et al. Locoregional outcomes of inflammatory breast cancer patients treated with standard fractionation radiation and daily skin bolus in the taxane era. *Int J Radiat Oncol Biol Phys* (2010) 77(4):1105–12. doi: 10.1016/j.ijrobp.2009.06.042

8. Peng X, Wei Z, Gerweck LE. Making radiation therapy more effective in the era of precision medicine. *Precis Clin Med* (2020) 3(4):272–83. doi: 10.1093/pcmedi/pbaa038

9. Dogan N, Glasgow GP. Surface and build-up region dosimetry for obliquely incident intensity modulated radiotherapy 6 MV x rays. *Med Phys* (2003) 30 (12):3091–6. doi: 10.1118/1.1625116

10. Behrens CF. Dose build-up behind air cavities for Co-60, 4, 6 and 8 MV. *Measurements Monte Carlo Simulations Phys Med Biol* (2006) 51(22):5937–50. doi: 10.1088/0031-9155/51/22/015

11. Xiang HF, Song JS, Chin DW, Cormack RA, Tishler RB, Makrigiorgos GM, et al. Build-up and surface dose measurements on phantoms using micro-MOSFET in 6 and 10 MV x-ray beams and comparisons with Monte Carlo calculations. *Med Phys* (2007) 34(4):1266–73. doi: 10.1118/1.2710951

12. Hou Y, Song Y, Sun X, Jiang Y, He M, Li Y, et al. Multifunctional composite hydrogel bolus with combined self-healing, antibacterial and adhesive functions for radiotherapy. *J Mater Chem B* (2020) 8(13):2627–35. doi: 10.1039/c9tb02967b

13. Demaria S, Golden EB, Formenti SC. Role of local radiation therapy in cancer immunotherapy. *JAMA Oncol* (2015) 1(9):1325–32. doi: 10.1001/jamaoncol.2015.2756

14. Wright JL, Takita C, Reis IM, Zhao W, Lee E, Hu JJ. Racial variations in radiation-induced skin toxicity severity: data from a prospective cohort receiving postmastectomy radiation. *Int J Radiat Oncol Biol Phys* (2014) 90(2):335–43. doi: 10.1016/j.ijrobp.2014.06.042

15. Tieu MT, Graham P, Browne L, Chin YS. The effect of adjuvant postmastectomy radiotherapy bolus technique on local recurrence. *Int J Radiat Oncol Biol Phys* (2011) 81(3):e165–71. doi: 10.1016/j.ijrobp.2011.01.002

16. Pignol JP, Vu TT, Mitera G, Bosnic S, Verkooijen HM, Truong P. Prospective evaluation of severe skin toxicity and pain during postmastectomy radiation therapy. *Int J Radiat Oncol Biol Phys* (2015) 91(1):157–64. doi: 10.1016/j.ijrobp.2014.09.022

17. Hui Z, Li Y, Yu Z, Liao Z. Survey on use of postmastectomy radiotherapy for breast cancer in China. *Int J Radiat Oncol Biol Phys* (2006) 66(4):1135–42. doi: 10.1016/j.ijrobp.2006.06.053

18. Nichol A, Narinesingh D, Raman S, Germain F, Chan EK, Tran E, et al. The effect of bolus on local control for patients treated with mastectomy and radiation therapy. *Int J Radiat Oncol Biol Phys* (2021) 110(5):1360–9. doi: 10.1016/j.ijrobp.2021.01.019

19. Turner JY, Zeniou A, Williams A, Jyothirmayi R. Technique and outcome of post-mastectomy adjuvant chest wall radiotherapy-the role of tissue-equivalent bolus in reducing risk of local recurrence. *Br J Radiol* (2016) 89(1064):20160060. doi: 10.1259/bjr.20160060

20. Kaidar-Person O, Dahn HM, Nichol AM, Boersma LJ, de Ruysscher D, Meattini I, et al. A Delphi study and international consensus recommendations: The use of bolus in the setting of postmastectomy radiation therapy for early breast cancer. *Radiother Oncol* (2021) 164:115–21. doi: 10.1016/j.radonc.2021.09.012

21. Dahn HM, Boersma LJ, de Ruysscher D, Meattini I, Offersen BV, Pignol JP, et al. The use of bolus in postmastectomy radiation therapy for breast cancer: A systematic review. *Crit Rev Oncol Hematol* (2021) 163:103391. doi: 10.1016/j.critrevonc.2021.103391

22. Vu TT, Pignol JP, Rakovitch E, Spayne J, Paszat L. Variability in radiation oncologists' opinion on the indication of a bolus in post-mastectomy radiotherapy: an international survey. *Clin Oncol (R Coll Radiol) Mar* (2007) 19(2):115–9. doi: 10.1016/j.clon.2006.10.004

23. Spierer MM, Hong LX, Wagman RT, Katz MS, Spierer RL, McCormick B. Postmastectomy CT-based electron beam radiotherapy: dosimetry, efficacy, and toxicity in 118 patients. *Int J Radiat Oncol Biol Phys* (2004) 60(4):1182–9. doi: 10.1016/j.ijrobp.2004.04.044

24. Kaidar-Person O, Vrou Offersen B, Hol S, Arenas M, Aristei C, Bourgier C, et al. ESTRO ACROP consensus guideline for target volume delineation in the setting of postmastectomy radiation therapy after implant-based immediate reconstruction for early stage breast cancer. *Radiother Oncol* (2019) 137:159–66. doi: 10.1016/j.radonc.2019.04.010

25. van der Velden J, Willmann J, Spalek M, Oldenburger E, Brown S, Kazmierska J, et al. ESTRO ACROP guidelines for external beam radiotherapy of patients with uncomplicated bone metastases. *Radiother Oncol* (2022) 173:197–206. doi: 10.1016/j.radonc.2022.05.024

26. Robar JL, Moran K, Allan J, Clancey J, Joseph T, Chytyk-Praznik K, et al. Intrapatient study comparing 3D printed bolus versus standard vinyl gel sheet bolus for postmastectomy chest wall radiation therapy. *Pract Radiat Oncol* (2018) 8 (4):221–9. doi: 10.1016/j.prro.2017.12.008

27. Park SY, Choi CH, Park JM, Chun M, Han JH, Kim JI. A patient-specific polylactic acid bolus made by a 3D printer for breast cancer radiation therapy. *PloS One* (2016) 11(12):e0168063. doi: 10.1371/journal.pone.0168063

28. Park K, Park S, Jeon MJ, Choi J, Kim JW, Cho YJ, et al. Clinical application of 3D-printed-step-bolus in post-total-mastectomy electron conformal therapy. *Oncotarget* (2017) 8(15):25660–8. doi: 10.18632/oncotarget.12829

29. Mayer HF. The use of a 3D simulator software and 3D printed biomodels to aid autologous breast reconstruction. *Aesthetic Plast Surg* (2020) 44(5):1396–402. doi: 10.1007/s00266-020-01733-y

30. Boman E, Ojala J, Rossi M, Kapanen M. Monte Carlo Investigation on the effect of air gap under bolus in post-mastectomy radiotherapy. *Phys Med* (2018) 55:82–7. doi: 10.1016/j.ejmp.2018.10.023

31. Michiels S, Barragan AM, Souris K, Poels K, Crijns W, Lee JA, et al. Patient-specific bolus for range shifter air gap reduction in intensity-modulated proton therapy of head-and-neck cancer studied with Monte Carlo based plan optimization. *Radiother Oncol* (2018) 128(1):161–6. doi: 10.1016/j.radonc.2017.09.006

32. Sharma SC, Johnson MW. Surface dose perturbation due to air gap between patient and bolus for electron beams. *Med Physics* (1993) 20(2):377–8. doi: 10.1118/1.597079

33. Butson MJ, Cheung T, Yu P, Metcalfe P. Effects on skin dose from unwanted air gaps under bolus in photon beam radiotherapy. *Radiat Measurements* (2000) 32 (3):201–4. doi: 10.1016/S1350-4487(99)00276-0

34. Kong M, Holloway L. An investigation of central axis depth dose distribution perturbation due to an air gap between patient and bolus for electron beams. *Australas Phys Eng Sci Med* (2007) 30(2):111–9. doi: 10.1007/BF03178415

35. Su S, Moran K, Robar JL. Design and production of 3D printed bolus for electron radiation therapy. *J Appl Clin Med Phys* (2014) 15(4):4831. doi: 10.1120/jacmp.v15i4.4831

36. Canters RA, Lips IM, Wendling M, Kusters M, van Zeeland M, Gerritsen RM, et al. Clinical implementation of 3D printing in the construction of patient specific bolus for electron beam radiotherapy for non-melanoma skin cancer. *Radiother Oncol* (2016) 121(1):148–53. doi: 10.1016/j.radonc.2016.07.011

37. Arenas M, Sabater S, Sintas A, Arguis M, Hernandez V, Arquez M, et al. Individualized 3D scanning and printing for non-melanoma skin cancer brachytherapy: a financial study for its integration into clinical workflow. *J Contemp Brachythер* (2017) 9(3):270–6. doi: 10.5114/jcb.2017.68134

38. Lukowiak M, Jezierska K, Boehlke M, Wiecko M, Lukowiak A, Podraza W, et al. Utilization of a 3D printer to fabricate boluses used for electron therapy of skin lesions of the eye canthi. *J Appl Clin Med Phys* (2017) 18(1):76–81. doi: 10.1002/acm2.12013

39. Ricotti R, Ciardo D, Pansini F, Bazani A, Comi S, Spoto R, et al. Dosimetric characterization of 3D printed bolus at different infill percentage for external photon beam radiotherapy. *Phys Med* (2017) 39:25–32. doi: 10.1016/j.ejmp.2017.06.004

40. Tejo-Otero A, Buj-Corral I, Fenollosa-Artes F. 3D printing in medicine for preoperative surgical planning: A review. *Ann BioMed Eng* (2020) 48(2):536–55. doi: 10.1007/s10439-019-02411-0

41. Baltz GC, Chi PM, Wong PF, Wang C, Craft DF, Kry SF, et al. Development and validation of a 3D-printed bolus cap for total scalp irradiation. *J Appl Clin Med Phys* (2019) 20(3):89–96. doi: 10.1002/acm2.12552

42. Zaid M, Bajaj N, Burrows H, Mathew R, Dai A, Wilke CT, et al. Creating customized oral stents for head and neck radiotherapy using 3D scanning and printing. *Radiat Oncol* (2019) 14(1):148. doi: 10.1186/s13014-019-1357-2

43. Albantow C, Hargrave C, Brown A, Halsall C. Comparison of 3D printed nose bolus to traditional wax bolus for cost-effectiveness, volumetric accuracy and dosimetric effect. *J Med Radiat Sci* (2020) 67(1):54–63. doi: 10.1002/jmrs.378

44. Park JW, Yea JW. Three-dimensional customized bolus for intensity-modulated radiotherapy in a patient with kimura's disease involving the auricle. *Cancer Radiother* (2016) 20(3):205–9. doi: 10.1016/j.canrad.2015.11.003

45. Park JW, Oh SA, Yea JW, Kang MK. Fabrication of malleable three-dimensional-printed customized bolus using three-dimensional scanner. *PloS One* (2017) 12(5):e0177562. doi: 10.1371/journal.pone.0177562

46. Chiu T, Tan J, Brenner M, Gu X, Yang M, Westover K, et al. Three-dimensional printer-aided casting of soft, custom silicone boluses (SCSBs) for head and neck radiation therapy. *Pract Radiat Oncol* (2018) 8(3):e167–74. doi: 10.1016/j.prro.2017.11.001

47. Offersen BV, Boersma LJ, Kirkove C, Hol S, Aznar MC, Biete Sola A, et al. ESTRO consensus guideline on target volume delineation for elective radiation therapy of early stage breast cancer. *Radiother Oncol* (2015) 114(1):3–10. doi: 10.1016/j.radonc.2014.11.030

48. Kaidar-Person O, Offersen BV, Boersma L, Meattini I, Dodwell D, Wyld L, et al. Tricks and tips for target volume definition and delineation in breast cancer: Lessons learned from ESTRO breast courses. *Radiother Oncol Sep* (2021) 162:185–94. doi: 10.1016/j.radonc.2021.07.015

49. Dai G, Xu X, Wu X, Lei X, Wei X, Li Z, et al. Application of 3D-print silica bolus for nasal NK/T-cell lymphoma radiation therapy. *J Radiat Res* (2020) 61 (6):920–8. doi: 10.1093/jrr/rraa084

50. Pignol JP, Truong P, Rakovitch E, Sattler MG, Whelan TJ, Olivotto IA. Ten years results of the Canadian breast intensity modulated radiation therapy (IMRT) randomized controlled trial. *Radiother Oncol* (2016) 121(3):414–9. doi: 10.1016/j.radonc.2016.08.021

51. Ehler E, Sterling D, Dusenbery K, Lawrence J. Workload implications for clinic workflow with implementation of three-dimensional printed customized bolus for radiation therapy: A pilot study. *PloS One* (2018) 13(10):e0204944. doi: 10.1371/journal.pone.0204944

52. Bjohle J, Onjukka E, Rintela N, Eloranta S, Wickman M, Sandelin K, et al. Post-mastectomy radiation therapy with or without implant-based reconstruction is safe in terms of clinical target volume coverage and survival - a matched cohort study. *Radiother Oncol* (2019) 131:229–36. doi: 10.1016/j.radonc.2018.07.005

53. Valenti M, Parisotto M, Angeletti F, Cucciarelli F, Mantello G, Maggi S. PO-1346: *In-vivo* surface dose measurements in breast cancer patient treated with helical radiation therapy. *Radiother Oncol* (2020) 152:S712–3. doi: 10.1016/s0167-8140(21)01365-7

54. Cox JD, Stetz J, Pajak TF. Toxicity criteria of the radiation therapy oncology group (RTOG) and the European organization for research and treatment of cancer (EORTC). *Int J Radiat Oncol Biol Physics* (1995) 31(5):1341–6. doi: 10.1016/0360-3016(95)00060-C

55. Khan Y, Villarreal-Barajas JE, Udowicz M, Sinha R, Muhammad W, Abbasi AN, et al. Clinical and dosimetric implications of air gaps between bolus and skin surface during radiation therapy. *J Cancer Ther* (2013) 04(07):1251–5. doi: 10.4236/jct.2013.47147

56. Zhao Y, Moran K, Yewondwossen M, Allan J, Clarke S, Rajaraman M, et al. Clinical applications of 3-dimensional printing in radiation therapy. *Med Dosim Summer* (2017) 42(2):150–5. doi: 10.1016/j.meddos.2017.03.001

57. Hou YJ, Yu JP, Wang YQ, Liu H, Da L, Xu J, et al. Fabrication and pre-clinical application of patient-specific 3D silicone rubber bolus for chest wall. *Chin J Radiat Oncol* (2018) 27(9):835–8. doi: 10.3760/cma.j.issn.1004-4221.2018.09.010

58. Anderson PR, Hanlon AL, Fowble BL, McNeeley SW, Freedman GM. Low complication rates are achievable after postmastectomy breast reconstruction and radiation therapy. *Int J Radiat Oncol Biol Phys* (2004) 59(4):1080–7. doi: 10.1016/j.ijrobp.2003.12.036

frontiers | Frontiers in Oncology

TYPE Case Report
PUBLISHED 02 September 2022
DOI 10.3389/fonc.2022.940678

OPEN ACCESS

EDITED BY
Nosheen Masood,
Fatima Jinnah Women University, Pakistan

REVIEWED BY
Hira Iqbal,
University of the Punjab, Pakistan
Saima Shakil,
Augusta University, United States

*CORRESPONDENCE
Reza Shirkoohi
rshirkoohi@tums.ac.ir
Bahram Andalib
b.andalib@yahoo.com

SPECIALTY SECTION
This article was submitted to Breast Cancer, a section of the journal Frontiers in Oncology

RECEIVED 10 May 2022
ACCEPTED 08 August 2022
PUBLISHED 02 September 2022

CITATION
Eskandarion MR, Tizmaghz Z, Andalib B, Parsa N, Emami SAH, Shahsiah R, Oghabian MA and Shirkoohi R (2022) A case report of the sustained and rapid response of bevacizumab in a TP53-positive breast cancer and liver metastatic patient through personalized medicine. *Front. Oncol.* 12:940678. doi: 10.3389/fonc.2022.940678

A case report of the sustained and rapid response of bevacizumab in a TP53-positive breast cancer and liver metastatic patient through personalized medicine

Mohammad Reza Eskandarion[1,2], Zahra Tizmaghz[2,3], Bahram Andalib[2,4]*, Nasser Parsa[2,5], Seyed Amir Hossein Emami[1,2,6], Reza Shahsiah[2,7], Mohammad Ali Oghabian[2,8] and Reza Shirkoohi[1,2]*

[1]Cancer Research Center, Cancer Institute, Imam Khomeini Hospital Complex, Tehran University of Medical Sciences, Tehran, Iran, [2]BESTforPM (Biomarker Evaluation and Supervision Team for Personalized Medicine), Imam Khomeini Hospital Complex, Tehran University of Medical Sciences, Tehran, Iran, [3]Department of Radiation Oncology, Cancer Institute, Imam Khomeini Hospital Complex, Tehran University of Medical Sciences, Tehran, Iran, [4]Radiation Oncology Central Clinic of Karaj (ROCK), Karaj, Iran, [5]Iranian Cancer Association, Tehran, Iran, [6]Department of Hematology and Medical Oncology, Imam Khomeini Hospital Complex, Tehran University of Medical Sciences, Tehran, Iran, [7]Department of Anatomical and Clinical Pathology, Cancer Institute, Imam Khomeini Hospital Complex, Tehran University of Medical Sciences, Tehran, Iran, [8]Medical Physics Department, Faculty of Medicine, Tehran University of Medical Sciences, Tehran, Iran

HER2-positive metastatic breast cancer is much less frequent than other subgroups of breast cancer. Treatment options for this cancer are mostly limited to systemic chemotherapy, which leads to moderate improvements. Targeted therapy against malignant breast cancer requires the identification of reliable biomarkers for personalized medicine to obtain the maximum benefit of this therapy. Any mutations in the TP53 signaling pathway can be considered as a significant causative factor of breast cancer, for which the identification of target genes plays an important role in selecting the appropriate treatment. The use of personalized gene expression profiling could be valuable to find the direct target of the treatment in this case. The present study assessed the genetic profile of an HER2-positive metastatic breast cancer patient (with a liver metastasis) and figured out a complete and sustained response to bevacizumab. According to the results of next-generation sequencing (NGS) analysis, the patient's genetic profile showed an increased expression of p4EBP1 and PTEN and the activation of the mTOR signaling pathway with a mutation in the TP53 gene. Based on the common treatment of similar profiling, we administrated bevacizumab/Taxol/Gemzar chemotherapy up to six courses. Accordingly, as the response to treatment was revealed by reducing the volume of the liver metastasis from 4 to 1.4 cm, metastasectomy was performed as a complementary treatment. Hence,

personalized gene expression profiling not only is useful for targeted therapy but also could be recommended to avoid prescription of non-responsive drugs.

KEYWORDS

breast cancer, liver metastasis, tumor markers, target therapy, personalized medicine, NGS

Introduction

Nowadays, personalized medicine has made it possible to diagnose, treat, or prevent a specific disease using the genetic structure of each patient. The ultimate goal of personalized medicine is to provide a set of markers that can be used to assess the risk of developing a disease throughout the life of each individual in the presence of environmental variables (1).

Most cancer cells do not respond well to conventional therapies, and there is still a risk of recurrence, indicating very high heterogeneity of the disease and the involvement of particular molecular mechanisms specific to each tumor. Therefore, each individual shows an exclusive response to treatment based on a specific genotype (2).

Breast cancer is a highly heterogeneous disease caused by genetic and epigenetic mutations and is one of the most important causes of cancer mortality (3). Different types of breast cancer including ductal carcinoma *in situ* (DCIS) and invasive lobular carcinoma (ILC) have been reported in terms of their clinical features (4). The most common types are invasive ductal carcinoma (IDC) and ILC. IDC makes up about 70%–80% of all breast cancers (4). As patients differently respond to each treatment, the molecular analysis as well as the clinical and pathological findings play an important role in the targeted therapy considering the advances in the genomic field (5).

One of the remarkable targets in cancer signaling pathway is tumor protein P53 (TP53) protein, which is a multifunctional transcription factor in the wild type and is involved in cell-cycle control, DNA maintenance, genome integrity, post-DNA damage repair, and apoptosis (6). The loss of TP53 function results in the replication of damaged DNA. Therefore, tumors with activated TP53 mutations are expected to have more mutations in other genes that lead to an increase or decrease in the expression of other genes (7).

TP53 is a multifunctional tumor-suppressor gene that is often active in neo-vascularization following a number of inhibitory mechanisms (8). For instance, TP53 promotes the degradation of the hypoxia-inducible factor 1 (HIF-1) in the cell. In reaction to oxygen deficiency, HIF-1 functions as a primary transcriptional activator of vascular endothelial growth factor-(VEGF-)mediated angiogenesis (9). Although the interaction between TP53 and HIF-1 is not well understood, TP53 tends to influence angiogenesis *via* other pathways. As compared with non-overexpressing tumors, the overexpression of VEGF in breast cancer patients contributes to shorter relapse-free and total survival periods (9).

Many patients with various cancers are referred to the Biomarker Evaluation & Supervision Team for Personalized Medicine (BESTforPM), Imam Khomeini Hospital Complex, Tehran University of Medical Sciences, Tehran, Iran. These patients usually suffer complicated, metastatic, or end-stage cancers, most of which are resistant to conventional chemotherapy methods. Therefore, patients' genetic profiles are usually checked with the development of personalized medicine based on the decision of a multidisciplinary team for some patients. The results of personal medical tests would lead to the presentation of a better treatment for those patients. In the present study, we described the case of a patient with phenotypic, metastatic breast cancer that unpredictably reacted to bevacizumab therapy. A single reportable somatic TP53 mutation was discovered during genomic profiling of her metastatic liver specimen. The available literature suggests conflicting evidence that supports the role of this mutation in cancer (3). Some evidence proposes that it may stimulate the angiogenesis signaling pathway (7). The reported case emphasizes the importance of further research examining the function of TP53 mutations in cancer development. Moreover, therapeutic response also highlights that personalized medicine, unlike traditional chemotherapy methods, can contribute to targeted therapy.

Materials and methods

Clinical presentation and family history

The patient was a 48-year-old woman at premenopausal stage. In November 2014, she was diagnosed with IDC, grade II, T1c N1 M0, and ER+/PR+ HER-2 weakly (+2) positive. There was no history of breast cancer and no proof of BRCA1/2 mutations among the patient's relatives. In December 2014, after the initial diagnosis of ductal carcinoma, the left breast underwent lumpectomy, and then chemotherapy was given by doxorubicin, cyclophosphamide (four courses), and Taxol (four

courses). The treatment process was kept going on with radiotherapy (50 Gy/25Fr + tumor bed electron boost 10 Gy/5Fr in 30 sessions) from May 2015 to July 2015. Following the chemotherapy, she received 17 courses of Herceptin (440 mg every 3 weeks).

Hormone therapy started by tamoxifen for 8 months from June 2015 to February 2016; however, due to some side effects it was switched to letrozole which was consumed for about 2.5 years from February 2016 to July 2018 (Figure 1). During the first 2 years, diagnostic follow-up was performed every 3 months, and then every 6 months by evaluating tumor markers using blood tests (CA 125, CA15-3, and CEA), the results of which were normal throughout the mentioned period.

In addition, other follow-up diagnostic modalities for this patient included breast ultrasound twice a year as well as the annual mammography, which indicated no evidence of recurrence or metastasis, other than a suspicious lesion located at the surgical incision site, which was reported normal by MR mammography. Furthermore, Pap smear tests and clinical gynecology investigations performed every 6 months were reported to be normal.

In July 2018, without any symptoms and only based on the patient's request for abdominal and pelvic ultrasonography, a hypodense mass with approximate dimensions of 32 × 41 mm was reported in the left liver lobe, and soon after a liver metastasis was confirmed by performing biopsy (Figure 2).

A positron emission tomography (PET) scan was performed. With the exception of the mentioned liver mass, the reports of other sites and phasic lung scan showed normal results. The patient was presented at the liver tumor board. Liver metastasectomy indications were discussed and recommended as a treatment modality along with the systemic therapy. Due to the limitations of approved common chemotherapy for breast cancer and the probability of developing chemoresistance, it was suggested to examine the patient in terms of genetic by NGS (the Ion Torrent Genexus System Platform) and tumor characteristics as well as the pattern of biomarkers to arrive at the best decision to choose effective systemic therapy agents including targeted therapy and find out clinical benefits or lack of benefits about each systemic therapy agent in order to raise the chance of treatment response before the golden time expiration.

Results

Genomic analysis

Among the 315 cancer-related genes studied, genomic profiling of the liver specimen in January 2019 reported a single reportable mutation: TP53 (Table 1 and Supplemental Table 1).

Mechanistic target of rapamycin (mTOR) activation was shown with a positive phosphorylation of 4EBP1 (p4EBP1) expression (an mTOR c1 effector) and phosphatase and tensin homologue (PTEN) positivity. In addition, PTEN was present to block the phosphatidylinositol-3-kinase (PI3K) pathway and fulfilled its function as a tumor suppressor, preventing cancer cell proliferation. Furthermore, NGS data (the Ion Torrent Genexus System Platform) revealed that this patient had wild-type PIK3CA. Overall, these data indicated that PI3K and dual PIK3/mTOR inhibitors were not correlated with therapeutic benefits in this patient. The immunogram test showed a poor propensity for immunotherapy. Despite the existence of CD8+ T cells in the tumor, we observed that PD-L1 expression was poor. Furthermore, no microsatellite instability (MSI), tumor mutational burden (TMB), or sensibility/resistance mutations were found. Preexisting CD8+ T cells, which were distinctly located at the invading tumor margin, were linked to PD-1/PD-L1 immune inhibitory axis expression and might predict therapy response. Furthermore, an improvement in CD8+ T cells in serial tumor samples was associated with a stronger response during treatment. However, since CD8 expression was impaired by tumor heterogeneity and temporal variability, measuring CD8+ T-cell infiltration alone did not have a strong predictive value. As a result, we could not rule out the possibility of a boost from immunotherapy care centered on the optimistic CD8 lymphocyte infiltration. The tumor ID profile in biopsy

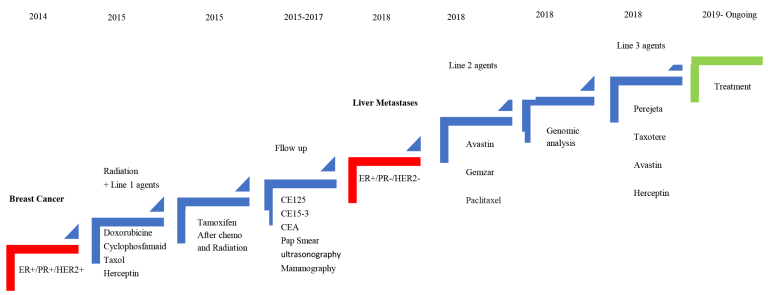

FIGURE 1
Schematic diagram of the patient's clinical course indicating treatment, duration, and disease recurrence.

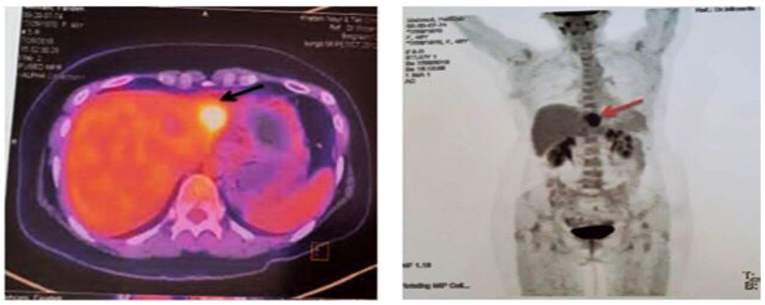

FIGURE 2
First PET/CT on 26 July 2018. The arrows show a fluorodeoxyglucose (FDG) avidity-standardized uptake value (SUVmax = 9.2) hypo-attenuating lesion with partial necrosis with the left liver lobe, compatible with metastatic disease.

showed a single reportable somatic mutation: TP53-cDNA: c.584T>C. AA: p.I195T. VarFreq: 35%.

Treatment outcomes

According to the results of the genetic profile report, chemotherapy with bevacizumab, Taxol, and Gemzar was continued for up to six courses. The response to treatment was achieved with a reduction of liver metastasis from 4 to 1.4 cm. Subsequently, the patient was referred for liver metastasectomy, which was performed first through laparoscopy procedure and then through liver metastasectomy as an open surgery.

At the end of the third line of treatment with Herceptin, Perjeta-Taxotere was started in March 2019. The reports of the PET scan provided in May 2019 and November 2019 indicated a complete response to treatment (Figures 3, 4). Moreover, the diagnostic follow-up demonstrated the patient's normal status currently.

Discussion

Despite their high occurrence in cancer, there are currently no approved targeted therapies for TP53 mutations. According to a newly released retrospective review, patients with advanced cancers harboring a TP53 mutation have a longer progression-free survival on drug regimens containing bevacizumab (Avastin®; Roche, Basel, Switzerland) (Figure 5) (7).

In the current study, the patient treatment was initiated in 2014 with conventional chemotherapy based on standard guidelines, and all treatment policies including surgery, chemotherapy, radiotherapy, hormone therapy, and patient follow-up were performed. In 2018, a liver metastasis was observed as a result of diagnostic follow-up performed due to the patient's request and without any specific symptoms or predicted risk factors. However, the multidisciplinary team consultation, oncologist–geneticist cooperation, and joint clinical decision making were benefited from in the second line of treatment, and the patient's treatment plan was determined considering the personalized medicine and genetic analysis in order to find out the best treatment approach. As explained above, based on NGS findings, bevacizumab was determined as the first and best recommended choice of treatment and led to the dramatic response of the liver metastasis and prolonged the patient's disease-free and overall survival rate. However, based on standard guidelines, bevacizumab is rarely employed in the therapeutic plan of patients with breast cancer and a liver metastasis and is more preferred in colorectal metastases and brain tumors. Therefore, it seems that if personalized medicine, rather than the conventional chemotherapy methods, was used from the very beginning of the treatment, a liver metastasis might not have occurred for this patient.

TABLE 1 A summary of the results of the patient's protein expression.

TP53	PTEN	TS	CD8	PosphoRb	p4EBP1	PD-L1	MSI	TMB	PIK3CA	BRCA1/2
+	+	+	+	-	↑	↓	No	No	WT	WT

+, Positive Expression.
-, Negative Expression.
↑, High Expression.
↓, Low Expression.
WT, Wild Type.

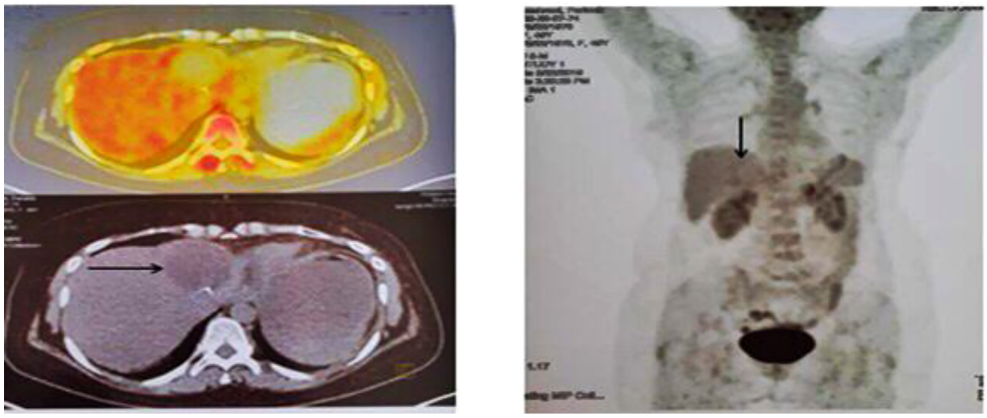

FIGURE 3
Second PET/CT on 23 May 2019. When compared with prior FDG PET/CT scan, the patient status post left liver lobe segment 4 resection, with non-FDG-avid post-surgical change in the surgical bed, which was compatible with an excellent complete metabolic response to therapy.

The valuable finding of this study is that in addition to the benefits of the personalized medicine and the corresponding treatment decision along with tumor identification, we also figured out the patient's resistance to a specific part of the first line of chemotherapy, which suggested that the main agent in her previous chemotherapy was not effective. It should be mentioned that the instructions provided in the guidelines always consider the personalized medicine for the second line of treatment as an inclusion criterion. If we had the option to apply the personalized medicine for this patient immediately after the initial diagnosis, it would have helped us to choose more effective chemotherapy agents or change the regimens in order to improve the treatment in the first line. Furthermore, by doing so, the prescription of ineffective drugs with their side effects would have been avoided.

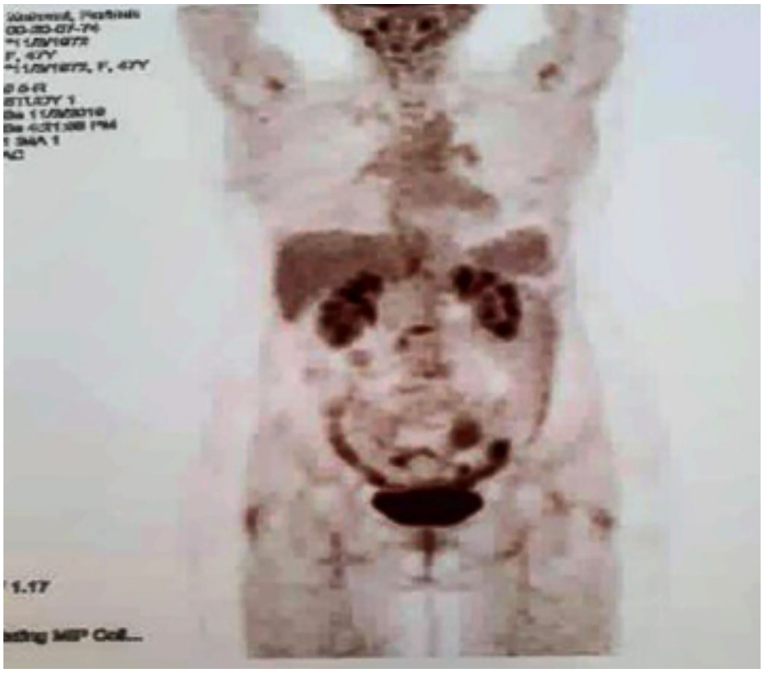

FIGURE 4
Third PET/CT on 03 November 2019. No metabolic evidence of malignancy in the images of the target parts of the body, which was compatible with continued remission.

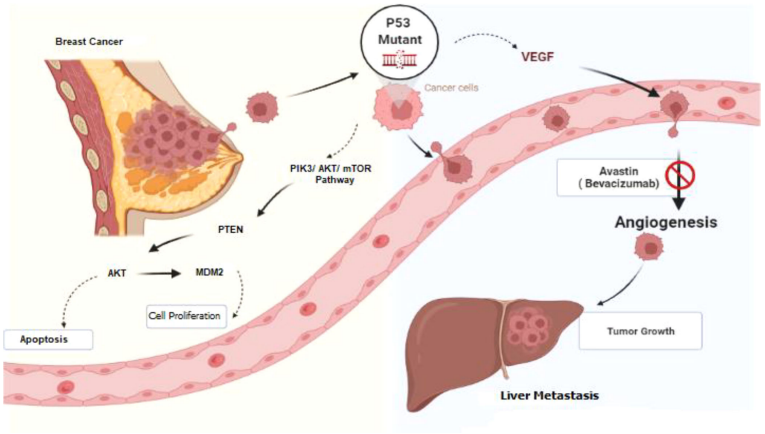

FIGURE 5
Schematic diagram of the signaling pathway from breast cancer to liver metastasis. TP53 protein is one of the important targets in the cancer signaling pathway and is involved in cell-cycle control, apoptosis, and angiogenesis. Bevacizumab is a VEGF-A monoclonal antibody against circulating VEGF and can inhibit tumor angiogenesis. This figure is created by Biorender.com.

However, very few studies have been published on the use of bevacizumab in the treatment of metastatic breast cancer along with a liver metastasis. In line with the present study, Ogata et al. (10) used the combination of bevacizumab/paclitaxel/carboplatin to treat the liver metastasis in triple-negative breast cancer with mutations in the BRCA2 gene.

Huemer et al.'s study also reported about a woman with HER2-positive breast cancer that was highly symptomatic because of extensive pulmonary involvement. They used the combination of docetaxel/trastuzumab/bevacizumab that led to a significant response. The mentioned study revealed a significant association between treatment success and the addition of anti-VEGF antibody. The employed treatment was in agreement with the current study (11).

The role of bevacizumab in breast cancer is still controversial. Several studies demonstrated an improvement in terms of progression-free survival when bevacizumab was added to standard chemotherapy. However, on the other hand, the toxicity rate was increased and no benefit was observed in terms of the overall survival rate (12, 13). In line with numerous previous studies that have used surgery to treat liver metastasis caused by breast cancer, the present study also employed surgery in addition to the targeted therapy (14, 15).

The majority of p53 mutations have been found in the core hot spots of the DNA-binding domain (16). The current result of tumor profiling on biopsy showed a somatic mutation in TP53-cDNA: c.584T>C. AA: p.I195T which was found in the protein's DNA-binding domain. This mutation was described as highly destabilized and linked to poor DNA-binding affinity (17). The variations found in TP53 in advanced cancers were scattered over multiple exons encoding the gene, suggesting that they were normal variations in exon 5 (n = 23. 33.3%), followed by exon 6 (n = 14, 20.3%), exon 7 (n = 12 17.4%), exon 4 (n = 9, 13.0%), exon 8 (n = 9 13.0%), and exon 9 (n = 2, 3.0%). More studies are required to specify which causes such as tissue of origin or a rare TP53 mutation influence bevacizumab responsiveness (7).

Several studies have been performed to examine the effect of somatic TP53 mutation in various cancers. One study in this respect showed a mutation in TP53 and its association with the increased expression of VEGF-A as the major ligand in the VEGF/VEGFR pathway, which can play a key role in regulating angiogenesis (18). The presented results refer to previous preclinical evidence, which connected TP53 to an increased VEGF expression and vessel density in head and neck tumors (18), breast carcinoma (19, 20), and bone marrow stromal cells in leukemia patients (21). Furthermore, the p53 protein controls angiogenesis, at least in part, by binding directly to the HIF-subunit and inducing HIF- degradation (9). Bevacizumab, as a VEGF-A monoclonal antibody against circulating VEGF, is one of the most common oncology medications. It inhibits tumor angiogenesis by blocking this ligand from communicating with its receptor (9, 22). This medication is licensed for implementation in a number of cancers including kidney cancer, colon cancer, non-small cell lung cancer (NSCLC), and glioblastoma. The effect of bevacizumab on survival in non-selected patients is limited, and the FDA revoked its approval in metastatic breast cancer in 2011 (23), although the National Comprehensive Cancer Network® (NCCN®) Clinical Practice Guidelines in Oncology for Breast Cancer define the recommendation as follows: "Bevacizumab in combination with Paclitaxel is an appropriate therapeutic option for metastatic breast cancer" (24). In phase II clinical trials in metastatic breast cancer, bevacizumab showed positive efficacy and was well tolerated as a single agent. In phase III trials,

bevacizumab with capecitabine, as compared with capecitabine alone, had little advantage in the progression-free survival, which may be attributed to the patient population, advanced stage at diagnosis, weak prognostic indicators, and also the employed chemotherapy protocol. Because of the role of other proangiogenic factors in breast cancer development and the variability of VEGF expression in breast cancer, a more targeted approach to anti-VEGF therapy may be advantageous (25). The association between TP53 mutations and positive results found in clinical trials of patients treated with anti-angiogenesis agents may be explained by attending to the relationship between TP53 mutations and the VEGF-A expression (7). Although previously published data on the predictive value of VEGF-A circulation have not been shown to correlate with patient recovery after bevacizumab treatment, it is also known that blood-derived VEGF-A levels are not well correlated with the VEGF-A tissue expression (25).

Other studies have also revealed that the p53 protein inhibits angiogenesis and neo-vascularization (8, 26). In addition, numerous tumor cell lines and xenograft tumor models have shown a connection between the p53 mutation and neo-vascularization (7). Scientific evidence indicated that p53 mutational status was not correlated with survival in patients with colorectal cancer treated with bevacizumab (27). As the pattern of cancer treatment changes from chemotherapy regimens to personalized medicine, the discovery of reliable biomarkers for treating cancer patients by targeted therapies is essential. Breast cancer treatment has so far been accepted using targeted HER2 therapies for HER2-positive and anti-hormonal therapies for ER +/PR + (28).

The basis of this type of treatment is the inhibition of growth factor receptors, inhibition of angiogenesis, and induction of apoptosis in tumor cells, which can be achieved using monoclonal antibodies and small-molecule inhibitors (29).

However, in order to extend this strategy, researchers will continue to specify biomarkers predicting therapeutic responses. Anti-angiogenic therapies (drugs targeting the neo-vascularization mechanism that helps tumors to self-sustain) will profit from the development of a new biomarker in particular.

Conclusion

The present study presented an identified case of breast cancer with a phenotype that caused several chemotherapy courses to fail. Therefore, cancer gene expression profiling was used to amend the treatment based on her genetic tumor information. Following the detection of a change in TP53, it was decided to add targeted therapy with bevacizumab, as a result of which the patient experienced an exceptional 6-month response to the bevacizumab regimen. It can be concluded that recommendation of personalized gene expression profiling from the beginning in guidelines could be beneficial to find specific targets and prevent the prescription of non-responsive drugs.

Data availability statement

The original contributions presented in the study are included in the article/Supplementary Material. Further inquiries can be directed to the corresponding authors.

Ethics statement

Ethical review and approval was not required for the study on human participants in accordance with the local legislation and institutional requirements. The patients/participants provided their written informed consent to participate in this study.

Author contributions

We are a team of multi-disciplinary known as experts BEST for pm (Biomarker Evaluation & Supervision Team for Personalized Medicine), in the field of medical oncology, radiation oncology, surgery, pathology, radiology, genetics, and medical physics in Imam Khomeini Hospital Complex, Tehran University of Medical Sciences have established and launched this center. We have several aims for diagnosis and treatment in cancer patients and one of them is using personalized medicine in end-stage patients. this team had much success in the project and this case report is one of them. ME is a researcher in the team and he wrote the manuscript with support from RSHi who is a Prof. of Genetic Medicine that the genetic profile of the patient is checked by him. ZT proved this manuscript and supervised radiation for this patient. BA is an oncologist who supervised the total of this project in collaboration with NP. SE and RSHa a were involved in the diagnosis and treatment of patients and MO was monitoring all processes of function as the head of the team. All authors contributed to the article and approved the submitted version.

Acknowledgments

The authors would like to thank Dr. Farideh Mehrani and Ms. Masoumeh Nezami for their excellent technical contribution to this manuscript.

Conflict of interest

The authors declare that the research was conducted in the absence of any commercial or financial relationships that could be construed as a potential conflict of interest.

Publisher's note

All claims expressed in this article are solely those of the authors and do not necessarily represent those of their affiliated organizations, or those of the publisher, the editors and the reviewers. Any product that may be evaluated in this article, or claim that may be made by its manufacturer, is not guaranteed or endorsed by the publisher.

Supplementary material

The Supplementary Material for this article can be found online at: https://www.frontiersin.org/articles/10.3389/fonc.2022.940678/full#supplementary-material

References

1. Burke W , Trinidad SB, Press NA., Editors. Essential elements of personalized medicine. In: *Urologic oncology: Seminars and original investigations*. Elsevier. 32 (2):193–19. doi: 10.1016/j.urolonc.2013.09.002

2. Verma M. Personalized medicine and cancer. *J pers Med* (2012) 2(1):1–14. doi: 10.3390/jpm2010001

3. Hosseini Bereshneh A, Soltani D, Veisi N, Khademi M, Modarressi MH. Horizons of personalized medicine in breast cancer treatment. *Tehran Univ Med J TUMS Publ* (2016) 74(9):607–13. doi: 10.14694/EdBook_AM.2014.34.e5

4. Gradishar WJ, Anderson BO, Abraham J, Aft R, Agnese D, Allison KH, et al. Breast cancer, version 3.2020, nccn clinical practice guidelines in oncology. *J Natl Compr Cancer Netw* (2020) 18(4):452–78. doi: 10.6004/jnccn.2020.0016

5. Parachoniak CA, Rankin A, Gaffney B, Hartmaier R, Spritz D, Erlich RL, et al. Exceptional durable response to everolimus in a patient with biphenotypic breast cancer harboring an Stk11 variant. *Mol Case Stud* (2017) 3(5):a000778. doi: 10.1101/mcs.a000778

6. Børresen-Dale AL. Tp53 and breast cancer. *Hum Mutat* (2003) 21(3):292–300. doi: 10.1002/humu.10174

7. Said R, Hong DS, Warneke CL, Lee JJ, Wheler JJ, Janku F, et al. P53 mutations in advanced cancers: Clinical characteristics, outcomes, and correlation between progression-free survival and bevacizumab-containing therapy. *Oncotarget* (2013) 4(5):705. doi: 10.18632/oncotarget.974

8. Teodoro JG, Evans SK, Green MR. Inhibition of tumor angiogenesis by P53: A new role for the guardian of the genome. *J Mol Med* (2007) 85(11):1175–86. doi: 10.1007/s00109-007-0221-2

9. Ravi R, Mookerjee B, Bhujwalla ZM, Sutter CH, Artemov D, Zeng Q, et al. Regulation of tumor angiogenesis by P53-induced degradation of hypoxia-inducible factor 1α. *Genes Dev* (2000) 14(1):34–44. doi: 10.1101/gad.14.1.34

10. Ogata H, Kikuchi Y, Natori K, Shiraga N, Kobayashi M, Magoshi S, et al. Liver metastasis of a triple-negative breast cancer and complete remission for 5 years after treatment with combined Bevacizumab/Paclitaxel/Carboplatin: Case report and review of the literature. *Medicine* (2015) 94(42):e1756. doi: 10.1097/MD.0000000000001756

11. Huemer F, Gampenrieder SP, Schlattau A, Greil R. Overcoming resistance against Her2-targeting agents in fifth-line therapy: Is there still a place for bevacizumab in Her2+ breast cancer? *Clin Breast Cancer* (2014) 14(1):e17–20. doi: 10.1016/j.clbc.2013.09.009

12. Gianni L, Romieu GH, Lichinitser M, Serrano SV, Mansutti M, Pivot X, et al. Averel: A randomized phase iii trial evaluating bevacizumab in combination with docetaxel and trastuzumab as first-line therapy for Her2-positive locally Recurrent/Metastatic breast cancer. *J Clin Oncol* (2013) 31(14):1719–25. doi: 10.1200/JCO.2012.44.7912

13. Rossari JR, Metzger-Filho O, Paesmans M, Saini KS, Gennari A, de Azambuja E, et al. Bevacizumab and breast cancer: A meta-analysis of first-line phase iii studies and a critical reappraisal of available evidence. *J Oncol* (2012) 2012:8. doi: 10.1155/2012/417673

14. Elias D, Di Pietroantonio D. Surgery for liver metastases from breast cancer. *HPB* (2006) 8(2):97–9. doi: 10.1080/13651820500471871

15. Weinrich M, Weiß C, Schuld J, Rau BM. Liver resections of isolated liver metastasis in breast cancer: Results and possible prognostic factors. *HPB Surg* (2014) 2014:6. doi: 10.1155/2014/893829

16. Kojima K, Konopleva M, McQueen T, O'Brien S, Plunkett W, Andreeff M. Mdm2 inhibitor nutlin-3a induces P53-mediated apoptosis by transcription-dependent and transcription-independent mechanisms and may overcome atm-mediated resistance to fludarabine in chronic lymphocytic leukemia. *Blood* (2006) 108(3):993–1000. doi: 10.1182/blood-2005-12-5148

17. Friedler A, Hansson LO, Veprintsev DB, Freund SM, Rippin TM, Nikolova PV, et al. A peptide that binds and stabilizes P53 core domain: Chaperone strategy for rescue of oncogenic mutants. *Proc Natl Acad Sci* (2002) 99(2):937–42. doi: 10.1073/pnas.241629998

18. Riedel F, GÖtte K, Schwalb J, SchÄfer C, HÖrmann K. Vascular endothelial growth factor expression correlates with P53 mutation and angiogenesis in squamous cell carcinoma of the head and neck. *Acta oto-laryngologica* (2000) 120(1):105–11. doi: 10.1080/00016480060203334

19. Linderholm B, Lindh B, Tavelin B, Grankvist K, Henriksson R. P53 and vascular-Endothelial-Growth-Factor (Vegf) expression predicts outcome in 833 patients with primary breast carcinoma. *Int J Cancer* (2000) 89(1):51–62. doi: 10.1002/(SICI)1097-0215(20000120)89:1<51::AID-IJC9>3.0.CO;2-8

20. Linderholm BK, Lindahl T, Holmberg L, Klaar S, Lennerstrand J, Henriksson R, et al. The expression of vascular endothelial growth factor correlates with mutant P53 and poor prognosis in human breast cancer. *Cancer Res* (2001) 61(5):2256–60. PMID: 11280795

21. Narendran A, Ganjavi H, Morson N, Connor A, Barlow JW, Keystone E, et al. Mutant P53 in bone marrow stromal cells increases vegf expression and supports leukemia cell growth. *Exp Hematol* (2003) 31(8):693–701. doi: 10.1016/S0301-472X(03)00159-0

22. Montero AJ, Escobar M, Lopes G, Glück S, Vogel C. Bevacizumab in the treatment of metastatic breast cancer: Friend or foe? *Curr Oncol Rep* (2012) 14 (1):1–11. doi: 10.1007/s11912-011-0202-z

23. Sasich LD, Sukkari SR. The us fdas withdrawal of the breast cancer indication for avastin (Bevacizumab). *Saudi Pharm J* (2012) 20(4):381–5. doi: 10.1016/j.jsps.2011.12.001

24. Gradishar WJ, Moran MS, Abraham J, Aft R, Agnese D, Allison KH, et al. Breast cancer, version 3.2022, nccn clinical practice guidelines in oncology. *J Natl Compr Cancer Netw* (2022) 20(6):691–722. doi: 10.6004/jnccn.2022.0030

25. Rugo HS. Bevacizumab in the treatment of breast cancer: Rationale and current data. *Oncol* (2004) 9:43–9. doi: 10.1634/theoncologist.9-suppl_1-43

26. Kamat CD, Green DE, Warnke L, Thorpe JE, Ceriello A, Ihnat MA. Mutant P53 facilitates pro-angiogenic, hyperproliferative phenotype in response to chronic relative hypoxia. *Cancer Lett* (2007) 249(2):209–19. doi: 10.1016/j.canlet.2006.08.017

27. Ince WL, Jubb AM, Holden SN, Holmgren EB, Tobin P, Sridhar M, et al. Association of K-ras, b-raf, and P53 status with the treatment effect of bevacizumab. *J Natl Cancer Inst* (2005) 97(13):981–9. doi: 10.1093/jnci/dji174

28. Longo R, Torino F, Gasparini G. Targeted therapy of breast cancer. *Curr Pharm des* (2007) 13(5):497–517. doi: 10.2174/138161207780162890

29. Wayteck L, Breckpot K, Demeester J, De Smedt SC, Raemdonck K. A personalized view on cancer immunotherapy. *Cancer Lett* (2014) 352(1):113–25. doi: 10.1016/j.canlet.2013.09.016

frontiers | Frontiers in Oncology

TYPE Original Research
PUBLISHED 15 September 2022
DOI 10.3389/fonc.2022.997306

OPEN ACCESS

EDITED BY
San-Gang Wu,
First Affiliated Hospital of Xiamen University, China

REVIEWED BY
Yigit Ali Üncü,
Akdeniz University, Turkey
Mircea-Sebastian Serbanescu,
University of Medicine and Pharmacy of Craiova, Romania

*CORRESPONDENCE
Dong Xu
xudong@zjcc.org.cn
Shu-Rong Wang
wsr7762808@hotmail.com

†These authors share first authorship

SPECIALTY SECTION
This article was submitted to Breast Cancer, a section of the journal Frontiers in Oncology

RECEIVED 18 July 2022
ACCEPTED 30 August 2022
PUBLISHED 15 September 2022

CITATION
Zhou Y, Feng B-J, Yue W-W, Liu Y, Xu Z-F, Xing W, Xu Z, Yao J-C, Wang S-R and Xu D (2022) Differentiating non-lactating mastitis and malignant breast tumors by deep-learning based AI automatic classification system: A preliminary study.
Front. Oncol. 12:997306.
doi: 10.3389/fonc.2022.997306

Differentiating non-lactating mastitis and malignant breast tumors by deep-learning based AI automatic classification system: A preliminary study

Ying Zhou[1†], Bo-Jian Feng[2†], Wen-Wen Yue[3†], Yuan Liu[1], Zhi-Feng Xu[1], Wei Xing[1], Zhao Xu[1], Jin-Cao Yao[2], Shu-Rong Wang[4*] and Dong Xu[2,5*]

[1]Department of Surgery, Hebei Provincial Hospital of Traditional Chinese Medicine, Shijiazhuang, China, [2]Department of Diagnostic Ultrasound Imaging and Interventional Therapy, The Cancer Hospital of the University of Chinese Academy of Sciences (Zhejiang Cancer Hospital), Hangzhou, China, [3]Department of Medical Ultrasound, Shanghai Tenth People's Hospital, Ultrasound Research and Education Institute, Shanghai, China, [4]Department of Ultrasound Medicine, Yantai Affiliated Hospital of Binzhou Medical College, Yantai, China, [5]Institute of Basic Medicine and Cancer (IBMC), Chinese Academy of Sciences, Hangzhou, China

Objective: To explore the application values of deep-learning based artificial intelligence (AI) automatic classification system, on the differential diagnosis of non-lactating mastitis (NLM) and malignant breast tumors, *via* its comparation with traditional ultrasound interpretations and the following interpretation conclusions made by the sonographers with various seniorities.

Methods: A total of 707 patients suffering from breast lesions (475 malignant breast tumors and 232 NLM), were selected from the following three medical centers, including Zhejiang Cancer Hospital, Hebei Province Hospital of Traditional Chinese Medicine, and Yantai Affiliated Hospital of Binzhou Medical University, and the time period was set from April 2020 to September 2021. All selected cases firstly accepted the routine breast ultrasound diagnosis, followed by the interpretations from a senior sonographer with more than 15 years of work experience, and an intermediate-aged sonographer with more than 5 years of work experience, independently. Meanwhile, a third physician also interpreted the same ultrasound images by deep learning–based AI automatic classification system, independent of the interpretation results from the previous two physicians. The kappa test was performed to evaluate the consistency between the conventional ultrasound interpretation results and pathological results interpreted from physicians with different working experiences.

Results: In total, 475 cases of malignant breast tumors (512 nodules) and 232 cases of NLM (255 nodules) were pathologically diagnosed. The accuracy, sensitivity, and specificity of conventional ultrasound interpretations vary from different sonographers with different working experiences. The accuracy,

sensitivity, and specificity for intermediate-aged sonographers and senior sonographers were 76.92% (590/767), 84.71% (216/255), and 73.95% (374/512) and 87.35% (670/767), 86.27% (220/255), and 87.89% (450/512), respectively (P<0.001). In contrast, if the threshold was set as 0.5, the accuracy, sensitivity, and specificity from deep learning–based AI automatic classification system were 83.00%, 87.20%, and 85.33%, separately, and the area under the curve was 92.6. The results of the kappa consistency test indicated that the diagnosis results from the image interpretations by senior physicians and deep-learning based AI automatic classification system showed high consistency with postoperative pathological diagnosis results, and the kappa values are 0.72 and 0.71, respectively, with the P-value of less than 0.001. In contrast, the consistency between the image interpretation results from intermediate-aged physicians with less working experience, and postoperative pathological diagnosis results, seemed to be relatively lower, with a kappa value of only 0.53 and P-value of less than 0.001.

Conclusions: The deep learning–based AI automatic classification system is expected to become a reliable auxiliary way to distinguish NLM and malignant breast tumors due to its high sensitivity, accuracy, and specificity.

KEYWORDS

deep-learning based AI automatic classification system, malignant breast tumors, nonlactating mastitis, plasma cell mastitis, granulomatous mastitis

Introduction

Generally, non-lactating mastitis (NLM) mainly includes plasma cell mastitis (PCM) (1) and granulomatous mastitis (GM) (2). It is a kind of inflammatory breast disease that occurs among the non-lactating women with the ages ranging between 30 and 40 years old (3, 4). It is relatively rare in clinical practice, and its rare incidence accounts for 1.41%–5.36% of the breast diseases in the same period, showing an increasing trend in recent years (5).

NLM belongs to a kind of rare, benign, and non-specific inflammatory breast disease and is usually misregarded as malignant breast tumors both clinically and radiologically (6, 7). Malignant breast tumors are a kind of common malignant tumors among women and show serious effects on both the physical and mental health of patients. The previous studies suggested that the 5-year survival for malignant breast tumors can be improved by more than 80% through early screening and diagnosis (8, 9). The breast imaging reporting and date system formulated by the American College of Radiology provided classification criteria for the ultrasound diagnosis of breast diseases (10). There are many clinical diagnostic methods, including nuclear magnetic resonance, tomography, three-dimensional reconstruction technology, and ultrasound examination (11–15). In some cases, due to the limited availability of medical imaging equipment, as well as the less working experience of physicians, misdiagnosis still occurs sometimes, leading to a patient's failure to be diagnosed correctly (16). Conventional magnetic-resonance-imaging (MRI) scans have good soft tissue resolution, can image in multiple directions, and have no radiation. The diagnostic sensitivity is as high as 90%, but the specificity is only 50%–70% (17), and the cost is relatively high and the examination time is long, so it cannot be widely used in clinical work. Digital mammography has good spatial resolution, which is conducive to the observation of the overall shape of the lesion, and is the most specific for the detection of calcification, but the sensitivity of breast diagnosis decreases with the increase of gland density (18). Diagnosis is difficult due to atypical imaging manifestations, and the diagnosis of early small malignant breast tumors is also difficult (19). Ultrasound examination is real time, non-invasive, and sensitive to the breast examination of dense glands. It has now become an important means of routine examination of female breasts in China. However, considering some overlapped features between NLM and malignant breast tumors, and the fact that the interpretations of image features are also susceptible to the subjective experience of physicians, it is difficult to distinguish (20). In recent years, the emergence of many new technologies has made up for the shortcomings of conventional ultrasound diagnosis (21). An

automated breast volume scanner (ABVS) is a fully automatic three-dimensional imaging scanner that can clearly display the information of the coronal plane of the lesion, but ABVS also has limitations: 1) it is not suitable for patients with large breasts, ulceration on the surface, partial depression, or an obvious protrusion of the tumor on the skin surface, and 2) it is impossible to superimpose technologies such as color Doppler and elastography like conventional ultrasound, and the diagnostic information is relatively simple (22). Elastography techniques mainly include strain elastography (SE) and shear wave elastography (SWE), which can qualitatively and quantitatively reflect the degree of softness and hardness of lesions in real time, but their diagnostic results are also affected by the operator's experience, technology, and the depth of the lesion and size, as well as the influence of factors such as the region of interest of the selected lesion (23). Contrast-enhanced ultrasound can sensitively capture low-velocity blood flow signals and improve the detection rate of early malignant breast tumors, but its shortcomings are: 1) the results of contrast-enhanced imaging are affected by the injection method, instrument adjustment, contrast artifact, and lesion location; 2) benign and malignant breasts. The microcirculation state of the lesions overlaps, and angiography may not be able to distinguish it; and 3) the qualitative or quantitative criteria for evaluating the enhancement pattern of benign and malignant breast lesions are not unified (24). AI is a new technical science based on mathematics, computer science, etc., which researches and develops theories, methods, and application systems for simulating the extension and expansion of human intelligence (25). The earliest development of breast medical imaging AI technology is the computer-aided design (CAD) system. Traditional CAD is affected by artificial delineation and feature extraction (26), and its accuracy is not high. Deep learning can autonomously extract the fine features of massive images to achieve end-to-end learning. The convolutional neural network (CNN) is the most representative model of deep learning, which has excellent performance in the detection and classification of breast ultrasound images (27). AI performs advanced learning based on large data sets and has the advantages of fast calculation speed and strong repeatability. It is expected to become the right-hand assistant of sonographers in the future.

Materials and methods

Materials

A total of 707 patients diagnosed as breast nodules (475 malignant breast tumor, 232 NLM) were selected from three tertiary centers (Zhejiang Cancer Hospital, Hebei Province Hospital of Traditional Chinese Medicine, and Yantai Affiliated Hospital of Binzhou Medical University) with the period from April 2020 to September 2021. The gold standards were set up based on puncture or surgical pathological diagnosis, and we tried to compare the differences between the deep-learning AI automatic classification system and routine examinations from sonographers with different working experiences, in the diagnosis of NLM and malignant breast tumors, followed by the discussion of identification values for the deep-learning AI automatic classification system in distinguishing the above two diseases. All the enrolled patients were proven by histopathological results after biopsy, surgery, or both. The inclusion criteria were: (1) nodules were confirmed by puncture or surgical pathology as NLM or malignant breast tumor; (2) solid breast lesions or predominant solid lesions (cystic part <25%); (3) have not received treatments such as incision and drainage, intervention, radiotherapy, and chemotherapy; (4) breast lesions detected by conventional United States (US) and had complete transverse and longitudinal standard cross-sectional views and image data. The exclusion criteria were: (1) ultrasonic examination showed unclear horizontal and vertical standard sections; (2) unclear pathological diagnosis or benign breast nodules; and (3) patients suffering from breastfeeding mastitis. This study was approved by the hospital ethics committee, and the subjects signed an informed consent form before all examinations.

Equipment and methods

Conventional ultrasound image interpretations

The above three medical centers used different types of ultrasound diagnostic equipment (LOGIQ E9 for Hebei Provincial Hospital of Traditional Chinese Medicine and Zhejiang Cancer Hospital, and Toshiba Aplio500 for Yantai Affiliated Hospital of Binzhou Medical University) to perform the routine breast ultrasound examinations, with the probe model of L11 and frequency of 5~13 MHz. The resulting ultrasound images were interpreted by two sonographers who have been engaged in breast ultrasound diagnosis for many years (one senior physician with more than 15 years of work experience, and another with more than 5 years of work experience), separately. This study was investigated according to the breast imaging reporting and data system developed by the American College of Radiology, with the precondition of not knowing a patient's personal clinical information and histopathological results (Figure 1).

Intelligence ultrasound image interpretations

The obtained ultrasound images were interpreted by a deep-learning based AI automatic classification system, which contains two parts including hardware and software. In terms

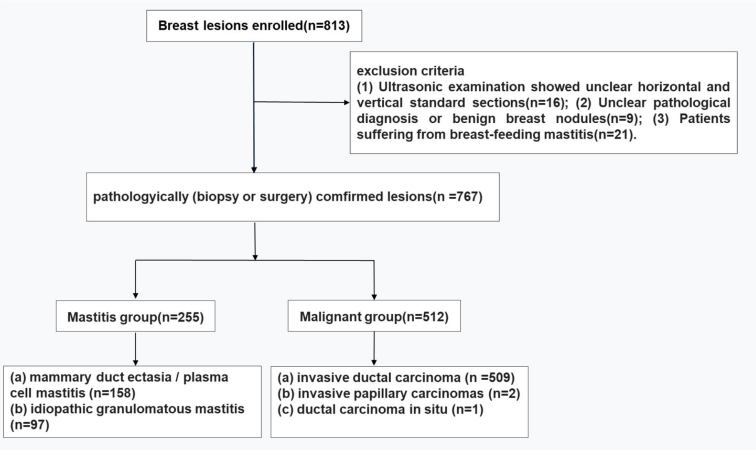

FIGURE 1
Flowchart for lesion selection.

of the software part, all methods were implemented in Python. CNNs have currently been applied widely in various fields (28–30), and the network in this study was based on Keras 2.1.5 and Tensorflow 1.6.0. The system runs under Ubuntu 16.04. For the hardware part, the system runs on Intel® Xeon(R) CPU E5-2678 v3 @ 2.5 GHz×48 and NVIDIA TITAN V 12 GB Graphic Processing Unit (GPU).

To verify whether it works for all proposed methods above, we used the B-mode ultrasound database of breast nodules originated from multicenters, which contains the 1808 B-mode ultrasound pictures of breast nodules (767 nodules in total). After obtaining the original database, we firstly constructed a rectangular frame in the nodule area based on the segmentation results to obtain the images of the nodule, followed by the diagnosis as malignant breast tumor or NLM (marked as 0: malignant breast tumor, 1: NLM) by a physician with working experience for more than 5 years. A total of 1,250 pictures (512 nodules) for malignant breast tumors were obtained, of which 558 were NLM pictures (255 nodules). Considering the imbalances in the data amount among different categories, the method of data amplification was applied to increase the pictures of both NLM and malignant breast tumors, up to 30,000, respectively, meanwhile keeping the ratio as 1:1, adjusting all the picture sizes as 224 × 224. We chose to use the pretrained InceptionV3 deep CNN from the ImageNet data set for transfer learning, and, meanwhile, the replacement of the fully connected layer, SoftMax layer, and classification output layer of InceptionV3. Of all the collected samples, 70% were selected as the training data set and 20% as the verification data set, and the remaining 10% were used as the test data set (Table 1).

For each nodule, we extracted the outer box of the nodule area according to the doctor's annotation of the nodule contour and then expanded it by 0.2 times in the up, down, left, and right directions to include the surrounding tissue and finally resized the cropped image to 224 × 224 and input it into the network. The entire procedure is shown in Figure 2.

ResNet is able to solve the problem of gradient disappearance in deep neural networks through identity mapping and accelerate the training process. The entire structure is shown in Figure 3.

Statistical analysis

Statistical Product Service Solutions (SPSS) 26.0 was used for statistical analysis. Data were indicated as the form of x ± s and shown as the number of cases and percentages. The pathology results were set as the gold standard, and the consistency of pathological and interpretation results, from conventional ultrasound interpretation by two physicians with different working experiences, and deep learning–based AI automatic classification system were evaluated using the consistency test based on the kappa coefficient (31), followed by the calculations of the kappa coefficient, accuracy, sensitivity and specificity. The larger the kappa coefficient, the higher the consistency. The kappa value with more than 0.70 was interpreted as good consistency and the kappa value of 0.40~<0.70 as general and the kappa value with less than 0.40 as poor consistency. The inspection level (α) was 0.05.

10.3389/fonc.2022.997306

TABLE 1 The baseline of the patients included in the data set.

	Intermediate-aged physician (n = 767)	Senior physician (n = 767)	AI (n = 767, 1,250 pictures for malignant breast tumors, 558 were NLM pictures)		
Pathologic stage			Training data set	Verification data set	Test data set
IDC	509	509	357 (899 pictures)	101 (216 pictures)	51 (125 pictures)
IPC	2	2	1 (4 pictures)	1 (4 pictures)	0
IC	1	1	1 (2 pictures)	0	0
PCM	158	158	110 (246 pictures)	32 (77 pictures)	16 (62 pictures)
GM	97	97	68 (111 pictures)	19 (24 pictures)	10 (38 pictures)
Age (y) (mean ± std)	46.52 ± 10.29	46.52 ± 10.29	46.17 ± 10.30	47.04 ± 10.80	46.78 ± 10.56
Nodule size					
0–1.0 cm	272(35.46%)	272(35.48%)	190(35.38%)	55(35.95%)	27(35.06%)
1.0–2.0 cm	400(52.15%)	400(52.13%)	277(51.58%)	79(51.63%)	40(51.95%)
>2.0 cm	95(12.39%)	95(12.39%)	70(13.04%)	19(12.42%)	10(12.99%)
Nodule location					
RU	273(35.59%)	273(35.59%)	192(35.85%)	53(34.64%)	24(35.06%)
RM	54(7.04%)	54(7.04%)	38(7.08%)	9(5.88%)	5(6.49%)
RD	129(16.82%)	129(16.82%)	89(16.57%)	27(17.65%)	13(16.88%)
LU	192(25.03%)	192(25.03%)	132(24.67%)	38(24.83%)	19(24.69%)
LD	119(15.52%)	119(15.52%)	85(15.83%)	26(17.00%)	13(16.88%)

DC, invasive ductal carcinomas; IPC, invasive papillary carcinomas; IC, intraductal carcinoma; PCM, plasma cell mastitis; GM, granulomatous mastitis; RU, right-up lobe; RM, right-middle lobe; RD, right-down lobe; LU, left-up lobe; LD, left-down lobe.

Results

Pathological results

A total of 707 patients (767 nodules) were collected in this study, and the malignant breast tumors diagnosed by puncture or surgical pathology were 475 cases (512 nodules), of which invasive ductal carcinomas account for 509 cases, invasive papillary carcinomas for 2 cases, and intraductal carcinoma for 1 case. The remaining 232 cases were diagnosed as NLM (255 nodules), including 158 cases of PCM and 97 cases of granulomatous mastitis.

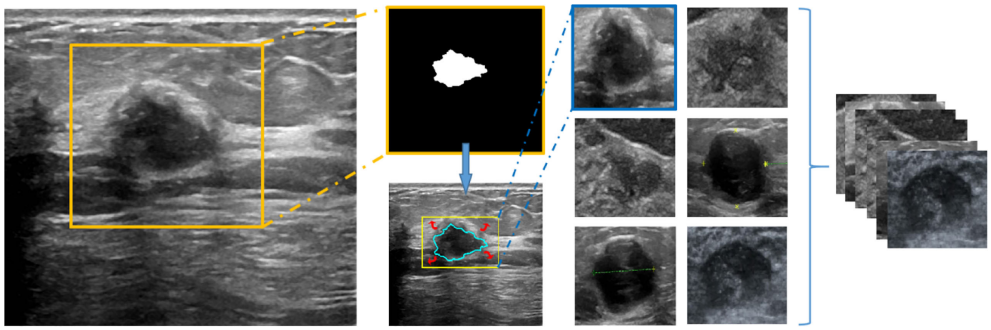

FIGURE 2
The working window of deep learning–based AI automatic classification system (the overall process of image preprocessing).

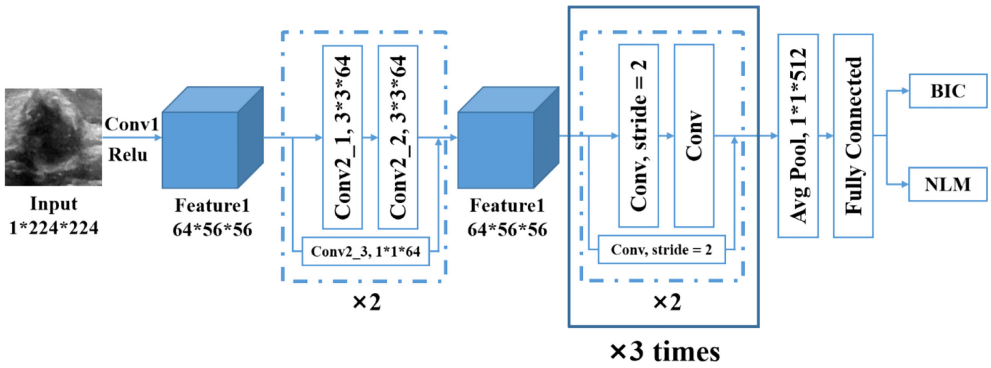

FIGURE 3
The network structure of ResNet-18.

Differential diagnosis of non-lactating mastitis and malignant breast tumors by sonographers with different working experiences and deep-learning based artificial intelligence automatic classification system

Of the total 767 nodules, NLM diagnosed by pathological analysis account for 255 cases, and the remaining 512 cases were diagnosed as malignant tumors. The intermediate-aged sonographer diagnosed 354 cases as NLM and 413 cases as malignant tumors. Furthermore, NLM and malignant tumors, diagnosed by the senior sonographer, were 214 cases and 553 cases, respectively. In contrast, if the threshold value was set as 0.5, the model accuracy, sensitivity, and specificity of the deep-learning based AI automatic classification system were 85.33%, 83.00%, and 87.20%, respectively, similar to the diagnosis results from the senior sonographers [accuracy 87.35% (670/767), sensitivity 86.27% (220/255), and specificity 87.89% (450/512)] and higher than that of sonographers with intermediate-aged working experience [respectively 76.92% (590/767), 84.71% (216/255), and 73.95% (374/512)]. Furthermore, the area under the curve (AUC) was 0.926 (as shown in Figure 4).

Here, if we defined "mastitis" as positive cases, and "malignant breast tumor" as negative cases, then, the positive predicted values and negative predicted values of all NLM or malignant breast tumors, diagnosed by intermediate-aged/senior experienced physicians and the deep learning–based AI automatic classification system, were 61.02%, 78.01%, and 83.84% and 90.56%, 92.78%, and 86.51%, respectively. It suggested that the interpretations by senior physicians, or the deep learning–based AI automatic classification system, showed higher consistency with the postoperative pathological diagnosis results, with the kappa value of 0.72 and 0.71 and P-value of less

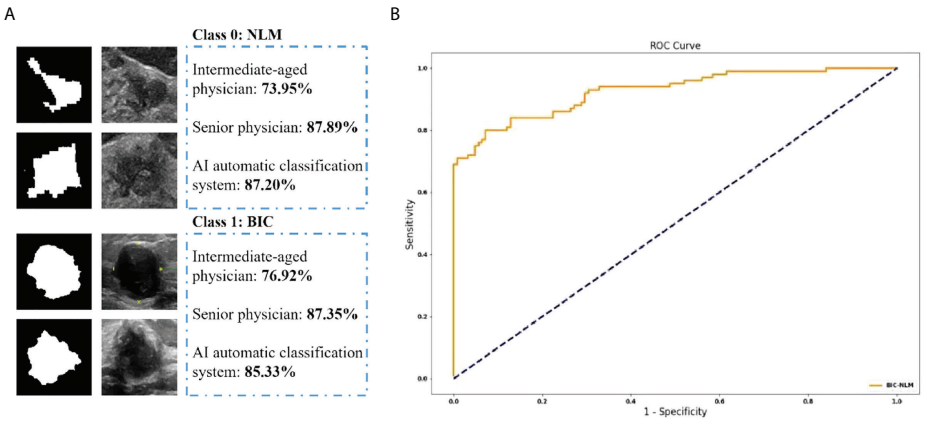

FIGURE 4
(A) The classification accuracy of physicians and AI automatic classification system in NLM and BIC. **(B)** The ROC curve of the proposed method.

than 0.001. In contrast, the results of image interpretations by physicians with intermediate-aged experience showed relatively lower consistency (its kappa value was 0.53 with the P-value of less than 0.001). For details, refer to Tables 2, 3.

Discussions

NLM is a kind of inflammatory disease in the breast tissues of non-breastfeeding women. It generally belongs to benign lesions and is mainly characterized with duct dilatation and massive inflammatory cell infiltration and followed by the infiltrating hyperplasia of ducts and adjacent tissues in the late stage (32, 33). Its main clinical manifestations (34) include breast swelling and pain accompanied with festering, long-lasting unhealed and repeated attacks. Generally, it belongs to intractable diseases among benign breast diseases. Therefore, NLM is also clinically called "undead cancers". The differentiation of this disease from malignant breast tumors can also lead to misdiagnosis easily. Malignant tumors in the breasts (35) are mostly invasive duct carcinoma, with the proliferation of fibrous tissues in the stroma. Thus, clinical manifestations are always presented as hard mass, an unclear boundary with the adjacent tissues, and poor mobility, along with some pains (36).

The ultrasound images of the above two diseases can show as hypoechoic or mixed-echo masses, obscure boundaries, irregular shapes, and heterogeneous internal echoes, along with or without strong echoes, and the partial attenuation of posterior echoes and CDFI show blood flow signals. The lesions of NLM become small along with the inhomogeneous internal echo; meanwhile, there are larger lesions existing in malignant breast tumors, along with necrosis liquefaction inside; the images of conventional ultrasound showed to be very similar, thus, to some degree, resulting in difficulties in differential diagnosis.

In recent years, with continuous update and improvement, AI-associated diagnosis technologies have been applied in the automatic segments and quick analysis of abnormal areas in tissues, as well as the quantification of lesions (37). Furthermore, AI can also be used for the accurate evaluations of detectable areas to reduce the medical mistakes caused by manual operations (38). AI-driven ultrasound is also becoming more and more mature, and its generated diagnosis results are also getting closer to the results of pathological diagnosis; the emergency of diagnosis by AI-driven ultrasound especially provides the beneficial supplements for early screening and benign/malignant assessments for high-risk diseases such as breast nodules and thyroid nodules (39).

In this study, the application of the deep learning–based AI automatic classification system reduced the probability of misreadings or misinterpretations, through the continuous input of cases, and followed with feature learning, lesion segmentation, and the extraction of features with multiple levels. However, considering the imbalances in the data amount among different categories, the method of data amplification was applied to increase the pictures of both

TABLE 2 The interpretation results by intermediate-aged/senior physicians based on working experience.

The interpretation ways		Pathological examination results	
		NLM (nodules)	Malignant breast tumors (nodules)
Intermediate-aged physician	NLM	216	138
	Malignant breast tumors	39	374
Senior physician	NLM	220	62
	Malignant breast tumors	35	450
AI	NLM	83	17
	Malignant breast tumors	16	109

NLM, non-lactating mastitis.

TABLE 3 The differential diagnosis of non-lactating mastitis and malignant breast tumors by both the deep learning–based AI automatic classification system and intermediate-aged/senior physicians.

Interpretation ways	Accuracy (%)	Sensitivity (%)	Specificity (%)	Positive predicted value (%)	Negative predicted value (%)	Kappa value	P-value
Intermediate-aged physician	76.92	84.71	73.95	61.02	90.56	0.53	<0.001
Senior physician	87.35	86.27	87.89	78.01	92.78	0.72	<0.001
AI automatic classification system	85.33	83.00	87.20	83.84	86.51	0.71	<0.001

NLM and malignant breast tumors, up to 30,000, respectively, meanwhile, keeping the ratio as 1:1 and adjusting all the picture sizes as 224 × 224.

We chose to use the pretrained InceptionV3 deep CNN from the ImageNet data set for the transfer learning and, meanwhile, the replacement of the fully connected layer, the SoftMax layer and classification output layer of InceptionV3. Then, the classification output layer was set up into two classes to generate the novel network model. The optimized algorithm uses the stochastic gradient descent method, and the hyperparameters of the model were set as follows: the initial learning rate was 0.001, the batch size was 128, the maximum epoch was 100, and the dropout probability was 0.5.

Furthermore, in this study, as for the AI analysis methods, the target areas were also preprocessed such as noise reduction, and enhancement/refinement for images, which improved the stability of AI interpretations, as well as the improvements in sensitivity, specificity, and accuracy. This research suggested that the differential diagnosis of NLM and malignant breast tumors by both the deep learning–based AI automatic classification system and the senior physicians with rich working experience showed high consistency with postoperative pathological diagnosis results. In contrast, the interpretation results from physicians with intermediate-aged working experience showed relatively lower consistency. When the threshold value was set as 0.5, the accuracy, sensitivity, and specificity of the model diagnosed by the deep learning–based AI automatic classification system were 85.33%, 83.00%, and 87.20%, respectively, and the AUC was 92.6. Both were close to the senior physicians [accuracy 87.35%, sensitivity 86.27%, and specificity 87.89%] and higher than those of middle-aged physicians [accuracy 76.92%, sensitivity 84.71%, and specificity 73.95%]. Since all the diagnostic results were compared with the pathological gold-standard diagnostic results, the consistency of kappa values between the middle-aged physicians/senior physicians/AI diagnosis and the pathological results was 0.53/0.72/0.71. The diagnostic efficiency of senior physicians/AI was significantly higher than that of the middle-aged physicians' results. For junior physicians, the introduction of AI-assisted diagnostic reading function in the future will help improve the accuracy of diagnosis, and AI-assisted diagnosis prompts provide feasibility for the rapid ability improvement of junior physicians in the future. If the clinical application of the deep learning AI automatic classification system technology for joint diagnosis will significantly improve the diagnostic efficiency of middle-aged sonographers, it is suitable for the training of ultrasound residents and shortens the training period; it is suitable for the primary screening of nodules in physical examinations. It avoids missed diagnosis and unnecessary needle biopsy and reduces the risk of overdiagnosis; it can also greatly reduce the workload of clinicians, make hospitals of different levels achieve homogeneity, and improve the differential diagnosis rate of non-lactation mastitis and malignant breast tumors.

Limitations

This study has several limitations: the amount of data in this study is small, the AI automatic classification system does not have a large amount of data for in-depth research, and the results may have certain bias and error, which requires multicenter and large-scale research verification. Currently, the latest version only processes and analyzes static gray-scale ultrasound images and cannot perform an intelligent diagnosis of breast nodule elastography, color Doppler flow imaging, and other multimodalities; the real-time dynamic comprehensive scanning of ultrasound helps. However, the AI automatic classification system technology can only analyze static ultrasound images, and the ultrasound characteristics of different sections of the same lesion are not completely consistent, which will affect the diagnostic results. Future research trends will focus on actively building open databases, optimizing the features of small data sets (fine annotation) on the basis of big data, and developing multimodal ultrasound AI that can effectively analyze dynamic videos, color Doppler images, and elastic images. It is a diagnostic tool that uses digital image processing technology to mark the ultrasound images accordingly and utilizes mammography, MRI, and pathological multimodal joint diagnosis to further improve the diagnostic performance, help clinicians deal with clinical problems more fully and freely, and provide breast imaging. The development of diagnostic disciplines provides new impetus and also shows the broad prospects of intelligent medical imaging in the future.

Conclusions

The deep-learning based AI automatic classification system is expected to become a reliable auxiliary way to distinguish NLM and malignant breast tumors due to its high sensitivity, accuracy, and specificity.

Data availability statement

The original contributions presented in the study are included in the article/supplementary material. Further inquiries can be directed to the corresponding authors.

Ethics statement

The studies involving human participants were reviewed and approved by Hebei Medical Ethics Committee. The patients/participants provided their written informed consent to participate in this study.

Author contributions

YZ and DX had full access to all of the data in the study and take responsibility for the integrity of the data and the accuracy of the data analysis. Concept and design: All authors. Acquisition, analysis, or interpretation of data: All authors. Drafting of the manuscript: YZ. Critical revision of the manuscript for important intellectual content: All authors. Statistical analysis: YZ, B-JF, and W-WY. Obtained funding: DX. Administrative, technical, or material support: DX and S-RW. Supervision: DX. All authors contributed to the article and approved the submitted version.

Funding

This study is funded by the National Natural Science Foundation of China (No. 82071946) and Zhejiang Provincial Natural Science Foundation of China (No. LSD19H180001).

Conflict of interest

The authors declare that the research was conducted in the absence of any commercial or financial relationships that could be construed as a potential conflict of interest.

Publisher's note

All claims expressed in this article are solely those of the authors and do not necessarily represent those of their affiliated organizations, or those of the publisher, the editors and the reviewers. Any product that may be evaluated in this article, or claim that may be made by its manufacturer, is not guaranteed or endorsed by the publisher.

References

1. Zhu L, Li P, Zhang P. Progress in the diagnosis and treatment of plasma cell mastitis. *Hejiang Med J* (2019) 41(5):497. doi: 10.12056/j.issn.1006-2785.2019.41.5.2017-2918

2. Altieri M, Barra F, Casabona F, Soriero D, Gustavino C, Ferrero ,S. Idiopathic granulomatous mastitis: Etiopathogenetic considerations on a rare benign inflammatory breast disease. *J Invest Surg* (2020) 34(9):998–9. doi: 10.1080/08941939.2020.1742403

3. Palmieri A, D'Orazi V, Martino G, Frusone F, Crocetti D, Amabile MI, et al. Plasma cell mastitis in men: A single-center experience and review of the literature. *In Vivo* (2016) 30(6):727–32. doi: 10.21873/invivo.10987

4. Nagaratnam N, Kannangara CS. Plasma-cell mastitis. *Postgrad Med J* (1958) 34(398):654–5. doi: 10.1136/pgmj.34.398.654

5. Wang Q. Observation on the effect of surgery combined with shengyang yiwei decoction and yanghe decoction in the treatment of plasma cell mastitis. *Henan J Surg* (2018) 24(3):74. doi: 10.16193/j.cnki.hnwk.2018.03.042

6. Pluguez-Turull CW, Nanyes JE, Quintero CJ, Alizai H, Mais DD, Kist KA, et al. Idiopathic granulomatous mastitis: Manifestations at multimodality imaging and pitfalls. *Radiographics* (2018) 38(2):330–56. doi: 10.1148/rg.2018170095

7. Oztekin PS, Durhan G, Kosar PN, Erel S, Hucumenoglu S. Imaging findings in patients with granulomatous mastitis. *Iran J Radiol* (2016) 13(3):e33900. doi: 10.5812/iranjradiol.33900

8. Bray F, Ferlay J, Soerjomataram I, Siegel RL, Torre LA, Jemal A, et al. Global cancer statistics 2018: GLOBOCAN estimates of incidence and mortality worldwide for 36 cancers in 185 countries. *CA Cancer J Clin* (2018) 68(6):394–424. doi: 10.3322/caac.21492

9. Allemani C, Matsuda T, Di Carlo V, Harewood R, Matz M, Nikšić M, et al. Global surveillance of trends in cancer survival 2000-14(concord-3):analysis of individual records for 37513025 patients diagnosed with one of 18 cancers from 322 population-based registries in 71 countries. *Lancet* (2018) 391(1125):1023–75. doi: 10.1016/S0140-6736(17)33326-3

10. Castro SM, Tseytlin E, Medvedeva O, Mitchell K, Visweswaran S, Bekhuis T, et al. Automated annotation and classification of BI-RADS assessment from radiology reports. *J BioMed Inform* (2017) 69:177–87. doi: 10.1016/j.jbi.2017.04.011

11. Üncü YA, Sevim G, Canpolat M. Approaches to preclinical studies with heterogeneous breast phantom using reconstruction and three-dimensional image processing algorithms for diffuse optical imaging. *Int J Imaging Syst Technol* (2021) 32(1):343–53. doi: 10.1002/IMA.22648

12. Üncü YA, Sevim G, Mercan T, Vural V, Durmaz E, Canpolat M, et al. Differentiation of tumoral and non-tumoral breast lesions using back reflection diffuse optical tomography: A pilot clinical study. *Int J Imaging Syst Technol* (2021) 31(4):2023–31. doi: 10.1002/IMA.22578

13. Shihab Uddin KM, Uddin KM, Zhang M, Anastasio M, Zhu Q. Optimal breast cancer diagnostic strategy using combined ultrasound and diffuse optical tomography. *Biomed Optics Express* (2020) 11(5):2722–37. doi: 10.1364/BOE.389275

14. Chae EY, Kim HH, Sabir S, Kim Y, Kim H, Yoon S, et al. Development of digital breast tomosynthesis and diffuse optical tomography fusion imaging for breast cancer detection. *Sci Rep* (2020) 10:13127. doi: 10.1038/s41598-020-70103-0

15. Xue F, Jiang J. Dynamic enhanced magnetic resonance imaging versus ultrasonic diffused optical tomography in early diagnosis of breast cancer. *J Healthc Eng* (2022) 2022. doi: 10.1155/2022/4834594

16. Larsen LJH, Peyvandi B, Klipfel N, Grant E, Iyengar G. Granulomatous lobular mastitis: imaging, diagnosis, and treatment. *AJR Am J Roentgenol* (2009) 193(2):574–81. doi: 10.2214/AJR.08.1528

17. Guo X. Application progress of diffusion weighted imaging in malignant breast tumors. *J Pract Radiol* (2011) 27:1581–3.

18. Ren H, Yu X. Application of ultrasound and X-ray mammography in the diagnosis of malignant breast tumors. *J Pract Radiol* (2011) 29:899–901. urged to enter the country.

19. Sun S. Advances in early diagnosis of malignant breast tumors. *J Clin Surg* (2013) 21:500–2.

20. Hongzhu T, Hua Z, Shufeng X, Tao WJ, Zeng XH. Evaluation result of early screening intervention among first-degree relatives familial malignant breast tumors. *Chin J Oper Proc Gen Surg (Electronic Edition)* (2017) 11(6):488–90. doi: 10.3877/cmajissn1674-3946.2017.;06014

21. Yang Y, Jiang W. Progress in the application of new ultrasound technologies in the diagnosis of benign and malignant breast lesions. *J Cancer Control Treat* (2020) 33(11):894–900. doi: 10.3969/j.issn.1674-0904.2020.11.012

22. Zhang G, Yan J, Ju Y, Song HP. Application progress of automatic breast ultrasound imaging system in malignant breast tumors screening and diagnosis.

Chin J Med Ultrasound (Electronic Edition) (2017) 14(11):805–9. doi: 10.3877/cma.j.issn.1672-6448.2017.11.002

23. Chen W, Zhang H, Peng Y. Application progress of ultrasound elastography in the diagnosis of breast diseases. *Biomed Eng Clin* (2020) 24(1):105–9. doi: 10.13339/j.cnki.sglc.20200107.021

24. Luo J, Chen J, Chen Q, Yue LX, Zhou G, Lan C, et al. Application value of contrast-enhanced ultrasound prediction model for benign and malignant breast lesions in the assessment of malignant risk of 4 types of breast lesions in breast imaging reporting and data system. *Chin J Med Ultrasound (Electronic Edition)* (2016) 13(6):459–65. doi: 10.3877//cma,j.issn.1672-6448.2016.06.012

25. Luo X, Li A. Application and thinking of artificial intelligence in diagnosis and treatment of malignant breast tumors. *Chin J Med Ultrasound (Electronic Edition)* (2019) 16(4):247–51. doi: 10.3877/cma.j.issn.1672-6448.2019.04.003

26. Wu GG, Zhou LQ, Xu JW, Wang JY, Wei Q, Deng YB, et al. Artificial intelligence in breast ultrasound. *World J Radiol* (2019) 11(2):19–26. 10.4329/wjr.v11.i2.19.

27. Liu R, Xia Y, Jiang Y. The application of artificial intelligence in the field of ultrasound medicine. *Concord Med J* (2018) 9(5):453–7. doi: 10.3969/j.issn.1674-9081.2018.05.015

28. Wu HB, Yao XY, Zeng LS, Huang F, Chen L. Application of artificial lintelligence technology based on convolutional neural network in early gastric cancer recognition. *J Third Military Med Univ* (2021) 43(18):1735–42. doi: 10.16016/j1000-5404202105018

29. Kumar Dash A, Mohapatra P. A fine-tuned deep convolutional neural network for chest radiography image classification on COVID-19 cases(2021). Available at: Multimedia Tools and Applications10.1007/S11042-021-11388-9.

30. Chen Y, Goorden MC. Convolutional neural network based attenuation correction for I-FP-CIT SPECT with focused striatum imaging(2021). Available at: Beekman F JPhysics in Medicine & Biology10.1088/1361-6560/AC2470.

31. Guo Y, Guo W, Qin Y, He Q, Zhang X, Wu C. Consistency check based on kappa coefficient and its software implementation. *China Health Stat* (2016) 33:169–170, 174.

32. Chen L, Zhang X, Ding HY, Zhao QF, Ding HY. Clinicopathological analysis of 300 cases of granulomatous lobular mastitis. *Zhonghua J Pathol* (2019) 48(3):231–6. doi: 10.3760/cma.j.issn.0529-5807.2019.03.012

33. Chao L, Linping P. Comparative analysis of 86 cases of plasma cell mastitis with ultrasound manifestations and pathological results. *Miscellaneous J Med Pharm Forum* (2017) 38(7):125–6. doi: 10.13339/j.cnki.1672-3422(2017)07-0125-02

34. Yan B-q, Zhao H-n. Analysis of clinical features and risk factors of non-lactating mastitis. *Smart Health* (2020) 6(30):56–8. doi: 10.19335/j.cnki.2096-1219.2020.30.027

35. Malignant breast tumors Professional Committee of Chinese Anti-Cancer Association. Guidelines and standards for the diagnosis and treatment of malignant breast tumors by the Chinese anti-cancer association (2019 edition). *China Oncol* (2019) 29(8):609–24. doi: 10.19401/j.cnki.1007-3639.2019.08.009

36. Zhou L. Application of color Doppler ultrasound in the differentiation of benign and malignant breast masses. *Med Equip* (2020) 33(17):44–5. doi: 10.19501/j.cnki.1002-2376(2020)17-0044-02

37. Lehman CD, Wellman RD, Buist DS, Kerlikowske K, Tosteson AN, Miglioretti DL. Malignant breast tumors surveillance consortium. diagnostic accuracy of digital screening mammography with and without computer-aided detection. *JAMA Intern Med* (2015) 175:1828–37. doi: 10.1001/jamainternmed.2015.5231

38. Shimauchi A, Giger ML, Bhooshan N, Lan L, Pesce LL, Lee JK, et al. Evaluation of clinical breast MR imaging performed with prototype computer-aided diagnosis breast MR imaging workstation: reader study. *Radiology* (2011) 258:696–704. doi: 10.1148/radiol.10100409

39. Akkus Z, Cai J, Boonrod A, Zeinoddini A, Weston AD, Philbrick KA, et al. A survey of deep-learning applications in ultrasound: artificial intelligence-powered ultrasound for improving clinical workflow. *J Am Coll Radiol* (2019) 16(9 Pt B):1318–28.doi: 10.1016/j.jacr.2019.06.004

frontiers | Frontiers in Oncology

TYPE Original Research
PUBLISHED 15 September 2022
DOI 10.3389/fonc.2022.981059

OPEN ACCESS

EDITED BY
San-Gang Wu,
First Affiliated Hospital of Xiamen University, China

REVIEWED BY
Swapnil Ulhas Rane,
Advanced Centre for Treatment, Research and Education in Cancer, India
Yu Min,
Sichuan University, China
Xiangyi Kong,
Chinese Academy of Medical Sciences and Peking Union Medical College, China

*CORRESPONDENCE
Yuanxi Huang
rxwk@163.com
Shiyuan Zhang
hmu_zsy@163.com

†These authors have contributed equally to this work

SPECIALTY SECTION
This article was submitted to Breast Cancer, a section of the journal Frontiers in Oncology

RECEIVED 29 June 2022
ACCEPTED 25 August 2022
PUBLISHED 15 September 2022

CITATION
Jiang C, Xiu Y, Qiao K, Yu X, Zhang S and Huang Y (2022) Prediction of lymph node metastasis in patients with breast invasive micropapillary carcinoma based on machine learning and SHapley Additive exPlanations framework. *Front. Oncol.* 12:981059. doi: 10.3389/fonc.2022.981059

Prediction of lymph node metastasis in patients with breast invasive micropapillary carcinoma based on machine learning and SHapley Additive exPlanations framework

Cong Jiang†, Yuting Xiu†, Kun Qiao, Xiao Yu, Shiyuan Zhang* and Yuanxi Huang*

Department of Breast Surgery, Harbin Medical University Cancer Hospital, Harbin, China

Abstract: Background and purpose: Machine learning (ML) is applied for outcome prediction and treatment support. This study aims to develop different ML models to predict risk of axillary lymph node metastasis (LNM) in breast invasive micropapillary carcinoma (IMPC) and to explore the risk factors of LNM.

Methods: From the Surveillance, Epidemiology, and End Results (SEER) database and the records of our hospital, a total of 1547 patients diagnosed with breast IMPC were incorporated in this study. The ML model is built and the external validation is carried out. SHapley Additive exPlanations (SHAP) framework was applied to explain the optimal model; multivariable analysis was performed with logistic regression (LR); and nomograms were constructed according to the results of LR analysis.

Results: Age and tumor size were correlated with LNM in both cohorts. The luminal subtype is the most common in patients, with the tumor size <=20mm. Compared to other models, Xgboost was the best ML model with the biggest AUC of 0.813 (95% CI: 0.7994 - 0.8262) and the smallest Brier score of 0.186 (95% CI: 0.799-0.826). SHAP plots demonstrated that tumor size was the most vital risk factor for LNM. In both training and test sets, Xgboost had better AUC (0.761 vs 0.745; 0.813 vs 0.775; respectively), and it also achieved a smaller Brier score (0.202 vs 0.204; 0.186 vs 0.191; 0.220 vs 0.221; respectively) than the nomogram model based on LR in those three different sets. After adjusting for five most influential variables (tumor size, age, ER, HER-2, and PR), prediction score based on the Xgboost model was still correlated with LNM (adjusted OR:2.73, 95% CI: 1.30-5.71, P=0.008).

Conclusions: The Xgboost model outperforms the traditional LR-based nomogram model in predicting the LNM of IMPC patients. Combined with SHAP, it can more intuitively reflect the influence of different variables on the LNM. The tumor size was the most important risk factor of LNM for breast IMPC

patients. The prediction score obtained by the Xgboost model could be a good indicator for LNM.

KEYWORDS

machine learning, SHAP, IMPC, nomogram, lymph node metastasis

Introduction

Invasive micropapillary carcinoma (IMPC), a special subtype of invasive breast cancer, was classified as a new histological type by the World Health Organization (WHO) in 2003 (1). Since Fisher et al. (2) first reported invasive papillary carcinoma with morula-like morphologic changes in 1980, there have been different reports on the pathological diagnostic criteria of IMPC. In all invasive breast cancers, the reported incidence of IMPC varies greatly from 2.0% to 8.0% (1), which is mainly because IMPC is most often part of invasive ductal carcinoma morphology, rather than the entirety of cancer.

Unlike invasive ductal carcinoma, patients with IMPC have a higher incidence of lymph node metastasis (LNM) and a shorter survival time (3–5). It has been known that LNM is correlated with a worse prognosis for breast cancer patients (6). Preoperative assessment of axillary lymph node metastasis can help physicians to implement some interventions such as neoadjuvant chemotherapy in advance, so that patients could benefit from individualized regimens. Regrettably, only core needle biopsy can provide the most direct evidence of lymph node metastasis, but it is expensive and time-consuming. Therefore, it is vital to develop an accurate and convenient model to evaluate the status of axillary lymph node metastasis.

Recently, Ye et al. constructed a nomogram to predict preoperative lymph node involvement of breast IMPC (7), but this LR-based model can only give low area under curve (AUC) of 0.735. Besides, the absence of external validation and the comparison of different models limit the application of the nomogram model. For the past few years, machine learning (ML) has drawn wide attention and has been applied to solve various medical problems, including outcome prediction and treatment support (8–10). Although ML has also been used to predict axillary lymph node metastasis in breast cancer (11, 12). it has not been used in IMPC. Besides, even with huge samples, these ML models lacked concrete explanations and intuitional understanding, limiting their wider applications. To solve the problem, SHapley Additive exPlanations (SHAP) framework, which was firstly proposed by Lundberg et al. (13) and is able to evaluate the contribution of each explanatory variable in any ML models (14), was introduced into this study.

This study aims to develop different ML models to predict axillary lymph node metastasis of breast IMPC and compare the predictive ability of different models. Furthermore, the SHAP framework was applied to intuitively explain the performance of the optimal model. Besides, the risk factors of LNM were also been explored.

Methods and patients

Patient selection

In this retrospective analysis, a total of 1405 patients diagnosed with breast IMPC ((ICD-O-3 8507) from Surveillance, Epidemiology, and End Results (SEER) database from 2010 to 2015 were incorporated for ML models construction; and 142 patients diagnosed with breast IMPC from Harbin Medical University Cancer Hospital between 2010-2015 were included for the external validation of the optimal ML model. In every state of the United States, cancer is a reportable disease, so no informed patient consent was required to release the SEER database. The ethics committee of Harbin Medical University Cancer Hospital approved this study. It complies with the World Medical Association Declaration of Helsinki in 1964 and subsequently amended versions. An informed consent form was signed prior to undergoing treatment.

Inclusion criteria (1): pathologically confirmed breast IMPC ((ICD-O-3 8507) (2); unilateral breast IMPC (3); patients diagnosed between 2010-2015; and (4) all patients in the external validation cohort underwent surgery in our hospital.

Exclusion criteria (1): bilateral, single primary breast IMPC; and (2) breast subtype record not available or unknown.

The flow chart for patient selection is shown in Figure S1.

Study outcome

The primary endpoint of this study was axillary lymph node metastasis. If the pathologist examines one or more axillary lymph nodes to be positive, then the axillary lymph node metastasis is confirmed.

Feature selection and data preprocessing

The method of KNNImputer was applied to variables with a missing age percentage of less than 30% (15). Features statistically correlated with LNM in univariable analysis were selected to develop ML models (Table 1). Notably, because the external validation cohort lacked male samples, gender features were excluded for model stability. Besides, other features, including estrogen receptor (ER), progesterone receptor (PR), human epidermal growth factor receptor2 (HER-2) and laterality (16–20), which had been proved to be related with LNM, were incorporated for model construction.

The development of ML models

We introduced seven ML algorithms using clinical and pathological data to predict axillary LNM, and these algorithms are LR, support vector machine (SVM), k-nearest neighbor (KNN), random forest (RF), Light Gradient Boosting Machine (lightGBM), adaptive boosting (AdaBoost) and extreme gradient boosting (XGBoost). LR models are commonly used to study the impact of trait variables on a binary classification variable (21). Based on hyperspace, SVM is often used to classify things with multidimensional properties into two categories (22). The KNN system, one of the most commonly used nonparametric classification techniques, works on the premise that if the k-nearest samples in the vicinity of a sample mostly belong to a certain class in the feature space, they must also belong to the same category (23). A classifier that uses multiple trees for training and predicting samples is known as the RF, which reduces training variance and improves integration and generalization (24). The Microsoft LightGBM is an ensemble algorithm that implements gradient boosting efficiently (25). AdaBoost, a powerful ensemble method, is an ensemble of weak learners that improves generalization ability (26). XGBoost is a machine learning technology that can efficiently and flexibly process missing data and build accurate

TABLE 1 Clinical and pathological characteristics of different cohorts.

Variable	SEER Cohort				External Validation Cohort			
	N=1405 (%)	Non-LNM n=687 (%)	LNM n=718 (%)	p	N=142 (%)	Non-LNM n=47 (%)	LNM n=95 (%)	p
Age	62 [52, 71]	64 [55, 73]	59 [49, 69]	**<0.001**	52.69 (10.22)	56.13 (9.69)	50.99 (10.10)	**0.004**
Sex				**0.027**				NA
female	1378 (98.1)	680 (99.0)	698 (97.2)		142 (100.0)	47 (100.0)	95 (100.0)	
male	27 (1.9)	7 (1.0)	20 (2.8)		NA	NA	NA	
Laterality				0.905				0.332
left	690 (49.1)	339 (49.3)	351 (48.9)		81 (57.0)	30 (63.8)	51 (53.7)	
right	715 (50.9)	348 (50.7)	367 (51.1)		61 (43.0)	17 (36.2)	44 (46.3)	
Subtype				0.134				0.888
luminal A	1042 (74.2)	526 (76.6)	516 (71.9)		51 (35.9)	16 (34.0)	35 (36.8)	
luminal B	242 (17.2)	111 (16.2)	131 (18.2)		91 (64.1)	31 (66.0)	60 (63.2)	
HER-2 OE	64 (4.6)	29 (4.2)	35 (4.9)		NA	NA	NA	
TNBC	57 (4.1)	21 (3.1)	36 (5.0)		NA	NA	NA	
ER				0.061				1
negative	128 (9.1)	52 (7.6)	76 (10.6)		3 (2.1)	1 (2.1)	2 (2.1)	
positive	1277 (90.9)	635 (92.4)	642 (89.4)		139 (97.9)	46 (97.9)	93 (97.9)	
PR				0.837				0.426
negative	274 (19.5)	136 (19.8)	138 (19.2)		17 (12.0)	4 (8.5)	13 (13.7)	
positive	1131 (80.5)	551 (80.2)	580 (80.8)		125 (88.0)	43 (91.5)	82 (86.3)	
HER-2				0.238				0.951
negative	1099 (78.2)	547 (79.6)	552 (76.9)		122 (85.9)	41 (87.2)	81 (85.3)	
positive	306 (21.8)	140 (20.4)	166 (23.1)		20 (14.1)	6 (12.8)	14 (14.7)	
Tumor Size				**<0.001**				**0.003**
<=20 mm	793 (56.4)	532 (77.4)	261 (36.4)		73 (51.4)	33 (70.2)	40 (42.1)	
20-50 mm	469 (33.4)	142 (20.7)	327 (45.5)		67 (47.2)	14 (29.8)	53 (55.8)	
>50 mm	143 (10.2)	13 (1.9)	130 (18.1)		2 (1.4)	0 (0.0)	2 (2.1)	

LNM, lymph node metastasis; HER2, human epidermal growth factor receptor2; TNBC, triple negative breast cancer; ER, estrogen receptor; PR, progesterone receptor. The bold values/numbers mean: p value < 0.05. NA, Not Available.

prediction models with weak prediction models (27). All the patients were randomly divided into two groups (training set and test set) in a ratio of 7:3. The ML model hyperparameters are optimized with ten-fold CV grid search. The training set was applied to construct ML models. The test set cohort was applied to evaluate the performance of different ML models. In order to avoid over-fitting and improve the prediction ability of the model, the hold-out method was applied. External validation cohort was used to validate the performance of the optimal ML model (Figure 1).

The interpretability of optimal ML model

ML models are often regarded as 'black boxes' because it is difficult to explain why they can accurately predict the special cohort of patients. Therefore, we bring in the SHAP value to determine the optimal ML model in this research. SHAP is a new method to explain the contribution of different variable in any ML models (14). Its interpretability performance had been validated in many cancers (28–31). In contrast to other methods, the SHAP method is based on sound theoretical groundwork, providing both local and global interpretability (32). We used SHAP values to assess the probability of LNM of whole cohort or an individual.

Statistical analysis

All the analysis were conducted by R software version 4.1.3 (forestmodel and dplyr packages) and python version 3.9.7 (scikitplot, sklearn, matplotlib.pyplot, lightgbm, xgboost, sklearn.neighbors, sklearn.svm, numpy, and shap packages).

Frequencies and percentages (%) were applied to describe categorical variables, while the chi-squared test or Fisher's exact test was applied to assess differences. The median and mean values of continuous variables were presented with the interquartile range (IQR) and standard deviation (SD). The AUC was applied to compare the performance of each ML model. The Brier score (33) was applied to evaluate the calibration of each ML model. The best cut-off value was determined by Youden's index. Multivariable analysis was conducted by LR. A nomogram was established on the basis of multivariate analysis, and a graphic analysis was performed on the differences between actual and predicted probabilities obtained by the nomograms. $P<0.05$ was deemed statistically significant.

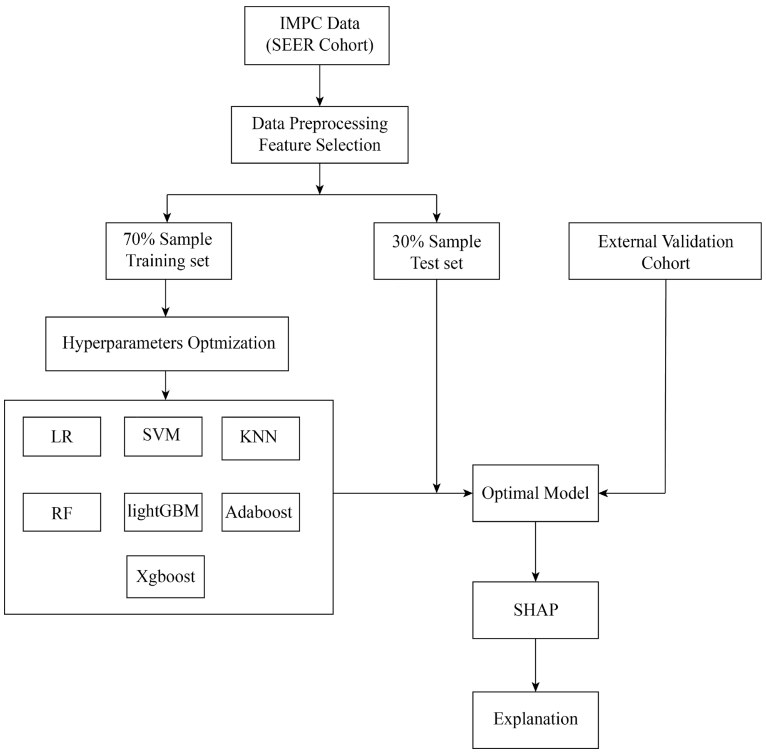

FIGURE 1
Flow chart for the development, explanation and validation of models.

Results

The baseline of breast IMPC patients

The SEER cohort included 1405 breast IMPC patients, 718 (51.1%) of whom suffered from LNM, the external validation cohort covered 142 breast IMPC patients, 95 (66.9%) of whom suffered from LNM, and most patients were female and belonged to luminal subtype in both cohorts. Besides, the patients among the SEER cohort and external validation cohort who belonged to ER accounted for respectively 90.9% and 97.9%, the ones belong to PR accounted for respectively 80.5% and 88.0%, while those diagnosed with HER-2 positive were 306 (21.8%), and 20 (14.1%), respectively.

The association between age and tumor size with LNM was observed in both cohorts (P <0.05). The relation between sex and LNM was confirmed in SEER cohort, while remaining untouched in external validation cohort because of the limited samples. (Table 1)

The predictive ability of different ML models

AUC and Brier score were adopted to compare seven ML models, revealing that model Xgboost outperformed with the biggest AUC of 0.813 (95% CI: 0.7994 - 0.8262; Figure 2A), the calibration curve (the red line) that was closest to the perfectly calibrated curve (the black line), and the smallest Brier score of 0.186 (95% CI: 0.799-0.826; Figure 2B). Therefore, model Xgboost was selected to predict LNM of IMPC.

The visualization of feature importance

SHAP was adopted to evaluate the effect of these selected variables on the LNM of IMPC, and to explain such variables. The feature importance of variables was ranked through the mean (|SHAP value|), and the tumor size stood out (Figure 3A). Figure 3B illustrated their detailed impact on LNM. The SHAP value (x-axis) referred to how the value or status of different variables influenced the LNM in the model, while the feature value (y-axis) the change of a certain variable. A bigger tumor size and smaller age increased the risk of LNM, while the status of ER, HER-2, PR and laterality exerted limited impact.

Molecular subtype-based analysis

Tumor size and age served as important risk factors for LNM in different molecular subtype of breast IMPC. ER status was the third important risk factor for LNM in luminal A, HER-2 OE, and TNBC subtypes, while HER-2 was the third in luminal B subtype. (Figure 4)

Individualized prediction

Based on the SHAP value, the risk of LNM in each patient was calculated. Two classical patients, including a 57-year-old without LNM and a 72-year-old with LNM, were explored to interpret the optimal model (Figure 5). The waterfall plot demonstrated the impact of variables on LNM, in which the red arrow indicated the increased risk, while the blue arrow the

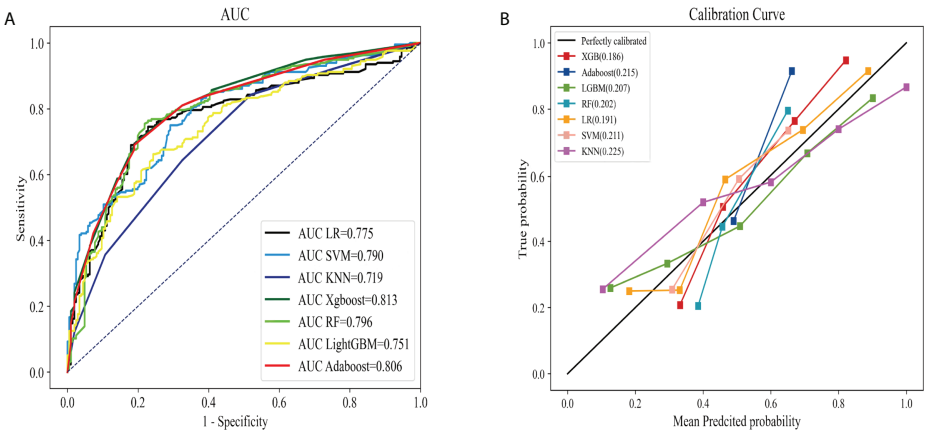

FIGURE 2
The perfomance comparison of different machine learning models in predicting lyph node metastasis. The receiver operating characteristic curves **(A)** and calibration curves **(B)** of different models.

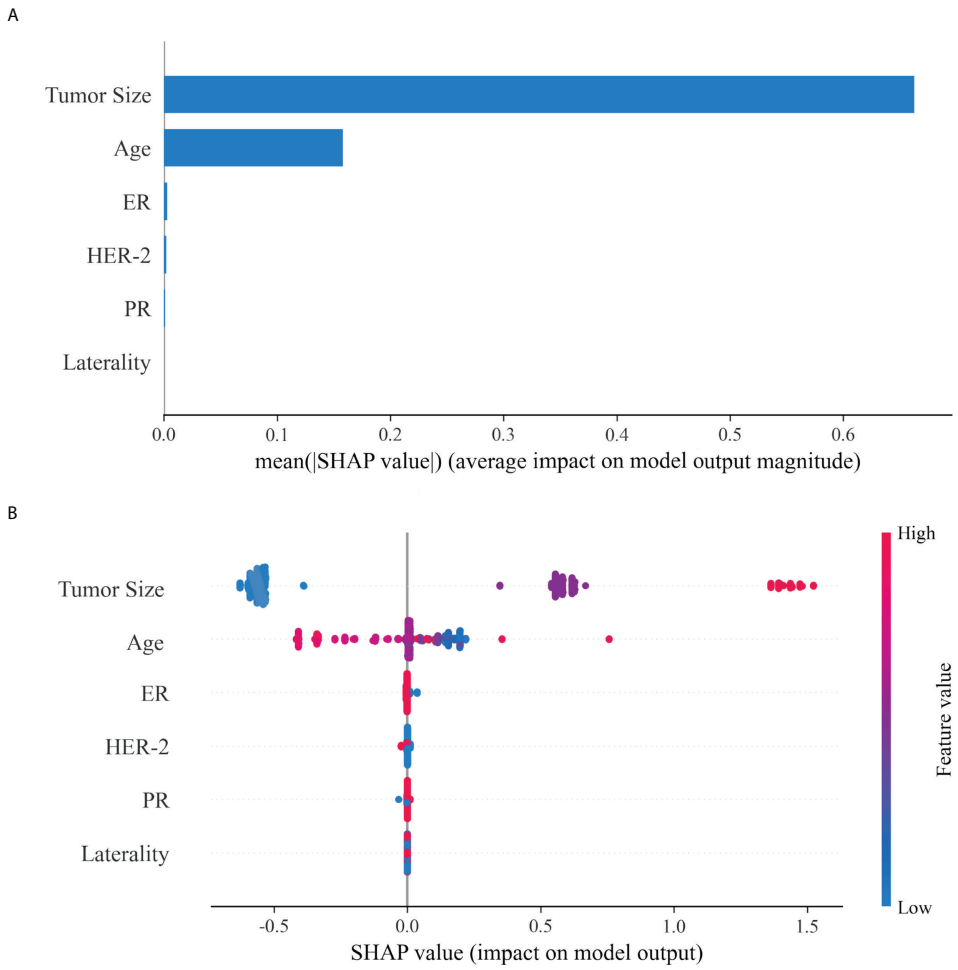

FIGURE 3
The interpretation of optimal model (Xgboost). **(A)**: The importance ranking of different variables according to the mean (|SHAP value|); **(B)**: The importance ranking of different risk factors with stability and interpretation using the optimal model. The higher SHAP value of a feature is given, the higher risk of lymph node metastasis the patient would have.The red part in feature value represents higher feature value.

decreased risk. The SHAP value was calculated by combining the effects of variables, which corresponded to the prediction score. The non-LNM patient (Figure 5A) performed a low SHAP value (-0.382) and prediction score (0.405529), and the LNM patient (Figure 5B) exhibited a high SHAP value (1.26) and prediction score (0.778945).

The multivariable logistic regression analysis

The Xgboost model was applied to predict LNM in the test set. All patients were divided into high and low risk groups according to the best cut-off value (0.42) determined by the Youden's index (Figure 6). The unadjusted LR analysis found that patients in the high-risk group were more prone to LNM (unadjusted OR:8.86, 95% CI: 5.71-13.99, P<0.001). Despite the adjustment of the five most influential variables (tumor size, age, ER, HER-2, and PR), prediction score was correlated with LNM (adjusted OR:2.73, 95% CI: 1.30-5.71, P=0.008; Figure 7).

The external validation for the predictive model

The Xgboost model, which outperformed in stability and accuracy compared with other ML models, was assessed by employing 142 breast IMPC samples from our hospital, so as to further identify its accuracy and stability. The result demonstrated that the model achieved a big AUC of 0.700 (95% CI: 0.682 - 0.72; Figure 8A), and a low Brier score of 0.220 (95% CI: 0.216-0.225; Figure 8B).

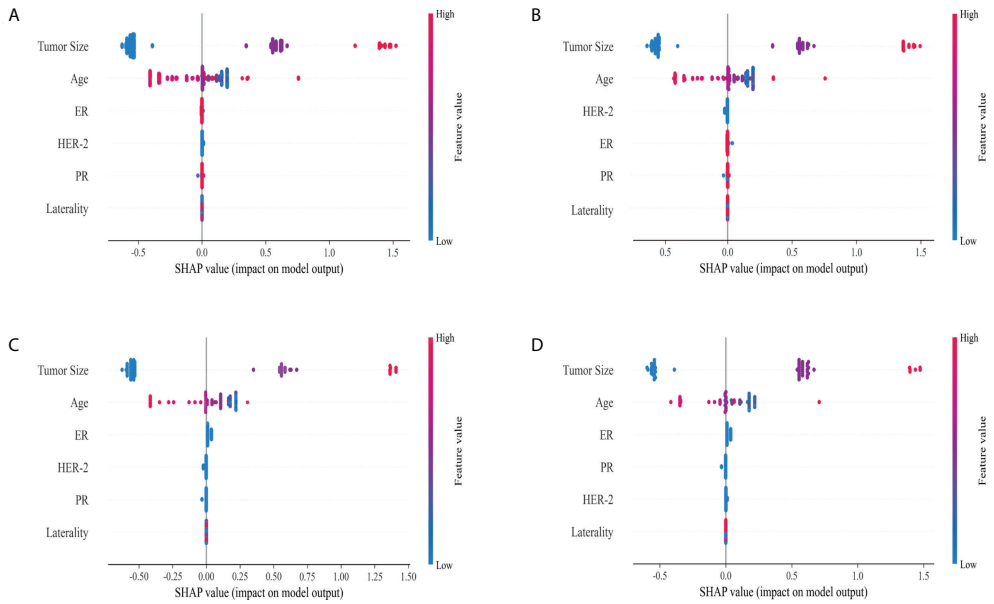

FIGURE 4
Variable importance in ML classification for Luminal A (**A**, n = 1042), Luminal B (**B**, n = 242), HER-2 overexpression (**C**, n = 64) and TNBC (**D**, n=57).

The performance of comparison of Xgboost and nomogram (LR) model

A nomogram was constructed in train set, test set, and external validation cohort, respectively, according to LR modes (Figure S2). All three nomograms based on clinical and pathological variables performed favorably. Nevertheless, the model Xgboost exhibited a bigger AUC in training (0.761 vs 0.745) and test sets (0.813 vs 0.775) compared with the LR model. The AUCs of these two models were similar (0.700 vs 0.703) in external validation cohort. Besides, Brier Score of Xgboost was smaller in these three sets (0.202 vs 0.204; 0.186 vs 0.191; 0.220 vs 0.221; respectively; Table 2).

Discussion

As a special subtype of breast cancer, IMPC cells was susceptible to invasion and metastasis because of special growth pattern and histological morphology induced by polarity reversal (34). Compared to breast invasive ductal carcinoma (IDC), breast IMPC had higher LNM rate and worse survival outcome (4, 35–37). Given the close association between LNM and survival outcome, a tool that identifies LNM can help doctors in instituting heal project and timely adjusting the treatment program. This paper chose the best ML model Xgboost following the comparison of seven powerful ML models to predict LNM of breast IMPC, whose performance was validated in the test set and external validation cohort. Through the SHAP values and plots, the feature importance rank and contribution to LNM of risk factors were intuitively demonstrated. Besides, the prediction score based on Xgboost was proved to be an independent predictive factor for LNM.

Nassar et al. found no significant differences in lymph node status, ER status, tumor size, grade, or lymph vascular invasion between tumors with different invasive micropapillary components (5). In addition, the difference of survival outcome between IMPC and IDC with similar stage was negligible. Therefore, despite their worse survival outcome than IDC patients, IMPC patients follow IDC treatment protocols, the current standard of care (38).

The correlation between LNM and worse survival time of breast cancer patients is known (6). Breast cancer patients with LNM underwent axillary lymph node dissection (ALND) in the past. The results of ACOSOG Z0011 (Alliance) Randomized Clinical Trial, however, indicated the similar 10-year overall survival between patients treated with ALND and those treated with sentinel lymph node dissection (SLNB) alone in T1 or T2 stage with 1 or 2 SLN metastasis (39), which explained the current wide application of SLNB for early operable invasive breast cancer patients with negative clinical lymph node. Nevertheless, it was still controversial if SLNB was suitable for breast IMPC (40). The information about the status of axillary lymph node facilitated doctors in developing an individualized treatment plan, thus avoiding overtreatment or undertreatment, which highlighted that the management of axillary lymph node deserved more attention.

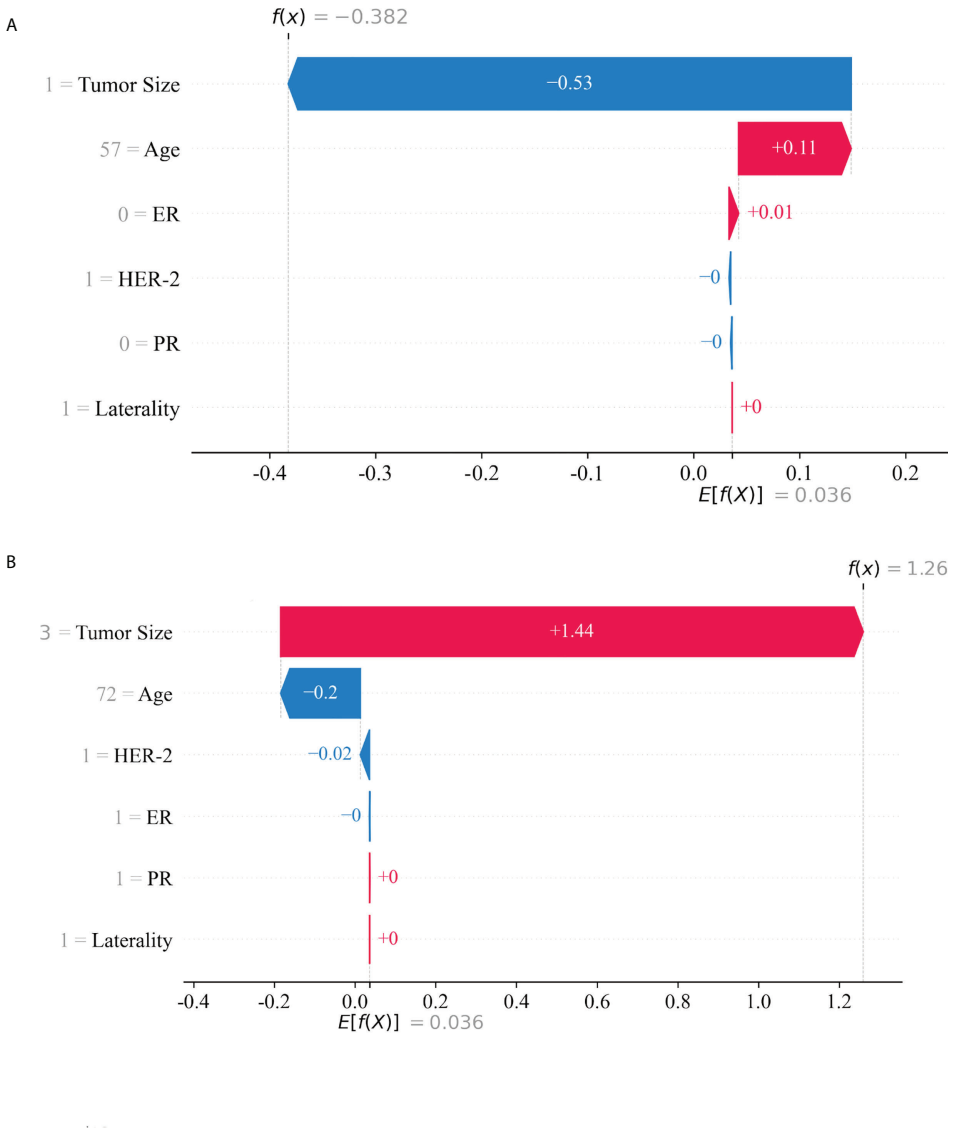

FIGURE 5
The interpretation of model prediction results with the two samples. A patient with no lymph node metastasis **(A)**. A patient with lymph node metastasis **(B)**.

In response, Ye and his team developed a nomogram to predict preoperative lymph node involvement for breast IMPC patients (7), and propose nomogram as a good tool for LNM prediction. Their study based on SEER database, however, lacked external validation and the comparison of model performance. Actually, the performance comparison between nomogram and ML models had been conducted in different disease. Rasheed et al. proved the higher accuracy of boosted decision tree than nomogram in predicting overall survival among patients with tongue cancer (41), and Thara and his team demonstrated the bigger AUC of random forest classifier model than nomogram in predicting intracranial injury following cranial CT of the brain (42), which unfortunately were also short of external validation and intuitive explanation to the model.

Previous studies took that most breast IMPC were ER positive (72%-75%), almost half were HR positive, and patients with HER-2 positive ranged from 10%-30% (43–45). In this paper, the proportion of patients in the SEER cohort and external validation cohort with ER positive was 90.9% and 97.9%, respectively, that with PR positive was respectively 80.5% and 88.0%, while that with HER-2 positive was respectively 21.8% and 14.1%, which shared the results of the above studies, and verified the stability and reliability of the samples adopted. Training set was adopted to develop the ML

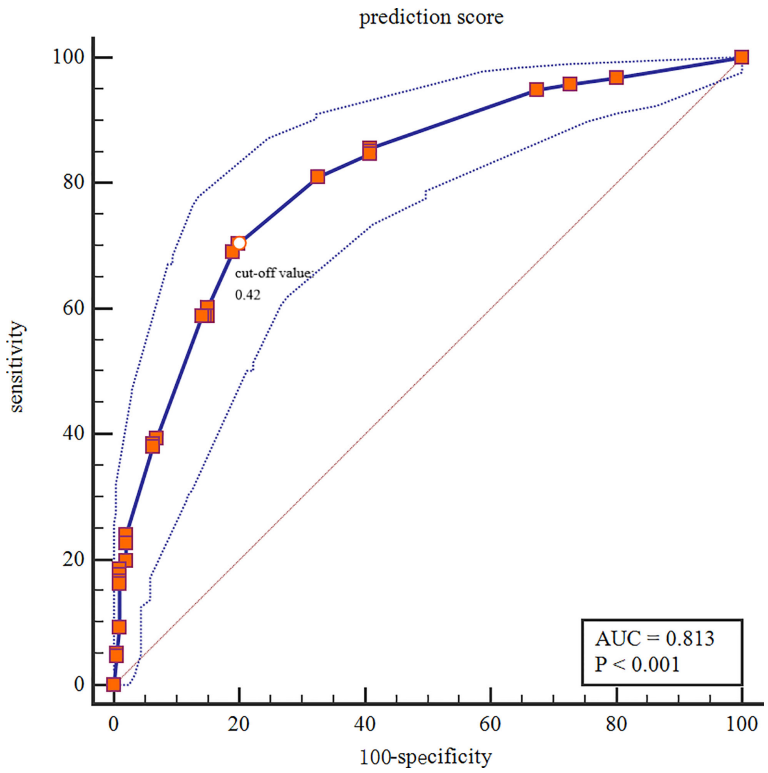

FIGURE 6
Categorization threshold of Prediction score.

models, and the ability of optimal model Xgboost and nomogram in test set and external validation cohort was compared, demonstrating the bigger AUC of model Xgboost in training (0.761 vs 0.745) and test sets (0.813 vs 0.775), and the smallest Brier Score of Xgboost in three sets (0.202 vs 0.204; 0.186 vs 0.191; 0.220 vs 0.221; respectively; Table 2). The AUC of Xgboost was slightly less than that of LR model (nomogram) in external validation cohort, which came down to small sample and racial difference (all patients in external validation cohort were Chinses while most patients in training and test sets came from US), but the Xgboost was still a better model than nomogram based on LR. Meanwhile, instead of nomogram which only showed the score of each variable in predicting LNM, SHAP was adopted in the paper to visually demonstrate the contribution of each variable. The SHAP plots intuitively displayed the increased or decreased contribution of each variable to LNM, and the bigger SHAP value indicated higher probability of LNM. In addition, SHAP values indicated the feature importance rank of each variable, and tumor size was the most influential risk factor for LNM. The feature importance of each variable in different molecular subtype was also compared, revealing tumor size to be the most important one. Instead, the application of nomogram failed to rank the importance of features, which validated the better practicability and predictive ability of model Xgboost. The contribution of prediction score was also evaluated based on Xgboost. After adjusting for confounding factors, prediction score was significantly associated with LNM, and patients in high prediction score group had higher risk for LNM. ML model was generally a better tool than nomogram based on LR in predicting LNM of breast IMPC patients.

Despite being the first to predict LNM of breast IMPC patients using ML models and compare its performance with nomogram based on LR to the authors' knowledge, this study was limited in the following aspects. Firstly, a prospective analysis was required to further identify the performance of Xgboost model even for the paper, a multicenter retrospective analysis. Secondly, the huge samples from SEER database could not make up for its limited clinical and pathological information, which required a cohort including more details of breast IMPC patients. Besides, the XGBoost model combined with more features (like Grade) could train more useful information about LNM, so as to promote its performance, which consolidated its clinical advantages compared with LR model. Thirdly, the clinical application of the ML model constructed based on SEER database was limited due to the highly homogenous feature of IMPC, a rare subtype of invasive breast cancer. Therefore, a larger sample contained different

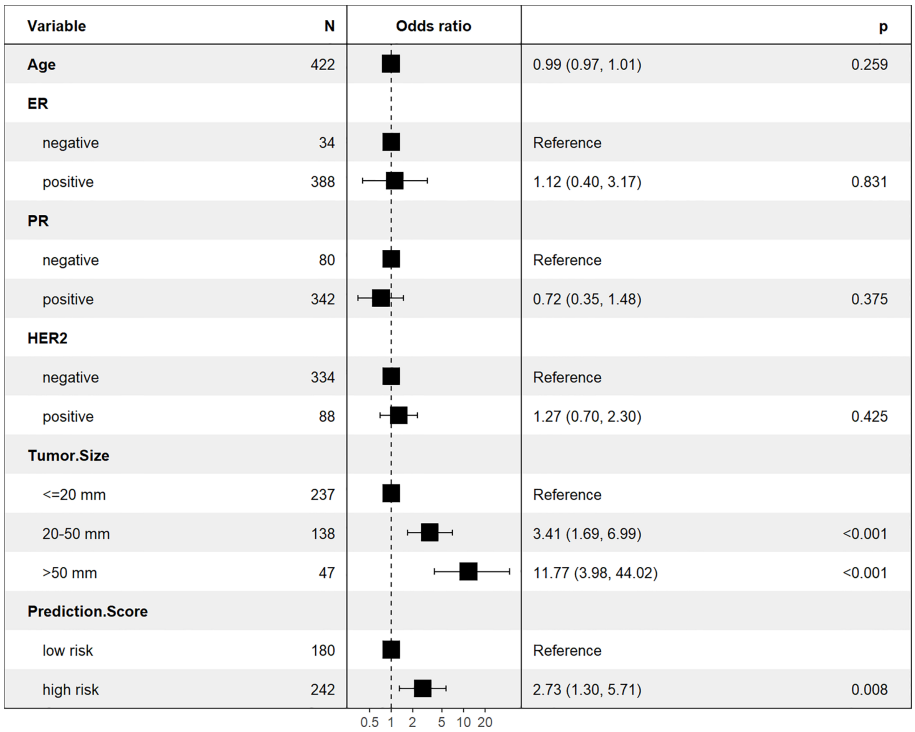

FIGURE 7
The multivariable logistic regression analysis for LNM prediction.

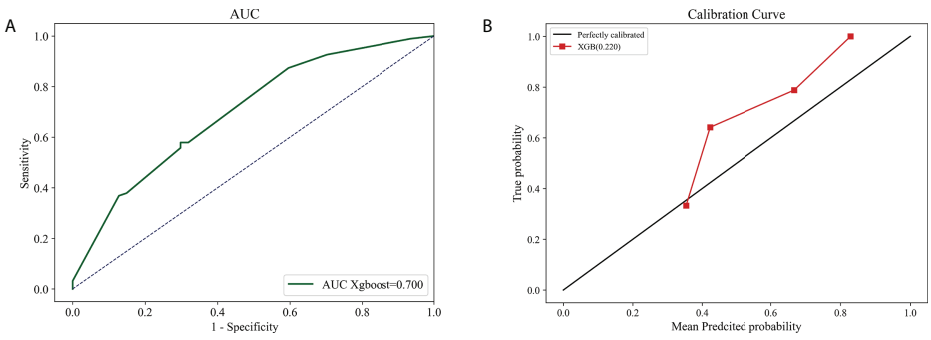

FIGURE 8
The external validation based on Xgboost model. The AUC curve **(A)** and calibration curve **(B)** 1n external validation cohort.

TABLE 2 The comparison of Xgboost and nomogram (LR) model.

Model	Training set		Test set		External validation cohort	
	AUC	Brier Score	AUC	Brier Score	AUC	Brier Score
LR	0.745 (0.730-0.758)	0.204 (0.199-0.210)	0.775 (0.761-0.790)	0.191 (0.186-0.197)	0.703 (0.685-0.718)	0.221 (0.215-0.225)
Xgboost	0.761 (0.746-0.776)	0.202 (0.197-0.206)	0.813 (0.799-0.826)	0.186 (0.182-0.190)	0.700 (0.683- 0.716)	0.220 (0.216-0.225)

histological types of breast cancer, like breast invasive ductal cancer, was needed to expand the clinical practicability of the best ML model.

Conclusions

The ML models, especially Xgboost, outperformed traditional LR-based nomogram model in predicting LNM of breast IMPC patients. The combination of Xgboost and SHAP intuitively reflected the influence of different variables on LNM, and the tumor size was the most important risk factor of LNM for breast IMPC patients. In addition, the prediction score derived from Xgboost model served as a good indicator for LNM.

Data availability statement

The raw data supporting the conclusions of this article will be made available by the authors, without undue reservation.

Ethics statement

This research was approved by the ethics committee of Harbin Medical University Cancer Hospital. It complies with the World Medical Association Declaration of Helsinki in 1964 and its later amendments. All patients signed the informed consent before each treatment.

Author contributions

CJ and YH conceptualized and designed the work. YX, KQ and XY collected all the data. CJ and SZ drafted and analyzed the manuscript. All authors contributed to the article and approved the submitted version.

Funding

This work was supported by the Haiyan Foundation of Harbin Medical University Cancer Hospital (Grant Number: JJQN2022-01). The funder played no role in the study design, data collection and analysis, decision to publish, or preparation of the manuscript.

Acknowledgments

Thanks for the data provided by Harbin Medical University Cancer Hospital.

Conflict of interest

The authors declare that the research was conducted in the absence of any commercial or financial relationships that could be construed as a potential conflict of interest.

Publisher's note

Supplementary material

The Supplementary Material for this article can be found online at: https://www.frontiersin.org/articles/10.3389/fonc.2022.981059/full#supplementary-material

References

1. Bocker W. WHO classification of breast tumors and tumors of the female genital organs: pathology and genetics. *Verh Dtsch Ges Pathol* (2002) 86:116–9. doi: 10.1111/j.1365-2141.1979.tb05888.x

2. Fisher ER, Palekar AS, Redmond C, Barton B, Fisher B. Pathologic findings from the national surgical adjuvant breast project (protocol no. 4). VI. invasive papillary cancer. *Am J Clin Pathol* (1980) 73(3):313–22. doi: 10.1093/ajcp/73.3.313

3. Li W, Han Y, Wang C, Guo X, Shen B, Liu F, et al. Precise pathologic diagnosis and individualized treatment improve the outcomes of invasive micropapillary carcinoma of the breast: a 12-year prospective clinical study. *Mod Pathol* (2018) 31(6):956–64. doi: 10.1038/s41379-018-0024-8

4. Chen L, Fan Y, Lang RG, Guo XJ, Sun YL, Cui LF, et al. Breast carcinoma with micropapillary features: clinicopathologic study and long-term follow-up of 100 cases. *Int J Surg Pathol* (2008) 16(2):155–63. doi: 10.1177/1066896907307047

5. Nassar H, Wallis T, Andea A, Dey J, Adsay V, Visscher D. Clinicopathologic analysis of invasive micropapillary differentiation in breast carcinoma. *Mod Pathol* (2001) 14(9):836–41. doi: 10.1038/modpathol.3880399

6. Pan H, Gray R, Braybrooke J, Davies C, Taylor C, McGale P, et al. 20-year risks of breast-cancer recurrence after stopping endocrine therapy at 5 years. *N Engl J Med* (2017) 377(19):1836–46. doi: 10.1056/NEJMoa1701830

7. Ye FG, Xia C, Ma D, Lin PY, Hu X, Shao ZM. Nomogram for predicting preoperative lymph node involvement in patients with invasive micropapillary carcinoma of breast: a SEER population-based study. *BMC Cancer* (2018) 18 (1):1085. doi: 10.1186/s12885-018-4982-5

8. Komura D, Ishikawa S. Machine learning approaches for pathologic diagnosis. *Virchows Arch* (2019) 475(2):131–38. doi: 10.1007/s00428-019-02594-w

9. Van Calster B, Wynants L. Machine learning in medicine. *N Engl J Med* (2019) 380(26):2588. doi: 10.1056/NEJMc1906060

10. Handelman GS, Kok HK, Chandra RV, Razavi AH, Lee MJ, Asadi H. eDoctor: machine learning and the future of medicine. *J Intern Med* (2018) 284 (6):603–19. doi: 10.1111/joim.12822

11. Yu Y, He Z, Ouyang J, Tan Y, Chen Y, Gu Y, et al. Magnetic resonance imaging radiomics predicts preoperative axillary lymph node metastasis to support surgical decisions and is associated with tumor microenvironment in invasive breast cancer: A machine learning, multicenter study. *EbioMedicine* (2021) 69:103460. doi: 10.1016/j.ebiom.2021.103460

12. Arefan D, Chai R, Sun M, Zuley ML, Wu S. Machine learning prediction of axillary lymph node metastasis in breast cancer: 2D versus 3D radiomic features. *Med Phys* (2020) 47(12):6334–42. doi: 10.1002/mp.14538

13. Lundberg S, Lee SI. A Unified Approach to Interpreting Model Predictions [J]. *Nips* (2017).

14. Rodríguez-Pérez R, Bajorath J. Interpretation of machine learning models using shapley values: application to compound potency and multi-target activity predictions. *J Comput Aided Mol Des*. (2020) 34(10):1013–1026. doi: 10.1007/s10822-020-00314-0

15. AlJame M, Ahmad I, Imtiaz A, Mohammed A. Ensemble learning model for diagnosing COVID-19 from routine blood tests. *Inform Med Unlocked* (2020) 21:100449. doi: 10.1016/j.imu.2020.100449

16. Van Calster B, Vanden Bempt I, Drijkoningen M, Pochet N, Cheng J, Van Huffel S, et al. Axillary lymph node status of operable breast cancers by combined steroid receptor and HER-2 status: triple positive tumours are more likely lymph node positive. *Breast Cancer Res Treat* (2009) 113(1):181–7. doi: 10.1007/s10549-008-9914-7

17. Tong ZJ, Shi NY, Zhang ZJ, Yuan XD, Hong XM. Expression and prognostic value of HER-2/neu in primary breast cancer with sentinel lymph node metastasis. *Biosci Rep* (2017) 37(4):BSR20170121. doi: 10.1042/BSR20170121

18. Rasponi A, Costa A, Bufalino R, Morabito A, Nava M, Marolda R, et al. Breast cancer: primary tumor characteristics related to lymph node involvement. *Tumori* (1981) 67(1):19–26. doi: 10.1177/030089168106700104

19. Mohammed H, Russell IA, Stark R, Rueda OM, Hickey TE, Tarulli GA, et al. Progesterone receptor modulates ERalpha action in breast cancer. *Nature* (2015) 523(7560):313–7. doi: 10.1038/nature14583

20. Bartlett JM, Ellis IO, Dowsett M, Mallon EA, Cameron DA, Johnston S, et al. Human epidermal growth factor receptor 2 status correlates with lymph node involvement in patients with estrogen receptor (ER) negative, but with grade in those with ER-positive early-stage breast cancer suitable for cytotoxic chemotherapy. *J Clin Oncol* (2007) 25(28):4423–30. doi: 10.1200/JCO.2007.11.0973

21. Nick TG, Campbell KM. Logistic regression. *Methods Mol Biol* (2007) 404:273–301. doi: 10.1007/978-1-59745-530-5_14

22. Noble WS. What is a support vector machine? *Nat Biotechnol* (2006) 24 (12):1565–7. doi: 10.1038/nbt1206-1565

23. Salvador-Meneses J, Ruiz-Chavez Z, Garcia-Rodriguez J. Compressed kNN: K-nearest neighbors with data compression. *Entropy (Basel)* (2019) 21(3):234. doi: 10.3390/e21030234

24. Jiang H, Mao H, Lu H, Lin P, Garry W, Lu H, et al. Machine learning-based models to support decision-making in emergency department triage for patients with suspected cardiovascular disease. *Int J Med Inform* (2021) 145:104326. doi: 10.1016/j.ijmedinf.2020.104326

25. Qi M. LightGBM: A highly efficient gradient boosting decision tree. *Neural Information Processing Systems* Curran Associates Inc. (2017).

26. Zhang PB, Yang ZX. A novel AdaBoost framework with robust threshold and structural optimization. *IEEE Trans Cybern* (2018) 48(1):64–76. doi: 10.1109/TCYB.2016.2623900

27. Yuan KC, Tsai LW, Lee KH, Cheng YW, Hsu SC, Lo YS, et al. The development an artificial intelligence algorithm for early sepsis diagnosis in the intensive care unit. *Int J Med Inform* (2020) 141:104176. doi: 10.1016/j.ijmedinf.2020.104176

28. Manikis GC, Ioannidis GS, Siakallis L, Nikiforaki K, Iv M, Vozlic D, et al (2021). Multicenter DSC-MRI-Based Radiomics Predict IDH Mutation in Gliomas. *Cancers* 13(16):3965. doi: 10.3390/cancers13163965

29. Li R, Shinde A, Liu A, Glaser S, Lyou Y, Yuh B, et al. Machine learning-based interpretation and visualization of nonlinear interactions in prostate cancer survival. *JCO Clin Cancer Inform* (2020) 4:637–46. doi: 10.1200/CCI.20.00002

30. Ladbury C, Li R, Shiao J, Liu J, Cristea M, Han E, et al. Characterizing impact of positive lymph node number in endometrial cancer using machine-learning: A better prognostic indicator than FIGO staging? *Gynecol Oncol* (2022) 164(1):39–45. doi: 10.1016/j.ygyno.2021.11.007

31. Chen X, Li Y, Li X, Cao X, Xiang Y, Xia W, et al. An interpretable machine learning prognostic system for locoregionally advanced nasopharyngeal carcinoma based on tumor burden features. *Oral Oncol* (2021) 118:105335. doi: 10.1016/j.oraloncology.2021.105335

32. Lundberg SM, Nair B, Vavilala MS, Horibe M, Eisses MJ, Adams T, et al. Explainable machine-learning predictions for the prevention of hypoxaemia during surgery. *Nat BioMed Eng* (2018) 2(10):749–60. doi: 10.1038/s41551-018-0304-0

33. Rufibach K. Use of brier score to assess binary predictions. *J Clin Epidemiol* (2010) 63(8):938–9. doi: 10.1016/j.jclinepi.2009.11.009

34. Fu L, Ikuo M, Fu XY, Liu TH, Shinichi T. [Relationship between biologic behavior and morphologic features of invasive micropapillary carcinoma of the breast]. *Zhonghua Bing Li Xue Za Zhi* (2004) 33(1):21–5. doi: 10.3760/j.issn:0529-5807.2004.01.006

35. Zekioglu O, Erhan Y, Ciris M, Bayramoglu H, Ozdemir N. Invasive micropapillary carcinoma of the breast: high incidence of lymph node metastasis with extranodal extension and its immunohistochemical profile compared with invasive ductal carcinoma. *Histopathology* (2004) 44(1):18–23. doi: 10.1111/j.1365-2559.2004.01757.x

36. Yu JI, Choi DH, Park W, Huh SJ, Cho EY, Lim YH, et al. Differences in prognostic factors and patterns of failure between invasive micropapillary carcinoma and invasive ductal carcinoma of the breast: matched case-control study. *Breast* (2010) 19(3):231–7. doi: 10.1016/j.breast.2010.01.020

37. Adrada B, Arribas E, Gilcrease M, Yang WT. Invasive micropapillary carcinoma of the breast: mammographic, sonographic, and MRI features. *AJR Am J Roentgenol* (2009) 193(1):W58–63. doi: 10.2214/AJR.08.1537

38. Tang SL, Yang JQ, Du ZG, Tan QW, Zhou YT, Zhang D, et al. Clinicopathologic study of invasive micropapillary carcinoma of the breast. *Oncotarget* (2017) 8(26):42455–65. doi: 10.18632/oncotarget.16405

39. Giuliano AE, Ballman KV, McCall L, Beitsch PD, Brennan MB, Kelemen PR, et al. Effect of axillary dissection vs no axillary dissection on 10-year overall survival among women with invasive breast cancer and sentinel node metastasis: The ACOSOG Z0011 (Alliance) randomized clinical trial. *JAMA* (2017) 318 (10):918–26. doi: 10.1001/jama.2017.11470

40. Paterakos M, Watkin WG, Edgerton SM, Moore DH2nd, Thor AD. Invasive micropapillary carcinoma of the breast: a prognostic study. *Hum Pathol* (1999) 30 (12):1459–63. doi: 10.1016/s0046-8177(99)90168-5

41. Alabi RO, Makitie AA, Pirinen M, Elmusrati M, Leivo I, Almangush A. Comparison of nomogram with machine learning techniques for prediction of overall survival in patients with tongue cancer. *Int J Med Inform* (2021) 145:104313. doi: 10.1016/j.ijmedinf.2020.104313

42. Tunthanathip T, Duangsuwan J, Wattanakitrungroj N, Tongman S, Phuenpathom N. Comparison of intracranial injury predictability between machine learning algorithms and the nomogram in pediatric traumatic brain injury. *Neurosurg Focus* (2021) 51(5):E7. doi: 10.3171/2021.8.FOCUS2155

43. Marchio C, Iravani M, Natrajan R, Lambros MB, Savage K, Tamber N, et al. Genomic and immunophenotypical characterization of pure micropapillary carcinomas of the breast. *J Pathol* (2008) 215(4):398–410. doi: 10.1002/path.2368

44. Luna-More S, de los Santos F, Breton JJ, Canadas MA. Estrogen and progesterone receptors, c-erbB-2, p53, and bcl-2 in thirty-three invasive micropapillary breast carcinomas. *Pathol Res Pract* (1996) 192(1):27–32. doi: 10.1016/S0344-0338(96)80126-9

45. Luna-More S, Casquero S, Perez-Mellado A, Rius F, Weill B, Gornemann I. Importance of estrogen receptors for the behavior of invasive micropapillary carcinoma of the breast. review of 68 cases with follow-up of 54. *Pathol Res Pract* (2000) 196(1):35–9. doi: 10.1016/S0344-0338(00)80019-9

frontiers | Frontiers in Oncology

TYPE Original Research
PUBLISHED 16 September 2022
DOI 10.3389/fonc.2022.951973

OPEN ACCESS

EDITED BY
San-Gang Wu,
First Affiliated Hospital of Xiamen University, China

REVIEWED BY
Xiaohong Fu,
Gongli Hospital, China
Cong Jiang,
Harbin Medical University, China

*CORRESPONDENCE
Fen Chen
chenfen0571@qq.com
Jun-Yan Zhu
junyan_zhu007@163.com
Han-Lu He
hhldoct@163.com

SPECIALTY SECTION
This article was submitted to Breast Cancer, a section of the journal Frontiers in Oncology

RECEIVED 24 May 2022
ACCEPTED 24 August 2022
PUBLISHED 16 September 2022

CITATION
Zhu J-Y, He H-L, Lin Z-M, Zhao J-Q, Jiang X-C, Liang Z-H, Huang X-P, Bao H-W, Huang P-T and Chen F (2022) Ultrasound-based radiomics analysis for differentiating benign and malignant breast lesions: From static images to CEUS video analysis. *Front. Oncol.* 12:951973. doi: 10.3389/fonc.2022.951973

Ultrasound-based radiomics analysis for differentiating benign and malignant breast lesions: From static images to CEUS video analysis

Jun-Yan Zhu[1*], Han-Lu He[1*], Zi-Mei Lin[2], Jian-Qiang Zhao[3], Xiao-Chun Jiang[1], Zhe-Hao Liang[1], Xiao-Ping Huang[1], Hai-Wei Bao[1], Pin-Tong Huang[2] and Fen Chen[1*]

[1]Department of Ultrasound, The First Affiliated Hospital of Zhejiang Chinese Medical University, Hangzhou, China, [2]Ultrasound in Medicine, The Second Affiliated Hospital, Zhejiang University School of Medicine, Hangzhou, China, [3]Technology Department, XENIRO, Shanghai, China

Background: Continuous contrast-enhanced ultrasound (CEUS) video is a challenging direction for radiomics research. We aimed to evaluate machine learning (ML) approaches with radiomics combined with the XGBoost model and a convolutional neural network (CNN) for discriminating between benign and malignant lesions in CEUS videos with a duration of more than 1 min.

Methods: We gathered breast CEUS videos of 109 benign and 81 malignant tumors from two centers. Radiomics combined with the XGBoost model and a CNN was used to classify the breast lesions on the CEUS videos. The lesions were manually segmented by one radiologist. Radiomics combined with the XGBoost model was conducted with a variety of data sampling methods. The CNN used pretrained 3D residual network (ResNet) models with 18, 34, 50, and 101 layers. The machine interpretations were compared with prospective interpretations by two radiologists. Breast biopsies or pathological examinations were used as the reference standard. Areas under the receiver operating curves (AUCs) were used to compare the diagnostic performance of the models.

Results: The CNN model achieved the best AUC of 0.84 on the test cohort with the 3D-ResNet-50 model. The radiomics model obtained AUCs between 0.65 and 0.75. Radiologists 1 and 2 had AUCs of 0.75 and 0.70, respectively.

Conclusions: The 3D-ResNet-50 model was superior to the radiomics combined with the XGBoost model in classifying enhanced lesions as benign or malignant on CEUS videos. The CNN model was superior to the radiologists,

and the radiomics model performance was close to the performance of the radiologists.

KEYWORDS

breast cancer, contrast enhanced ultrasonography (CEUS), machine learning, convolutional neural network (CNN), radiomics

Introduction

Contrast-enhanced ultrasound (CEUS) is the latest and most important technology in the field of ultrasound imaging (1). Using microbubbles, it obtains detailed information about the tumor blood supply and provides dynamic perfusion information in real time with few application limitations (2, 3). Different from the relatively mature static image radiomics studies, there are technical difficulties in applying static image radiomics analysis methods to video analysis with a length of more than 1 min (4). Given that the practice of medicine is constantly evolving in response to new technology, there is interest in using the latest imaging methods to obtain data for radiomics learning (5, 6).

CEUS is one of the most advanced techniques in clinical tumor treatments, ranging from early screening and differential diagnosis to treatment response evaluation (7). It is particularly useful for the detection and characterization of lesions and has been used in breast cancer diagnosis as a feasible alternative screening modality (1, 8). Breast cancer is the most common malignant cancer in women, and it has a high mortality rate; there were over 1.6 million cases in 2010, and 2.1 million cases are projected by 2030 (9–12). Therefore, early detection and treatment play important roles in reducing mortality rates.

Several studies have reported training a radiomics or convolutional neural network (CNN) architecture to automatically extract features from CEUS cine images. Among them, the application of deep neural networks that can extract continuous spatiotemporal information is quite rare. In this context, we extracted the spatiotemporal information of dynamic CEUS by using 3D-CNN models. We aimed to compare the diagnostic performance of radiomics combined with the ML model, the 3D-CNN model, and human-read interpretations based on CEUS video for the differentiation of benign and malignant breast lesions.

Materials and methods

Study design and patients

The study was approved by the ethical committee of the local institutional board and complied with the Declaration of Helsinki. Informed consent was waived for this retrospective research. Written informed consent was obtained from each participant. From April 2021 to November 2021, 123 patients with breast tumors who underwent CEUS examination were enrolled from The First Affiliated Hospital of Zhejiang Chinese Medical University in Hangzhou, China. From August 2018 to August 2021, 92 patients with breast tumors who underwent CEUS examination were enrolled from The Second Affiliated Hospital, Zhejiang University School of Medicine in Hangzhou, China.

The two centers used the same patient inclusion and exclusion criteria. The inclusion criteria were as follows: (a) each patient underwent pathological examination; (b) CEUS examinations were performed before surgery and prior to any treatment, including biopsy or neoadjuvant therapies; and (c) each patient had complete demographic information and clinical data. The exclusion criteria were as follows: (a) poor-quality CEUS cine (e.g., the entire tumor and surrounding breast parenchyma were not clearly displayed on the ultrasound image at the same time) and (b) extreme motion existed during CEUS examination. Finally, the CEUS cines of 190 patients acquired before treatment were analyzed.

There were 190 patient CEUS videos in our dataset, the tumors were classified as benign or malignant, and the dataset included 109 benign and 81 malignant lesions. A detailed flowchart of patient selection for the study is shown in Figure 1.

CEUS data acquisition

CEUS was performed by two experienced radiologists (X-CJ and Z-ML). There were two different ultrasound instruments used in this study (Esaote MyLabTM Twice, Mindray Resona R9).

During the examination, breast tumors were imaged in the transverse plane of the largest tumor dimension. A single focus was always placed at the bottom of the image, and the selected plane remained unchanged. The probe was stabilized manually to ensure that no pressure was exerted to avoid weakening the contrast-enhanced signals. Patient movement was also avoided.

One-minute minimum continuous cine images were acquired after injecting 4.8 ml of the second-generation

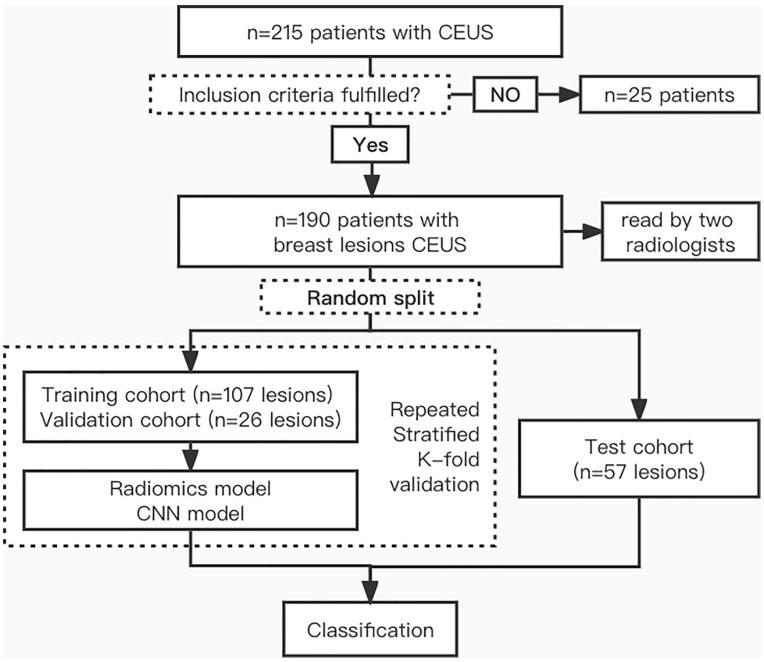

FIGURE 1
Flowchart of patient enrollment.

contrast agent (SonoVue, Bracco Imaging, Milan, Italy) *via* the elbow, followed by a 5-ml saline flush. Time was activated promptly from the beginning of the SonoVue injection.

The selected imaging plane remained unchanged during the examination. The whole CEUS cine process was recorded in an ultrasound workstation by using digital imaging and communication in medicine (DICOM) format. The recorded CEUS videos were used for further analysis.

Tumor segmentation and preprocessing

Tumors were manually segmented by a single radiologist (FC, with more than 20 years of experience in breast CEUS interpretation). For segmentation, the radiologist first reviewed the complete video to identify tumor boundaries. Then, we extracted a rectangular image with a fixed length–width ratio enclosing the nodule and its surrounding tissues, saved it in JSON format, kept it unchanged in the sequence, adjusted the image size to 160 × 160 pixels, and preprocessed it.

FFmpeg was used to cut the first 10 s and the last 5 s from the dynamic 1.0- to 2.0-min video data. The frame rate of the original data was between 15 and 30 frames/s. We tried to unify it into (15, 18, 21, 24, and 25) different frame rates. After selecting the 18 frames/s video, which had better results, we uniformly converted it into frame pictures.

We used a total of 107 CEUS for the training cohort and 26 CEUS for the validation cohort. A total of 57 CEUS videos were used for the test cohort. We split the dataset using sklearn (version 1.0.2) (13). The train_test_split function with parameter stratifies so that the benign/malignant proportion of training, validation, and test cohorts remains the same as the overall data. The data used in the test cohort were independent and were not used in the training and validation cohorts.

Radiomics feature extraction and model building

Features were extracted from the ROI using PyRadiomics (version 3.0.1) (14–16). Extracted texture features were calculated on the first-order statistics (19 features), gray-level cooccurrence matrix (24 features), gray-level run-length matrix (16 features), gray-level size-zone matrix (16 features), neighboring gray tone difference matrix (5 features), and gray-level dependence matrix (14 features). A detailed definition of all image features can be found online (http://pyradiomics.readthedocs.io/en/latest/features.html).

The minimum analysis time of a CEUS video is 1 min; a rate of 18 frames/s was applied for a total of 1,080 images. The difference between each picture is small and changes over time. According to expert experience, the degree of change over time should be more valuable for diagnosis. We have tried a variety of

data sampling methods: all 60 s of data enter the follow-up; the mean value is taken every 10 s; the mean value is taken every 20 s; one frame is taken every 10 s; one frame is taken every 20 s; the differences between the above values and the 30th second frame are taken; and the differences between the above values and the 60th second frame are taken.

The XGBoost algorithm implements decision trees with a boosted gradient, enhanced performance, and a faster speed. It was applied to the super parameter setting process of gridsearchcv.

CNN model building

In the training cohort, data augmentation was performed by using random cropping, random rotations, flipping vertically or horizontally, and color jitter (17, 18).

To efficiently utilize the dynamic characteristics of the CEUS modality, multichannel convolution models that can learn the spatiotemporal characteristics of different enhancement models were considered. 3D-ResNet is a subgroup of CNN methods and is widely used in video analysis because it has good performance in dealing with both spatial and temporal features at the same time (19).

Pretrained 3D-ResNet on Kinetics-400 (https://arxiv.org/abs/1705.06950) is used for classification *via* transfer learning (20). To find the most suitable model for benign and malignant discrimination, 18-layer, 34-layer, 50-layer, and 101-layer ResNet models were fine-tuned. Clinical features and lesion size were not included as radiomics and CNN model parameters. The ResNet models were trained by performing Repeat-Stratified K-Fold validation (n_**repeats** = **10**; K = 5) on the dataset to obtain more reliable generalization errors. The dataset was shuffled and equally divided into three cohorts. One was used as the test cohort to evaluate the trained model. Another cohort was further divided into a training set and a validation set according to 80%:20%.

The details of ROI segmentation and the flowchart of radiomics and CNN are shown in Figure 2. The following link can be accessed for additional code details: https://github.com/kenshohara/3D-ResNets-PyTorch.

Reader study

All the digital cine clips of the study population were retrospectively reviewed by two different readers (X-PH and Z-HL, with 8 and 15 years of clinical experience, respectively). The readers were blinded to each other's interpretations, to the original radiologist's interpretations, and to the model's assessment. None of the readers were involved in the CEUS examinations, and both were blinded to the clinical and other imaging information of the patients.

The two readers assessed the possibility of malignancy in CEUS cines based on the Breast Imaging Reporting and Data System (BI-RADS) and the reported BI-RADS categories per patient, which were 3, 4a, 4b, 4c, and 5. Then, the readers combined CEUS, grayscale US, and color Doppler flow imaging (CDFI) for classification in the same way.

Statistical analysis

All statistical analyses were performed using SPSS (Version 26.0, IBM Corporation, Armonk, USA) and R software (Version 3.4.1, R Foundation for Statistical Computing, Vienna, Austria). Student's *t*-tests or the Mann–Whitney test, as appropriate, was used to compare continuous variables. The chi-square test was

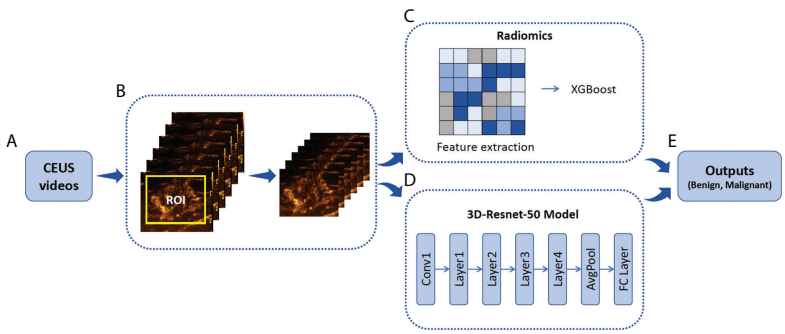

FIGURE 2
Illustration of ROI annotation in CEUS videos and the design of Radiomics and 3D-Resnet-50 models. **(A)** CEUS examinations were performed for each breast tumor. **(B)** An example of the yellow bounding box ROI drawn in one CEUS frame. **(C)** Schematic of radiomics combined with the XGBoost model. **(D)** A three-dimensional ROI (2D in space and 1D in time) of CEUS videos was fed into the 3D-Resnet-50 model to obtain the discriminative features by automatic feature learning. **(E)** The features obtained from the radiomics and 3D-Resnet-50 models are used to calculate the prediction probability. ROI, region of interest; CEUS, contrast-enhanced ultrasound; ResNet, residual network.

used to compare categorical variables. A p-value less than 0.05 was considered statistically significant.

To evaluate the predictions of the three different methods (the radiomics, CNN, and radiologist methods), receiver operating characteristic (ROC) curves were constructed. The areas under the ROC curve (AUCs) with 95% confidence intervals (CIs), sensitivity, specificity, accuracy, and F1 score were investigated.

Results

Clinical characteristics

A total of 190 female patients with breast tumors were enrolled for analysis, namely, 109 with benign breast tumors and 81 with malignant tumors, and were divided into two groups. The baseline characteristics of all patients and breast tumors (including age, pathological findings, and US BI-RADS category) are presented in Table 1.

The final diagnosis included 109 (57.4%) benign and 81 (42.6%) malignant breast lesions (Table 2). Malignant lesions were larger than benign lesions on US, and patients with malignant lesions were significantly older than those with benign lesions. The results showed that the differences between all clinical factors (including age, size, and BI-RADS category) of the patients with benign and malignant tumors were statistically significant ($p < 0.05$).

Radiologist diagnosis results

The ROC curves (Figure 3) showed that the prediction performance of the senior radiologist (radiologist 1) was better than that of the junior radiologist (radiologist 2), and the AUC values were 0.75 and 0.70, respectively (Table 3). Comparing radiologist diagnoses before and after combining CEUS with grayscale US and CDFI, p-values for AUC were not statistically significant ($p > 0.05$).

TABLE 1 Characteristics of patients and images.

Characteristics	Benign	Malignant	*p*
Patient number (*n*)	109 (57.4%)	81 (42.6%)	
Age (years)	24–78	35–82	<0.05
Range/mean ± SD	45.1 ± 11.2	56.0 ± 10.1	
Size of lesions (cm)	0.32–4.47	0.34–4.54	<0.05
Range/mean ± SD	1.28 ± 0.78	1.97 ± 0.88	
BI-RADS (*n*)			<0.05
3	41 (37.5%)	0 (0.0%)	
4a	49 (45.0%)	13 (16.0%)	
4b	10 (9.2%)	21 (26.0%)	
4c	5 (4.5%)	18 (22.2%)	
5	4 (3.7%)	29 (35.8%)	

SD, standard deviation; BI-RADS, Breast Imaging Reporting and Data System.

Performance of the radiomics models

The best XGBoost algorithm had the following parameters: learning_rate = 0.02, subsample = 1, min_child_weight = 1, n_estimators = 148, gamma = 0.1, max_depth = 3, and colsample_bytree = 1.

In the radiomics model of XGBoost Group e4c2, the difference between the frames every 20 s and the frame at the 60th second is taken by using RepeatS Stratified 5-Fold validation in the training and validation cohorts. In the training cohort, after 28 epochs, the max mean AUC was 1.00 (Figure 4A). In the validation cohort, after 28 epochs, the max mean AUC was 0.74 (Figure 4B).

Among various data packets, the best result is obtained when the differences between the frames at every 10 s and the frame at the 30th second are taken (group e3d, test cohort sensitivity: 77.4%, specificity: 66.7%, accuracy: 65.5%, F1 score: 0.68, AUC: 0.75). The worst result is obtained when the difference between the frames every 20 s and the frame at the 60th second is taken (group e4c2, test cohort sensitivity: 54.8%, specificity: 75.0%, accuracy: 60.0%, F1 score: 0.66, AUC 0.61) (Table 2).

Performance of the 3D-ResNet models

The 3D-ResNet-50 with the best classification effect is selected. The hyperparameters of 3D-ResNet-50 were learning_rate = 1e-4, weight_decay = 1e-5, momentum = 0.9, ft_begin_module = layer1, sample_size = 136, sample_duration = 108, n_epochs = 30, and batch_size = 8. Details of the network architecture are provided in https://github.com/kenshohara/3D-ResNets-PyTorch.

In the 3D-ResNet-50 model, repeat-stratified fivefold validation was used in the training and validation cohorts. In the training cohort, after 30 epochs, the max mean AUC was 0.85 (Figure 4C). In the validation cohort, after 29 epochs, the max mean AUC was 0.82 (Figure 4D).

In the test cohort, the 3D-ResNet-50 algorithm achieved sensitivity, specificity, accuracy, F1 score, and AUC values of 70.8%, 85.9%, 76.0%, 0.72, and 0.84, respectively. The AUC of the test cohort was the same as that of the training cohort.

AI system performance compared with the performance of the radiologists

The ROC curves of radiomics, 3D-ResNet-50, and radiologists in the test cohort are shown in Figure 3. The AUC

10.3389/fonc.2022.951973

TABLE 2 Histopathology of breast lesions.

Lesion type	No. of lesions
Benign lesions	109 (57.4%)
Adenosis	32 (29.4%)
Fibroadenoma	28 (25.7%)
Papilloma	15 (13.8%)
Inflammatory process	13 (11.9%)
Other*	21 (19.2%)
Malignant lesions	81 (42.6%)
Invasive	67 (82.7%)
Ductal carcinoma in situ	14 (17.3%)

There were a total of 190 lesions. Unless otherwise indicated, data in parentheses are percentage.
*The "other" category included enhancement around fat necrosis, fresh scar tissue, pseudo angiomatous stromal hyperplasia, and other benign-appearing enhancement because of focal or regional background enhancement.

of the 3D-ResNet-50 model was 0.84, which was significantly higher than that of both the radiomics and radiologist approaches. The NRI (Net Reclassification Index) of the 3D-ResNet-50 model compared with the radiomics models and radiologists was >0.

The best sensitivity and specificity results for the radiomics model were 77.4% and 66.7%, respectively. The sensitivity and specificity for senior radiologists were 74.3% and 74.1%, respectively. The sensitivity and specificity results for the junior radiologist were 66.0% and 71.6%, respectively (Table 2). The NRIs of the best radiomics model compared with the senior radiologist and junior radiologist were <0 and >0, respectively.

Decision curve analysis (DCA) was used to assess the clinical usefulness of the 3D-ResNet-50 model, radiomics model, and radiologists' diagnosis in the test cohort (Figure 5). If the threshold probability was more than 7%, using the 3D-ResNet-50 model to predict malignancy added more benefit than either the treat-all scheme (assuming that all lesions were malignant) or the treat-none scheme (assuming that all lesions were benign). In addition, using the 3D-ResNet-50 model to predict malignancy added more benefit than using either radiomics or radiologists.

Discussion

The diameters, volumes, shapes, and contrast-enhanced models of lesions usually described by radiologists based on diagnosis are called semantic features. They can be generated by algorithms that capture imaging data patterns, such as first-order, second-order, and high-order statistical determinants, shape-based features, and fractal features, which are called radiomics features. At present, the research hotspot of image analysis uses CNNs to extract the so-called "deep" feature phase in the training process, which is a very powerful nonlinear mapping. To distinguish CNNs from radiomics algorithms, the medical image task that uses CNNs to extract features is called deep learning radiomics (DL-radiomics) by some scholars. Most radiomics studies use less than 10 images per case, and 1-min CEUS videos have three times more data than static ultrasound images. To our knowledge, this is the first study to attempt to use the above three methods to interpret breast CEUS

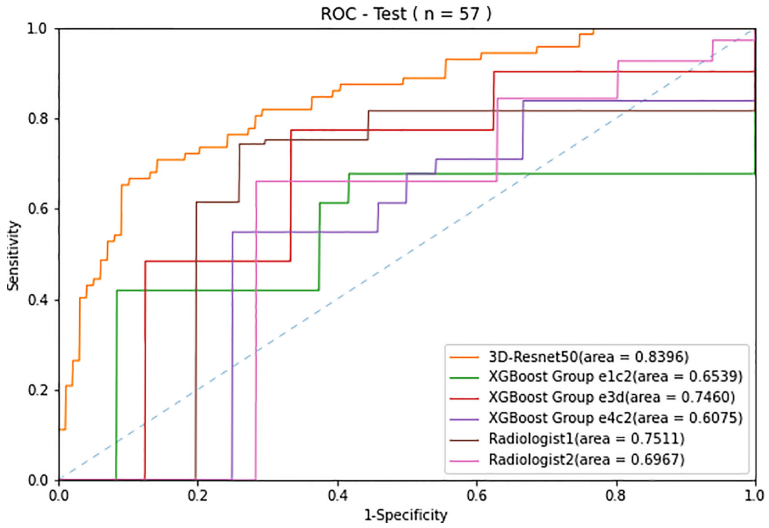

FIGURE 3
Receiver operating characteristic (ROC) curves of the two radiologists compared with the 3D-Resnet-50 model and radiomics combined with the XGBoost model with three different data sampling methods in the test cohort.

TABLE 3 Comparison of the predictive performance in 3D-Resnet 50, radiomics, and radiologists in the training, validation and test cohort.

Models	Datasets	Sensitivity (%)	Specificity (%)	Accuracy (%)	F1 score	AUC
3D-Resnet 50	Training	83.4	75.7	76.6	0.75	0.84
	Validation	83.4	75.7	75.5	0.74	0.82
	Test	70.8	85.9	76.0	0.72	0.84
XGBoost Group e1c2	Training	72.8	77.6	92.2	0.85	0.98
	Validation	61.8	67.8	69.3	0.92	0.75
	Test	67.7	58.3	54.6	0.55	0.65
XGBoost Group e3d	Training	84.2	79.8	96.7	0.92	0.99
	Validation	65.7	69.5	67.0	0.61	0.74
	Test	77.4	66.7	65.5	0.68	0.75
XGBoost Group e4c2	Training	83.5	84.8	98.7	0.98	1.00
	Validation	64.0	70.9	67.7	0.68	0.74
	Test	54.8	75.0	60.0	0.66	0.61
Radiologist 1	All data	74.3	74.1	74.2	0.77	0.75
Radiologist 2	All data	66.0	71.6	68.4	0.71	0.70

Resnet, residual network; AUC, area under the receiver operating characteristic curve.

and evaluate whether CEUS can be used to classify benign and malignant breast lesions.

For the three different methods, we chose a relatively mainstream method combined with the analyzed data. Sufficient time was provided for the semantic analysis of the experts in reading the CEUS. The experts were invited to classify benign and malignant lesions and perform BI-RADS scoring. When processing video for more than 1 min, the conventional

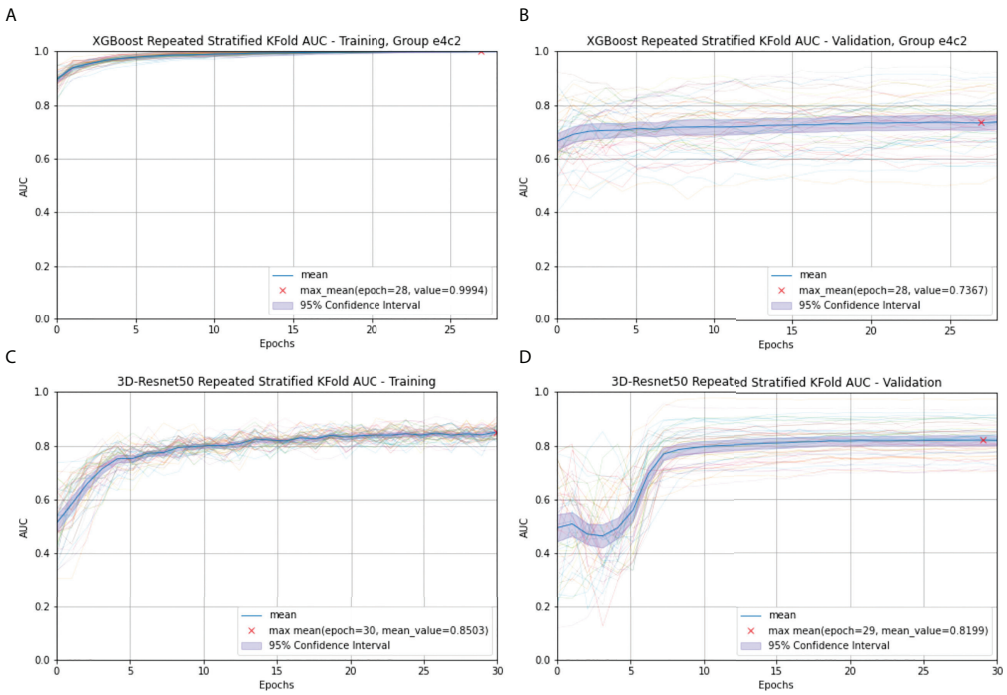

FIGURE 4
Radiomics **(A)** and 3D-Resnet-50 **(C)** Repeated Stratified 5-Fold AUC in the training cohort; Radiomics **(B)** and 3D-Resnet-50 **(D)** Repeated Stratified 5-Fold AUC in the validation cohort. The epochs are depicted on the *x*-axis, each representing the process of training all training samples once. The thick blue curve represents the mean AUC value. The blue area represents the 95% confidence interval (CI). The red fork represents the maximum mean of the AUC value after repeating multiple epochs.

radiomics information extraction combined with machine learning classification method must contend with extracting effective information from more than 1,000 times the amount of data from static images. To extract effective information from the massive radiomics data in a video, we referred to the clinical significance (biological underpinnings) and attempted to analyze the difference in the radiomics data at different time points. Data combinations were selected from a variety of time differences. XGBoost, a classical and effective machine learning classification method, was selected, as CNNs can handle a large number of images. We transformed 1 min of video (18 frames/s) into 1,080 pictures, all of which were entered into the follow-up analysis. To obtain the spatiotemporal information of dynamic CEUS and the total amount of data used in this study, we chose to use the 3D-ResNet model for transfer learning.

Our department performs a large number of traditional breast ultrasonography examinations; thus, these radiologists have gained rich experience in interpreting breast ultrasonography images. However, the diagnostic accuracy of radiologists in CEUS video diagnosis is relatively low, with poor CEUS diagnosis consistency among different radiologists, indicating that the human eye has low specificity when observing contrast images in breast lesions (21, 22). Making accurate qualitative cancer diagnoses using ultrasound is still a challenge for radiologists.

The same situation appears in radiomics analysis, which shows that careful selection of image types is very important for obtaining meaningful results. The AUC value we obtained was between 0.65 and 0.75, which is similar to that of human experts. The optimal radiomics analysis in our study involved the expert knowledge of radiologists and data scientists.

Our study with the 3D-ResNet-50 model for predicting breast cancer yielded satisfactory performance, obtaining an AUC of 0.84 on the test cohort. The CEUS-based 3D-ResNet-50 model had excellent performance in identifying benign and malignant breast lesions. Consistent with computer vision trends, CNN spatiotemporal features can help better process video data from CEUS.

In this study, we analyzed the performance of the ML-radiomics method on CEUS videos and found that it exceeded the recognition ability of the human-eye approach. The promising results in this study were attributed to the advantages of the standardized CEUS acquisition criteria and the acquisition of samples from a multicenter database, which created good conditions for our follow-up analysis and made our results more authentic and reliable.

Our work has several limitations.

First, comparing radiologist diagnoses before and after combining CEUS with grayscale US and CDFI, the *p*-values for the AUC were not statistically significant. However, given the scientific nature of research, we should repeat this process for the radiomics and CNN models.

Additionally, a larger cohort of subjects should be included to ensure that the varying perfusion patterns of specific breast lesions can be captured, thus further improving the prediction accuracy and reducing the risk of overfitting.

Conclusion

Our 3D-ResNet-50 model showed excellent diagnostic performance in differentiating between benign and malignant

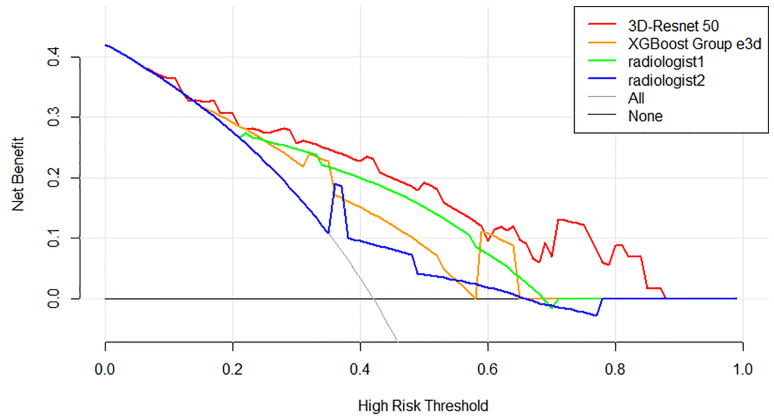

FIGURE 5
Decision curve analysis (DCA) of the models and radiologists from the test cohort. The net benefit measured on the *y*-axis is determined by calculating the difference between the expected benefit and the expected harm associated with each proposed model. The red curve, green curve, orange curve, and blue curve represent the performance of the 3D-Resnet-50 model, the best XGBoost model, radiologist 1, and radiologist 2, respectively. The gray line represents the assumption that all lesions were malignant (the treat-all scheme). The black line represents the assumption that all lesions were benign (the treat-none scheme). If the threshold probability was more than 7%, using the 3D-Resnet-50 model to predict malignancy added more benefit than either the treat-all scheme or the treat-none scheme (dark black line).

breast lesions compared with the radiomics combined with the XGBoost model and human readers on CEUS. DL-radiomics may have better results than mathematic-radiomics in the analysis of ultrasonic dynamic images.

Data availability statement

The original contributions presented in the study are included in the article/supplementary material. Further inquiries can be directed to the corresponding authors.

Ethics statement

The study was approved by the ethical committee of the local institutional board and complied with the Declaration of Helsinki. Informed consent was waived for this retrospective research.

Author contributions

Conceptualization: FC. Data curation: H-WB. Formal Analysis: J-YZ, FC. Methodology: J-YZ, FC. Project: P-H. Software: J-YZ. Supervision: Z-HL, X-CJ. Validation: Z-HL, X-PH. Writing – original draft: J-YZ, H-LH. Writing – review and editing: FC. All authors contributed to the article and approved the submitted version.

Acknowledgments

We thank all participants in this study.

Conflict of interest

Author J-QZ was employed by XENIRO.

The remaining authors declare that the research was conducted in the absence of any commercial or financial relationships that could be construed as a potential conflict of interest.

Publisher's note

References

1. Balleyguier C, Opolon P, Mathieu MC, Athanasiou A, Garbay JR, Delaloge S, et al. New potential and applications of contrast-enhanced ultrasound of the breast: Own investigations and review of the literature. *Eur J Radiol* (2009) 69(1):14–23. doi: 10.1016/j.ejrad.2008.07.037

2. Wan CF, Du J, Fang H, Li FH, Zhu JS, Liu Q. Enhancement patterns and parameters of breast cancers at contrast-enhanced US: correlation with prognostic factors. *Radiology* (2012) 262(2):450–9. doi: 10.1148/radiol.11110789

3. Wan CF, Liu XS, Wang L, Zhang J, Lu JS, Li FH. Quantitative contrast-enhanced ultrasound evaluation of pathological complete response in patients with locally advanced breast cancer receiving neoadjuvant chemotherapy. *Eur J Radiol* (2018) 103:118–23. doi: 10.1016/j.ejrad.2018.04.005

4. Sollini M, Antunovic L, Chiti A, Kirienko M. Towards clinical application of image mining: a systematic review on artificial intelligence and radiomics. *Eur J Nucl Med Mol Imaging* (2019) 46(13):2656–72. doi: 10.1007/s00259-019-04372-x

5. Giger ML. Machine learning in medical imaging. *J Am Coll Radiol* (2018) 15 (3 Pt B):512–20. doi: 10.1016/j.jacr.2017.12.028

6. Qi TH, Hian OH, Kumaran AM, Tan TJ, Cong TRY, Su-Xin GL, et al. Multi-center evaluation of artificial intelligent imaging and clinical models for predicting neoadjuvant chemotherapy response in breast cancer. *Breast Cancer Res Treat* (2022) 193(1):121–38. doi: 10.1007/s10549-022-06521-7

7. Dijkmans PA, Juffermans LJ, Musters RJ, van Wamel A, ten Cate FJ, van Gilst W, et al. Microbubbles and ultrasound: from diagnosis to therapy. *Eur J Echocardiogr* (2004) 5(4):245–56. doi: 10.1016/j.euje.2004.02.001

8. Tang MX, Mulvana H, Gauthier T, Lim AK, Cosgrove DO, Eckersley RJ, et al. Quantitative contrast-enhanced ultrasound imaging: a review of sources of variability. *Interface Focus* (2011) 1(4):520–39. doi: 10.1098/rsfs.2011.0026

9. Sammut SJ, Crispin-Ortuzar M, Chin SF, Provenzano E, Bardwell HA, Ma W, et al. Multi-omic machine learning predictor of breast cancer therapy response. *Nature* (2022) 601(7894):623–9. doi: 10.1038/s41586-021-04278-5

10. Harbeck N, Penault-Llorca F, Cortes J, Gnant M, Houssami N, Poortmans P, et al. Breast cancer. *Nat Rev Dis Primers* (2019) 5(1):66. doi: 10.1038/s41572-019-0111-2

11. Forouzanfar MH, Foreman KJ, Delossantos AM, Lozano R, Lopez AD, Murray CJ, et al. Breast and cervical cancer in 187 countries between 1980 and 2010: a systematic analysis. *Lancet* (2011) 378(9801):1461–84. doi: 10.1016/S0140-6736(11)61351-2

12. Yasaka K, Akai H, Abe O, Kiryu S. Deep learning with convolutional neural network for differentiation of liver masses at dynamic contrast-enhanced CT: A preliminary study. *Radiology* (2018) 286(3):887–96. doi: 10.1148/radiol.2017170706

13. Pedregosa F, Varoquaux G, Gramfort A, Michael V., Thirion B., Grisel O., et al. Scikit-learn: machine learning in python. *JMLR* (2012) Q12:2825–30.

14. van Griethuysen JJM, Fedorov A, Parmar C, Hosny A, Aucoin N, Narayan V, et al. Computational radiomics system to decode the radiographic phenotype. *Cancer Res* (2017) 77(21):e104–7. doi: 10.1158/0008-5472

15. Pinto Dos Santos D, Dietzel M, Baessler B. A decade of radiomics research: are images really data or just patterns in the noise? *Eur Radiol* (2021) 31(1):1–4. doi: 10.1007/s00330-020-07108-w

16. Bao H, Chen T, Zhu J, Xie H, Chen F. CEUS-based radiomics can show changes in protein levels in liver metastases after incomplete thermal ablation. *Front Oncol* (2021) 11:694102. doi: 10.3389/fonc.2021.694102

17. Kataoka H, Wakamiya T, Hara K, Satoh Y. Would mega-scale datasets further enhance spatiotemporal 3D CNNs? *arXiv* (2020). doi: 10.48550/arXiv.2004.04968

18. Ji S, Yang M, Yu K. 3D convolutional neural networks for human action recognition. *IEEE Trans Pattern Anal Mach Intell* (2013) 35(1):221–31. doi: 10.1109/TPAMI.2012.59

19. Zheng X, Yao Z, Huang Y, Yu Y, Wang Y, Liu Y, et al. Deep learning radiomics can predict axillary lymph node status in early-stage breast cancer. *Nat Commun* (2020) 11(1):1236. doi: 10.1038/s41467-020-15027-z

20. He K, Zhang X, Ren S, Sun J. Spatial pyramid pooling in deep convolutional networks for visual recognition. *IEEE Trans Pattern Anal Mach Intell* (2015) 37 (9):1904–16. doi: 10.1109/TPAMI.2015.2389824

21. Li W, Li L, Zhuang BW, Ruan SM, Hu HT, Huang Y, et al. Inter-reader agreement of CEUS LI-RADS among radiologists with different levels of experience. *Eur Radiol* (2021) 31(9):6758–67. doi: 10.1007/s00330-021-07777-1

22. Chen C, Wang Y, Niu J, Liu X, Li Q, Gong X. Domain knowledge powered deep learning for breast cancer diagnosis based on contrast-enhanced ultrasound videos. *IEEE Trans Med Imaging* (2021) 40(9):2439–51. doi: 10.1109/TMI.2021.3078370

frontiers | Frontiers in Oncology

TYPE Original Research
PUBLISHED 10 November 2022
DOI 10.3389/fonc.2022.1017435

OPEN ACCESS

EDITED BY
San-Gang Wu,
First Affiliated Hospital of Xiamen University, China

REVIEWED BY
Congchong Yan,
Soochow University, China
Youqun Lai,
Fujian Medical University Xiamen Humanity Hospital, China

*CORRESPONDENCE
Xiadong Li
lixiadong2019@outlook.com
Yu Kuang
yu.kuang@unlv.edu

†These authors have contributed equally to this work and share first authorship

SPECIALTY SECTION
This article was submitted to Breast Cancer, a section of the journal Frontiers in Oncology

RECEIVED 12 August 2022
ACCEPTED 27 September 2022
PUBLISHED 10 November 2022

CITATION
Feng H, Wang H, Xu L, Ren Y, Ni Q, Yang Z, Ma S, Deng Q, Chen X, Xia B, Kuang Y and Li X (2022) Prediction of radiation-induced acute skin toxicity in breast cancer patients using data encapsulation screening and dose-gradient-based multi-region radiomics technique: A multicenter study. *Front. Oncol.* 12:1017435. doi: 10.3389/fonc.2022.1017435

Prediction of radiation-induced acute skin toxicity in breast cancer patients using data encapsulation screening and dose-gradient-based multi-region radiomics technique: A multicenter study

Huichun Feng[1,2†], Hui Wang[1,3†], Lixia Xu[1,3], Yao Ren[1,3], Qianxi Ni[4], Zhen Yang[5], Shenglin Ma[1,6], Qinghua Deng[1,2], Xueqin Chen[1,2], Bing Xia[1,2], Yu Kuang[7*] and Xiadong Li[1,3*]

[1]Medical Imaging and Translational Medicine Laboratory, Hangzhou Cancer Center, Hangzhou, China, [2]Patient follow-up center, Hangzhou Cancer Hospital, Hangzhou, China, [3]Department of Radiotherapy, Affiliated Hangzhou Cancer Hospital, Zhejiang University School of Medicine, Hangzhou, China, [4]Department of Radiology, Hunan Cancer Hospital, Affiliated Cancer Hospital of Xiangya School of Medicine, Central South University, Changsha, China, [5]Department of Radiotherapy, Xiangya Hospital Central South University, Changsha, China, [6]Medical Oncology, Xiaoshan Hospital Affiliated to Hangzhou Normal University, Hangzhou, China, [7]Medical Physics Program, University of Nevada, Las Vegas, NV, United States

Purpose: Radiation-induced dermatitis is one of the most common side effects for breast cancer patients treated with radiation therapy (RT). Acute complications can have a considerable impact on tumor control and quality of life for breast cancer patients. In this study, we aimed to develop a novel quantitative high-accuracy machine learning tool for prediction of radiation-induced dermatitis (grade ≥ 2) (RD 2+) before RT by using data encapsulation screening and multi-region dose-gradient-based radiomics techniques, based on the pre-treatment planning computed tomography (CT) images, clinical and dosimetric information of breast cancer patients.

Methods and Materials: 214 patients with breast cancer who underwent RT between 2018 and 2021 were retrospectively collected from 3 cancer centers in China. The CT images, as well as the clinical and dosimetric information of patients were retrieved from the medical records. 3 PTV dose related ROIs, including irradiation volume covered by 100%, 105%, and 108% of prescribed dose, combined with 3 skin dose-related ROIs, including irradiation volume covered by 20-Gy, 30-Gy, 40-Gy isodose lines within skin, were contoured for radiomics feature extraction. A total of 4280 radiomics features were extracted from all 6 ROIs. Meanwhile, 29 clinical and dosimetric characteristics were included in the data analysis. A data encapsulation screening algorithm was applied for data cleaning. Multiple-variable logistic regression and 5-fold-

cross-validation gradient boosting decision tree (GBDT) were employed for modeling training and validation, which was evaluated by using receiver operating characteristic analysis.

Results: The best predictors for symptomatic RD 2+ were the combination of 20 radiomics features, 8 clinical and dosimetric variables, achieving an area under the curve (AUC) of 0.998 [95% CI: 0.996-1.0] and an AUC of 0.911 [95% CI: 0.838-0.983] in the training and validation dataset, respectively, in the 5-fold-cross-validation GBDT model. Meanwhile, the top 12 most important characteristics as well as their corresponding importance measures for RD 2+ prediction in the GBDT machine learning process were identified and calculated.

Conclusions: A novel multi-region dose-gradient-based GBDT machine learning framework with a random forest based data encapsulation screening method integrated can achieve a high-accuracy prediction of acute RD 2+ in breast cancer patients.

KEYWORDS

Breast cancer, radiation therapy, radiation-induced skin toxicity, machine learning, radiomics, gradient boosting decision tree

1 Introduction

Surpassing lung cancer as the leading cause of global cancer incidence, breast cancer accounted for 11.7% of all new cancer cases with 685,000 deaths, ranking the fifth leading cause of cancer mortality worldwide in 2020 (1). Most patients with breast cancer are treated with surgery (e.g., lumpectomy or mastectomy) followed by radiation therapy (RT) on the residual ipsilateral breast or chest wall, with alternative dose boost to the tumor bed and/or regional lymph node irradiation applied (2–4). Treatment-induced acute skin toxicity (i.e., acute radiodermatitis) with a different degree, ranging from erythema to desquamation (dry or moist), ulceration, and necrosis, is one of the most common acute side effects of RT underwent by breast cancer patients, with approximately 90% of treated patients experiencing erythema and 30% experiencing moist desquamation (5–8). Such acute skin toxicity negatively affects multiple aspects of quality of life (QOL) of breast cancer radiotherapy patients, such as physical discomfort, emotional distress, and body image disturbance, and so on (9).

The acute skin reactions are prone to progress during the treatment and remain after completion of the treatment. In addition, severe acute reactions may be prodromal of subsequent late effects (10), and the RT schedule might be changed or even terminated due to these negative reactions. Therefore, early prediction of acute radiodermatitis when formulating a radiation therapy regimen could potentially reduce the risk of skin toxicity. Furthermore, early management of acute radiodermatitis in breast cancer patients can improve both day-to-day functioning and satisfaction with radiation treatment, and therefore QOL and outcome of patients.

Qualitative evaluation of acute skin toxicity mainly by visual inspection of the skin-related symptoms of breasts is subject to practitioner bias, variability in grading dermatitis as well as differentiating the severe dermatitis (e.g., moist desquamation) due to clinician expertise, and underreporting by patients (9, 11). Most importantly, this method detects early signs of dermatitis with low sensitivity and specificity. Based on the semi-quantitative analysis of clinical and dosimetric predictors of acute skin toxicity, the normal tissue complication probability (NTCP) models can be established to predict severe acute skin toxicity in breast cancer patients (10). However, the prediction performance was relatively poor with an area under the curve (AUC) as low as 0.77 (10).

To improve the prediction performance, quantitative early thermal imaging biomarkers were identified and used in machine learning frameworks (i.e., thermoradiomics) to build the predict model, and a high prediction accuracy (test accuracy = 0.87) on the independent test data at treatment fraction of 5 was achieved for predicting acute skin toxicity at the end of RT (12, 13). However, the prediction performance is not sufficient enough to be as an effective clinical decision support tool for intervention and management of dermatitis in breast cancer patients, probably due to the 2-D surface imaging with limited information provided rather than 3-D volume imaging with one more dimension information offered. The models built on 2-D surface thermal

imaging constrain their usage for 3-D dose distribution optimization guidance. Furthermore, the extra usage of thermal imaging devices and additional procedures involved might increase the labor burdens in the breast radiation oncology clinic and reduce the patient throughput.

In this study, we investigated 3-D planning CT volume imaging and machine learning frameworks to develop a quantitative prediction tool for radiation-induced acute radiodermatitis in breast cancer patients before RT treatment. This multicenter retrospective study was performed using a novel 3-D dose-gradient-based multi-region radiomics technique with the data encapsulation screening method integrated. The gradient boosting decision tree (GBDT) algorithm was used to build the predictive model. We hypothesized that acute radiodermatitis is associated with the 3-D region-based characteristic radiomics signatures in breast cancer patients before RT.

2 Methods and materials

2.1 Patients and CT scans

This study retrospectively reviewed 256 patients with stage 0-IV breast cancer, who underwent post-surgery (i.e., lumpectomy, mastectomy, or breast reconstruction) intensity-modulated radiation therapy or volumetric modulated arc therapy RT with or without concurrent chemotherapy and/or Hormone therapy, at 3 cancer centers including our hospital from October 2018 to August 2021 under institutional review board approval. The patients received a prescription dose of whole breast and/or chest wall irradiation mainly using regimens of 50 Gy in 25 fractions or 42.5 Gy in 16 fractions with an optional boost of 10 Gy in 5 fractions to the tumor bed using the 6 MV photons. The patients were monitored for skin symptoms from the start of RT to at least 1 month after the completion of RT. A total of 214 patients (144 patients with ≥ 2 grade skin toxicity) were selected based on the exclusion criteria including (1) prior or subsequent RT to the chest, (2) previous skin disorder, (3) with dose boost using electron therapy, (4) male patients, (5) loss of clinical characteristics records. Informed consent from all the patients was obtained before the study. All study participates were graded for skin toxicity using Radiotherapy Oncology Group (RTOG), Common Terminology Criteria for Adverse Events (CTCAE) Ver. 4 (6, 7).

In our study, all patients underwent breathing training before radiotherapy; 88 of them with left-sided breast cancer were treated with deep inhalation breath-hold (DIBH) radiotherapy technique, and their CT scans were completed in breath-hold state. Other 126 of them with right-sided breast cancer underwent 4D-CT scans in free-breathing state. CT scans of the patients for treatment planning were mainly conducted using a Philips Brilliance Big Bore CT (Philips Medical Systems, Cleveland, OH, USA) 2 to 7 days before RT. The imaging parameters of the CT scans include voltage (120 kVp), tube current (325 mA or 375mA), exposure time (800 ms or 933 ms), pixel size (0.5×0.5 mm or 0.6×0.6 mm), slice thickness (5 mm), and image size (XY: 768×1024, Z: around 80). The Pinnacle (Philips Medical Systems, Andover, MA) or Eclipse treatment planning systems (Varian Medical Systems, Palo Alto, CA) were used for the calculation of the radiation dose distribution of contoured treatment volumes.

The planning CT scans and associated dose distributions of eligible patients were collected for data analysis and model building (Figure 1). Clinical characteristics of the patients include age, body mass index (BMI), body temperature, tumor laterality, tumor quadrant positions, pathological tumor size (e.g., tumor maximum diameter), tumor grade, tumor histology type, TNM stage, overall stage, CRP, ER, PR, HER-2, surgery method, chemotherapy, hormone therapy, etc. (Table 1).

All patients were informed by nurses about the basic skin cares before treatment, including daily rinsing of the breast skin surface with warm water, keeping the breast skin moist and clean, and avoiding friction of the skin of breasts by hard clothing. If the patients are prone to RD 2+, they may be advised to use silver sulfadiazine 1% three times per day for 5 weeks. All the patients and family members confirmed the consensus of cooperation.

2.2 Data processing and model building

2.2.1 Radiomics feature extraction

The construction and application of a radiation dermatitis prediction model was illustrated in Figure 1. A total of 884 radiomics features were extracted from each delineated ROI by using the open-source image biomarker explorer (IBEX) software platform (14). The radiomics features extracted includes seven categories: shape, intensity direct, intensity histogram, gray-level co-occurrence matrix (GLCM) (2.5D), neighbor intensity difference (2.5D), gray level run length matrix (2.5D), and intensity histogram Gaussian fit. Radiomics features were extracted from PTV regions defined with 100%, 105%, 108% of the prescribed dose and skin regions defined with 20-Gy, 30-Gy, 40-Gy isodose of the skin for the following model building.

2.2.2 Null interpolation

Based on the fact that missing of clinical and dosimetric variable values are types of data missing completely at random (MCAR) or missing at random (MAR), two methods of maximum likelihood (ML) and multiple imputation (MI) can be used to fill null variable values. We used the ML method to impute the linear null data; the MI method was applied to fill the

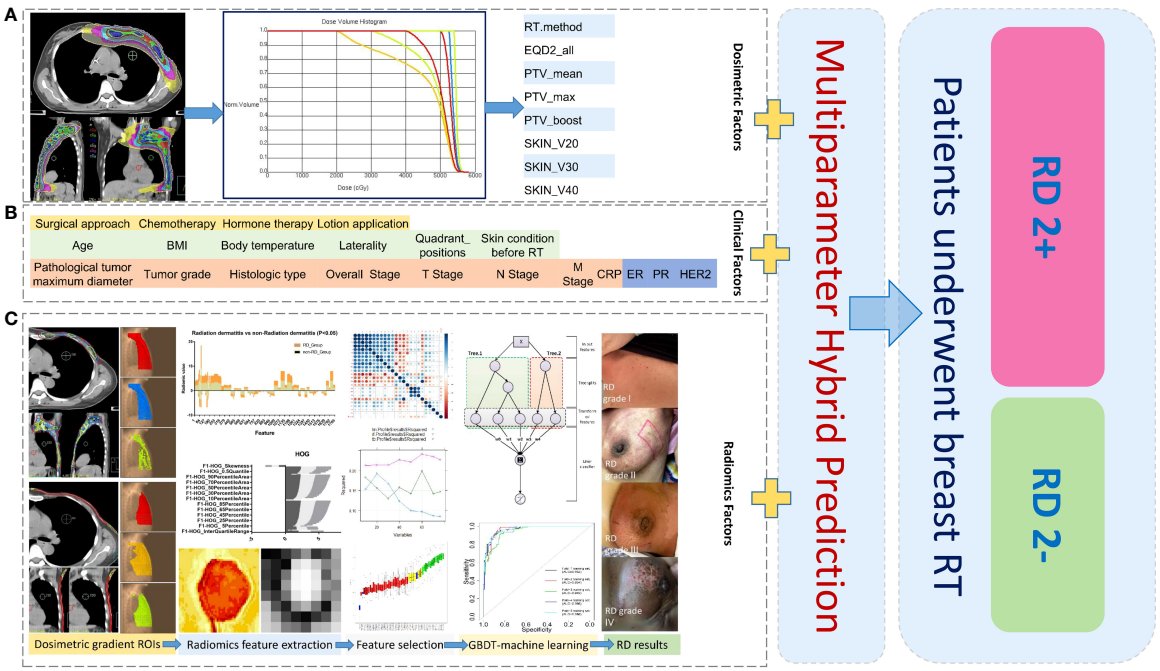

FIGURE 1
Schematic diagram of data analysis for machine learning in this study: Collection and analysis based on dosimetric factors **(A)**, patient clinical factors **(B)**, and radiomics factors **(C)** extracted from different dose-gradient regions of patients. ROIs, regions of interest; RD 2+, radiodermatitis with ≥ 2 grade; RD 2-, radiodermatitis with< 2 grade.

non-linear null data. For radiomics features, since the proportion of null data is very low (<10%) and the correlation between feature variables is high, the method of directly removing null data should not generate the biased estimation.

2.2.3 Unbalanced data handling

Training on imbalanced dataset would create a biased prediction in the minority class of dataset. The degree of imbalance of dataset is based on the proportion of a minority class in the whole dataset and could range from mild (20-40%), moderate (1-20%) to extreme (<1%) imbalances (15). Previous studies showed that resampling approach is a useful pre-processing step to handle the imbalanced dataset (16, 17). This method modifies the imbalance distribution of the majority and minority classes at the data level before training with classifiers. In this study, due to a mild imbalanced dataset used (non-RD2+ patients/total patients =32.7%), an imbalanced adjustment strategy of Synthetic Minority Oversampling Technique (SMOTE) was utilized before all the data sets were trained. SMOTE is a very popular algorithm for oversampling of the minor class data. Briefly, SMOTE takes k data from k-NN (near neighbors) for each data in the minor class to perform oversampling, and then generates new data by obtaining "in-line" data with one of the randomly chosen k-NN data results for a number of magnification.

2.2.4 Screening of prediction variable

The p values were calculated for clinical and dosimetric variables (Table 1), in which the chi-square test was used by default for categorical variables, and the MUW test was used by default for continuous variables. If the data did not meet the conditions for the chi-square test, the fisher's exact test was used instead. The variables with P value< 0.5 were selected for multiple-variable logistic regression analysis in the following step. Because the sample size of this study is relatively not large, the current data might not represent the actual situation, and the low p value might cause missing of important variables that account for the prediction model. In performing multiple-variable logistic regression of clinical and dosimetric variables, we set a relatively high P value of 0.5 (compared to P< 0.1 or P< 0.05) to avoid too few variables included in the regression analysis, which may loss valuable variables for further analysis. This resulted in 8 variables included in the regression equation (Table 2).

For the radiomics data extracted from the 6 ROIs, the MWU test was firstly performed with P value < 0.05 set, and then redundant features with variance ≤ 0.05 were deleted. In the next step, the pairwise correlation coefficient between one variable and all the remaining variables was calculated, and variables with correlation coefficient ≥ 0.9 were deleted. When the correlation coefficients of two variables are the same, the

TABLE 1 Demographic and clinical information of the patients (n=214) in the study.

Demographic and clinical characteristics		Grade ≤ 1(n = 70)	Grade ≥ 2(n = 144)	P value (Chi-squared/MUW test)
Age (mean (SD))		50.04 (9.44)	49.48 (9.62)	0.804
BMI (mean (SD))		22.94 (3.03)	23.25 (2.70)	0.773
Body temperature (mean (SD))		36.67 (0.33)	36.70 (0.35)	0.692
Laterality (%)	Left	44 (62.9)	82 (56.9)	0.411
	Right	26 (37.1)	62 (43.1)	
Quadrant position (%)	Upper-Outer	17 (24.3)	23 (15.9)	0.207
	Upper-Inner	26 (37.1)	57 (39.6)	
	Lower-Outer	13 (18.6)	54 (37.5)	
	Lower-Inner	14 (20.0)	10 (6.9)	
Tumor maximum diameter (cm) (mean SD)		1.97 (0.91)	2.28 (1.68)	0.759
Tumor grade (%)	I	5 (7.2)	13 (9.0)	0.958
	II	36 (51.4)	69 (47.9)	
	III	29 (41.4)	62 (43.1)	
Histologic type (%)	DCIS	10 (14.3)	13 (9.0)	0.114
	IDC	59 (84.3)	124 (86.1)	
	ILC	1 (1.4)	5 (3.5)	
	IMC	0 (0.0)	1 (0.7)	
	LCIS/DCIS	0 (0.0)	1 (0.7)	
Overall Stage (%)	0	4 (5.7)	9 (6.3)	0.189
	I	14 (20.0)	16 (11.1)	
	IIA	17 (24.3)	31 (21.5)	
	IIB	0 (0.0)	1 (0.7)	
	IIIA	3 (4.3)	12 (8.3)	
	IIIB	18 (25.7)	30 (20.8)	
	IIIC	13 (18.6)	40 (27.8)	
	IV	1 (1.4)	5 (3.5)	
T Stage (%)	Tx~is	1 (1.4)	4 (2.8)	0.109
	T0	3 (4.3)	5 (3.4)	
	T1	4 (5.7)	5 (3.5)	
	T2	43 (61.4)	74 (51.4)	
	T3	17 (24.3)	48 (33.3)	
	T4	2 (2.9)	8 (5.6)	
N Stage (%)	0	36 (51.4)	66 (45.8)	0.595
	1	18 (25.7)	46 (31.9)	
	2	11 (15.7)	21 (14.6)	
	3	5 (7.2)	11 (7.7)	
M Stage (%)	0	70 (100.0)	143 (99.3)	0.002
	1	0 (0.0)	1 (0.7)	
CRP (mg/l) (mean (SD))		2.27 (4.19)	2.36 (5.03)	0.876
ER (%)	Positive	55 (78.6)	114 (79.2)	0.960
	Negative	15 (21.4)	30 (20.8)	
PR (%)	Positive	50 (71.4)	112 (77.8)	0.312
	Negative	20 (28.6)	32 (22.2)	
HER2 (%)	Positive	14 (20.0)	34 (23.6)	0.554
	Negative	56 (80.0)	110 (76.4)	
Surgery method (%)	Lumpectomy	41 (58.6)	84 (58.3)	0.928
	Mastectomy	27 (38.6)	59 (41.0)	
	Reconstruction	2 (2.8)	1 (0.7)	

(Continued)

TABLE 1 Continued

Demographic and clinical characteristics		Grade ≤ 1(n = 70)	Grade ≥ 2(n = 144)	P value (Chi-squared/MUW test)
Chemotherapy (%)	No	13 (18.6)	32 (22.2)	0.541
	Yes	57 (81.4)	112 (77.8)	
Hormone therapy (%)	No	44 (62.9)	77 (53.5)	0.195
	Yes	26 (37.1)	67 (46.5)	
EQD2_all (mean (SD))		52.16 (5.18)	52.66 (4.16)	0.466
Lotion application (%)	No	6 (8.6)	5 (3.5)	0.115
	Yes	64 (91.4)	139 (96.5)	
PTV_mean (mean (SD))		5098.71 (325.99)	5139.06 (317.50)	0.838
PTV_max (mean (SD))		5773.97 (477.05)	5839.24 (454.27)	0.937
PTV_boost (%)	Yes	41(58.6)	80(55.6)	0.678
	No	29(41.4)	64(44.4)	
SKIN_mean (mean (SD))		3608.40 (493.26)	3587.22 (570.25)	0.730
SKIN_max (mean (SD))		5447.94 (489.98)	5535.82 (464.63)	0.504
SKIN_V20 (mean (SD))		87.26 (10.00)	85.65 (12.01)	0.316
SKIN_V30 (mean (SD))		70.60 (14.74)	69.69 (15.31)	0.461
SKIN_V40 (mean (SD))		44.59 (21.24)	43.83 (20.93)	0.626

SD, standard deviation; BMI, body mass index; DCIS, ductal carcinoma in situ; IDC, invasive ductal carcinoma; ILC, invasive lobular carcinoma; IMC, invasive mammary carcinoma; LCIS, lobular carcinoma in situ; HER2, human epidermal growth factor receptor 2; ER, estrogen receptor; PR, progesterone receptor; EQD2_all,equivalent dose of all treatment phase at 2Gy/fraction.

variable with the larger correlation with the classification result was kept. Meanwhile, a variance inflation factor (VIF) was calculated for multiple linear tests on the remaining variables, in which all variables with VIF ≥ 10 were removed. Then, a decision tree encapsulation screening method was applied to filter the variables for the following prediction model building. The encapsulation screening method integrated the feature selection process with the training process, and used the predictive ability of the model as a measure of feature selection to select a high-quality subset of variables.

2.2.5 Model training and validation

The GBDT machine learning algorithm was used to train and validate the clinical and dosimetric, radiomics, and combined prediction models, respectively. Gradient boosting is an integrated boosting method, which iterates the new learner through the gradient descent algorithm, and boosting refers to connecting multiple weak learners in series to generate a new strong learner.

For binary GBDT in this study, the loss function is defined as (18)

$$L(y,f(x)) = log(1 + \exp(-yf(x))) \quad (1)$$

where y is the label, and $f(x)$ denotes the prediction value. Then the negative gradient error at the current time is defined as

$$r_{ti} = -\left[\frac{\partial L(y,f(x))}{\partial f(x)}\right]_{f(x)=f_{t-1}(x)} = \frac{y_i}{1 + \exp(y_i f(x_i))} \quad (2)$$

For the generated decision tree, the best residual fitting value of each leaf node is

$$c_{tj} = \arg\min \sum_{x_i \in R_{tj}} (log(1 + exp(y_i f_{t-1}(x_i + c)))) \quad (3)$$

TABLE 2 Multiple-variable logistic regression of selected clinical and dosimetric variables.

Variable	Coefficient	Wald Z	Pr (>|Z|)
Laterality	0.6983	1.86	0.0628
Quadrant position	0.1183	2.09	0.0362
Histologic type	0.2709	0.68	0.4967
T Stage	0.1641	0.69	0.4923
PR	-0.2727	-0.73	0.4631
Hormone therapy	0.4601	1.35	0.1776
EQD2_all	-0.1483	-0.75	0.4525
Lotion application	0.7188	1.08	0.2789

Since the above equation is difficult to be optimized in a computer, we use the following loss function to approximate it instead:

$$c_{tj} = \frac{\sum_{x_i \in R_{tj}} r_{ti}}{\sum_{x_i \in R_{tj}} |r_{ti}| * (1 - |r_{ti}|)} \quad (4)$$

The pseudocode of the binary GBDT is as follows:

Gradient Boosting Trees Algorithm

1 Initialize $f_0(x) = \arg\min_\gamma \sum_{i=1}^{N} L(y_i, \gamma)$

2. For m=1 to M:

(a) For i=1,2,…,N compute: $r_{im} = -[\frac{\partial L(y_i, f(x_i))}{\partial f(x_i)}]_{f=f_{m-1}}$

(b) Fit a regression tree to the targets r_{im} gibing terminal regions, R_{jm}, j = 1,2,…,Jm compute:

(c) For j = 1,2,…,Jm compute: $\gamma_{jm} = argmin_\gamma \sum_{x_i \in Rjm} L(y_i, f_{m-1}(x_i) + \gamma)$

(d) Update $f_m(x) = f_{m-1}(x) + \sum_{j=1}^{Jm} \gamma_{jm} I(x_i \in R_{jm})$

3. Output. $\hat{f}(x) = f_M(x)$

ALGORITHM

The entire data set was divided into 5 equal sub-folds with the ratio of close to 1:1 for RD 2+ and non-RD 2+ patients in each sub-fold, and the patients in each sub-fold do not appear repeatedly. 70% of the data in each sub-fold were used for GBDT model training, and the remaining 30% were used for validation. A *gbm* package in *Rstudio* was used to implement the GBDT algorithm (19). Since the problem is a classification problem, the Bernoulli distribution was selected in the loss function. The learning rate shrinkage parameter was set at 0.05, and the number of decision tree was set to 10000. The optimal number of iterations and the importance of each explanatory variable were determined by using a 5-fold cross-validation.

3 Results

3.1 Variable selection and data handling

With the null imputation method being applied to the clinical and dosimetric datasets, total of 29 clinical and dosimetric variables were retained for further analysis. The number of remained non-null radiomics features extracted from the PTV_100PD, PTV_105PD, PTV_108PD, SKIN_20Gy, SKIN_30Gy, and SKIN_40Gy were 812, 789, 674, 684, 657, and 664, respectively.

After the SMOTE method was applied, the total number of samples was increased from 214 to 280, and the number of non-RD 2+ cases was increased from 70 to 140. In the new balanced data, the ratio of RD 2+ and non-RD 2+ patients was close to 1:1.

3.2 Model training and validation

As mentioned above, the 8 clinical and dosimetric variables selected were fed into the GBDT model for training. The performance of GBDT model in the training and validation datasets using the selected clinical and dosimetric variables is shown in Table 3. It is observed that the clinical and dosimetric characteristics showed moderate predictive power for RD 2+, even in the best performance in the second and third sub-folds in the training and validation set (i.e., AUC of 0.839 with 95% CI of 0.788-0.891, and AUC of 0.816 with 95% CI of 0.705-0.927).

With the MWU test, zero-variance test, correlation test, VIF verification and tree encapsulation screening method being successively applied to the radiomics dataset, we obtained 20 radiomics features from the 2 types of ROIs with 6 dose levels. The VIFs of these radiomics features and their AUCs in predicting RD 2+ were shown in Table 4. As can be observed from the table, these radiomics features showed limited prediction performance on their own, such as PTV_100PD_radiomics_average (AUC, 0.566 [95% CI: 0.497-0.632]), SKIN_20Gy _radiomics_average (AUC, 0.569 [95% CI: 0.501-0.636]), and so on.

As can be observed in Table 5, using combined radiomics features from all the ROIs, the prediction was improved significantly for the GBDT model both in training and validation sub-folds (e.g., AUC of 0.998 [95% CI, 0.996-1] for the training set, AUC of 0.907 [95% CI, 0.829-0.985] for the validation set).

As shown in Table 6, in the GBDT model built on the combined clinical, dosimetric and radiomics characteristics, the best performance of the model resided in the first and fourth sub-fold in the training and validation set, with a AUC of 0.998 [95% CI:0.996-1.0] and a AUC of 0.911 [95% CI: 0.838-0.983], respectively. The best performance with the highest AUC value of each sub-folds in training and validation set of the three GBDT models were summarized in Figure 2.

3.3 Important predictor analysis

Meanwhile, the top 12 most important characteristics as well as their corresponding importance measures (i.e., mean and standard deviation) for RD 2+ prediction in the combined GBDT model were shown in Figure 3. Three clinical characteristics were selected in this top variable list, including Hormone.therapy, T.Stage, and Quadrant.positions. Four radiomics features from the SKIN_30Gy region, including

TABLE 3 The GBDT model performance in training and validation dataset using selected clinical and dosimetric variables. The bold values indicate the best prediction performance in the training set and validation set, respectively.

Type-GBDT	Folds	1-foldsModel-1	2-foldsModel-2	3-foldsModel-3	4-foldsModel-4	5-foldsModel-5
Training-set	RD 2 +/Non-RD 2+	0.830 95% CI: 0.777-0.884 (DeLong)	**0.839** 95% CI: 0.788-0.891 (DeLong)	0.786 95% CI: 0.727-0.845 (DeLong)	0.802 95% CI: 0.744-0.861 (DeLong)	0.811 95% CI: 0.754-0.867 (DeLong)
Validation-set	RD 2 +/Non-RD 2+	0.725 95% CI: 0.587-0.863 (DeLong)	0.743 95% CI: 0.611-0.877 (DeLong)	**0.816** 95% CI: 0.705-0.927 (DeLong)	0.748 95% CI: 0.618-0.879 (DeLong)	0.759 95% CI: 0.631-0.886 (DeLong)

ID_Local Range Max, IH_Gauss Fit1 Gauss_Std, GOH_MAD and GLCM-25225.4Contrast, were identified as important features for prediction of RD 2+. Five radiomics features, including GLCM_2590.7_IV, Shape_Number Of Objects and GOH_0.975_Quantile from PTV_108PD, IH_Gauss Fit1 Gauss_Mean and ID_Local Entropy Max from PTV_105PD, were chosen in this top list. Most of these features focus on describing the region heterogeneity and complexity of the textures in patients' PTV and skin volumes.

As illustrated in Figure 4, changes of the top 12 variable values were correlated with risk scores of RD 2+. For instance, the increase of SKIN_30Gy.GLCM-25225.4Contrast value was correlated to the decreased risk score for the occurrence of RD 2 +; and it seems like that a threshold of SKIN_30Gy.IH_Gauss Fit1 Gauss_Std can be set to identify the patients with a high risk for RD 2+. We further explored the distributions (i.e., spatial and amplitude) of feature values, calculated from sliding sub-volumes (e.g., containing 7×7×7 voxels) within the ROIs, of several variables in the top list. Figure 5 shows the exemplary amplitude and spatial distributions of the feature values of IH_Gauss Fit1 Gauss Mean, GLCM_25225.4Contrast, and IH_Gauss Fit1 Gauss_Std extracted from the sub-volumes within the ROIs of PTV_100PD, SKIN_30Gy, SKIN_30Gy, respectively, for patients with and without RD 2+.

TABLE 4 AUC of 20 radiomics features after variable screening using decision tree encapsulation screening method. The bold values indicate the average values across the dose regions.

Feature	VIF	AUC	95%CI(DeLong)
PTV_100Pd_F2.GLCM25270.7_Corr	8.608	0.591	0.524-0.658
PTV_100Pd_F4.ID_LocalStdMedian	8.945	0.604	0.537-0.670
PTV_100PD_F4.ID_Range	1.407	0.510	0.441-0.577
PTV_100PD_F8.ShapeMax3Ddiameter	1.551	0.544	0.476-0.612
PTV_100PD_F6.IHGaussFit1GaussMean	1.311	0.576	0.507-0.644
PTV_100PD_radiomics_average	**4.364**	**0.566**	**0.497-0.632**
PTV_105PD_F2.GLCM25.333.7_Corr	1.208	0.592	0.525-0.659
PTV_105PD_F4.ID_LocalEntropyMax	1.080	0.570	0.502-0.637
PTV_105PD_F8.ShapeMeanBreadth	1.123	0.587	0.520-0.655
PTV_105PD_radiomics_average	**1.137**	**0.583**	**0.516-0.650**
PTV_108PD_F1.GOH0.975Quantile	1.277	0.588	0.519-0.656
PTV_108PD_F2.GLCM25180.1Dissimilarity	1.831	0.574	0.506-0.642
PTV_108 PD_F8.ShapeNumberOfObjects	1.292	0.606	0.540-0.672
PTV_108PD_F2.GLCM2590.7_IV	1.301	0.568	0.500-0.636
PTV_108PD_radiomics_average	**1.425**	**0.584**	**0.516-0.652**
SKIN_20Gy.F2.GLCM25225.4Contrast	3.749	0.570	0.503-0.637
SKIN_20Gy.F8.ShapeConvexHullVolume3D	1.827	0.554	0.486-0.622
SKIN_20Gy.F8.ShapeMeanBreadth	7.401	0.582	0.515-0.650
SKIN_20Gy _radiomics_average	**4.326**	**0.569**	**0.501-0.636**
SKIN_30Gy_F2.GLCM25225.4Contrast	1.411	0.577	0.510-0.645
SKIN_30Gy_F4.ID_LocalRangeMax	1.286	0.613	0.546-0.680
SKIN_30Gy_F6.IHGaussFit1GaussStd	1.255	0.641	0.576-0.706
SKIN_30Gy_F1.GOH_MAD	1.351	0.591	0.524-0.658
SKIN_30Gy_F8.ShapeMax3DDiameter	1.075	0.655	0.59040.719
SKIN_30Gy _radiomics_average	**1.276**	**0.615**	**0.549-0.682**

TABLE 5 The GBDT model performance in training and validation dataset using 20 selected radiomics features. The bold values indicate the best prediction performance in the training set and validation set, respectively.

Type-GBDT	Folds	1-foldsModel-1	2-foldsModel-2	3-foldsModel-3	4-foldsModel-4	5-foldsModel-5
Training-set	RD 2+/Non-RD 2+	0.998 95% CI: 0.996-1.0 (DeLong)	0.997 95% CI: 0.993-1.0 (DeLong)	0.997 95% CI: 0.994-1.0 (DeLong)	0.974 95% CI: 0.954-0.993 (DeLong)	**0.998** 95% CI: 0.996-1.0 (DeLong)
Validation-set	RD 2+/Non-RD 2+	0.881 95% CI: 0.782-0.981 (DeLong)	**0.907** 95% CI: 0.829-0.985 (DeLong)	0.901 95% CI: 0.814-0.987 (DeLong)	0.867 95% CI: 0.777-0.958 (DeLong)	0.875 95% CI: 0.769-0.980 (DeLong)

4 Discussion

There is currently no gold standard for the prevention and management of RD 2+ for breast cancer patients. Many interventions are based on the experience of physicians and nurses, anecdotal evidence, or low-level evidence, and there are very limited prospective data to guide interventions currently. The goal of treatment is primarily to improve patient comfort, minimize the risk of further damages, and promote wound healing. This study aimed to provide an innovative method to quantitatively assess the risk of radiation dermatitis before treatment, which will greatly reduce the clinical cost of trial and error for high-risk patients, and offer the opportunity to optimize the radiotherapy plan for high-risk patients just before treatment.

Ionizing radiation essentially damages the mitotic ability of clonogenic or stem cells within the basal layer of epidermis, thus preventing the process of repopulation and weakening the integrity of the skin. The degrees of damage range from mild to severe as telangiectasias, erythema, desquamation, keratinocyte cell death, fibrosis and inflammatory response (10). The incidence of grade 2 or higher radiation dermatitis in this study (approximately 67.3%) was similar to that in previous studies (31%-50%) (20). In this study, we extracted radiomics features from skin- and PTV-related ROIs defined by different dose gradients in the planning CT images. It was found that these radiomics characteristics combined with clinical and dosimetric factors significantly improved the predictive accuracy of RD 2+. The results showed the potential of taking the risk of RD 2+ and the radiation sensitivity of multiple ROIs into account in the RT planning procedures, which facilitates personalized radiation dose distribution at the planning stage of RT to improve outcomes for patients at the high risk of RD 2+.

In this study, all patients were divided into three groups: (1) lumpectomy (i.e., partial breast resection surgery or breast conserving surgery) group, (2) mastectomy group, (3) breast reconstruction group. Previous studies found that lumpectomy was associated with a higher rate of moderate or severe dermatitis than mastectomy (63% vs. 24%, P = 0.003) (21–23), which might be due to the local dose escalation after breast conserving surgery. However, our data did not show the same situation. In the lumpectomy cohort, RD 2+ was found in 80 (66.1%) out of 121 patients who underwent a dose escalation to the tumor bed. In the mastectomy cohort, 68.6% (59/86) patients developed RD 2+. There was no significant statistical difference between the two groups (p = 0.556), which suggested that local increase of radiation dose might not be an important risk factor for RD 2+. Meanwhile, it was found that there was no significant difference in the occurrence probability of RD 2+ between lumpectomy and mastectomy groups (p=0.441), which indicated that the surgery method might not be a risk factor for RD 2+.

Previous study demonstrated that higher biologically equivalent dose was correlated to an increase in the rate of moderate or severe dermatitis (12). Our results showed that there were no statistically significant differences in EQD2_all (P = 0.457) between patients with and without RD 2+ by using the MUW test. Patient large breast size and high BMI have been found to be independent risk factors of acute skin toxicity,

TABLE 6 The GBDT model performance in training and validation dataset using selected radiomics combined with clinical and dosimetric variables. The bold values indicate the best prediction performance in the training set and validation set, respectively.

Type-GBDT	Folds	1-foldsModel-1	2-foldsModel-2	3-foldsModel-3	4-foldsModel-4	5-foldsModel-5
Training-set	RD 2+/Non-RD 2+	**0.998** 0.996-1.0 (DeLong)	0.996 0.991-1.0 (DeLong)	0.998 0.991-1.0 (DeLong)	0.996 0.991-1.0 (DeLong)	**0.983** 0.970-0.995 (DeLong)
validation-set	RD 2+/Non-RD 2+	0.857 0.755-0.960 (DeLong)	0.908 0.835-0.982 (DeLong)	0.816 0.706-0.927 (DeLong)	**0.911** 0.838-0.983 (DeLong)	0.837 0.723-0.950 (DeLong)

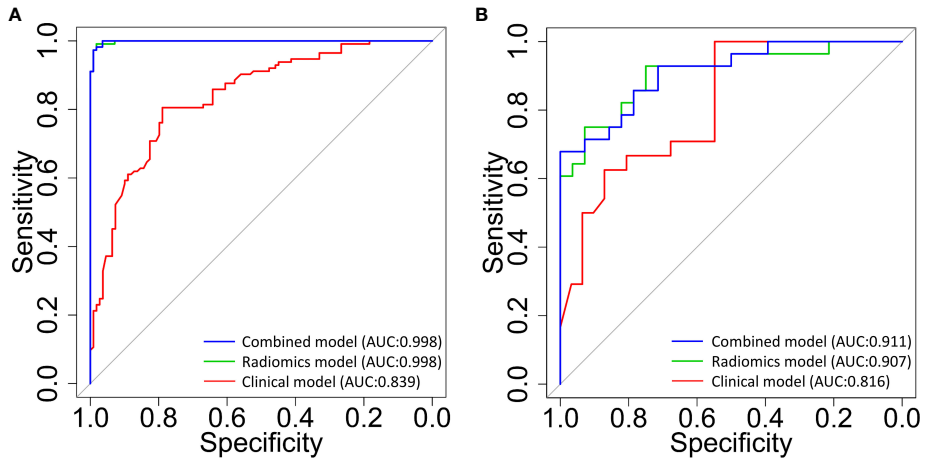

FIGURE 2
The receiver operating characteristic (ROC) curves for the classification of patients with and without radiodermatitis (RD 2+). The 3 curves are for classifiers that were built using clinical and dosimetric (red line), radiomics signatures within multiple ROIs (green line), and the combination of clinical, dosimetric, and radiomics features within multiple ROIs (blue line), respectively. **(A)**: prediction model performance in the training set; **(B)**: prediction model performance in the validation set. AUC, area under the curve; ROIs, regions of interest.

including moist desquamation (24). A greater self-bolusing effect is supposed to increase toxicity in the inframammary and axillary folds, due to the dose buildup of skin-on-skin. Therefore, patients with large breast size and/or high BMIs are prone to RD 2+ due to the greatest areas of skin-on-skin overlap. However, our results showed that the BMI, as well as chemotherapy, expression of hormone receptors or HER2, were not directly associated with RD 2+, which was consistent with the similar study carried by a French study team (13).

Although the clinical and dosimetric characteristics were not significantly predictive of symptomatic RD 2+ in multivariable logistic modeling, they showed good performance both in the training and validation datasets when the GBDT algorithm was adopted (e.g., best AUCs in 5-flod CV in training and validation dataset are 0.839 with 95% CI of 0.788-0.891 and 0.816 with 95% CI of 0.705-0.927, respectively) (Table 3). This suggested that the GBDT algorithm was the appropriate choice for the problem in this study.

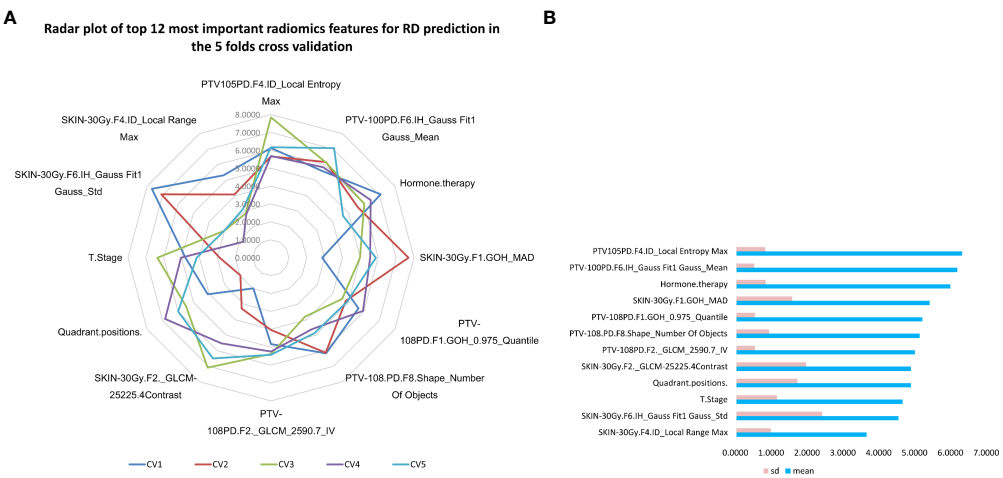

FIGURE 3
Top 12 most important variables in the combined GBDT model for radiodermatitis prediction. **(A)** the radar plot of top 12 most important prediction features in 5 folds cross validation GBDT machine learning process; **(B)** The mean and standard deviation of importance measures of the top 12 most important radiodermatitis prediction features sorted by the average measures.

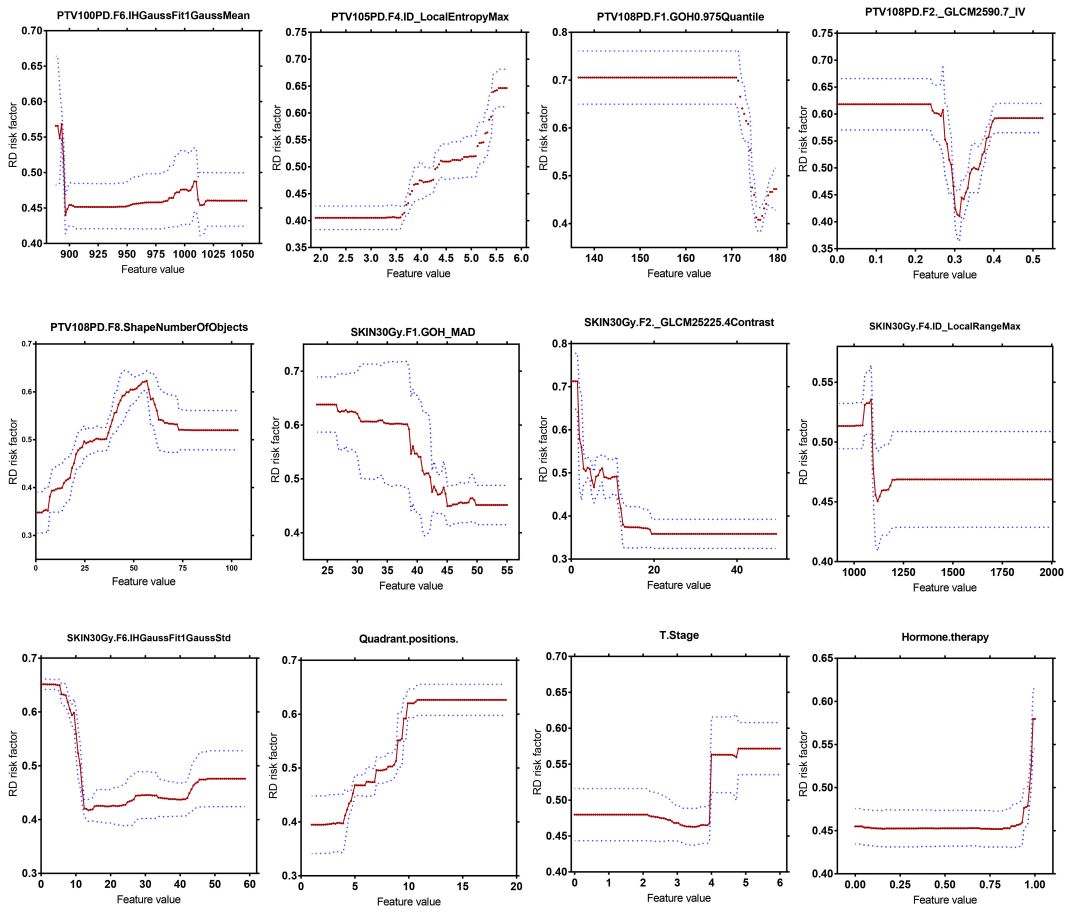

FIGURE 4
Quantitative correlation analysis of changes in top 12 most important variables in the GBDT model with changes in risk scores of radiodermatitis.

By using decision tree encapsulation screening method, we screened out 5, 3, 4, 3, and 5 features from the 5 ROIs of PTV_100PD, PTV_105PD, PTV_108PD, SKIN_20Gy, and SKIN_30Gy, respectively. The number of radiomics features retained from the PTV ROIs was greater than the skin ROIs. The predictive ability of radiomics features of a single ROI was relatively low, which indicated that it was difficult to extract predictors with excellent prediction performance from a single ROI. However, when we used all the screened 20 radiomics features from multiple ROIs, the best AUC values of the prediction model reached 0.998 with 95% CI of 0.996-1.0 and 0.907 with 95% CI of 0.829-0.985 in the training and validation set, respectively. Therefore, we speculate that the occurrence of RD 2+ is not only directly related to the patient's skin, but also the characteristics of the PTV adjacent to the skin which will also have an important impact on the occurrence of RD 2+.

In this study, our analysis found that RD 2+ was not strongly correlated to the dose characteristics of the skin as well as those of PTV adjacent to the skin, whereas the radiomics indicators of PTV_100PD, PTV_105PD, PTV_108PD, SKIN_20Gy, and SKIN_30Gy showed strongly correlated to the occurrence of RD 2+. This suggested that radiomics characteristics of these ROIs of the skin and PTV play more important role in the prediction of RD 2+ than the dosimetric characteristics for breast cancer patients treated with RT. For the sake of safety, driving those PTV and skin regions to the low-abundance regions of RD 2+-sensitive radiomics features holds the potential to reduce the occurrence of RD 2+.

In the combined prediction model, radiomics features extracted from the SKIN_30Gy, PTV_100PD, PTV_105PD, and PTV_108PD were the most important predictors of RD2+; while clinical characteristics, including estrogen therapy, tumor T stage, and tumor quadrant positions, were also important predictors. A previous study reported the volume of skin receiving a dose >35 Gy (SKIN_V35), PTV-V100%, PTV-V105%, PTV-V107% (i.e., volumes receiving percentage of prescribed dose within PTV) were the most significant dosimetric predictors associated with >50% probability of RD 2+ toxicity (20). Although our

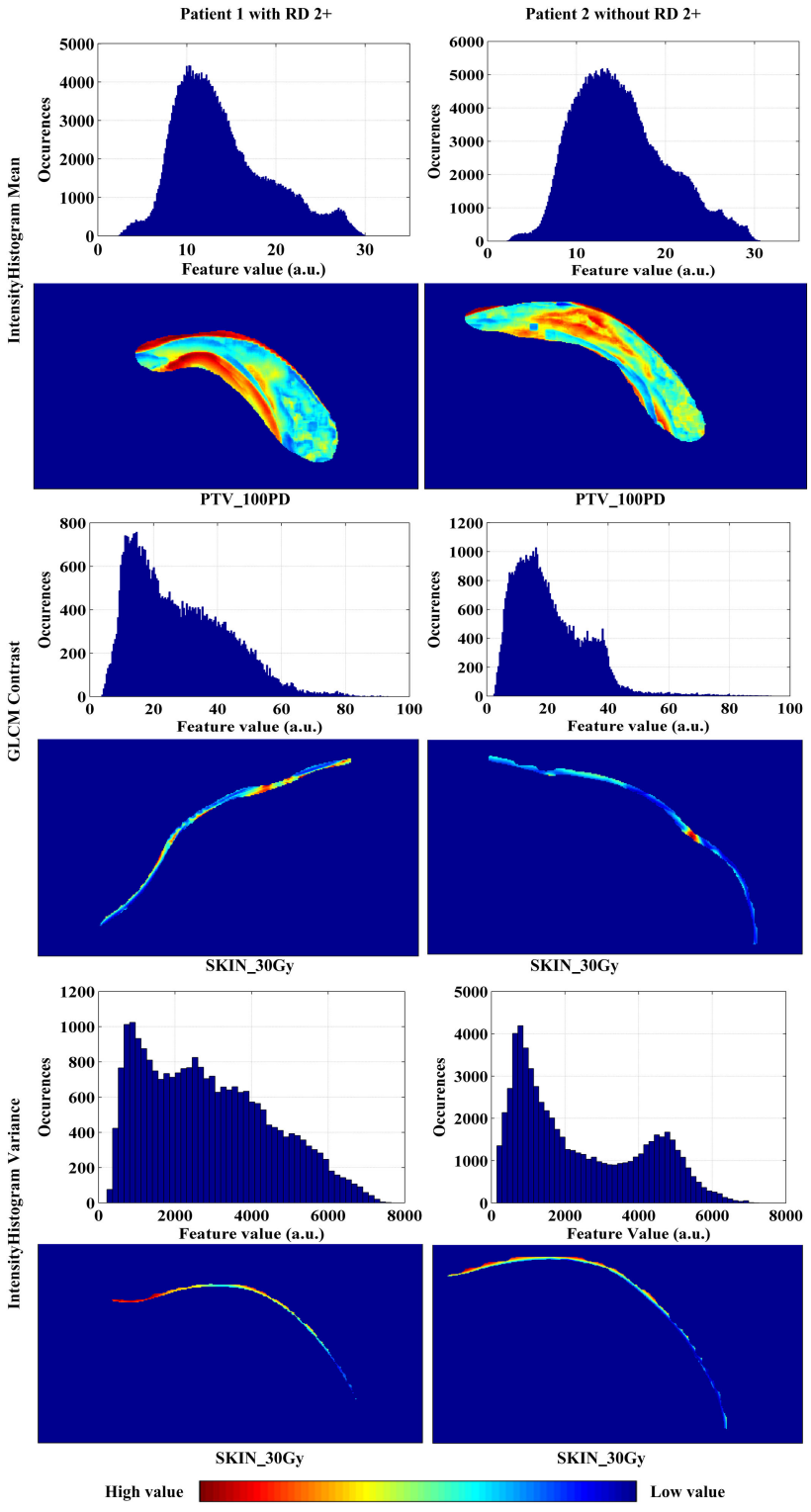

FIGURE 5
The amplitude and spatial distributions of the feature values of IH_Gauss Fit1 Gauss Mean, GLCM_25225.4Contrast, and IH_Gauss Fit1 Gauss_Std extracted from the sub-volumes within the ROIs of PTV_100PD, SKIN_30Gy, SKIN_30Gy, respectively, for patients with and without RD 2+.

results did not show the strong correlation between the volumes of SKIN_V30 and/or SKIN_V40 and the occurrence of RD 2+, and the correlations between the volumes of PTV-V100%, PTV-V105%, and/or PTV-V107% and the occurrence of RD 2+ were not analyzed, our results revealed strong correlations between specific radiomics features extracted from these volumes and the occurrence of RD 2+.

As can be found from Tables 5, 6 and Figure 2, the model performance was not improved significantly when the clinical and dosimetric characteristics were added for training. This fact highlighted the role of radiomics features, extracted from the multiple dose-gradient-based ROIs of planning CT images of the patients, in the prediction of RD 2+ before treatment using the GBDT modeling method. This can be very helpful if clinical and/or dosimetric details of the patients were lost, as collecting these data is a labor intensive and time consuming task in practice.

The reason why we chose CT images for radiomics study rather than MRI images is that planning CT images were obtained within a week before the start of RT, whereas MRI images were usually acquired at the beginning of patient admission. As such, the patients' CT images reflect the baseline of the skin condition before RT more than MRI images do. Although MRI has advantages over CT in breast imaging, Wang et al. conducted a predictive model for the fibrotic level of neck muscles after radiotherapy by using radiomic features extracted from the MRI images before and after radiotherapy and planning CT in nasopharyngeal carcinoma patients, and they found that the prediction model based on CT radiomics features has better performance in the prediction of the grade of post-radiotherapy neck fibrosis (25). Therefore, we adopted extraction of radiomics features from patients' CT images instead of MRI images, which are usually not available due to the high cost.

The robustness of radiomics features was usually influenced by respiratory motion (26). For the patients with breast cancer, the respiratory motion was mainly manifested in the anterior-posterior direction. In our study, the left-side breast cancer patients underwent CT scans in the breath-holding state, therefore, the CT radiomics features from these patients was relatively reliable. For patients with right-side breast cancers, 4D-CT scans were performed using the free-breathing scan protocol. In this scenario, the maximum respiratory motion was restrained not to exceed 1.5cm; the respiratory rate was maintained at about 13 times per minute, and the optimal scanning pitch was set based on our previous studies (27). Furthermore, the contouring of ROIs and the extraction of the radiomics features were conducted in the MIP image mode. Therefore, the impact of respiratory motion on the training and verification of the machine learning model should be negligible.

Although the prediction model of this study requires further validation on an additional center as an independent test, we believed that the partition of the dataset into training set and validation set is good practice to ensure the reliability of the predictive models developed. In building GBDT model, we used the internal data cross-validation method (i.e., 75% of patients as the training set, and the remaining 25% as the validation set). Given the small sample size, this cross-validation method can make full use of the data. This internal cross-validation method may be more suitable for small sample dataset and can improve the generalization ability of the model, as reported in previous studies on machine learning applications (28, 29). Part of procedures of this method is similar to that reported previously by Kocak et al. They performed feature extraction and dimensionality reduction on CT images of all patients before adopting a 10-fold cross validation random forest training and validation (30). In our future work, we will consider to combine the dataset of our center with other regions in China, in which an independent test cohort can be obtained to achieve improved reliability of the prediction model.

Inflammatory response has been shown to be generally associated with RD 2+. In the initial period of RT, there is an immediate generation of an inflammatory response. The early inflammatory response to radiation is mainly caused by pro-inflammatory cytokines (e.g., IL-1, IL-3, IL-5, IL-6, and tumor necrosis factor [TNF]-a), chemokines, receptor tyrosine kinase, and adhesions molecules. These factors can create local inflammatory response of eosinophils and neutrophils. Janko et al. have ascertained that IL-1 had an important role in the development of RD 2+. They found that mice that lack either IL-1 or the IL-1 receptor developed less inflammation and less severe pathological changes in their skin (31). On the other hand, 80% of tissues and cells are composed of water. Most of the radiation damage from exposure of low-LET rays is due to the radiolysis of water resulting in the production of free radicals (ROS) and reactive nitrogen species (RNS). Radiation leads to an upregulation of free radicals and oxidases in tissues, and the distributions of which in cells, tissues and organs are heterogeneous.

Given these facts, we expect that the distributions of pro-inflammatory cytokines, ROS and RNS in the skin are individualized and specific in patients, and these specificities or differences might be reflected by the different distributions of radiomics features, such as distributions of the feature values of IH_Gauss Fit1 Gauss Mean, GLCM_25225.4Contrast, and IH_Gauss Fit1 Gauss_Std shown in Figure 5. The specific relationship between the distributions of cytokines and enzymes and radiomics signatures needs to be further investigated.

As can be observed in Figure 5, the high values of IH_Gauss Fit1 Gauss Mean feature in PTV_100PD of the patient with RD 2+ mainly appeared close to the body surface and chest wall, and distributed in strip pattern. Whereas the high value of this feature in the patient without RD 2+ appeared in the middle of PTV_100PD in a cluster style. The GLCM_25225.4Contrast

feature has a scatter-like distribution in the SKIN_30Gy of the patient with RD 2+, whereas the feature of the patient without RD 2+ has a single-hot-spot distribution. The IHGaussFit1GaussStd feature has little difference in the heat map within SKIN_30Gy; however, the histograms (i.e., amplitude distribution) of the feature values between the patient with and without RD 2+ exhibit apparently different envelopes. These exemplary distributions of radiomics features between patients with and without RD 2+ demonstrated their potential to identify the patients at the high risk of RD 2+. However, the correlation between the occurrence location of RD 2+ and the spatial distribution of radiomics feature needs to be further investigated in the future study. We envision that the prediction of the locations where RD 2+ occurs in advance of RT will be possible, which would facilitate personalized skin care prior to the occurrence of severe RD 2+.

5 Conclusion

In this study, we developed a novel dose-gradient based GBDT machine learning model using 20 CT radiomics features within PTV_100PD, PTV_105PD, PTV_108PD, SKIN_20Gy and SKIN_30Gy volumes and 8 clinical and dosimetric characteristics to predict RD 2+ in breast cancer patients before radiotherapy treatment. Our results demonstrated that combining features within multiple ROIs related to different dosimetric gradient in treatment planning CT images can achieve the best prediction performance compared to using single ROI as well as clinical or dosimetric characteristics only. The model offers the opportunity to take the risk of RD 2+ and the sensitivity of multiple ROIs into account in the radiation therapy planning procedures, thus enabling the personalized radiation dose distribution at the planning stage of RT to improve outcomes for patients at high risk for RD 2+.

Data availability statement

The original contributions presented in the study are included in the article/supplementary material. Further inquiries can be directed to the corresponding authors.

Ethics statement

The studies involving human participants were reviewed and approved by Medical Ethics Committee of Hangzhou Cancer Hospital. The patients/participants provided their written informed consent to participate in this study.

Author contributions

XL and YK created the study design. HF, QN, ZY, LX and YR collected the clinical and CT data and processed the data. HF, XL and HW conducted data analysis. XL and HW wrote the manuscript. SM, QD, XC and BX gave suggestions regarding the radiodermatitis grading. All authors contributed to the article and approved the submitted version.

Funding

This study was supported by the Natural Science Foundation of Zhejiang Province, China (LGF22H220007), Hunan Provincial Natural Science Foundation, China (2022JJ30976), Hangzhou Health Science and Technology Project, China (A20200746).

Conflict of interest

The authors declare that the research was conducted in the absence of any commercial or financial relationships that could be construed as a potential conflict of interest.

Publisher's note

References

1. Sung H, Ferlay J, Siegel RL, Laversanne M, Soerjomataram I, Jemal A, et al. Global cancer statistics 2020: GLOBOCAN estimates of incidence and mortality worldwide for 36 cancers in 185 countries. *CA Cancer J Clin* (2021) 71(3):209–49. doi: 10.3322/caac.21660

2. Haussmann J, Corradini S, Nestle-Kraemling C, Bolke E, Njanang FJD, Tamaskovics B, et al. Recent advances in radiotherapy of breast cancer. *Radiat Oncol* (2020) 15(1):71. doi: 10.1186/s13014-020-01501-x

3. Darby S, McGale P, Correa C, Taylor C, Arriagada R, Clarke M, et al. Effect of radiotherapy after breast-conserving surgery on 10-year recurrence and 15-year breast cancer death: meta-analysis of individual patient data for 10,801 women in 17 randomised trials. *Lancet* (2011) 378(9804):1707–16. doi: 10.1016/S0140-6736(11)61629-2

4. Ebctcg, McGale P, Taylor C, Correa C, Cutter D, Duane F, Ewertz M, et al. Effect of radiotherapy after mastectomy and axillary surgery on 10-year recurrence and 20-year breast cancer mortality: meta-analysis of individual patient data for

8135 women in 22 randomised trials. *Lancet* (2014) 383(9935):2127–35. doi: 10.1016/S0140-6736(14)60488-8

5. Hymes SR, Strom EA, Fife C. Radiation dermatitis: clinical presentation, pathophysiology, and treatment 2006. *J Am Acad Dermatol* (2006) 54(1):28–46. doi: 10.1016/j.jaad.2005.08.054

6. Cox JD, Stetz J, Pajak TF. Toxicity criteria of the radiation therapy oncology group (RTOG) and the European organization for research and treatment of cancer (EORTC). *Int J Radiat Oncol Biol Phys* (1995) 31(5):1341–6. doi: 10.1016/0360-3016(95)00060-C

7. *Common terminology criteria for adverse events v.4.0 (CTCAE)*. (Bethesda, Md. : USA, Department of Health and Human Services, National Institutes of Health, National Cancer Institute) (2009).

8. Chan RJ, Larsen E, Chan P. Re-examining the evidence in radiation dermatitis management literature: an overview and a critical appraisal of systematic reviews. *Int J Radiat Oncol Biol Phys* (2012) 84(3):e357–62. doi: 10.1016/j.ijrobp.2012.05.009

9. Schnur JB, Ouellette SC, Dilorenzo TA, Green S, Montgomery GH. A qualitative analysis of acute skin toxicity among breast cancer radiotherapy patients. *Psychooncology* (2011) 20(3):260–8. doi: 10.1002/pon.1734

10. Pastore F, Conson M, D'Avino V, Palma G, Liuzzi R, Solla R, et al. Dose-surface analysis for prediction of severe acute radio-induced skin toxicity in breast cancer patients. *Acta Oncol* (2016) 55(4):466–73. doi: 10.3109/0284186X.2015.1110253

11. Murray CS, Rees JL. How robust are the dermatology life quality index and other self-reported subjective symptom scores when exposed to a range of experimental biases? *Acta Derm Venereol* (2010) 90(1):34–8. doi: 10.2340/00015555-0768

12. Saednia K, Tabbarah S, Lagree A, Wu T, Klein J, Garcia E, et al. Quantitative thermal imaging biomarkers to detect acute skin toxicity from breast radiation therapy using supervised machine learning. *Int J Radiat Oncol Biol Phys* (2020) 106(5):1071–83. doi: 10.1016/j.ijrobp.2019.12.032

13. Maillot O, Leduc N, Atallah V, Escarmant P, Petit A, Belhomme S, et al. Evaluation of acute skin toxicity of breast radiotherapy using thermography: Results of a prospective single-centre trial. *Cancer Radiother* (2018) 22(3):205–10. doi: 10.1016/j.canrad.2017.10.007

14. Zhang L, Fried DV, Fave XJ, Hunter LA, Yang J, Court LE. IBEX: an open infrastructure software platform to facilitate collaborative work in radiomics. *Med Phys* (2015) 42(3):1341–53. doi: 10.1118/1.4908210

15. Data Preparation and Feature Engineering in Machine Learning, Available at: https://developers.google.com/machine-learning/data-prep/construct/sampling-splitting/imbalanced-data, the website was obtained on June 2022.

16. Chen Z, Li X, Li J, Zhang S, Zhou P, Yu X, et al. A COVID-19 risk score combining chest CT radiomics and clinical characteristics to differentiate COVID-19 pneumonia from other viral pneumonias. *Aging (Albany NY)* (2021) 13(7):9186–224. doi: 10.18632/aging.202735

17. Varotto G, Susi G, Tassi L, Gozzo F, Franceschetti S, Panzica F. Comparison of resampling techniques for imbalanced datasets in machine learning: Application to epileptogenic zone localization from interictal intracranial EEG recordings in patients with focal epilepsy. *Front Neuroinform* (2021) 15:715421. doi: 10.3389/fninf.2021.715421

18. Helmy M, Eldaydamony E, Mekky N, Elmogy M, Soliman H. Predicting Parkinson disease related genes based on PyFeat and gradient boosted decision tree. *Sci Rep* (2022) 12(1):10004. doi: 10.1038/s41598-022-14127-8

19. Rstudio package source, https://CRAN.R-project.org/package=gbm. The website was obtained on June 2021.

20. Lee TF, Sung KC, Chao PJ, Huang YJ, Lan JH, Wu HY, et al. Relationships among patient characteristics, irradiation treatment planning parameters, and treatment toxicity of acute radiation dermatitis after breast hybrid intensity modulation radiation therapy. *PloS One* (2018) 13(7):e0200192. doi: 10.1371/journal.pone.0200192

21. Ramseier JY, Ferreira MN, Leventhal JS. Dermatologic toxicities associated with radiation therapy in women with breast cancer. *Int J Womens Dermatol* (2020) 6(5):349–56. doi: 10.1016/j.ijwd.2020.07.015

22. Spalek M. Chronic radiation-induced dermatitis: challenges and solutions. *Clin Cosmet Investig Dermatol* (2016) 9:473–82. doi: 10.2147/CCID.S94320

23. Issoufaly I, Petit C, Guihard S, Eugene R, Jung L, Clavier JB, et al. Favorable safety profile of moderate hypofractionated over normofractionated radiotherapy in breast cancer patients: a multicentric prospective real-life data farming analysis. *Radiat Oncol* (2022) 17(1):80. doi: 10.1186/s13014-022-02044-z

24. Kole AJ, Kole L, Moran MS. Acute radiation dermatitis in breast cancer patients: challenges and solutions. *Breast Cancer (Dove Med Press)* (2017) 9:313–23. doi: 10.2147/BCTT.S109763

25. Wang J, Liu R, Zhao Y, Nantavithya C, Elhalawani H, Zhu H, et al. A predictive model of radiation-related fibrosis based on the radiomic features of magnetic resonance imaging and computed tomography. *Transl Cancer Res* (2020) 9(8):4726–38. doi: 10.21037/tcr-20-751

26. Du Q, Baine M, Bavitz K, McAllister J, Liang X, Yu H, et al. Radiomic feature stability across 4D respiratory phases and its impact on lung tumor prognosis prediction. *PloS One* (2019) 14(5):e0216480. doi: 10.1371/journal.pone.0216480

27. Li X, Chen E, Guo B, Yang W, Han R, Hu C, et al. The impact of respiratory motion and CT pitch on the robustness of radiomics feature extraction in 4DCT lung imaging. *Comput Methods Programs BioMed* (2020) 197:105719. doi: 10.1016/j.cmpb.2020.105719

28. Vabalas A, Gowen E, Poliakoff E, Casson AJ. Machine learning algorithm validation with a limited sample size. *PloS One* (2019) 14(11):e0224365. doi: 10.1371/journal.pone.0224365

29. Maleki F, Muthukrishnan N, Ovens K, Reinhold C, Forghani R. Machine learning algorithm validation: From essentials to advanced applications and implications for regulatory certification and deployment. *Neuroimaging Clin N Am* (2020) 30(4):433–45. doi: 10.1016/j.nic.2020.08.004

30. Kocak B, Durmaz ES, Ates E, Ulusan MB. Radiogenomics in clear cell renal cell carcinoma: Machine learning-based high-dimensional quantitative CT texture analysis in predicting PBRM1 mutation status. *AJR Am J Roentgenol* (2019) 212(3):W55–63. doi: 10.2214/AJR.18.20443

31. Janko M, Ontiveros F, Fitzgerald TJ, Deng A, DeCicco M, Rock KL. IL-1 generated subsequent to radiation-induced tissue injury contributes to the pathogenesis of radiodermatitis. *Radiat Res* (2012) 178(3):166–72. doi: 10.1667/RR3097.1

frontiers | Frontiers in Oncology

TYPE Review
PUBLISHED 21 November 2022
DOI 10.3389/fonc.2022.980513

OPEN ACCESS

EDITED BY
San-Gang Wu,
First Affiliated Hospital of Xiamen University, China

REVIEWED BY
Hans-Christian Kolberg,
Marienhospital Bottrop, Germany
Wiktoria Maria Suchorska,
Greater Poland Cancer Center (GPCC), Poland

*CORRESPONDENCE
Mohammad Esmaeil Akbari
profmeakbari@gmail.com
Hakimeh Zali
hakimehzali@gmail.com;
h.zali@sbmu.ac.ir

SPECIALTY SECTION
This article was submitted to Breast Cancer, a section of the journal Frontiers in Oncology

RECEIVED 28 June 2022
ACCEPTED 19 October 2022
PUBLISHED 21 November 2022

CITATION
Jeibouei S, Shams F, Mohebichamkhorami F, Sanooghi D, Faal B, Akbari ME and Zali H (2022) Biological and clinical review of IORT-induced wound fluid in breast cancer patients.
Front. Oncol. 12:980513.
doi: 10.3389/fonc.2022.980513

Biological and clinical review of IORT-induced wound fluid in breast cancer patients

Shabnam Jeibouei[1,2], Forough Shams[3], Fariba Mohebichamkhorami[4], Davood Sanooghi[1], Bahareh Faal[5], Mohammad Esmaeil Akbari[1]* and Hakimeh Zali[4]*

[1]Cancer Research Center, Shahid Beheshti University of Medical Sciences, Tehran, Iran, [2]Future Foods Lab, Virginia Seafood Agricultural Research and Extension Center, Virginia Tech, Hampton, VA, United States, [3]Department of Medical Biotechnology, School of Advanced Technologies in Medicine, Shahid Beheshti University of Medical Sciences, Tehran, Iran, [4]Department of Tissue Engineering and Applied Cell Sciences, School of Advanced Technologies in Medicine, Shahid Beheshti University of Medical Sciences, Tehran, Iran, [5]Department of Biology, Central Tehran Branch, Islamic Azad University, Tehran, Iran

Intraoperative radiotherapy (IORT) has become a growing therapy for early-stage breast cancer (BC). Some studies claim that wound fluid (seroma), a common consequence of surgical excision in the tumor cavity, can reflect the effects of IORT on cancer inhibition. However, further research by our team and other researchers, such as analysis of seroma composition, affected cell lines, and primary tissues in two-dimensional (2D) and three-dimensional (3D) culture systems, clarified that seroma could not address the questions about IORT effectiveness in the surgical site. In this review, we mention the factors involved in tumor recurrence, direct or indirect effects of IORT on BC, and all the studies associated with BC seroma to attain more information about the impact of IORT-induced seroma to make a better decision to remove or remain after surgery and IORT. Finally, we suggest that seroma studies cannot decipher the mechanisms underlying the effectiveness of IORT in BC patients. The question of whether IORT-seroma has a beneficial effect can only be answered in a trial with a clinical endpoint, which is not even ongoing.

KEYWORDS

breast cancer, IORT, seroma, personalized medicine, tumor microenvironment

1 Introduction

Breast cancer is the fifth most important reason for cancer death worldwide (1). Global statistics show that in 2020 female breast cancer caused 11.7% and 6.9% of new cases and deaths from all cancer types, respectively (2). Surgical intervention is the primary option for BC patient management. Based on prolonged research, the standard

procedure is either an excision plus radiotherapy or a total mastectomy to achieve clear margins. It has been demonstrated that these two strategies are consistently equivalent in relapse-free and overall survival (3). In the early stages of BC, radiotherapy has been approved as a critical part of breast-conserving therapy (4). Following lumpectomy, radiation therapy is associated with fewer BC recurrences (distant or locoregional) and mortality (5). Hypofractionation and dose escalation were used as a standard of care. External beam radiotherapy (EBRT), which is typically administered in daily fractional doses during 5-6 weeks (45–50 Gy fractionated in 1.8–2.0 Gy per day), six weeks after surgery (6), while IORT is a high single dose of irradiation _either electrons (12Gy as boost dose/21Gy as radical dose) or X-rays (21Gy) _ given to the negative tumor margin during the surgery immediately after removing the tumor. Because electrons penetrate deeper than low-energy X-rays, breast tissue must be mobilized, and shields put into the posterior lumpectomy cavity to protect tissues inside the thorax. For measured depth, 20–21 Gy doses are regularly delivered at low-electron energy. Intraoperative electron radiation therapy (IOERT) is a common term for this method (7). Recently, the survival outcomes and local control of electron intraoperative radiotherapy (ELIOT) (using 50 kv IORT) and TARGIT (using 21 Gy IOERT) were released as two randomized clinical trials. They compared IORT and whole-breast EBRT (8, 9). TARGIT: means intraoperative radiotherapy with photon made by ZEISS COMPANY from Germany which is named “Intrabeam”. The dose of partial breast irradiation is 20 GY as Low KV-X Ray, which, based on biological and clinicopathological criteria is called: BOOST or RADICAL dose. ELLIOT: in completing different IORT procedures, here we are using Electron by two different doses: BOOST= 12 GY irradiation by an electron at the flap prepared during surgery that should be completed after surgery by EBRT. RADICAL: 21 GY irradiation by the electron during surgery as the radical dose which does not need EBRT anymore; it takes time less than 2 min. Moreover, the TARGIT-A trial showed risk-adapted targeted intraoperative radiotherapy (TARGIT-IORT) during lumpectomy for BC as impressive as whole-breast EBRT. TARGIT-IORT aims to achieve an accurately-positioned and accelerated form of tumor-bed irradiation, focusing on the target tissues alone, sparing normal tissues and organs such as lung, skin, heart, and chest wall structures from unnecessary and potentially harmful radiation treatment (10). Through ELIOT technique, the mobile linear accelerator delivers a single dose of radiation with electrons to the involved quadrant of the breast during surgery, reducing the radiotherapy course from six weeks to one single session during surgery (11). Both trials announced low local recurrence rates for IORT with tolerable toxicity and remarkable outcomes of overall survival (8, 9). In addition to these trials, emerging studies clarify the benefits and mechanisms underlying the local and systemic IORT in BC patients. Recently, wound fluid (seroma) has attracted the particular interest of researchers. It is typically formed in remained space after surgical excision. It leads to an inflammatory response in wound healing and seroma fluid accumulation in the subcutaneous area. During two recent decades, many studies have been done to clarify the impacts of seroma derived from IORT-treated tumor bed on the decrease of cancer recurrence. Studies by Belletti et al. and Herskind et al. have notified that seroma obtained from patients treated with IORT caused a reduction in proliferation and invasion of BC cell lines *in vitro* compared to seroma from non-treated patients.

Moreover, IORT treatment reported significant results in invasion (3-D Matrigel) and migration assays. No significant effects were observed on the proliferative capacity of seroma in 2D cell culture using BC cell lines (12, 13). Belletti et al. discovered an anti-cancer effect of TARGIT through changes in cytokines and growth factors in the resection cavity (12). Despite the promising results from these studies that introduced IORT-seroma as a tumor-inhibiting factor, there are many growing kinds of research on the analysis of seroma composition and effects of seroma on cell lines of BC and primary tissues that show contrary outcomes. Some of these studies performed using 3D *ex vivo* models have recently been performed by our research team. In this review, we will mention critical factors involved in BC recurrence, focusing on the direct and indirect effects of IORT on BC. Then we will discuss all the findings in this field of study to elucidate the benefit of removing or preserving IORT-seroma.

1.1 Factors involved in breast cancer recurrence

Ninety percent of all local relapses happen within proximity of the removed tumor site (14), and it may be due to remaining cancer cells in peritumoral tissue, which is developed by positive resection margins or perilymphatic and perivascular invasion (15). Studies showed that one of the important factors involved in BC recurrences could be the molecular subtype of the removed tumor. On the other hand, the heterogeneity of a single tumor results in drug resistance and recurrence. Moreover, the role of the microenvironment of the tumor bed and immune system in the development of recurrences would be significant. Figure 1 schematically presents the factors that influence the recurrence of the disease.

1.1.1 Molecular subtype

Different patterns of cancer recurrence have been suggested between various BC subtypes. According to Figure 1 (left side), it seems that estrogen receptor (ER)-negative breast cancers are susceptible to higher recurrence during the first five years than ER-positive breast cancers following diagnosis. For the next ten years, the recurrence risk will chronically enhance in ER-positive

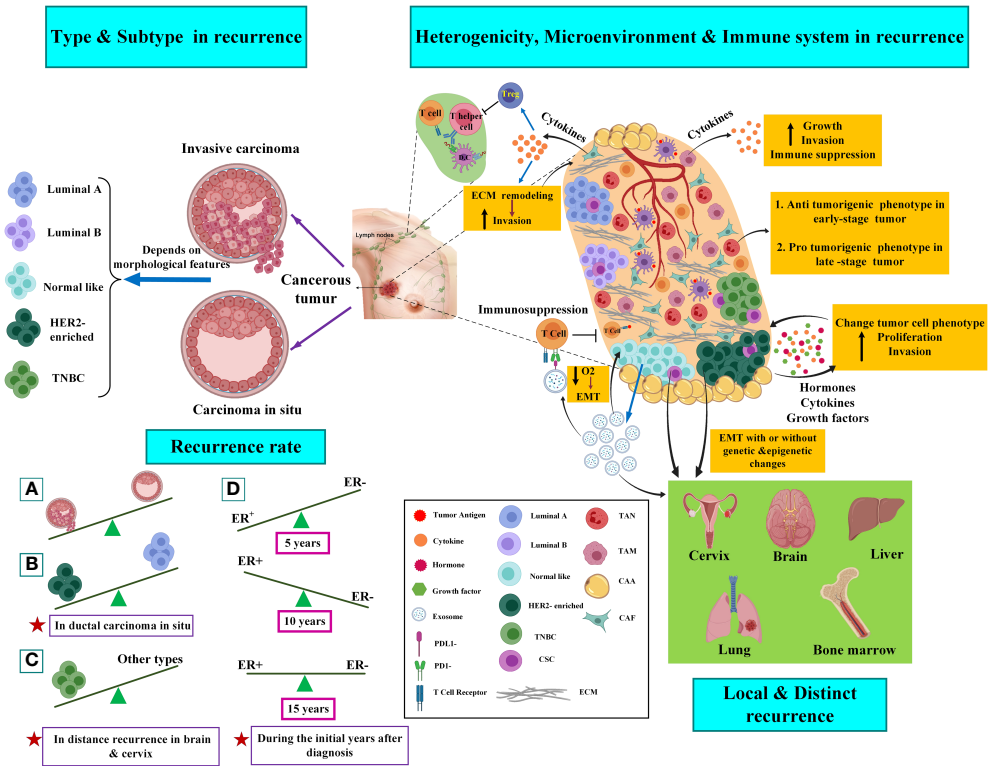

FIGURE 1
Factors involved in breast cancer recurrence. The left side of the picture shows the histopathologic types and molecular subtypes of the tumors in the recurrence of the disease. The right side of the picture shows the role of tumor heterogeneity, microenvironment, and immune system in breast cancer recurrence. Several clonal tumors containing CSCs are seen in tumor bulk and CSCs can affect the heterogenic migration of various clones in a single tumor. CSC also promote the EMT process and cause metastasis of BC tumor cell to the cervix, brain, liver, lung, and bone marrow. Cancer cells can recruit the immune system to progress tumor or even metastasis. Specific immune cells, including macrophages, lymphocytes, NK cells, dendritic cells (DCs), and neutrophils, are abundant and actively involved in the progression or suppression of cancer dissemination at the site of metastasis. Indeed, cancer cells can indirectly modulate and suppress the immune response (30, 32). CAFs promote tumor progression by initiating extracellular matrix remodeling through cytokine secretion. CAFs could suppress or avoid the immune response by promoting the recruitment of regulatory T cells (Treg), which is mediated by inflammation, or stopping the proliferation of T helper cells and killer T cells (28, 29). Work as tumor-modifying cells that may induce a change in cancer cell phenotype. CAAs produce hormones, growth factors, and cytokines. TAMs are the predominant immune cell types with immunosuppressive M2 polarized phenotypes that secrete tumor cytokines. Exosomes are essential in impairing both the adaptive and innate immune systems. It was shown that exosomal PDL1 derived from BC promotes and protects tumor growth by attaching to the PD-1 receptor of the CD8 T cells; thus, their adaptive killing activities are inhibited. Moreover, T-cells inhibit exosome secretion significantly through their anti-tumor immunity. In addition, uncontrolled cell proliferation induced by exosomes leads to inadequate nutrient and oxygen flow that derives the tumor microenvironment from becoming hypoxic. This process further triggers Epithelial-to-Mesenchymal Transition (EMT) and also promotes a more invasive phenotype. Further explanations are available in the text. TAN, tumor-associated neutrophil; TAM, tumor-associated macrophage; CAA, cancer-associated adipocyte; CAF, cancer-associated fibroblast; ECM, extracellular matrix; EMT, epithelial to mesenchymal transition; TNBC, triple-negative breast cancer; CSC, cancer stem cell. The figure was created using Biorender (https://biorender.com).

breast cancers, and fifteen years after diagnosis, the risk seems to be equivalent for both subtypes. It has been demonstrated that in ductal carcinoma in situ, the human epidermal growth factor receptor 2 (HER2)-positive/progesterone (PR)-negative/ER-negative cancers showed a higher recurrence risk than HER2-negative/PR-positive/ER-positive cancers. Triple-negative breast cancer (TNBCs), which are typified by the absence of PR/ER/HER2, are commonly related to a higher risk of recurrence compared to receptor-positive tumors, particularly with a higher rate of recurrences in distant tissues (in the brain and visceral metastases) (16).

1.1.2 Heterogeneity

Histopathologic, genetic, epigenetic, and single-cell sequencing studies, as well as the application of CTC-based assays in breast tumors, indicate that a single primary tumor can affect different regions and also, it may be able to phenotypic and genotypic change over time (17, 18). Tumor heterogeneity can be observed between cells within an individual patient's tumor (intra-tumoral) or between cells of the same subgroup of tumors in different patients (inter-tumoral). At the genetic level, heterogeneity is connected to the copy number variation

(CNV), down-regulation, and overexpression of a gene (due to missense, nonsense, or frameshift mutations) (19). Based on two concepts, including the cancer stem cell (CSC) hypothesis and the clonal evolution/selection model, primary single cells can undergo multiple molecular alterations and develop infinitive proliferative potential. The clonal evolution/selection model implies natural selection and explains how clones with higher epigenetic and genetic complexity can comply more under pressures than clones with low complexity (18). Unlike this model, the concept of CSC mentions self-renewal, capacity for clonal tumor initiation, and the potential for the clonal long-term repopulation (20). Interaction between CSCs and their niche (CSC surrounding microenvironment in a tumor) promotes invasion and metastasis of the tumor due to the production of factors, and the density of CSCs can affect the heterogenic migration of various clones in a single tumor (21, 22).

1.1.3 Tumor microenvironment and immune system

Researchers are increasingly supporting evidence that acellular and cellular components in the tumor microenvironment (TME) play a principal role in tumor growth and response to treatment. Cancer-associated fibroblasts (CAFs) are the main components in cancer stroma and TME. They promote tumor progression by initiating extracellular matrix remodeling through the secretion of cytokines (23). Adipocytes are other cell types that form TME. The most abundant component covering the cells in breast tumors is adipose tissue. Cancer-associated adipocytes (CAAs) work as tumor-modifying cells that may induce a change in cancer cell phenotype (24). Adipocytes produce hormones, growth factors, and cytokines. However, their role in the expansion of BC has not been fully discovered yet (25). Numerous types of immune cells, including macrophages, various phenotypes of T cells, B lymphocytes, natural killer (NK) cells, mast cells, and neutrophils, are found in breast tumors as part of normal tumor anatomy (26). Tumor-associated macrophages (TAMs) are the predominant immune cell types with immunosuppressive M2 polarized phenotypes that secrete tumor cytokines (IL-4, IL-10, and IL-13). These cytokines promote tumor growth by stimulating immune cell differentiation into mature macrophages (27). The interaction of tumor cells and the matured macrophages cause the secretion of various factors, such as vascular endothelial growth factor (VEGF) and colony-stimulating factor–1 (CSF1), *via* tumor cells, promoting tumor growth and invasion (28).

TAMs, through expressing heme oxygenase-1 (HO-1), an enzyme that inhibits immune system, suppress the endothelial cells' response to tumor necrosis factor-a (TNFα), an immunogenic cytokine, and then maintain the immunosuppressive tumor microenvironment (29). Cancer progression and anti-cancer response also depend on interactions between cancer cells and the immune system. The interaction can be categorized into four groups: First, the process of immunosurveillance; second, the anti-cancer immune response; third, immunosuppression; and fourth, the cancer assistance program. Through the immunosurveillance mechanism, the healthy immune system continually checks tissues for the manifestation of cancer, particularly the existence of tumor antigens, including abnormally expressed, mutated, or oncoviral proteins. Following prosperous detection of tumor cells, the anti-cancer immune responses proceed and are identified by killer cells and T helper cells and then lyse the cancer cells. Furthermore, cancer cells can indirectly modulate and suppress the immune response. The c activation of b-catenin mediated by cancer cells in DCs is a specific example of this process.

DCs are responsible for presenting killer T cells adhered to the particular tumor antigens with the ability to direct the anti-tumor immune response. DCs cause a repressed cross-priming of CD8+ T cells adhered to tumor antigens following high levels of activated b-catenin; therefore, the entire process of anti-tumor immune response mediated by CD8+ T cell is dampened (30). Then, the immune cells can have a dual function in the tumor microenvironment; while specific features of tumor stroma can trigger immune cells to develop tumor suppression, other signals and features of the tumor can promote immune system-mediated tumor invasion (31–34).

Among acellular components of TME, exosomes possess a crucial role in shaping the microenvironment of the local tumor through paracrine crosstalk between stromal cells and tumor and in organizing future sites of metastasis. Exosomes are small extracellular vesicles with an average size of 100 nm with an endosomal origin that deliver various types of molecular and genetic information (e.g., lipids, proteins, and nucleic acids) to neighbor and distant cells. In pioneering studies, David C. Lyden et al. demonstrated that exosomes have a critical role in pre-metastatic niche formation in distant organs. Furthermore, the studies highlighted the role of exosomal integrins in directing organotropic metastasis. These findings bring further insight into cancer development's complexity while demonstrating the existing gaps in our knowledge (35).

1.2 Responses of tumor and tumor bed to IORT

IORT is used in a high single dose that targets the wound cavity with a higher recurrence risk while spars the surrounding tissue and providing acceptable cosmetic and toxicological results (36–39). The IORT with direct effects removes survived tumor cells in the margin and non-irradiated neighbor cells through the bystander effect. The tumor microenvironment also receives significant modifications

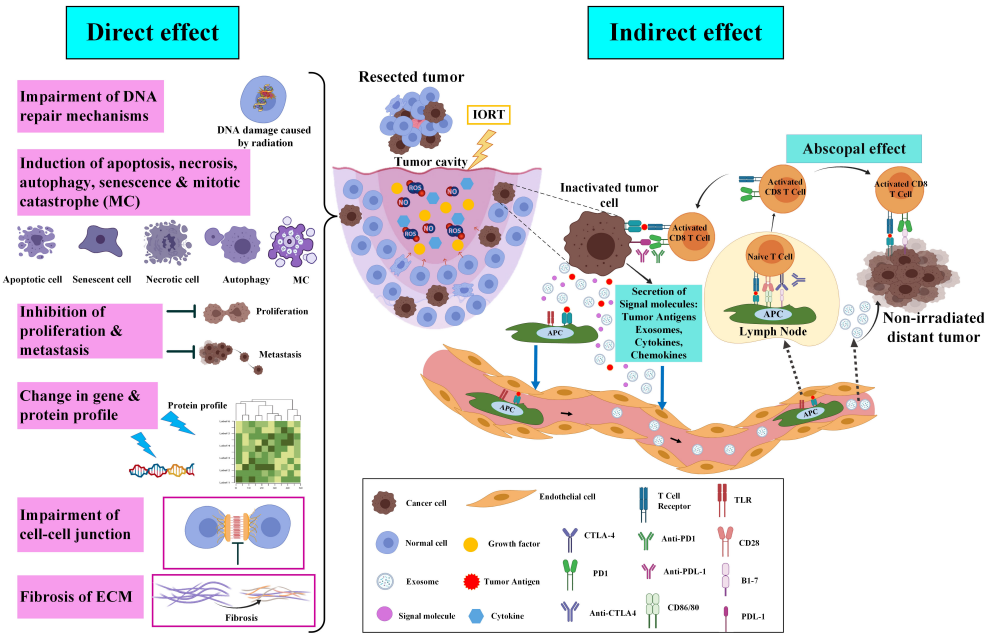

FIGURE 2
Direct and indirect effects of IORT on cancer inhibition and recurrence. After the breast-conserving surgery, molecular and probably remained cancer cells in the tumor cavity will be affected by IORT. Briefly, irradiation on the tumor cavity impairs DNA repair mechanisms, induces cell death, inhibits proliferation and metastasis, alters gene and protein profiles, impairs the cell-cell junction, and induces ECM fibrosis. In indirect effects of IORT, inactivated remained tumor cells release exosomes and tumor antigens which move and deliver to lymphatic vessels through the circulating system and APCs, respectively. IORT-induced tumor antigens and exosomes effects non-irradiated tumor cells in the body via a mechanism named "abscopal effect" (33). The figure was created using Biorender (https://biorender.com).

(39). Discovered direct and indirect biological responses of probably remained tumor cells as well as tumor bed cells to IORT are represented here and schematically presented in Figure 2.

1.2.1 DNA repair mechanisms

Mainly, due to less time to repair their damages, IR induces more efficient cell death in proliferative cells than quiescent cells. Oxygen concentration is decreased in tumor tissue, and it was demonstrated that poor-oxygenated cells are less sensitive to IR radiation compared to those well-oxygenated cells. Cancer cells are more susceptible to unrepaired damage due to faster proliferation than normal cells; they often have several mutations that cause continual stimulation of the repair process. It can lead to their survival from damage; however, it may lead to the death of surrounding normal cells (40–42).

1.2.2 Metastasis, proliferation, and metabolism

After BC surgery, IORT targets tumor bed cells through modifying their growth conditions, such as preventing mammary mesenchymal stromal cells (MSC) from outgrowth after IORT (43). Segatto et al. supported this concept by finding the expression of miR-223 in the cells of the tumor bed that undergo IORT. This expression causes the reduction of epidermal growth factor (EGF) expression that finally abrogates cell growth and tumor recurrence (44). The main signaling pathway mediated by growth factors responsible for cancer cell survival and proliferation is the PI3K/AKT/mTOR (45), in which we recently observed downregulation of proteins that are part of the PI3K-Akt signaling pathway led to disrupted proliferation following radiation (46, 47). The tumor margin of cancer after 24h following IORT showed downregulation of central carbon metabolism. Cancer cells alter their metabolism to promote unrestricted cellular proliferation and respond to energetic and biosynthetic demands (48). Warburg first discovered that cancer cells have more demands for glucose; then, the glycolysis process is increased in them (49). After irradiation, processes associated with Glycolysis/Gluconeogenesis were suppressed, and several carbon metabolisms, including citrate cycle and fatty acid and amino acid degradation, were activated. After IORT, changes in the metabolisms could aid the environment in infiltrating immune cells and restrict the proliferation of remaining tumor cells (50).

1.2.3 Cell death mechanisms

Growing evidence shows that triggering the cell death mechanism as a therapeutic effect of radiotherapy would be a complicated process. Notably, nowadays, it is detected that suppression of the proliferative capacity of tumor cells behind irradiation happens through various mechanisms, including apoptosis, necrosis, senescence, autophagy, and mitotic

catastrophe (MC) (51, 52). In high LET (linear energy transfer) radiation, direct ionization of cell macromolecules such as DNA, RNA, proteins, and lipids induce cell damage. Radiation with low LET leads to indirect damage to these macromolecules because of reactive oxygen species (ROS) production, particularly hydroxide and superoxide radicals produced from the radiolysis process of reactive nitric oxide species (RNOS) and intracellular H2O. These sources of ROSs trigger several intracellular signaling pathways and oxidate macromolecules, which lead to inflammation and stress responses (53–57). IR stimulates pro- and anti-proliferative signaling pathways that unbalance cell decisions about survival/apoptosis (58), which are regulated by several factors and genes involved in DNA repair, inflammation, cell cycle progression, and cell survival/or death (58–61). Altogether, various kinds of tumor cells, including immortalized keratinocytes, lung, colon, and prostate cancer, experience apoptosis after IR radiation (from 1 to 20 Gy). Many non-immortalized cells require higher irradiation doses (>20 Gy) to show apoptosis (51, 62, 63). Moreover, several data support the notion that IR treatment may stimulate p53-independent apoptosis by the mechanism of the membrane stress pathway, *in vitro* and *in vivo*, by sphingomyelin transmembrane signaling through the production of ceramide second messenger (57, 64). Radiation-triggered necrosis, unlike apoptosis, is mainly linked with intensified inflammation in the surrounding normal tissue (65). Necrosis is a type of cell death that has commonly been highlighted as a consequence of high IR doses (32 to 50 Gy) (57, 66). Senescence is a recognized procedure throughout aging and tissues under IR-treated or several stress stimuli such as chemotherapeutic agents, oxidative stress, and prolongation of signaling through some cytokines. The senescent cells can consequently initiate the pathology process (67–70). The primary cell response of lower doses of IR is senescence, while higher doses of IR induce necrosis or apoptosis in the same cells. In a study, X-ray irradiation of endothelial cells of the pulmonary artery showed that an intensifying dose of IR radiation induces a range of cell responses from senescence in lower doses and autophagy/apoptosis and necrosis at higher doses (62). Much data have been proposed that senescence in cancer cells-treated with IR could cause a decrease in self-renewal capacity (71, 72). Despite the potential tumor suppression role of senescent cancer cells, they could secrete a particular profile of the Senescence-Associated Secretory Phenotype (SASP), which contains a various range of cytokines, proteases, and growth factors. SASP changes the tissue microenvironment and triggers tumorigenesis and angiogenesis, as well as the EMT process and invasion. Although, SASP has anti-tumor function through tumor cell clearance *via* the immune system (73–75). Autophagy is a primary catabolic mechanism of cell degradation through lysosomal action that lyses dysfunctional or unnecessary cell components (76). Autophagy is a procedure to maintain metabolic homeostasis in tumor cells undergoing nutrient depletion and chronic hypoxia (41). This pathway can stimulate survival or cell death in IR-treated cells; the mechanisms depend on the gene expression controlling apoptosis, which is also cell and tissue-specific (77, 78). Mitotic catastrophe (MC) is associated with different biochemical and morphological changes. A cell death process occurs after or during aberrant mitosis and incomplete DNA synthesis following radiation (79). Checkpoint deficiencies in tumor cells cause defective DNA replication and malfunctioned repair mechanisms in the aberrant segregation of chromosomes that may lead to MC. Therefore, the control loss of checkpoints in IR-treated cancer cells may generate aneuploid progeny and cell death due to MC (57).

1.2.4 Cell-cell and cell-(extracellular matrix) ECM interaction

Crosstalk between PI3K/AKT/mTOR signaling pathway mediated by growth factors and cell adhesion to the ECM activates several vital biological processes, such as regulation of gene expression as well as proliferation, differentiation, survival, and motility of cells (80, 81). We also found a number of downregulated proteins through analysis of the KEGG pathways 24h after indirect irradiation of the tumor margins of breast-conserving surgery (BCS) plus IORT. The proteins are involved in the processes associated with focal adhesion, ECM-receptor interaction, and Rap1 signaling pathway (46, 82).

1.2.5 Gene and protein expression profile

Despite many significant research interests in the scientific community about the clinical application of IORT on different types of cancers, a limited number of papers were concerned about induced gene expression following treatment with IORT. A recent study on BC cell lines (both tumorigenic and non-tumorigenic cell lines) exposed with doses of 10 and 23 Gy identified differences among various types of cell lines and treatment after using microarray for gene expression profiling (83). According to our previous omics investigations on the tissue of negative tumor margins, radical and boost doses of IOERT change different molecular pathways (82). They could stimulate the activity of some signaling pathways, such as nuclear factor kappa B (NF-κB), TNF, forkhead Box O1 (FoxO), and hypoxia-inducible factors1 (HIF-1). We also detected that apoptosis, B cell receptor, Toll-like receptor, and metabolic pathways were upregulated, known to have systemic and local effects. The proteome profile was obtained from the isobaric tag for relative and absolute quantitation (ITRAQ) technique of tumor margin samples of patients under treatment with IOERT, 21Gy (sample collected before and 24 h of after treatment with IOERT). According to our results, the tumor margin

samples collected before and after IORT showed alterations in the expression of many genes and enhanced pathways linked to cell growth, survival, programmed cell death, and cell cycle arrest. In addition, downregulated proteins that were part of the phosphatidylinositol 3-kinase (PI3K)-AKT signaling pathway showed disruption of proliferation after IORT (82). Besides, inhibition of this pathway, directly and indirectly, could influence the radiation results (82).

1.2.6 Abscopal effect

Local IR treatment of tumors often results in systemic responses at distant sites. This phenomenon is termed the "abscopal effect," which induces and enhances the innate and adaptive immune responses against tumors (84). The abscopal effect is an antitumor consequence of radiation that can be seen in metastatic conditions away from irradiated tissue (85). In radiation therapy, diverse mechanisms are associated with the abscopal effect. Generally, the mechanisms include increasing the lymphocyte infiltration into the tumor's microenvironment, improving detection and tumor cell death by enhancing the tumor's antigens expression and antigen presentation machinery, increasing tumor sensitivity, and activating ascending modulatory pathways. The radiation-induced abscopal effect depends on the immune system through various strategies. In some cases, radiation therapy can activate the host immune system, especially in immunogenic cancers such as melanoma, hepatocellular carcinoma, and renal cell carcinoma. The synergistic effect between the host immune response and the abscopal effect induced by radiation therapy stimulates antitumor effects against micro-metastases beyond the irradiated area. A combination of immunotherapy and radiation therapy is used in some other cases, mainly involving less immunological cancers such as BC. Thus, immunogenic reagents, including immune checkpoint blockers and targeted immunomodulators, are combined with radiation therapy in this type of cancer. This combination promotes the host immune response against tumor cells and stimulates the abscopal effect after radiation therapy (86). However, in a rare case, Azami and colleagues reported that local radiation monotherapy in advanced BC, with extensive lymph node, lung, and bone metastases, effectively induced an abscopal effect in non-irradiated metastatic regions. A few months after radiation therapy, they observed that metastatic lesions regressed in the irradiated breast tumors and all non-irradiated areas (87). Generally, in the first antitumor strategy, high-dose radiation therapy with a direct effect on tumor cells kills these cells. It releases the remnants of dead tumor cells that contain potentially immunogenic molecules. These factors stimulate the immune system and lead to immunological cell death through T-regulatory cells, DCs, and suppressive cells (88). The combination of radiation therapy and granulocyte-macrophage colony-stimulating factor (GM-CSF) in some solid metastatic cancers can induce an abscopal effect and increase the overall survival of patients. Formenti and colleagues showed that in metastatic BC, the combination of radiation therapy with a systemic transforming growth factor-β (TGF-β) blocking antibody called Fresolimumab induces a dose-dependent systemic immune response and improves overall survival (89).

1.2.7 Effect of drainage on clinical outcome

Several studies have explored the safety of seroma drainage according to multiple clinical endpoints (Table 1). Quality of life has been reported in various kinds of results in different studies. Better quality of life was seen in long-term drainage (90), reduction of hospital stays, and early drain removal in some studies provided a better quality of life by decreasing post-operative complications or in some studies reported no adverse effects, so early drain removal was preferred by patients (98, 99). To the best of our knowledge, in IORT, no results were reported regarding drainage tube removal time, length of hospitalization, and post-operative complications. However, IORT had promising results, both in terms of saving healthy tissue and local control (74% to 100% at 5 years) and 96.2% disease-free survival (101, 103). The local relapse prompted a series of clinical trials and studies to investigate whether localized IORT could be as efficient at preventing recurrence at local site as standard postoperative radiotherapy of the whole breast while also being more patient-friendly in terms of decreasing the treatment duration. As we mentioned earlier, IORT decreases the possible risk of tumor cell repopulation during the wound healing process through direct radiation therapy of diseased tissue within the tumor bed during the surgical procedure (9).

1.3 Studies associated with effects of IORT-seroma on breast cancer progression

Key information related to all the studies about breast surgery IORT- and non-IORT-seroma and their effects on BC (according to our knowledge) is available in Table 2. See also Figure 3.

1.3.1 Composition of breast surgery-induced seroma; benign, malignant, IORT-treated

Seroma is an inflammatory exudate most commonly found during the first step of wound healing (104). It has been illuminated that seroma inoculation near the tumor site in mice with syngeneic BC xenografts led to enhanced tumor growth (105). Seroma derived from surgical sites may show brief information about the cell activity in terms of the release of growth factors, chemokines, and cytokines that are vital in repair and healing (106, 107). The differential expression of pro-oncogenic growth factors and cytokines is secreted from malignant to benign lesions in the post-surgical seroma in breast tumors. Valeta-Magara and

TABLE 1 Evidence Summary of drain policy and its clinical effects.

	Patient Numbers	Standards are regarding drains (days after surgery)	Standards are regarding drains (volume of seroma)	Influence on infection rate or wound healing	Improves quality of life or not	Outcome	Ref
surgery	88	24 hours compared to 5 days after surgery	Higher seroma formation in the 1-day group (161.25 ml) compared to the 5-day group (7.50 ml) one week after surgery	The lower frequency of wound infection in the long-term compared to short-term drainage	Quality of life is better in the long-term (5 days) drainage	long-term drainage reduces the risk of seroma formation compared to short-term	Jafari Nedooshan J et al., 2022 (90)
	187	24h after surgery	Three groups (10ml, 20ml, 30ml)	Wound infection was similar at different drain removal times	Yes, the Significantly better quality of life in the 20 mL group	The 20 mL group had relatively low postoperative complication rates	Wen N et al., 2022 (91)
	40	off-drain day I compared to day III post-surgery	Mean 157.31 ml in 1-day compared to 149.58 ml in 3-day post-operative drain removal	–	Early drain removal reduces the symptoms felt by breast cancer patients related to drain.	Early drain removal does not reduce seromas incidence seven days after discharge	Ramadanus et al., 2022 (92)
	A meta-analysis including 11 RCTs	Early drain removal was defined between postoperative days 1-7 and late drain removal was dependent on the output	20mL/24h to 50mL/24h (The mean total seroma formation was 326 mL in 3 d)	Early removal did not increase surgical site infection	Early drain removal has no proven clinical benefit except the reduction of hospital stays	Early drain removal shortens hospital stay length while increasing the risk of seroma formation	Shima H et al., 2021 (47)
	88	The Redon drain and the Quadrain drain with a mean duration of drains *in situ* 42.6 *h* and 50.1 h respectively	The standard of drain removal was less than 30ml/24h. mean volume was 12.3 ml for the Redon drain and 13.0 ml for the Quadrain drain (Not different for both drains)	No difference in surgical site infections between the two groups	Did not differ concerning either efficacy or safety	Not significantly different concerning duration in the surgical site, post-operative pain, seroma volume, and cosmetic result	Schmidt G et al., 2019 (93)
	202	The mean postoperative day of drain removal is 14 days (9 patients had no drainage in a surgical modality)	Drain removed when the drainage fluid volume was 20 ml or less per day and the total volume was 1456 ml	Relative higher risk of seroma infection without drainage	surgical modality affected the quality of life post-operation	A high rate of seroma formation and prolonged fluid discharge were observed without drainage	Isozaki H et al., 2019 (94)
	251	Two groups, including quilting sutures with and without wound drainage	–	The incidence of postoperative infection significantly decreased without postoperative drain	- (Postoperative drain could be omitted based on the operation technique)	The group without a postoperative drain had lower seroma incidence and wound complications compared to the group with a drain	Ten Wolde B et al., 2019 (95)
	99	Early removal (4–5 days postoperative) compared to output-based drain removal when	Less than 30 ml/day in the early removal group. Total volumes of fluid drained were significantly lower in the early-removal group (median 752 ml versus 1745 ml)	No negative influence on the wound infection rate in the early removal group	Yes, Early drain removal was associated with a significant improvement in quality of life	Early drain removal has no negative effect on clinical outcomes with considerably lower home care nursing	Vos H et al., 2018 (96)
	214	Average day 5 (1–5) postoperative as the study group and	Drain removal when was less than 50 ml/24 h. Mean total volume was 351 ml in the	No significant difference	Yes, no adverse effect on the quality of life in early drain removal	Early drain removal is safe with a shorter hospital stay despite the	Okada N et al., 2013 (97)

(Continued)

TABLE 1 Continued

	Patient Numbers	Standards are regarding drains (days after surgery)	Standards are regarding drains (volume of seroma)	Influence on infection rate or wound healing	Improves quality of life or not	Outcome	Ref
		Day 6 (3–15) as the control group	study and 416 ml in the control group	between the two groups		slightly increased chance of seroma formation	
	87	Early (day 4) to late (day 10) drain removal	Drain removal when was less than 30 ml/24h. Total drainage volume was significantly higher (1123ml) in late than those with early drain removal (571 ml)	The lower wound infection rate in early removal	No negative effect on the quality of life in early drain removal so it was preferred by patients	Shorter hospital stay and slightly higher risk of seroma formation in early drain removal	Clegg-Lamptey JN et al., 2007 (98)
	100	Short (24 h) versus long-term (up to 7 days) postoperative drainage	Drainage removal when was less than 50 ml/24h. No significant difference was seen in the mean volumes of aspirations (213 ml in short vs 186 ml in long-term drainage)	Lower Infectious complications in short-term drainage	Yes, short-term drainage provided a better quality of life by decreasing post-operative complications	Short-term (24 h) drainage was associated with a shorter hospital stay, a higher risk of seroma formation, and lower wound-related complications	Baas-Vrancken Peeters MJ et al., 2005 (99)
	121	5-day vs. 8-day groups	Drain removal when was less than 30 ml/24h. no significant difference in the volume of seroma drainage between the two groups	No negative effect on the wound infection in both group	Yes, 5-day postoperative drain removal allowed for better utilization of community resources without adversely impacting patients' physical or psychological welfare or outpatient facilities	Five-day post-operative drainage was as safe as 8-day however increased the risk of seroma formation requiring aspiration	Gupta R et al., 2001 (100)
IORT	797	- IOERT vs whole breast irradiation groups	179 patients (22.46% of cases) who developed seroma	Surgical wound infection in one patient	Yes, by providing long-term efficacy and acceptable cosmetic result	IOERT-boost improves local control with 96.2% disease-free survival and reduces local recurrence at long-term follow-up (Mean 5 years)	Ciabattoni et al., 2022 (101)
	160	5.9 days in $IORT^{+}$ versus 5.0 days in the $IORT^{-}$ groups	No difference between groups in incidences of seroma	No difference in infection	Yes, IORT safely delivers radiation therapy with acceptable acute toxicity, is well-tolerated	No difference in terms of drainage tube removal time, length of hospitalization, and postoperative complications	Hu X et al., 2020 (102)
	90	- IORT vs TARGIT E groups	Seroma formation occurred in 15 patients (16.5% of cases)	15 patients (16.5% of cases) had an infection	Yes. IORT had promising results in saving healthy tissue and local control	In the IORT group, overall survival was 100% After a median follow-up of 27.4 months, and the local recurrence rate was 2.4%	d'Illiers et al., 2018 (103)

colleagues detected that seroma from the surgical cavity of BC patients expresses a higher level of fundamental tumor-promoting cytokines. In contrast, benign surgical lesions in non-cancer patients express a lower level of principal tumor-inhibiting factors. They assessed 80 different cytokines, growth factors, and chemokines in 59 post-surgical seroma (24 patients with benign and 35 with malignant lesions). Although the results showed that 28 cytokines were overexpressed in both groups of seroma. Malignant-derived seroma showed higher expression of 9 biologically important factors. In particular, Leptin, tissue inhibitor of metalloproteinases 2 (TIMP-2), growth-regulated protein (GRO), and epithelial neutrophil-activating peptide 78/chemokine (C-X-C motif) ligand 5 (ENA-78/CXCL5) were highly overexpressed in malignant seroma. At the same time,insulin-like factor binding protein-1 (IGFBP-1), IL-3, IL-16, fibroblast growth factors-9 (FGF-9), and IFN-γ showed down-regulation in malignant compared to the benign seroma. The post-surgical cavity of a breast tumor contains pro-inflammatory factors, regardless of being malignant or benign; however, in malignant tumors, a higher amount of additional pro-oncogenic cytokines, chemokines, and growth

TABLE 2 Summary of studies associated with effects of seroma and IORT-seroma on breast cancer.

	Method	Results	Author	Year
Seroma composition	Hematological and biochemical analysis of 3 or 4-day seroma from 18 BC patients undergoing mastectomy with complete axillary clearance or wide local excision.	Reflection of the exudative phase of wound healing in seroma.	McCaul et al.	2000
	Quantitative assessment of CEA and CK-19 in 24h seroma from 126 BC patients.	The high sensitivity of CEA and CK-19 for detection of locoregional recurrence in BC patients.	Zhang et al.	2006
	Wound fluid injection near the tumor site in syngeneic BC xenografts in mice.	Enhanced tumor growth.	Christina et al.	2008
	Evaluating proteomic profile of 24h seroma from 45 BC patients.	Increase of 10 and decrease of 20 tumor progression associated proteins in IORT-seroma compared with non-IORT-seroma.	Belletti et al.	2008
	Assessment of 80 cytokines, chemokines, and growth factors in 1 or 2-week seroma from 59 patients with benign or malignant lesions.	Increased expression levels of key tumor-triggering cytokines and decreased expression of important tumor-inhibiting factors in seroma from BC patients compared to seroma collected from non-cancer patients.	Valeta-Magara et al.	2015
	Assessment of 34 chemokines, cytokines, and growth factors in 24h seroma collected from 27 BC patients.	Association of the composition of seroma with molecular features of the excised tumor.	Agresti et al.	2019
	Quantitative analysis of the factor composition of 48h seroma from 38 BC patients.	Decreased level of IL-7, IL-8, MIF, IL-13, and TNF-beta and increased level of CTACK, HGF, G-CSF, TNF-alpha, and IL-1 beta in IORT-seroma compared with non-IORT-seroma.	Kulcenty et al.	2019
	Analysis of immune cell populations and cytokines in 24h seroma from 42 patients.	No significant difference in cell count between IORT group and control. Increased level of Leptin and decreased level of GRO-α, IL-1β, and Oncostatin-M in IORT group.	Wuhrer et al.	2021
Seroma on cell lines	Evaluating proliferative effects of 24h seroma from 13 BC patients on SKBR-3, MDA-MB361, MDA-MB-453, MDA-MB-231, MDA-MB435, and MCF-7 cell lines in 2D system.	Induction of proliferative effects in all the cell lines.	Tagliabue et al.	2003
	Evaluation of cell growth and motility in MCF-7, T47D, MDA-MB-453, MDA-MB-231, and SKBR-3 cell lines under 24h seroma from 45 BC (IORT and non-IORT) patients in 2D and 3D systems.	Stimulation of proliferation, invasion, and migration of BC cell lines under seroma treatment. Abrogated stimulatory effects under IORT-seroma treatment.	Belletti et al.	2008
	Evaluation of proliferation in MCF-7, HCC1937, and under treatment of 24h or 48h seroma from 30 patients (in 3 groups) in 2D system.	Induction of proliferation in HCC1937 and MCF-7 in a similar manner.	Ramolu et al.	2014
	Evaluation of clonigenic and long-term proliferation effects of 24h seroma from 30 BC (IORT and non-IORT) patients on MCF-7 cell line in 2D system.	No significant difference between IORT- and non-IORT-seroma groups.	Veldwijk et al.	2015
	Evaluation of cancer stem cell phenotype in MDA-MB-231, BT-20, MDA-MB-468, SK-BR-3, BT-549, BT-474, MCF7, and T47D cell lines under seroma treatment from 44 BC patients (IORT and non-IORT).	Decreased CSC population in IORT-seroma affected in cell lines of MDA-MB-468 and BT-549. Inhibition of CSC populations in both IORT- or non-IORT-seroma affected MCF-7 cell line.	Zaleska et al.	2016
	Evaluation of mammosphere formation in BT-474, MDA-MB-231, MDA-MB-468, and MCF-7 cell lines under treatment of 24h seroma from BC patients in 2D system.	Stimulation of mammosphere formation and also STAT3 activation.	Segatto et al.	2018
	Evaluation of apoptosis pathways in MCF-7 cell line under treatment of 7-day seroma from BC patients (IORT and non-IORT).	Activation of extrinsic apoptosis pathway by IORT-seroma.	Kulcenty et al.	2018
	Evaluation of proliferation and migration of MDA-MB-231, HCC1937, BT-549, SKBR-3, T-47D and, MCF-7 under 24h seroma treatment from 27 BC patients in 2D system.	Stimulation of proliferation and migration in all the cell lines over 4 days.	Agresti et al.	2019
	Measurement of the level of breaks double-strand DNA, apoptosis induction and the changes in DNA repair associated gene expression in MDA-MB-468 and MCF-7 cell lines under 48h seroma from 16 BC patients (IORT and non-IORT) in 2D system.	Induction of breaks in double-strand DNA and enhanced expression of DNA repair-associated genes in IORT-seroma group.	Piotrowski et al.	2019
	Evaluation of changes in CSC phenotype and EMT in MCF-7 and MDA-MB-468 cell lines under 48h seroma from 16 BC patients (IORT and non-IORT) in 2D system.	Stimulation of phenotype of CSC and EMT process in non-IORT group and abrogation of them in IORT group.	Kulcenty et al.	2019
	Microarray analysis of biological processes in MDA-MB-468 under 48h seroma from 43 BC patients (IORT and non-IORT) in 2D system.	Common biological processes in both IORT- and non-IORT groups.	Kulcenty et al.	2020

(Continued)

TABLE 2 Continued

	Method	Results	Author	Year
	Evaluation of behavior and secretome of MDA-MB-231 and mesenchymal stromal cells under 24h seroma from 42 BC patients (IORT and non-IORT) in 2D system.	Reduced proliferation of MSCs, capacity of wound healing and activity of chemotactic migration under IORT-seroma treatment.	Wuhrer	2021
	Evaluation of viability, proliferation, migration and invasion in MCF-7, MDA-MB-231, and SK-BR-3 cell lines under treatment of 24h seroma from 20 BC patients (IORT and non-IORT) in 2D system.	Decreased number of colonies in IORT-seroma affected MCF-7 cells. No significant difference between two groups in expression levels of P21, P16 and Cas3.	Jeibouei et al.	2022
Seroma on primary cells	Evaluation of survival rates in cells from human-derived BC cells under 3-day 21 seroma treatment in 2D system.	Increased survival rates and promote drug resistance in seroma-treated cells.	Zhang et al.	2016
	Evaluation of proliferation and migration in human-derived BC tumor spheroids from 4 specimens under seroma treatment from the patients in 3D microfluidic system (IORT and non-IORT) using time laps imaging.	Increased proliferation and migration rate in IORT-treated group compared with control.	Javadi et al.	2021
	Evaluation of cell viability of human-derived BC tumor spheroids from 23 specimens under seroma treatment from the patients in 3D microfluidic system.	Induction of cell viability in 22 specimens under seroma treatment compared with control. Inhibition of cell viability under seroma treatment in 1 specimen compared with control.	Jeibouei et al.	2021
	Evaluation of cell viability and measurement of the expression levels of apoptosis and migration/invasion-related proteins in human-derived BC tumor spheroids from 20 specimens under treatment of seroma from the patients (IORT and non-IORT) in 3D microfluidic system.	No significant difference in the percentage of live cells in IORT-seroma and non-IORT-seroma groups. No significant difference in Cas3 expression level between two groups. Higher level of E-cad expression in IORT group.	Jeibouei et al.	2021

Studies are divided into 3 sections, including seroma composition studies, effects of seroma on BC cell lines, and studies on the effects of seroma on primary tumor tissues.

factors and a reduction in tumor-inhibiting factors are detected. These results showed the preconditioning effect of normal surrounding tissue on the tumor and provided a pro-oncogenic environment that remains after the removal of the tumor by surgery (108). In a recent study, Agresti and collaborators detected 34 cytokines, growth factors, and chemokines in seroma of 27 BC patients that promote the initiation and development of cancer. The results clarified that the molecular characteristics of the removed tumor influence the final composition of the secreted seroma. Specifically, MIP-1a, MIP-1b, IP-10, IL-6, G-CSF, monocyte chemoattractant protein1- monocyte chemotactic and activating factor (MCP1-MCAF), and osteopontin were expressed higher in more aggressive tumors. Furthermore, differential expression of several small molecules was detected in the seroma of BC patients with mastectomy or quadrantectomy. In mastectomized patients, IL-1ra, IL-1b, IFN-γ, IL-6, G-CSF, osteopontin, IP-10, and MIP-1b were significantly higher than in quadrantectomized patients (109). The quantitative molecular diagnosis of cytokeratin-19 (CK19) and carcinoembryonic antigen (CEA) that target cancer cells in axillary seroma showed that they are a predictor of locoregional recurrence in mastectomized BC patients (110). In pioneering research, Belletti et al. compared non-IORT-seroma with IORT-seroma and revealed that TARGIT might possess an anti-tumor effect and surpass cancer cell kill *via* radiation therapy through altering the cytokines and growth factors existing in the resection cavity. They evaluated the proteomic content of seromas and detected that in seroma derived from TARGIT-treated patients compared to non-treated ones, 10 proteins enhanced while 20 proteins decreased (12). Kulcenty et al. conducted a quantitative investigation of the composition of seroma in patients with BC subtypes of luminal A and luminal B and between two groups of non-treated and treated with IORT. The comparison showed that TNF-beta, macrophage migration inhibitory factor (MIF), IL-7, IL-8, and IL-13 were significantly reduced in IORT-seroma; However, these findings were obtained without a differential diagnosis of molecular subtypes in the seroma groups. Moreover, enhanced concentrations of G-CSF, cutaneous T-cell-attracting chemokine (CTACK), IL-1 beta, hepatocyte growth factor (HGF), and TNF-alpha were characterized in IORT-seroma. They found that several cytokines were overexpressed in the luminal A subtype in the IORT-treated group, which may have anti-tumor characteristics (111). In a recent study, Wuhrer et al. analyzed seromas collected 24h after breast-conserving surgery (from 42 patients) with and without IORT treatment and observed dramatic changes in populations of immune cells and levels of cytokine (112). None of the investigated subpopulations, such as Treg, T cells, and myeloid cells, showed alteration in their activation states or their counts in cellular fraction analysis of the seroma and blood samples of the patients 24 h after IR treatment compared to control. Moreover, both groups did not alter the leucocyte fraction's apoptosis rate. Thus, IORT did not affect the processes in cellular immunity during the first 24h after surgery in the local environment. In this study, levels of cytokines in seroma were significantly changed in the IORT-treated group; results showed that cytokines including GRO-α, oncostatin-M, and IL-1β are reduced while Leptin is enhanced with IORT treatment. All of these cytokines are linked to inflammation and tumor growth. Figure 4 summarizes the studies related to seroma composition regarding protein changes.

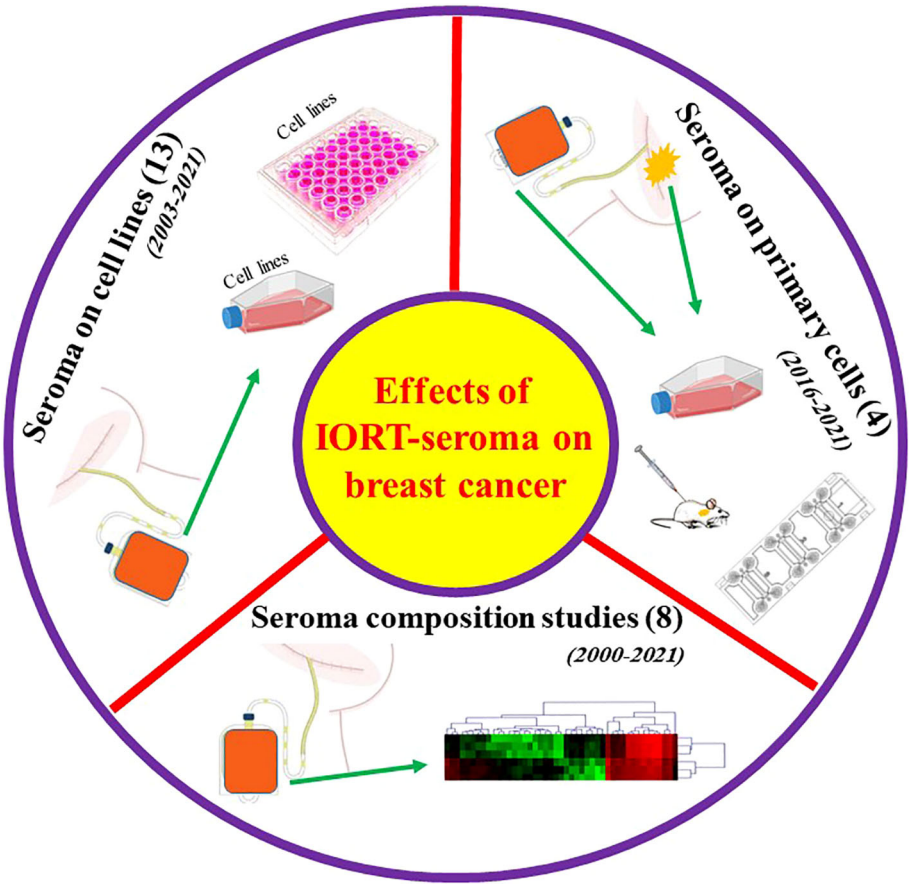

FIGURE 3
Graphical abstract for performed studies in breast surgery IORT- and non-IORT-seroma and their effects on breast cancer.

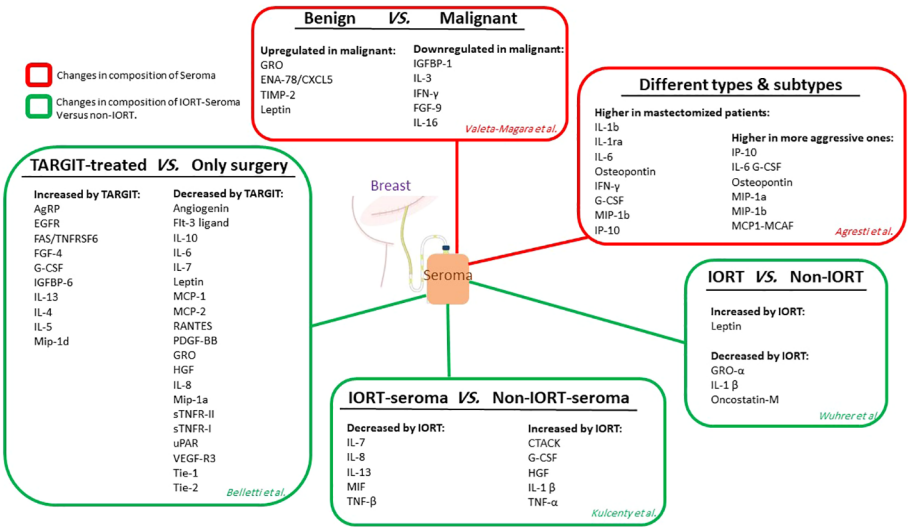

FIGURE 4
The studies related to seroma composition. Red boxes show the level of protein expression in seroma without considering radiotherapy. Green boxes show protein expression levels in an IORT-affected seroma compared to non-IORT-affected seroma.

1.3.2 Effects of seroma on breast cancer cell lines; IORT vs non-IORT

Tagliabue and collaborators first described the proliferative effects of seroma on cultures of BC cells, who tested 24h post-surgical seroma and serum from 13 BC patients on SKBR-3, MDA-MB-453, MDA-MB361, MDA-MB231, MDA-MB-435, MCF- 7 cell lines. The results clarified that all of the cell lines were stimulated to proliferate in response to the drainage fluids, although the HER2-positive cell lines showed more proliferation levels than the HER2-negative ones. Their findings showed that seroma and post-surgical serum samples comprised growth factors capable of inducing the proliferation of HER-2-positive breast cancers. Although surgical wounds provided favorable conditions for the proliferation of tumor cells, carcinomas with overexpression of HER-2 revealed a higher rate of stimulating growth. It suggests several factors secreted during repair and healing are particularly active in inducing the HER-2-positive cells (113). In their several studies, Belletti and colleagues highlighted that collected seroma from BC patients within 24 hours after surgery plays a principal role in the proliferation, survival, and motility of BC cells (12, 114, 115). Segatto et al. found that the post-surgical collected seroma highly stimulates mammosphere formation in BC cells. The researchers used EGF (as a standard stimulative agent) and seroma on cell lines of MDA-MB-231, BT-474, MDA-MB-468, and MCF-7 to test mammosphere formation. The seroma-stimulated cell lines showed a higher mammosphere forming efficacy (MFE) than those induced with EGF. Seroma highly activates signal transducer and activator of transcription 3 (STAT3) in BC cell lines. The STAT3 affects the proliferative phenotype of BC cells, and its signaling is essential for the self-renewal ability of the seroma-induced cells (116). Another study on the effects of seroma on BC cell lines by Ramolu et al. showed the capability of three types of seroma to induce the proliferation of BC cell lines. They collected seroma from 30 patients who had tumor surgery (10 patients) or underwent induction chemotherapy after tumor surgery (10 patients) or breast reconstruction (10 patients). The seromas were used to grow MCF-7 and HCC1937 cell lines. The results showed that all three groups of seromas induced the proliferation of the cells.

Interestingly, the proliferation index from culturing HCC1937 cells was significantly higher than MCF-7 cells, suggesting more sensitivity of triple-negative cell lines to stimulation by seroma (117). In studies by Belletti et al. and, Herskind et al., seroma obtained from patients treated with IORT led to more reduced invasion and proliferation of BC cell lines *in vitro* compared to those induced by seroma from non-IORT patients. However, in the short-term 2D cell culture of BC cell lines with molecular types of ER/PR, -Her2/neu, and ER/PR–, Her2/neu+, IORT had no significant effect on the proliferative capacity of seroma; although, it showed the significant effects on invasion assay on 3-D Matrigel and migration test (12, 13). To confirm the results of previous studies, Veldwijk and collaborators evaluated the clonogenic and long-term proliferation effects of IORT-seroma and non-IORT-seroma on the MCF-7 cell line. Their results showed that the difference between these groups was insignificant and that the cells required 3% FBS in addition to seroma for short-term and clonogenic proliferation (118). Recently, Agresti et al. treated MDA-MB-231, MCF-7, SKBR-3, HCC1937, BT-549, and T-47D with post-surgery seroma (collected 24h after surgery) from 27 BC patients. Measurement of cell growth in 2D culture over 4 days showed that seroma stimulated robust cell proliferation and migration in all cell lines (109).

Zaleska et al. treated 8 BC cell lines with seroma collected from conservative–breast surgery (WF) and compared data to that of seroma from IOERT treatment RT-WF (≤10 Gy) for 4 days to indicate the effect of seromas on the phenotype of cancer stem cells. Then, the differentiation cluster of CD44+/CD24-/low phenotype and activity of aldehyde dehydrogenase 1 (ALDH1) were characterized. Each of the two types of fluids impacted the CD44+/CD24-/low phenotype. They showed different consequences between cell lines, even in histologically similar subtypes. RT–WF led to the decreased CD44+/CD24-/low population in basal–like MDA–MB–468 and BT–549, while the two fluids inhibited these populations in the luminal type MCF7 cell line. The HER2 –overexpressing subtypes protected a minimal population of CD44+/CD24-/low, but the two postoperative fluids stimulated the growth of SK–BR–3. Compared to RT–WF, WF showed a more substantial effect on ALDH1 activity. Depending on the histological subtype of the cell lines, a different stimulatory effect was observed. The most robust stimulation was in the control group for the luminal subtypes with low dehydrogenase activity (119).

In a recent study, Kulcenty and colleagues published reports about the effects of IORT-seroma on BC cells. To evaluate the marker expression related to extrinsic and intrinsic apoptosis pathways, they incubated MCF-7 cell lines with IORT-seroma and non-IORT-seroma from BC patients for 4 days. Their result indicated the activation of the extrinsic apoptosis pathway by IORT-seroma (120). To clarify bystander effects of IORT-seroma on BC cells, they incubated MDA-MB-468 and MCF-7 cell lines with non-IORT-seroma, IORT-seroma from 16 patients, and conditioned media (CM) from irradiated cells. They measured the level of apoptosis induction, the rate of breaks in double-strand DNA, and the alterations in DNA repair-associated gene expression. They found that despite the induction by non-IORT-seroma, the induction by IORT-seroma and non-IORT-seroma+CM stimulated the double-strand breaks and enhanced the expression of DNA repair-associated genes (121). They incubated MDA-MB-468 and MCF-7 cell lines with non-IORT-seroma and IORT-seroma to determine the underlying mechanisms leading to the reduced tumorigenic

potential of IORT-seroma and confirm its effect on the activation of bystander effects in cell lines. The phenotype modification of CSCs in the EMT process was investigated to determine the inductive migration effect of seroma on BC cells. Their results showed that seroma triggers the phenotype of CSC and EMT process in BC cell lines; however, its impact was partly questioned when incubated with IORT-seroma. In addition, the radiation-stimulated bystander effect's role in changing WF properties to persuade the EMT process and CSC phenotype formation was confirmed (122). To compare the biological effects of seroma and IORT-seroma on non-irradiated neighbors of the cancer cells (bystander effects), the MDA-MB-468 cell line was treated with non-IORT-seroma, IORT-seroma, and CM derived from irradiated cells. Then, the microarray analysis was carried out. The analysis showed that IORT-seroma and non-IORT-seroma+RIBE groups have a similar effect on the same biological processes, such as enhancing cell-cycle regulation, oxidative phosphorylation, and DNA repair. The non-IORT-seroma group has its effect through over-activation of the involved pathways on the inflammatory response, INF-α and INF-γ response, and the signaling pathway of IL6 JAK/STAT3. These results showed that MDA-MB-468 cells induced by IORT-seroma and cells stimulated with non-IORT-seroma plus RIBE share common biological processes (123). A recent study on IORT-seroma and non-IORT-seroma on MDA-MB-231 and mesenchymal stromal cells clarified that seroma from IORT-treated patients affected the MSC behavior and modified the secretome of these cells. After 34h, IORT-seroma inhibits the proliferation of the MSCs with a similar method and kinetics related to the MSC's doubling time (30–40 h). Overall, these studies provide the results that IORT alters the factor composition of seroma, which decreases the proliferation of the MSCs, the capacity of wound healing, and the activity of chemotactic migration.

Moreover, analysis of MSCs-CM cultured in 0.5% IORT- and control-seroma and collected after 72h showed significantly decreased RANTES, GRO-α, and VEGF in the IORT-seroma group (112). To confirm the tumor inhibitory effects of IORT-seroma compared with non-IORT-seroma, we evaluated migration, proliferation, viability, and invasion in three BC cell lines. The viability and proliferation results clarified that MDA-MB-231 cells benefit more than SKBR-3 and MCF-7 from the anticancer effects of IORT-seroma. The findings of the clonal survival assay in MCF-7 cells showed that the number of colonies was reduced in IORT-seroma-treated cells compared with the other groups. IORT-seroma-treated and non-IORT-seroma-treated cells showed no significant change in expression levels of proteins associated with cell cycle arrest (P16, P21) and the expression level of Caspase 3. Furthermore, our results confirmed the previous findings about tumor progressive effects of seroma on these three BC cell lines (124). Figure 5 presents the studies related to the effects of seroma on BC cell lines.

1.3.3 Effects of seroma on breast cancer primary cells; IORT vs non-IORT

Most data indicate post-surgery seroma strongly induces proliferative and aggressive phenotypes in BC cell lines. To achieve more reliable results, these findings *in vivo* outcomes are required. Zhang et al. cultured primary cells from BC cells with or

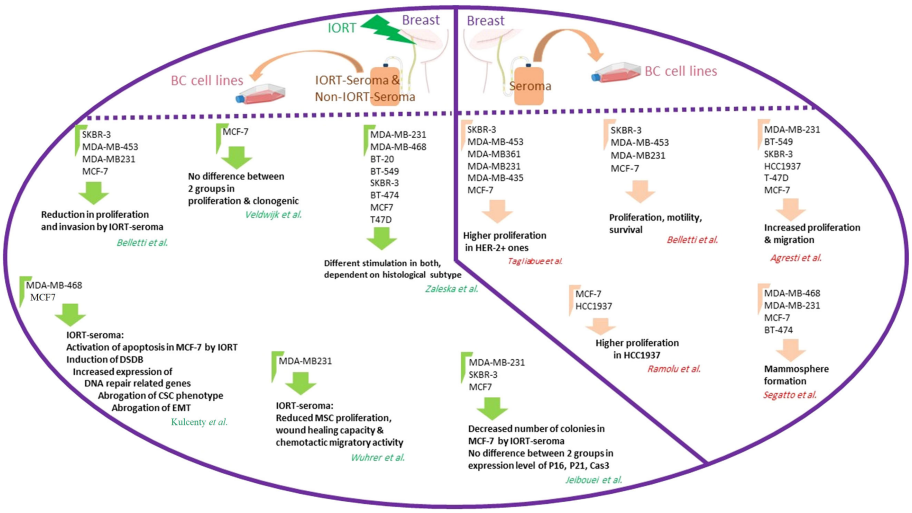

FIGURE 5
The studies related to the effects of seroma on BC cell lines. The right part of the circle shows the results from the effects of breast cancer seroma on breast cancer cell lines. The left part of the circle shows the results of the effects of IORT-treated and non-IORT-treated breast cancer seroma on breast cancer cell lines.

without seroma and then treated the cells with different anticancer drugs. Generally, a remarkable enhancement in survival rates was observed in the seroma-treated cells compared to the non-treated cells among different subgroups of the various anticancer drugs. The BC cells treated with seroma collected from premenopausal patients displayed a significantly higher rate of survival compared to those of the control group in all anticancer drugs. Finally, seroma-treated primary BC cells reported higher resistance to chemotherapy drugs (125). To mimic the tumor's *in vivo* microenvironment and re-evaluate previous *in vitro* effects of seroma on breast tumor cells, we designed a 3D model using human-derived specimens. Spheroids from 23 breast tumors were cultured in the collagen matrix in microfluidic devices. Spheroids derived from each patient were treated for six days with the 24h seroma collected from the patients. Final data from fluorescent live/dead staining on day 6 showed that in 22 samples, the percentage of live cells was significantly higher in seroma-treated samples compared to cells treated with Roswell Park Memorial Institute (RPMI) (as a control for each sample) (124).

Interestingly, one sample displayed the opposite result. We concluded that, however, most BC patients take advantage of removing seroma, the effects of seroma on tumor progression may not show a similar effect in all patients, and it can depend on many unknown factors (126). In another study, we assessed the radiobiological impact of IORT-seroma on human-derived specimens in a 3D model mentioned above. No significant difference in the percentage of live cells was observed between IORT-seroma-treated specimens with non-IORT-seroma-treated specimens after six days of treatment. The caspase 3 and E-cadherin expression levels in these specimens showed that despite similar caspase 3 in both groups, IORT-seroma-treated spheroids showed a higher level of E-cadherin compared to non-IORT-seroma-treated spheroids. It is worth noting that in both IORT-seroma and non-IORT-seroma groups, the expression levels of both E-cadherin and Caspase 3 were significantly higher in seroma-treated spheroids compared to RPMI-treated spheroids (as control). This study suggested IORT-seroma as a fluid containing inhibitory factors for tumor migration in the microfluidic system (124). Also, we showed increased proliferative and migrative characteristics of spheroids from four BC patients under IORT-seroma treatment using time-lapse imaging (127). Figure 6 presents studies on seroma's effects on primary BC cells.

2 Conclusion

Suction drainage placement after BCS is popular to prevent seroma formation in BC cases. However, it has some distinct drawbacks, such as an infection caused by the retrograde entry of skin bacteria through the drain, patient discomfort due to drain placement, and a need for daily nursing at home. Moreover, policies of drain removal are broadly different across various BC centers. Several studies have explored the safety of early drain removal according to multiple clinical endpoints. Studies revealed that seroma acts as a stimulative factor in tumor development through its interaction with cytokines, chemokines, and MMPs. According to data indicating beneficial direct and indirect effects of IORT on BC patients, some researchers assumed that IORT-induced seroma might mediate a part of these therapeutic effects of IORT. However, many studies such as analysis of IORT-seroma composition, treatment of BC cell lines and human tumor tissues,

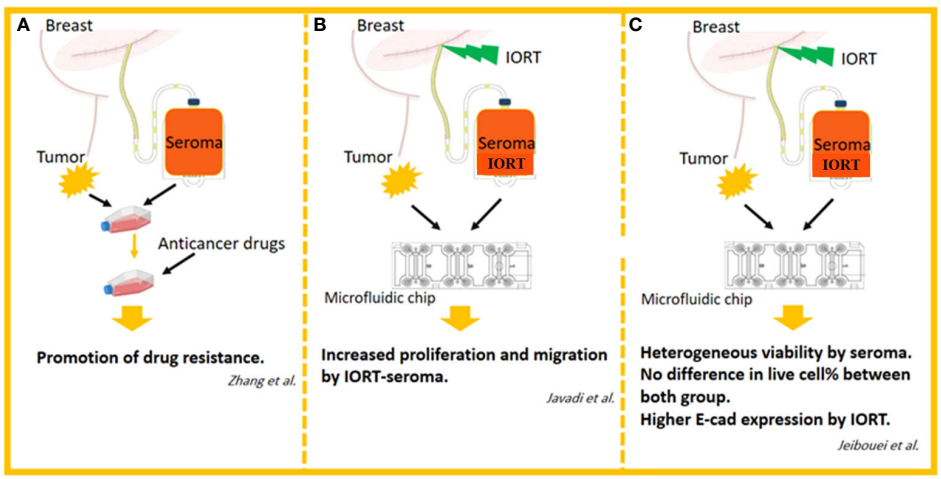

FIGURE 6
The studies related to the effects of seroma on primary BC cells. **(A)** Effects of drugs on seroma-treated human-derived breast cancer cells in 2D cell culture system. **(B)** Effects of IORT-treated and non-IORT-treated seroma on human-derived breast tumor spheroids in 3D microfluidic chips (visual evaluation of proliferation and migration). **(C)** Effects of IORT-treated and non-IORT-treated seroma on human-derived breast tumor spheroids in 3D microfluidic chips (visual and molecular evaluation of proliferation, apoptosis, migration, and heterogeneity).

and assessment of their behavior under treatment of the collected seroma in 2D and 3D systems revealed that IORT-seroma has the same results as non-IORT-seroma in tumor cavity after the surgery.

The tumor heterogeneity could be a role player in the effectiveness of seroma on tumor behavior. Furthermore, in a 3D microfluidic study, we observed that heterogeneity of tumor and seroma have different effects in different patients. Our proteomic and transcriptomic data from tumor bed analysis also showed that IORT could affect tumor bed and probably remain cancer cells in tumor margins through immune system infiltration. Overall, evidence indicates that studies on seroma or IORT could not discover their mechanisms of tumor inhibition because of the variation in body reactions of patients. It seems that it is related to the immune system and probably unknown or unstudied factors in this area, such as microbiota in the body of patients. Deciphering mechanisms associated with immune system infiltration and abscopal effects consider personalized medicine by using profiling to address the questions about the inhibiting effects of IORT. In conclusion, we cannot provide a rationale for preserving or removing seroma in IORT-treated BC patients. The question of whether IORT-seroma has a beneficial effect can only be answered in a trial with a clinical endpoint, which needs to be investigated.

Author contributions

The concept of the manuscript was conceived by MA and HZ. SJ drafted the manuscript, and the other authors made direct intellectual and substantial contributions to the work, and accepted the manuscript for publication. All authors contributed to the article and approved the submitted version.

Acknowledgments

Authors thank Dr. Ebrahim Mostafavi for his unconditional support. Authors apologize to the scientists whose helps to IORT and personalized medicine in breast cancer could not be acknowledged because of space limitations.

Conflict of interest

The authors declare that the research was conducted in the absence of any commercial or financial relationships that could be construed as a potential conflict of interest.

Publisher's note

References

1. Fitzmaurice C, Abate D, Abbasi N. Global burden of disease cancer collaboration. global, regional, and national cancer incidence, mortality, years of life lost, years lived with disability, and disability-adjusted life-years for 29 cancer groups, 1990to 2017: A systemic analysis for the global burden of disease study (vol 5, pg 1749, 2019). *JAMA Oncol* (2020) 6(3):444–4. doi: 10.1001/jamaoncol.2019.2996

2. Sung H, Ferlay J, Siegel RL, Laversanne M, Soerjomataram I, Jemal A, et al. Global cancer statistics 2020: GLOBOCAN estimates of incidence and mortality worldwide for 36 cancers in 185 countries. *CA: Cancer J Clin* (2021) 71(3):209–49. doi: 10.3322/caac.21660

3. Fisher B, Anderson S, Bryant J, Margolese RG, Deutsch M, Fisher ER, et al. Twenty-year follow-up of a randomized trial comparing total mastectomy, lumpectomy, and lumpectomy plus irradiation for the treatment of invasive breast cancer. *New Engl J Med* (2002) 347(16):1233–41. doi: 10.1056/NEJMoa022152

4. Vaidya JS, Bulsara M, Baum M, Wenz F, Massarut S, Pigorsch S, et al. Long term survival and local control outcomes from single dose targeted intraoperative radiotherapy during lumpectomy (TARGIT-IORT) for early breast cancer: TARGIT-a randomised clinical trial. *Bmj* (2020) 370:m2836. doi: 10.1136/bmj.m2836

5. Waks AG, Winer EP. Breast cancer treatment: a review. *Jama* (2019) 321 (3):288–300. doi: 10.1001/jama.2018.19323

6. Ruano-Ravina A, Cantero-Munoz P, Urién AE. Efficacy and safety of intraoperative radiotherapy in breast cancer: A systematic review. *Cancer Lett* (2011) 313(1):15–25. doi: 10.1016/j.canlet.2011.08.020

7. Harris EE, Small WJr. Intraoperative radiotherapy for breast cancer. *Front Oncol* (2017) 7:317. doi: 10.3389/fonc.2017.00317

8. Veronesi U, Orecchia R, Maisonneuve P, Viale G, Rotmensz N, Sangalli C, et al. Intraoperative radiotherapy versus external radiotherapy for early breast cancer (ELIOT): A randomised controlled equivalence trial. *Lancet Oncol* (2013) 14 (13):1269–77. doi: 10.1016/S1470-2045(13)70497-2

9. Vaidya JS, Wenz F, Bulsara M, Tobias JS, Joseph DJ, Keshtgar M, et al. Risk-adapted targeted intraoperative radiotherapy versus whole-breast radiotherapy for breast cancer: 5-year results for local control and overall survival from the TARGIT-a randomised trial. *Lancet* (2014) 383(9917):603–13. doi: 10.1016/S0140-6736(13)61950-9

10. Vaidya JS, Bulsara M, Baum M, Wenz F, Massarut S, Pigorsch S, et al. New clinical and biological insights from the international TARGIT-a randomised trial of targeted intraoperative radiotherapy during lumpectomy for breast cancer. *Br J Cancer* (2021) 125(3):380–9. doi: 10.1038/s41416-021-01440-8

11. Veronesi U, Orecchia R, Luini A, Galimberti V, Gatti G, Intra M, et al. Full-dose intra-operative radiotherapy with electrons (ELIOT) during breast-conserving surgery: experience with 1246 cases. *ecancermedicalscience* (2008) 242(1):101–6. doi: 10.3332/eCMS.2008.65

12. Belletti B, Vaidya JS, D'Andrea S, Entschladen F, Roncadin M, Lovat F, et al. Targeted intraoperative radiotherapy impairs the stimulation of breast cancer cell proliferation and invasion caused by surgical wounding. *Clin Cancer Res* (2008) 14 (5):1325–32. doi: 10.1158/1078-0432.CCR-07-4453

13. Herskind C, Wenz F. Radiobiological aspects of intraoperative tumour-bed irradiation with low-energy X-rays (LEX-IORT). *Transl Cancer Res* (2014) 3(1):3–17. doi: 10.1667/rr3292

14. Kurtz JM, Amalric R, Brandone H, Ayme Y, Jacquemier J, Pietra JC, et al. Local recurrence after breast-conserving surgery and radiotherapy. frequency, time

course, and prognosis. *Cancer* (1989) 63(10):1912–7. doi: 10.1002/1097-0142(19890515)63:10<1912

15. Veronesi U, Luini A, Del Vecchio M, Greco M, Galimberti V, Merson M, et al. Radiotherapy after breast-preserving surgery in women with localized cancer of the breast. *New Engl J Med* (1993) 328(22):1587–91. doi: 10.1056/NEJM199306033282202

16. Ahmad A. Pathways to breast cancer recurrence. *Int Sch Res Not* (2013) 2013:290568. doi: 10.1155/2013/290568

17. Turashvili G, Brogi E. Tumor heterogeneity in breast cancer. *Front Med* (2017) 4:227. doi: 10.3389/fmed.2017.00227

18. Martelotto LG, Ng CK, Piscuoglio S, Weigelt B, Reis-Filho JS. Breast cancer intra-tumor heterogeneity. *Breast Cancer Res* (2014) 16(3):1–11. doi: 10.1186/bcr3658

19. Jeibouei S, Akbari ME, Kalbasi A, Aref AR, Ajoudanian M, Rezvani A, et al. Personalized medicine in breast cancer: pharmacogenomics approaches. *Pharmacogenomics person Med* (2019) 12:59. doi: 10.2147/PGPM.S167886

20. Clarke MF, Dick JE, Dirks PB, Eaves CJ, Jamieson CH, Jones DL, et al. Cancer stem cells–perspectives on current status and future directions: AACR workshop on cancer stem cells. *Cancer Res* (2006) 66(19):9339–44. doi: 10.1158/0008-5472.CAN-06-3126

21. Oskarsson T, Batlle E, Massagué J. Metastatic stem cells: sources, niches, and vital pathways. *Cell Stem Cell* (2014) 14(3):306–21. doi: 10.1016/j.stem.2014.02.002

22. Ye J, Wu D, Wu P, Chen Z, Huang J. The cancer stem cell niche: cross talk between cancer stem cells and their microenvironment. *Tumor Biol* (2014) 35(5):3945–51. doi: 10.1007/s13277-013-1561-x

23. Shiga K, Hara M, Nagasaki T, Sato T, Takahashi H, Takeyama H. Cancer-associated fibroblasts: their characteristics and their roles in tumor growth. *Cancers* (2015) 7(4):2443–58. doi: 10.3390/cancers7040902

24. Iyengar P, Combs TP, Shah SJ, Gouon-Evans V, Pollard JW, Albanese C, et al. Adipocyte-secreted factors synergistically promote mammary tumorigenesis through induction of anti-apoptotic transcriptional programs and proto-oncogene stabilization. *Oncogene* (2003) 22(41):6408–23. doi: 10.1038/sj.onc.1206737

25. Tan J, Buache E, Chenard M-P, Dali-Youcef N, Rio M-C. Adipocyte is a non-trivial, dynamic partner of breast cancer cells. *Int J Dev Biol* (2011) 55(7-8-9):851–9. doi: 10.1387/ijdb.113365jt

26. DeNardo DG, Andreu P, Coussens LM. Interactions between lymphocytes and myeloid cells regulate pro-versus anti-tumor immunity. *Cancer Metastasis Rev* (2010) 29(2):309–16. doi: 10.1007/s10555-010-9223-6

27. Mantovani A, Sozzani S, Locati M, Allavena P, Sica A. Macrophage polarization: tumor-associated macrophages as a paradigm for polarized M2 mononuclear phagocytes. *Trends Immunol* (2002) 23(11):549–55. doi: 10.1016/S1471-4906(02)02302-5

28. Roland CL, Dineen SP, Lynn KD, Sullivan LA, Dellinger MT, Sadegh L, et al. Inhibition of vascular endothelial growth factor reduces angiogenesis and modulates immune cell infiltration of orthotopic breast cancer xenografts. *Mol Cancer Ther* (2009) 8(7):1761–71. doi: 10.1158/1535-7163.MCT-09-0280

29. Arnold JN, Magiera L, Kraman M, Fearon DT. Tumoral immune suppression by macrophages expressing fibroblast activation protein-α and heme oxygenase-1. *Cancer Immunol Res* (2014) 2(2):121–6. doi: 10.1158/2326-6066.CIR-13-0150

30. Liang X, Fu C, Cui W, Ober-Blöbaum JL, Zahner SP, Shrikant PA, et al. β-catenin mediates tumor-induced immunosuppression by inhibiting cross-priming of CD8+ T cells. *J leukocyte Biol* (2014) 95(1):179–90. doi: 10.1189/jlb.0613330

31. Spiegel A, Brooks MW, Houshyar S, Reinhardt F, Ardolino M, Fessler E, et al. Neutrophils suppress intraluminal NK cell–mediated tumor cell clearance and enhance extravasation of disseminated carcinoma cells. *Cancer Discovery* (2016) 6(6):630–49. doi: 10.1158/2159-8290.CD-15-1157

32. Mattner J, Wirtz S. Friend or foe? the ambiguous role of innate lymphoid cells in cancer development. *Trends Immunol* (2017) 38(1):29–38. doi: 10.1016/j.it.2016.10.004

33. Zamarron BF, Chen W. Dual roles of immune cells and their factors in cancer development and progression. *Int J Biol Sci* (2011) 7(5):651. doi: 10.7150/ijbs.7.651

34. Kim J, Bae J-S. Tumor-associated macrophages and neutrophils in tumor microenvironment. *Mediators Inflammation* (2016) 2016:6058147. doi: 10.1155/2016/6058147

35. Murdocca M, Torino F, Pucci S, Costantini M, Capuano R, Greggi C, et al. Urine LOX-1 and volatilome as promising tools towards the early detection of renal cancer. *Cancers* (2021) 13(16):4213. doi: 10.3390/cancers13164213

36. Wenz F, Welzel G, Blank E, Hermann B, Steil V, Sütterlin M, et al. Intraoperative radiotherapy as a boost during breast-conserving surgery using low-kilovoltage X-rays: The first 5 years of experience with a novel approach. *Int J Radiat Oncol Biol Phys* (2010) 77(5):1309–14. doi: 10.1016/j.ijrobp.2009.06.085

37. Vaidya J, Baum M, Tobias J, Massarut S, Wenz F, Hilaris B, et al. Targeted intraoperative radiotherapy (Targit) boost after breast conserving surgery results in a remarkably low recurrence rate in a standard risk population: 5 year results. *AACR* (2009) 69(24):4104. doi: 10.1158/0008-5472.SABCS-09-4104

38. Kraus-Tiefenbacher U, Bauer L, Scheda A, Fleckenstein K, Keller A, Herskind C, et al. Long-term toxicity of an intraoperative radiotherapy boost using low energy X-rays during breast-conserving surgery. *Int J Radiat Oncol Biol Phys* (2006) 66(2):377–81. doi: 10.1016/j.ijrobp.2006.05.042

39. Pez M, Keller A, Welzel G, Abo-Madyan Y, Ehmann M, Tuschy B, et al. Long-term outcome after intraoperative radiotherapy as a boost in breast cancer. *Strahlentherapie und Onkologie* (2020) 196(4):349–55. doi: 10.1007/s00066-019-01525-7

40. Ghardi M, Moreels M, Chatelain B, Chatelain C, Baatout S. Radiation-induced double strand breaks and subsequent apoptotic DNA fragmentation in human peripheral blood mononuclear cells. *Int J Mol Med* (2012) 29(5):769–80. doi: 10.3892/ijmm.2012.907

41. Minafra L, Bravatà V. Cell and molecular response to IORT treatment. *Transl Cancer Res* (2014) 3(1):32–47. doi: 10.3978/j.issn.2218-676X.2014.02.03

42. Huber SM, Butz L, Stegen B, Klumpp D, Braun N, Ruth P, et al. Ionizing radiation, ion transports, and radioresistance of cancer cells. *Front Physiol* (2013) 4:212. doi: 10.3389/fphys.2013.00212

43. Uhlig S, Wuhrer A, Berlit S, Tuschy B, Sütterlin M, Bieback K. Intraoperative radiotherapy for breast cancer treatment efficiently targets the tumor bed preventing breast adipose stromal cell outgrowth. *Strahlentherapie und Onkologie* (2020) 196(4):398–404. doi: 10.1007/s00066-020-01586-z

44. Fabris L, Berton S, Citron F, D'andrea S, Segatto I, Nicoloso M, et al. Radiotherapy-induced miR-223 prevents relapse of breast cancer by targeting the EGF pathway. *Oncogene* (2016) 35(37):4914–26. doi: 10.1038/onc.2016.23

45. Miricescu D, Totan A, Stanescu-Spinu I-I, Badoiu SC, Stefani C, Greabu M. PI3K/AKT/mTOR signaling pathway in breast cancer: From molecular landscape to clinical aspects. *Int J Mol Sci* (2020) 22(1):173. doi: 10.3390/ijms22010173

46. Yu C-C, Hung S-K, Lin H-Y, Chiou W-Y, Lee M-S, Liao H-F, et al. Targeting the PI3K/AKT/mTOR signaling pathway as an effectively radiosensitizing strategy for treating human oral squamous cell carcinoma in vitro and in vivo. *Oncotarget* (2017) 8(40):68641. doi: 10.18632/oncotarget.19817

47. Shima H, Kutomi G, Sato K, Kuga Y, Wada A, Satomi F, et al. An optimal timing for removing a drain after breast surgery: A systematic review and meta-analysis. *J Surg Res* (2021) 267:267–73. doi: 10.1016/j.jss.2021.05.031

48. Vander Heiden MG, DeBerardinis RJ. Understanding the intersections between metabolism and cancer biology. *Cell* (2017) 168(4):657–69. doi: 10.1016/j.cell.2016.12.039

49. Warburg O, Wind F, Negelein E. The metabolism of tumors in the body. *J Gen Physiol* (1927) 8(6):519. doi: 10.1085/jgp.8.6.519

50. Jiang W, Chan CK, Weissman IL, Kim BY, Hahn SM. Immune priming of the tumor microenvironment by radiation. *Trends Cancer* (2016) 2(11):638–45. doi: 10.1016/j.trecan.2016.09.007

51. Surova O, Zhivotovsky B. Various modes of cell death induced by DNA damage. *Oncogene* (2013) 32(33):3789–97. doi: 10.1038/onc.2012.556

52. Jason CY, Formenti SC. Integration of radiation and immunotherapy in breast cancer-treatment implications. *Breast* (2018) 38:66–74. doi: 10.1016/j.breast.2017.12.005

53. Hall EJ. Radiation biology for pediatric radiologists. *Pediatr Radiol* (2009) 39(1):57–64. doi: 10.1007/s00247-008-1027-2

54. Zhao W, Diz D, Robbins M. Oxidative damage pathways in relation to normal tissue injury. *Br J Radiol* (2007) 80(special_issue_1):S23–31. doi: 10.1259/bjr/18237646

55. Lomax M, Folkes L, O'neill P. Biological consequences of radiation-induced DNA damage: relevance to radiotherapy. *Clin Oncol* (2013) 25(10):578–85. doi: 10.1016/j.clon.2013.06.007

56. Mladenov E, Magin S, Soni A, Iliakis G. DNA Double-strand break repair as determinant of cellular radiosensitivity to killing and target in radiation therapy. *Front Oncol* (2013) 3:113. doi: 10.3389/fonc.2013.00113

57. Golden E, Pellicciotta I, Demaria S, Barcellos-Hoff MH, Formenti SC. The convergence of radiation and immunogenic cell death signaling pathways. *Front Oncol* (2012) 2:88. doi: 10.3389/fonc.2012.00088

58. Multhoff G, Radons J. Radiation, inflammation, and immune responses in cancer. *Front Oncol* (2012) 2:58. doi: 10.3389/fonc.2012.00058

59. Kuribayashi K, Finnberg NK, Jeffers JR, Zambetti GP, El-Deiry WS. The relative contribution of pro-apoptotic p53-target genes in the triggering of apoptosis following DNA damage *in vitro* and *in vivo*. *Cell Cycle* (2011) 10(14):2380–9. doi: 10.4161/cc.10.14.16588

60. Pant V, Xiong S, Jackson JG, Post SM, Abbas HA, Quintás-Cardama A, et al. The p53–Mdm2 feedback loop protects against DNA damage by inhibiting p53

activity but is dispensable for p53 stability, development, and longevity. *Genes Dev* (2013) 27(17):1857–67. doi: 10.1101/gad.227249.113

61. Chipuk JE, Bouchier-Hayes L, Kuwana T, Newmeyer DD, Green DR. PUMA couples the nuclear and cytoplasmic proapoptotic function of p53. *Science* (2005) 309(5741):1732–5. doi: 10.1126/science.1114297

62. Panganiban RAM, Mungunsukh O, Day RM. X-Irradiation induces ER stress, apoptosis, and senescence in pulmonary artery endothelial cells. *Int J Radiat Biol* (2013) 89(8):656–67. doi: 10.3109/09553002.2012.711502

63. Han Y, Wang Y, Xu H-T, Yang L-H, Wei Q, Liu Y, et al. X-Radiation induces non-small-cell lung cancer apoptosis by upregulation of axin expression. *Int J Radiat Oncol Biol Phys* (2009) 75(2):518–26. doi: 10.1016/j.ijrobp.2009.05.040

64. Kolesnick R, Fuks Z. Radiation and ceramide-induced apoptosis. *Oncogene* (2003) 22(37):5897–906. doi: 10.1038/sj.onc.1206702

65. Mullins ME, Barest GD, Schaefer PW, Hochberg FH, Gonzalez RG, Lev MH. Radiation necrosis versus glioma recurrence: Conventional MR imaging clues to diagnosis. *Am J Neuroradiol* (2005) 26(8):1967–72.

66. Jella KK, Garcia A, McClean B, Byrne HJ, Lyng FM. Cell death pathways in directly irradiated cells and cells exposed to medium from irradiated cells. *Int J Radiat Biol* (2013) 89(3):182–90. doi: 10.3109/09553002.2013.734942

67. Campisi J. Aging, cellular senescence, and cancer. *Annu Rev Physiol* (2013) 75:685. doi: 10.1146/annurev-physiol-030212-183653

68. Muller M. Cellular senescence: molecular mechanisms, in vivo significance, and redox considerations. *Antioxid Redox Signaling* (2009) 11(1):59–98. doi: 10.1089/ars.2008.2104

69. Tchkonia T, Zhu Y, Van Deursen J, Campisi J, Kirkland JL, et al. Cellular senescence and the senescent secretory phenotype: therapeutic opportunities. *J Clin Invest* (2013) 123(3):966–72. doi: 10.1172/JCI64098

70. Tominaga K, Pereira-Smith OM. The role of chromatin reorganization in the process of cellular senescence. *Curr Drug Targets* (2012) 13(13):1593–602. doi: 10.2174/138945012803529983

71. Muñoz-Espín D, Serrano M. Cellular senescence: from physiology to pathology. *Nat Rev Mol Cell Biol* (2014) 15(7):482–96. doi: 10.1038/nrm3823

72. Fumagalli M, Rossiello F, Mondello C, d'Adda di Fagagna F. Stable cellular senescence is associated with persistent DDR activation. *PloS One* (2014) 9(10): e110969. doi: 10.1371/journal.pone.0110969

73. Young AR, Narita M. SASP reflects senescence. *EMBO Rep* (2009) 10 (3):228–30. doi: 10.1038/embor.2009.22

74. Coppé J-P, Desprez P-Y, Krtolica A, Campisi J. The senescence-associated secretory phenotype: the dark side of tumor suppression. *Annu Rev Pathol* (2010) 5:99. doi: 10.1146/annurev-pathol-121808-102144

75. Davalos AR, Coppe J-P, Campisi J, Desprez P-Y. Senescent cells as a source of inflammatory factors for tumor progression. *Cancer Metastasis Rev* (2010) 29 (2):273–83. doi: 10.1007/s10555-010-9220-9

76. Denton D, Nicolson S, Kumar S. Cell death by autophagy: facts and apparent artefacts. *Cell Death Differ* (2012) 19(1):87–95. doi: 10.1038/cdd.2011.146

77. Rodriguez-Rocha H, Garcia-Garcia A, Panayiotidis MI, Franco R. DNA Damage and autophagy. *Mutat Res/Fundam Mol Mech Mutagen* (2011) 711(1-2):158–66. doi: 10.1016/j.mrfmmm.2011.03.007

78. Palumbo S, Comincini S. Autophagy and ionizing radiation in tumors: the "survive or not survive" dilemma. *J Cell Physiol* (2013) 228(1):1–8. doi: 10.1002/jcp.24118

79. Castedo M, Perfettini J-L, Roumier T, Andreau K, Medema R, Kroemer G. Cell death by mitotic catastrophe: A molecular definition. *Oncogene* (2004) 23 (16):2825–37. doi: 10.1038/sj.onc.1207528

80. Desgrosellier JS, Cheresh DA. Integrins in cancer: biological implications and therapeutic opportunities. *Nat Rev Cancer* (2010) 10(1):9–22. doi: 10.1038/nrc2748

81. Hamidi H, Ivaska J. Every step of the way: integrins in cancer progression and metastasis. *Nat Rev Cancer* (2018) 18(9):533–48. doi: 10.1038/s41568-018-0038-z

82. Shahani M, Shakeri J, Akbari ME, Arefnezhad B, Tafti A, Zali H, et al. Transcriptomic and proteomic approaches reveal biological basis of intraoperative radiotherapy-treated tumor bed modification in breast cancer patients: A pilot study. *J Proteomics* (2020) 212:103596. doi: 10.1016/j.jprot.2019.103596

83. Bravatà V, Minafra L, Cammarata FP, Pisciotta P, Lamia D, Marchese V, et al. Gene expression profiling of breast cancer cell lines treated with proton and electron radiations. *Br J Radiol* (2018) 91(1089):20170934. doi: 10.1259/bjr.20170934

84. Welsh J, Bevelacqua J, Dobrzyński L, Mortazavi S. Abscopal effect following radiation therapy in cancer patients: A new look from the immunological point of view. *J Biomed Phys Eng* (2020) 10(4):537. doi: 10.31661/jbpe.v0i0.1066

85. Van de Walle M, Demol J, Staelens L, Rottey S. Abscopal effect in metastatic renal cell carcinoma. *Acta Clin Belg* (2017) 72(4):245–9. doi: 10.1080/17843286.2016.1201614

86. Hu ZI, McArthur HL, Ho AY. The abscopal effect of radiation therapy: what is it and how can we use it in breast cancer? *Curr Breast Cancer Rep* (2017) 9(1):45–51. doi: 10.1007/s12609-017-0234-y

87. Azami A, Suzuki N, Azami Y, Seto I, Sato A, Takano Y, et al. Abscopal effect following radiation monotherapy in breast cancer: A case report. *Mol Clin Oncol* (2018) 9(3):283–6. doi: 10.3892/mco.2018.1677

88. Farias VdA, Tovar I, Del Moral R, O'Valle F, Expósito J, Oliver FJ, et al. Enhancing the bystander and abscopal effects to improve radiotherapy outcomes. *Front Oncol* (2020) 9:1381. doi: 10.3389/fonc.2019.01381

89. Formenti SC, Lee P, Adams S, Goldberg JD, Li X, Xie MW, et al. Focal irradiation and systemic TGFβ blockade in metastatic breast cancer. *Clin Cancer Res* (2018) 24(11):2493–504. doi: 10.1158/1078-0432.CCR-17-3322

90. Jafari Nedooshan J, Dashti Rahmatabadi MH, Kargar S, Lotfi MH. Evaluation of complications of short-term and long-term drainage following mastectomy with removal of axillary lymph nodes: A randomized clinical trial. *Asian Pac J Cancer Prev* (2022) 23(8):2873–8. doi: 10.31557/APJCP.2022.23.8.2873

91. Wen N, Ouyang C, Hu X, Hou L, He L, Liu C, et al. What is the optimal strategy for drain removal after mastectomy and axillary surgery in breast cancer patients? a multicenter, three-arm randomized clinical trial. *J Surg Res* (2022) 277:148–56. doi: 10.1016/j.jss.2022.02.034

92. Khambri D, Harahap WA. Association of early drain removal with formation of seroma in breast cancer patients after modified radical mastectomy. *Biosci Med: J Biomed Trans Res* (2022) 6(7):1989–93. doi: 10.37275/bsm.v6i7.544

93. Schmidt G, Zuschlag M, Gerlinger C, Endrikat J, Müller C, Gabriel L, et al. Efficacy and safety of two post-operative drains: Results of a prospectively randomized clinical study in breast cancer patients after breast conserving surgery. *Arch Gynecol Obstet* (2019) 300(6):1687–92. doi: 10.1007/s00404-019-05360-0

94. Isozaki H, Yamamoto Y, Murakami S, Matsumoto S, Takama T. Impact of the surgical modality for axillary lymph node dissection on postoperative drainage and seroma formation after total mastectomy. *Patient Saf Surg* (2019) 13:20. doi: 10.1186/s13037-019-0199-z

95. Ten Wolde B, Strobbe FFR, Schlooz-de Vries M, van den Wildenberg FJH, Keemers-Gels M, de Wilt JHW, et al. Omitting postoperative wound drainage after mastectomy with skin-flap quilting. *Ann Surg Oncol* (2019) 26(9):2773–8. doi: 10.1245/s10434-019-07411-x

96. Vos H, Smeets A, Neven P, Laenen A, Vandezande L, Nevelsteen I. Early drain removal improves quality of life and clinical outcomes in patients with breast cancer - results from a randomised controlled trial. *Eur J Oncol Nurs* (2018) 36:112–8. doi: 10.1016/j.ejon.2018.08.007

97. Okada N, Narita Y, Takada M, Kato H, Ambo Y, Nakamura F, et al. Early removal of drains and the incidence of seroma after breast surgery. *Breast Cancer* (2015) 22(1):79–83. doi: 10.1007/s12282-013-0457-3

98. Clegg-Lamptey JN, Dakubo JC, Hodasi WM. Comparison of four-day and ten-day post-mastectomy passive drainage in Accra, Ghana. *East Afr Med J* (2007) 84(12):561–5. doi: 10.4314/eamj.v84i12.9592

99. Baas-Vrancken Peeters MJ, Kluit AB, Merkus JW, Breslau PJ. Short versus long-term postoperative drainage of the axilla after axillary lymph node dissection. a prospective randomized study. *Breast Cancer Res Treat* (2005) 93(3):271–5. doi: 10.1007/s10549-005-5348-7

100. Gupta R, Pate K, Varshney S, Goddard J, Royle GT. A comparison of 5-day and 8-day drainage following mastectomy and axillary clearance. *Eur J Surg Oncol* (2001) 27(1):26–30. doi: 10.1053/ejso.2000.1054

101. Ciabattoni A, Gregucci F, Llange K, Alessandro M, Corazzi F, Ivaldi GB, et al. Intra-operative electron radiation therapy (IOERT) anticipated boost in breast cancer treatment: An Italian multicenter experience. *Cancers* (2022) 14 (2):292. doi: 10.3390/cancers14020292

102. Hu X, He Y, Chen X, Xia T, Cao T, Jia H, et al. Impact of intraoperative radiotherapy on the perioperative period of patients after breast-conserving surgery. *Gland Surg* (2020) 9(5):1535–42. doi: 10.21037/gs-20-727

103. Patas d'Illiers LB, Lafay F, Faure C, Klingler S, Pleynet E, Racadot S. Up to 5 years outcomes following intraoperative radiotherapy for early breast cancer. *Trans Cancer Res* (2018) 7(4):859–70. doi: 10.21037/tcr.2018.06.07

104. McCaul J, Aslaam A, Spooner R, Louden I, Cavanagh T, Purushotham A. Aetiology of seroma formation in patients undergoing surgery for breast cancer. *Breast* (2000) 9(3):144–8. doi: 10.1054/brst.1999.0126

105. Stuelten CH, Barbul A, Busch JI, Sutton E, Katz R, Sato M, et al. Acute wounds accelerate tumorigenesis by a T cell–dependent mechanism. *Cancer Res* (2008) 68(18):7278–82. doi: 10.1158/0008-5472.CAN-08-1842

106. Yussof SJM, Omar E, Pai DR, Sood S. Cellular events and biomarkers of wound healing. *Indian J Plast Surg* (2012) 45(02):220–8. doi: 10.4103/0970-0358.101282

107. Werner S, Grose R. Regulation of wound healing by growth factors and cytokines. *Physiol Rev* (2003) 83(3):835–70. doi: 10.1152/physrev.2003.83.3.835

108. Valeta-Magara A, Hatami R, Axelrod D, Roses DF, Guth A, Formenti S, et al. Pro-oncogenic cytokines and growth factors are differentially expressed in the post-surgical wound fluid from malignant compared to benign breast lesions. *SpringerPlus* (2015) 4(1):1–11. doi: 10.1186/s40064-015-1260-8

109. Agresti R, Triulzi T, Sasso M, Ghirelli C, Aiello P, Rybinska I, et al. Wound healing fluid reflects the inflammatory nature and aggressiveness of breast tumors. *Cells* (2019) 8(2):181. doi: 10.3390/cells8020181

110. Zhang Y, Ma QY, Dang CX, Moureau-Zabotto M, Chen WK. Quantitative molecular diagnosis of axillary drainage fluid for prediction of locoregional failure in patients with one to three positive axillary nodes after mastectomy without adjuvant radiotherapy. *Int J Radiat Oncol Biol Phys* (2006) 64(2):505–11. doi: 10.1016/j.ijrobp.2005.07.984

111. Kulcenty K, Piotrowski I, Wróblewska JP, Wasiewicz J, Suchorska WM. The composition of surgical wound fluids from breast cancer patients is affected by intraoperative radiotherapy treatment and depends on the molecular subtype of breast cancer. *Cancers* (2019) 12(1):11. doi: 10.3390/cancers12010011

112. Wuhrer A, Uhlig S, Tuschy B, Berlit S, Sperk E, Bieback K, et al. Wound fluid from breast cancer patients undergoing intraoperative radiotherapy exhibits an altered cytokine profile and impairs mesenchymal stromal cell function. *Cancers* (2021) 13(9):2140. doi: 10.3390/cancers13092140

113. Tagliabue E, Agresti R, Carcangiu ML, Ghirelli C, Morelli D, Campiglio M, et al. Role of HER2 in wound-induced breast carcinoma proliferation. *Lancet* (2003) 362(9383):527–33. doi: 10.1016/S0140-6736(03)14112-8

114. Segatto I, Berton S, Sonego M, Massarut S, D'Andrea S, Perin T, et al. Inhibition of breast cancer local relapse by targeting p70S6 kinase activity. *J Mol Cell Biol* (2013) 5(6):428–31. doi: 10.1093/jmcb/mjt027

115. Segatto I, Berton S, Sonego M, Massarut S, Fabris L, Armenia J, et al. p70S6 kinase mediates breast cancer cell survival in response to surgical wound fluid stimulation. *Mol Oncol* (2014) 8(3):766–80. doi: 10.1016/j.molonc.2014.02.006

116. Segatto I, Berton S, Sonego M, Massarut S, Perin T, Piccoli E, et al. Surgery-induced wound response promotes stem-like and tumor-initiating features of breast cancer cells, via STAT3 signaling. *Oncotarget* (2014) 5(15):6267. doi: 10.18632/oncotarget.2195

117. Ramolu L, Christ D, Abecassis J, Rodier J-F. Stimulation of breast cancer cell lines by post-surgical drainage fluids. *Anticancer Res* (2014) 34(7):3489–92.

118. Veldwijk MR, Neumaier C, Gerhardt A, Giordano FA, Sütterlin M, Herskind C, et al. Comparison of the proliferative and clonogenic growth capacity of wound fluid from breast cancer patients treated with and without intraoperative radiotherapy. *Transl Cancer Res* (2015) 4(2):173–7. doi: 10.3978/j.issn.2218-676X.2015.04.01

119. Zaleska K, Suchorska WM, Przybyła A, Murawa D. Effect of surgical wound fluids after intraoperative electron radiotherapy on the cancer stem cell phenotype in a panel of human breast cancer cell lines. *Oncol Lett* (2016) 12 (5):3707–14. doi: 10.3892/ol.2016.5167

120. Kulcenty KI, Piotrowski I, Zaleska K, Murawa D, Suchorska WM. Wound fluids collected from patients after IORT treatment activates extrinsic apoptotic pathway in MCF7 breast cancer cell line. *Ginekol Polska* (2018) 89(4):175–82. doi: 10.5603/GP.a2018.0030

121. Piotrowski I, Kulcenty K, Murawa D, Suchorska W. Surgical wound fluids from patients treated with intraoperative radiotherapy induce radiobiological response in breast cancer cells. *Med Oncol* (2019) 36(2):1–12. doi: 10.1007/s12032-018-1243-z

122. Kulcenty K, Piotrowski I, Zaleska K, Wichtowski M, Wróblewska J, Murawa D, et al. Wound fluids collected postoperatively from patients with breast cancer induce epithelial to mesenchymal transition but intraoperative radiotherapy impairs this effect by activating the radiation-induced bystander effect. *Sci Rep* (2019) 9(1):1–11. doi: 10.1038/s41598-019-44412-y

123. Kulcenty K, Piotrowski I, Rucinski M, Wroblewska JP, Jopek K, Murawa D, et al. Surgical wound fluids from patients with breast cancer reveal similarities in the biological response induced by intraoperative radiation therapy and the radiation-induced bystander effect–transcriptomic approach. *Int J Mol Sci* (2020) 21(3):1159. doi: 10.3390/ijms21031159

124. Jeibouei S, Hojat A, Mostafavi E, Aref AR, Kalbasi A, Niazi V, et al. Radiobiological effects of wound fluid on breast cancer cell lines and human-derived tumor spheroids in 2D and microfluidic culture. *Sci Rep* (2022) 12(1):1–21. doi: 10.1038/s41598-022-11023-z

125. Zhang Y, Yan D, Zhang H, Ou X, Zhao Z, Wang D, et al. Influence of wound fluid on chemotherapy sensitivity in primary breast cancer cells. *Oncotarget* (2016) 7(40):65034. doi: 10.18632/oncotarget.11345

126. Hojat A, Jeibouei S, Aref AR, Kalbasi A, Moghaddam M, Mohammadi F, et al. Effects of wound fluid on breast cancer-derived spheroids in a 3D culture system: A case series study. *Iranian J Pharm Res* (2022) 21(1):e123828. doi: 10.5812/ijpr.123828

127. Javadi SM, Abdolahad M, Hashemi S, Khayamian M, Parizi MS, Vanaei S, et al. Effect of post IORT wound fluid secretion (PIWFS) on the behavior of breast cancer cells: Stimulator or inhibitor; report of an experimental study on breast cancer. *Arch Iranian Med* (2022) 25(2):78. doi: 10.34172/aim.2022.13

frontiers | Frontiers in Oncology

TYPE Original Research
PUBLISHED 28 November 2022
DOI 10.3389/fonc.2022.1034171

OPEN ACCESS

EDITED BY
San-Gang Wu,
First Affiliated Hospital of Xiamen University, China

REVIEWED BY
Xiaorong Luan,
Qilu Hospital, Shandong University, China
Mónica Oliveira,
University of Lisbon, Portugal

*CORRESPONDENCE
Xiuni Gan
300650@cqmu.edu.cn

†These authors have contributed equally to this work and share first authorship

SPECIALTY SECTION
This article was submitted to Breast Cancer, a section of the journal Frontiers in Oncology

RECEIVED 01 September 2022
ACCEPTED 09 November 2022
PUBLISHED 28 November 2022

CITATION
Liang Y, Gao Y, Yin G, Chen W and Gan X (2022) Development of a breast cancer case management information platform (BC-CMIP) module based on patient-perceived value. *Front. Oncol.* 12:1034171. doi: 10.3389/fonc.2022.1034171

Development of a breast cancer case management information platform (BC-CMIP) module based on patient-perceived value

Yinyin Liang[1†], Yan Gao[2†], Guobing Yin[1], Wenjun Chen[1] and Xiuni Gan[2*]

[1]Department of Breast and Thyroid Surgery, Second Affiliated Hospital of Chongqing Medical University, Chongqing, China, [2]Nursing Department, Second Affiliated Hospital, Chongqing Medical University, Chongqing, China

Objective: To construct a content module for a breast cancer case management information platform (BC-CMIP) based on patient-perceived value (PPV).

Methods: A questionnaire was used to investigate the service needs of breast cancer patients and their families for the information platform. Based on the value dimensions of PPV, the module content of the BC-CMIP was initially constructed, and the Delphi method was used to justify and revise the module content. Excel 2019 and SPSS 26.0 were used for statistical analysis.

Results: The information platform includes the patient side and the medical side. The index content includes four primary indicators: functional value, emotional value, efficiency value and social value; it can realize all patient case management needs, such as diagnosis and treatment services, health education, telemedicine, treatment tracking, psychological support, case assessment and positive warning.

Conclusion: Based on the PPV, the module design of the BC-CMIP is reasonable and comprehensive, and it can scientifically and effectively meet the health needs of patients and provide a theoretical basis for subsequent platform development and application.

KEYWORDS

patient-perceived value, breast cancer, case management, informatization, telemedicine

1 Introduction

Breast cancer (BC) is one of the most common malignant tumours in women, ranking first in incidence. Statistics released by the World Health Organization (WHO) in 2018 showed that 2.09 million new cases of BC were diagnosed, accounting for 11.6% of the total number of new cancer cases worldwide (18 million) (1). In China, approximately 250,000 women develop BC, and approximately 60,000 die from it yearly (2). Although BC is the most common cancer among women, it is the sixth most common cause of cancer death among women and has a relatively good prognosis compared to other cancers, with a 5-year observed survival rate of 72.7%, making it a cancer with a high survival rate (3, 4). However, due to the heterogeneity of BC, the treatment protocol requires rationalized therapy in individual cases according to the characterization and stage of the disease; thus, the treatment is complex and requires a long follow-up period (5, 6). Patients face many difficulties during treatment, care and recovery, for example, stress during treatment, emotional needs, and need for knowledge about the disease (7–9). Therefore, there is an urgent need to establish an individualised model for the management of BC patients throughout the course of their care.

Currently, various management models are also being explored for BC patients. For example, the self-management model based on empowerment theory can benefit postoperative chemotherapy patients in the process of physical and psychological recovery and improve their quality of life; the model has facilitative effects and practical significance in enhancing psychological resilience, psychological adjustment, disease awareness and self-management ability (10). The multidisciplinary management model has a good effect on chemotherapy-induced nausea and vomiting among BC patients (11). The 5S health education management model is used in the health education of patients with BC (12). However, these models currently focus on a single function and fail to create a full continuum of patient care from prehospital to posthospital.

The case management model meets the need for versatility. Case management (CM) is a system of assessment, planning, service delivery, coordination and monitoring of health care for a particular condition aimed at providing and coordinating care for a specific group of patients (13, 14). In 1985, the New England Medical Center in Boston was the first to implement a nursing care system with nurses as case managers in response to a prospective payment system, and the CM model has since been applied to acute care and long-term care systems (15). In Taiwan, in response to the implementation of universal health care, CM was established for patients in 2005 (16), with significant success, especially in oncology case care (17).At present, CM is more widely used in diseases with a long course, complex treatment and high medical costs, such as patients with severe mental illness (18), dementia (19) and cancer (20). CM is an extension of in-hospital care that integrates traditional fragmented health care systems to ensure that patients receive continuous and complete care that is high in quality and efficiency (21). A case manager, who is trained in CM, is responsible for coordinating with physicians, the health care team and the patient to develop a treatment plan and goals and to ensure that the patient completes the required tests and treatments on schedule to achieve the desired goals within a predetermined time frame. Case managers can be physicians or nursing staff but are primarily nurses (22). In countries such as the USA, Australia and Taiwan, clinical practice has proven that CM led by case managers is a successful model (23, 24). Studies (25) have also found that applying a CM model to BC patients can help them return to work as soon as possible and that case managers can play an active role in screening programmes for breast and cervical cancer (26).

Convenience, comfortable environment, and faster assessment related to the treatment surroundings could foster more relaxed emotions, accompanied by patient-perceived fairness and efficiency (27, 28). Delays in appointments has increased tension and conflict (29). Patients' dissatisfaction led many Chinese hospitals to adopt IT systems to improve convenience and workflow efficiency for patients. These e-programs in hospitals, such as electronic registration machines, electronic health record (EHR) systems, electronic payment machines, and online appointment systems, are becoming widely used in an effort to reduce the time it takes to receive medical treatment. However, the current mHealth platform for breast cancer patients does not enable management of the entire process from prehospital to posthospital.

Patient-perceived value (PPV) is an extension of customer-perceived value in the healthcare sector (30). The concept of customer-perceived value is the overall assessment of the effectiveness of a product or service when the customer's perceived benefit is weighed against the cost to the customer. The introduction of mobile healthcare has promoted the study of PPV. Hu Rong et al. (31) proposed four dimensions of PPV as functional, emotional, social and efficiency values in the context of mobile healthcare. PPV is a better indicator of the effectiveness of healthcare services than indicators such as patient satisfaction and service experience (30).

Following an extensive literature search, we first constructed a questionnaire on patient and family needs and evaluated the information platform services, applied the PPV theoretical framework, arranged the needs in order from prehospital to posthospital, and constructed the BC-CMIP modules. After two rounds of Delphi expert consultation, the contents of the modules for constructing the BC-CMIP were finally determined, providing a theoretical basis for the subsequent construction and evaluation of the platform. This study aims to i) investigate the demand and evaluation of BC and their families for CM service programs; ii) build a BC-CMIP module based on the PPV, the demand survey results and two rounds of Delphi

expert validation; and iii) construct a preliminary operational framework for the BC-CMIP.

2 Methods

2.1 Establishment of expert discussion groups

The expert discussion group consisted of 10 experts in clinical nursing management, including 3 masters, 2 masters in progress and 5 undergraduates; 1 chief nurse, 1 chief physician, 1 deputy chief nurse and 7 nurses in charge, mainly engaged in the specialist direction of BC treatment and care, nursing management and nursing education. The discussion group was responsible for developing the demand questionnaire and distributing it, extensive literature collection to develop the correspondence questionnaire, selecting the correspondence experts, statistically analysing the importance ratings of the correspondence experts for each indicator and collating the experts' comments and suggestions, revising the strategy according to the revision principles and providing feedback to the experts.

2.2 Construction of the content framework

2.2.1 Literature search

The literature search was conducted using a combination of subject terms and free words. PubMed, Web of Science, Embase, OVID, Cochrane Library, the Australian JBI Centre for Evidence-Based Health Care website, the US National Guideline Clearinghouse (NGC) website, and the UK National Institute for Health and Clinical Excellence (NICE) website were searched for studies published from database inception to April 1, 2022. The search strategy was built on the application of Boolean logic operators to the following keywords: (((Breast Neoplasms) OR (Breast Cancer)) OR (Mammary Cancer)) AND (((((((Mobile Applications) OR (Mobile healthmobile)) OR (Telemedicine)) OR (Telehealth)) OR (Mobile Health)) OR (Information flat)) OR (Information platform)). Using the PPV as a framework, information relevant to this study was extracted from the four dimensions of patient functional value, efficiency value, emotional value and social value, and a questionnaire on the needs of the BC-CMIP was constructed and distributed to BC patients who met the requirements.

2.2.2 Survey of demand for full case management services based on perceived value theory

Prior to the distribution of the questionnaire, the expert discussion group reviewed and discussed the format and the content of the statements in the first draft of the questionnaire (Appendix 1). From 25 April to 30 May 2022, questionnaires were distributed to patients diagnosed with BC and their family members in a tertiary hospital in Chongqing through the online survey tool "Questionnaire Star" (an online crowdsourcing platform in China), and the purpose of the survey was first explained to them. After obtaining informed consent, they were invited to respond *via* microscan to understand the patients' perceptions of the content and evaluation of the CM of BC patients. Inclusion criteria: (i) age ≥ 18 years; (ii) patients diagnosed with BC; (iii) family member who most often cares for the patient (limit one family member per patient); and (iv) voluntary participation in this survey. Data analysis and collation: The four dimensions of functional value, efficiency value, emotional value and social value of patients, each stage was divided into levels according to prehospital, in-hospital and posthospital, and patients and their families were asked to evaluate the specific functions of the information platform with the help of the BC case manager.

2.3 Correspondence method

The Delphi method is a qualitative research approach used to gain consensus through expert opinion on a real-world problem (32). The process aims to structure information on a topic about which little is known; the research questions can be answered by a panel of geographically diverse experts (32). Researchers using this method are able to obtain accurate and reliable data through multiple rounds of queries (33). The Delphi method is an appropriate choice when the research question requires gathering subjective information from experts and those working in the field (34), either to set priorities or to reach consensus where none existed before (33).

2.3.1 Criteria for the selection of experts

Inclusion criteria for correspondence experts: i) long-term engagement in BC management, treatment and care; ii) high academic level in BC and CM, with outstanding research ability; iii) intermediate level or above; iv) bachelor's degree or more; and v) voluntary participation in the consultation.

2.3.2 Method of correspondence

Letters of enquiry were sent to experts by letter or email in June-July 2022 due to study site constraints. Experts rated the importance of each indicator on a 5-point Likert scale as very important, relatively important, generally important, not very important and very unimportant, assigning a score of 5, 4, 3, 2 and 1, respectively (35), and made comments, suggested changes in the revision comments column, and added new indicators (Appendix 2). Experts were also asked to complete a questionnaire on basic information, familiarity and basis of

judgement. The degree of familiarity is divided into very familiar, familiar, generally familiar, unfamiliar and unfamiliar according to the experts' knowledge of the issue, with values of 1.0, 0.8, 0.6, 0.4 and 0.2, respectively (36), and the basis of judgement is mainly theoretical analysis, practical experience, domestic and international references and subjective judgement. A table quantifying the basis for assigning points and their level of impact is provided in Appendix 3.

Principles for revision of indicators: The following cases shall be evaluated and validated by the expert discussion group to decide whether to retain, add, delete or revise the indicators, including indicators with mean importance score x< 4 or coefficient of variation CV≥25% (36), indicators proposed by experts for addition or deletion, and indicators proposed by experts for comments and suggestions. After each round of the Delphi, responses for each item are summarized and fed back.

within the subsequent questionnaire, enabling participants to consider the views of others before rerating (Appendix 4).

2.4 Statistical analysis

Data were exported in an Excel file (Microsoft Corp., Redmond, WA, USA) and analysed by SPSS 26.0 statistical software (IBM Corp., Group NY). The expert positivity factor (E) is generally expressed in terms of the questionnaire return rate and measures the level of motivation and involvement of experts in the consultation. According to previous studies, the expert motivation factor should be at least 50% or more; above 60% indicates a high level of motivation, and 70% and above indicate a high level of motivation (37). The degree of authority of the experts' opinions is reflected by the coefficient of the basis of the experts' judgements on each indicator (Ca) and the coefficient of their familiarity with each indicator (Cs). The authority coefficient (Cr) is equal to the arithmetic mean of the coefficient of judgement basis and the coefficient of familiarity, i.e., Cr=(Ca+Cs)/2. The range of values for Cr was 0-0.95, and the critical value for more credible results was ≥0.7 (36). Coefficients of variation and Kendall's coefficient of coordination (W-values) are used to indicate the degree of consistency of expert opinion.

3 Results

3.1 Demand for case management information platforms from breast cancer patients and families

A total of 231 questionnaires were collected, including 189 patients (81.8%) and 42 family members (18.2%), who had an average age of 50.3 years. The vast majority of the respondents in this survey were women (207, 89.6%), and they were married (187,81.0%). The vast majority of patients were in the surgery stage (55, 23.8%) or chemotherapy stage (60, 26.0%). Regarding the progression of the disease, 46.3% of the participants were unaware of it. Specific information can be found in Appendix 5. The results of the evaluation of the content of the CM information module based on the theoretical framework of PPV by patients and their families are shown in Table 1.

3.2 Basic information and positive coefficients for experts

Twenty-two experts in clinical areas, nursing education and nursing management related to BC care were purposively selected from nursing schools and departments of major universities and tertiary hospitals in the southwest region according to predetermined criteria for the selection of experts. In the first round of the study, 22 consultation questionnaires were distributed, and 18 valid questionnaires were returned, for a positive coefficient of 81.8%; in the second round of the study, 18 consultation questionnaires were distributed, and 18 valid questionnaires were returned, for a positive coefficient of 100%. The distribution of the general information of the included experts is shown in Table 2.

3.3 Expert authority factor

The results show that four experts were very familiar with the indicators, 11 were more familiar and three were generally familiar. In addition, the experts judged each indicator on the basis of Table 3. The authority level of the experts' opinions in this study was 0.87, indicating that the experts were more authoritative.

3.4 The degree of coordination of expert opinion

The mean values of the coefficients of variation of the indicators in the 2 rounds of the study ranged from 0.094 to 0.175, and the differences were statistically significant (p< 0.05). The values of the Kendall harmonic coefficients for the various levels are shown in Table 4.

3.5 Selection and identification of indicators

Through two rounds of expert consultation, the average importance score for all indicators ranged from 4.50 to 5.00, and the coefficient of variation ranged from 0 to 0.181; items were screened on the basis of an average importance score > 3.50 and

TABLE 1 Content needs and evaluation of the information management platform by breast cancer patients and family members.

Function	Time	Sevices	$\bar{X} \pm S$
Functional value	**Pre-admission**	Provide appointment booking service	4.60 ± 0.603
		If not	2.77 ± 1.436
		Push information about the treatment process	4.53 ± 0.631
		If not	2.76 ± 1.381
	In hospital	Establishing a health record	4.56 ± 0.662
		If not	2.85 ± 1.415
		Individualised care plans	4.54 ± 0.587
		If not	2.84 ± 1.353
		Tracking Management	4.57 ± 0.577
		If not	2.75 ± 1.398
		Prevention and management of complications	4.54 ± 0.617
		If not	2.74 ± 1.351
		Dietary and lifestyle guidance	4.54 ± 0.609
		If not	2.70 ± 1.352
	After hospital	Targeted health education	4.55 ± 0.629
		If not	2.76 ± 1.358
		Management of concomitant symptoms during treatment and rehabilitation	4.54 ± 0.580
		If not	2.78 ± 1.357
		Out of hospital follow up	4.51 ± 0.632
		If not	2.76 ± 1.338
		Health education for carers	4.48 ± 0.684
		If not	2.92 ± 3.104
		Promote online health education knowledge	4.49 ± 0.678
		If not	2.77 ± 3.750
Emotional value	**Pre-admission**	Contact the medical team online at any time for a consultation	4.56 ± 0.607
		If not	2.72 ± 1.365
	In hospital	Provide a dedicated person (case manager) for long-term follow-up	4.54 ± 0.631
		If not	2.76 ± 1.365
		Regular assessments by case managers	4.56 ± 0.608
		If not	2.74 ± 1.370
		Multiple approaches to psycho-emotional support	4.52 ± 0.617
		If not	2.96 ± 3.506
	After hospital	Provide case manager contact details	4.52 ± 0.638
		If not	2.74 ± 1.361
		Patient Exchange Platform	4.55 ± 0.594
		If not	2.79 ± 1.338
		Real-time online consultation	4.52 ± 0.596
		If not	2.74 ± 1.358
Value of efficiency	**Pre-admission**	Case managers to book specialist appointments for you	4.52 ± 0.617
		If not	2.75 ± 1.366
		Special Disease Process	4.79 ± 3.370
		If not	2.75 ± 1.370
		Hospital access information support	4.54 ± 0.580
		If not	2.78 ± 1.341
	In hospital	Full rehabilitation needs assessment	4.56 ± 0.600
		If not	2.84 ± 1.397
		Information on Venous Access Maintenance Clinics and Community Maintenance Sites	4.42 ± 0.730
		If not	2.79 ± 1.322

(Continued)

TABLE 1 Continued

Function	Time	Sevices	$\bar{X} \pm S$
		Regional medical referrals	4.42 ± 0.718
		If not	2.77 ± 1.320
	After hospital	Nurse visits	4.41 ± 0.697
		If not	2.85 ± 1.312
		Teleconsultation	4.46 ± 0.664
		If not	2.83 ± 1.342
Social values	**Pre-admission**	Green channel to medical treatment	4.55 ± 0.601
		If not	2.69 ± 1.372
	In hospital	Provide individualised guidance to enhance patients' ability to manage their own rehabilitation	4.70 ± 2.016
		If not	2.77 ± 1.337
	After hospital	Health Education Seminar Live Event	4.51 ± 0.618
		If not	2.78 ± 1.344
		Provide addresses and contact numbers of health care centres and communities in each district and county	4.49 ± 0.652
		If not	2.79 ± 1.332
		Provide contact details for social assistance agencies (e.g. Cancer Relief Foundation)	4.48 ± 0.678
		If not	2.81 ± 1.336

a coefficient of variation< 0.25, and no indicators were deleted. However, it was noted that B2.2 Health lectures were a duplicate of A3.2 Health education and therefore, the item was removed. Three new secondary indicators were added: "B2.2 Counselling", "B3.3 Family support" and "D3.3 Emergency access". The content of the indicators A3.1 Follow-up tracking and C1.1 Consultation services was revised and adjusted in conjunction with expert opinion. Through the second round of consultation,

TABLE 2 Basic information on the 18 experts included in this correspondence.

Items	Number	Percentage (%)
Title		
Intermediate	12	66.7
Associate Senior	5	27.8
Senior	1	5.6
Academic qualifications		
Bachelor's degree	10	55.6
Master's degree	7	38.9
Doctor	1	5.6
Fields of work		
Clinical	10	55.6
Education	2	11.1
Management	6	33.3
Age (years)		
<30	4	22.2
30~40	6	33.3
41~50	6	33.3
>50岁	2	11.1
Years of work(years)		
<10	7	38.9
10~20	5	27.8
21~30	5	27.8
>30	1	5.6

TABLE 3 Analysis of the basis of judgement of the 18 experts.

Basis of judgement	Degree of impact		
	Great	Medium	Little
Theoretical analysis	12	6	0
Practical experience	12	6	0
Bibliography	7	6	5
Subjective judgement	4	3	11

four primary indicators and 31 secondary indicators were identified, and their mean scores, standard deviations and coefficients of variation are shown in Table 5.

3.6 Model framework for a case management information platform for breast cancer patients

The BC-CMIP is divided into a medical side for healthcare professionals and a patient side for patients and family members. The overall framework is shown in Figure 1. The medical end of the platform connects to the medical systems of each treatment unit through mobile medical technology, storing the medical examination data, consultation cases, examination results, medication prescriptions and health data uploaded by patients and their families in the platform, forming a complete BC patient's personal electronic health file and updating the health management records in real time. The case manager and medical staff can access the treatment records of BC patients at any time to understand the consultation results, examination and recovery and implement health management, health guidance, tracking management and business supervision. The management side provides statistics and analysis of health data, identifies alert values when compared with defined criteria, and dynamically monitors the whole process of BC patient management services. The patient side provides an online hospital, health testing, health assessment, expert consultation, patient home and access to health knowledge for patients and family members.

4 Discussion

In this study, based on the service needs and evaluation of breast cancer patients and family members on the case management platform, the content module of the whole information platform for breast cancer patients' case management was initially constructed through two rounds of expert correspondence based on the framework of patients' perceived value. It is scientific and practical and provides a theoretical basis for the subsequent construction of the case management platform and its clinical application.

As payment models change, with more clinicians and health care entities accepting financial risk for outcomes, health care systems are using digital health to manage their populations and improve access, patient experience, and control costs (38). At the same time, patients' interest in using technology to manage their health is increasing. Many patients seek information from the internet to learn more about their symptoms, diagnoses, and treatments. An increasing number are also using wearable devices and mobile applications to track their health. In addition, numerous studies now highlight the importance of designing and developing software platforms based on user requirements (38). The first principle of the software platform is to meet the needs of the people who use it because the software platform developed under the guidance of the needs will be more humane and practical and more likely to obtain long-term, stable support from the people who use it and higher application satisfaction. Therefore, this study first investigated the demand for and evaluation of case management information platform services by breast cancer patients and family members, and the results showed that patients and their families have a high opinion of the functional content of the information module for breast cancer patients, with mean scores ranging from 4.41 ± 0.697 to 4.60 ± 0.603, while without the implementation of these items, patient satisfaction scores are all less than 3, i.e., not satisfied. It can be seen that the content of the module of the information platform for case management of breast cancer patients based on the perceived value of patients constructed in this study meets the health needs of patients and is an essential health link.

Studies have shown that case managers spend considerable time recording patient-related information and case management processes (39) and that the key to the effective implementation of breast cancer case management is a well-functioning web-based platform (40). Wang et al. (41) investigated the application of professional case management based on the WeChat platform in BC patients. A total of 149 BC patients were randomly divided into two groups. The difference between the two groups was statistically significant ($P<0.05$), and the difference between the two groups' health promotion behaviour scores at 3 months after discharge was statistically significant ($P<0.001$). Thus, with specialized CM through the information platform, patients can proactively and timely communicate with healthcare professionals

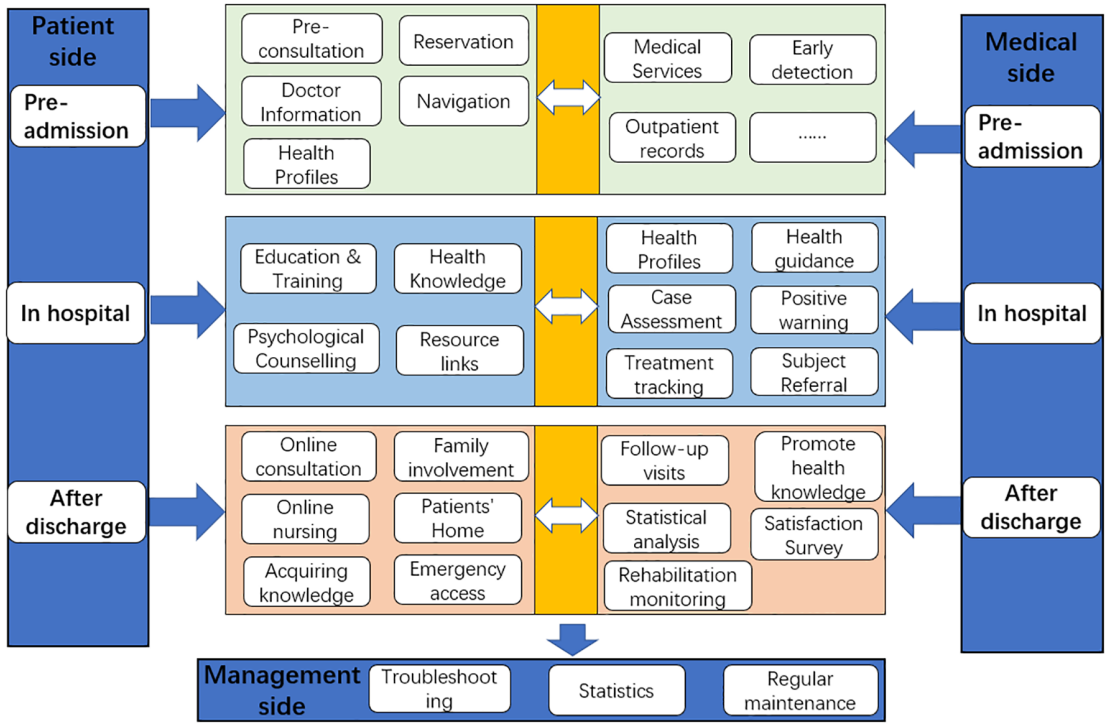

FIGURE 1
Framework for a case management information platform for breast cancer patients.

and obtain the most direct and reliable professional information. Members of the CM team track, follow up, monitor, intervene and record BC patients' life and compliance behaviour, forming a feedback system and providing targeted one-to-one guidance, improving the quality of out-of-hospital care, promoting patient self-healing and maintaining the permanence of patient health management.

Bettencourt et al. (42) pointed out in 2008 that service innovation is not a study of how the service is achieved but of how the customer wants to achieve the service. As healthcare is a professional service industry, it is not enough for the healthcare industry to focus on the clinical value of the patient from the doctor's perspective alone to obtain service innovation; the development of healthcare services also needs to revolve around the patients' multidimensional perceived value. This study systematically and comprehensively reflects the health needs of patients from prehospital to posthospital based on the four value dimensions of patient-perceived value, namely, functional, efficiency, emotional and social values. In addition, indicators were screened with the help of the Delphi method (32), combining expert opinions with statistical analysis of data, integrating consistency and coordination based on the original opinions of experts, while satisfying the requirement of overall opinion convergence to obtain the optimal solution for group decision-making and indicators with credibility. This combination of subjective and objective methods makes the selection of the indicator system more scientific and appropriate. Therefore, this study constructs a case management information platform for breast cancer patients based on patient-perceived value theory, which is scientific and comprehensive and can meet the needs of patient disease management.

TABLE 4 Level of coordination of expert opinion.

Rounds	Levels	Mean value of coefficient of variation	W value	X^2	df	P
Round 1	Tier 1 indicators	0.069	0.178	8.538	3	0.036
	Secondary indicators	0.070	0.084	37.412	28	0.110
Round 2	Tier 1 indicators	0.080	0.296	14.186	3	0.003
	Secondary indicators	0.081	0.136	65.499	30	<0.001

W, Kendall cofficient of concordance; X^2, Chi-square test; df, degree of freedom.

10.3389/fonc.2022.1034171

TABLE 5 Evaluation of secondary indicators of the Breast Cancer Case Management Information Platform module.

Tier 1 Indicator		Secondary Indicator	Importance score		Coefficient of variation
			$\bar{X}$	S	
Functional value (A)	Pre-Admission (A1)	Consultation services (A1.1)	4.75	.577	0.121
		Early screening (A1.2)	5.00	.000	0
		Outpatient medical records (A1.3)	4.88	.500	0.102
	In hospital (A2)	Health record (A2.1)	4.88	.342	0.070
		Inpatient records (A2.2)	4.94	.250	0.051
		Treatment tracking management (A2.3)	5.00	.000	0
		Health guidance (A2.4)	4.88	.342	0.070
	After hospital (A3)	Follow-up tracking (A3.1)	5.00	.000	0
		Health education (A3.2)	4.81	.403	0.084
Emotional value (B)	Pre-admission(B1)	Pre-visit consultation (B1.1)	4.56	.512	0.112
	In hospital (B2)	Case assessment (B2.1)	4.94	.250	0.051
		Psychological counselling (B2.2)	4.56	.629	0.138
	After hospital(B3)	Recovery monitoring (B3.1)	4.94	.250	0.051
		Patients' homes (B3.2)	4.81	.403	0.084
		Family support (B3.3)	4.88	.342	0.070
Value of efficiency (C)	Pre-admission (C1)	Consultation services(C1.1)	4.75	.683	0.144
	In hospital (C2)	Early warning of positive tests(C2.1)	4.94	.250	0.051
		Specialist referrals(C2.2)	4.69	.602	0.128
		Multidisciplinary medical teams(C2.3)	4.75	.447	0.094
	After hospital (C3)	Follow-up(C3.1)	5.00	.000	0
		Online consultation(C3.2)	4.81	.403	0.084
		Network nursing(C3.3)	4.56	.727	0.159
		Statistical analysis(C3.4)	4.88	.342	0.070
Social values (D)	Pre-admission (D1)	Treatment services(D1.1)	4.81	.403	0.084
	In hospital (D2)	Health education(D2.1)	4.94	.250	0.051
		Links to resources(D2.2)	4.75	.447	0.094
		Graded diagnosis and treatment(D2.3)	4.63	.719	0.155
	After hospital (D3)	Online consultation(D3.1)	4.94	.250	0.051
		Patients' Home(D3.2)	4.88	.342	0.070
		First aid channel(D3.3)	4.50	.816	0.181
		Satisfaction surveys(D3.4)	4.81	.403	0.084

This study has the following limitations. First, there was a lack of information engineers on the expert discussion group for guidance. Second, although we included fill-in-the-blank questions in the needs questionnaire, patients and their family members did not provide much data. This may mean that the needs of patients and some of their family members were not fully included.

5 Conclusion

This study takes the PPV of BC patients as the theoretical framework, is demand oriented, and constructs the content of the BC-CMIP module with the help of the Delphi method, which has the scientific and comprehensive ability to meet the health management needs of patients. The information platform can provide patients with convenient access to information and medical and nursing consultation carriers. With the information platform as a carrier, medical and nursing staff can participate in the whole cycle of patients' disease treatment and rehabilitation, meet patients' needs for professional guidance, effectively improve breast cancer patients' self-management ability and improve their survival quality. It can be used as a new mode of case management for BC patients. Due to the limited duration of this study, the next step is to apply this management model to clinical practice and conduct a multicentre, large sample study to further improve the confidence platform for breast cancer case management.

Data availability statement

The raw data supporting the conclusions of this article will be made available by the authors, without undue reservation.

Author contributions

XG, supervising the subject throughout, looking for correspondence experts; YL, Extensive literature review, data collection, constructing questionnaires, distributing questionnaires, checking papers. YG, Data collection, constructing questionnaires, data collation, data analysis and collation, writing the thesis and thesis reworking. YL and YG contributed equally to this work and share first authorship. GY, Data collection, methodological guidance. WC, Data collection. All authors contributed to the article and approved the submitted version.

Funding

Project title: Study on the impact of chemotherapy-induced peripheral neuropathy on the quality of life of breast cancer patients and its countermeasures Item No.:2019MSXM068

Conflict of interest

The authors declare that the research was conducted in the absence of any commercial or financial relationships that could be construed as a potential conflict of interest.

Publisher's note

All claims expressed in this article are solely those of the authors and do not necessarily represent those of their affiliated organizations, or those of the publisher, the editors and the reviewers. Any product that may be evaluated in this article, or claim that may be made by its manufacturer, is not guaranteed or endorsed by the publisher.

Supplementary material

The Supplementary Material for this article can be found online at: https://www.frontiersin.org/articles/10.3389/fonc.2022.1034171/full#supplementary-material

References

1. Organization WH. *World health organization projections of mortality and causes of death* . Available at: https://www.Who.int/healthinfo/global_burden_disease/projections/en.

2. Chen W, Zheng R, Baade PD, Zhang S, Zeng H, Bray F, et al. Cancer statistics in China, 2015. *CA Cancer J Clin* (2016) 66(2):115–32. doi: 10.3322/caac.21338

3. Feng RM, Zong YN, Cao SM, Xu RH. Current cancer situation in China: good or bad news from the 2018 global cancer statistics. *Cancer Commun (Lond).* (2019) 39(1):22. doi: 10.1186/s40880-019-0368-6

4. Global Burden of Disease Cancer Collaboration, Fitzmaurice C, Akinyemiju TF, Al Lami FH, Alam T, Alizadeh-Navaei R, et al. Global, regional, and national cancer incidence, mortality, years of life lost, years lived with disability, and disability-adjusted life-years for 29 cancer groups, 1990 to 2016: A systematic analysis for the global burden of disease study. *JAMA Oncol* (2018) 4(11):1553–68. doi: 10.1001/jamaoncol.2018.2706

5. Thorat MA, Balasubramanian R. Breast cancer prevention in high-risk women. *Best Pract Res Clin Obstet Gynaecol.* (2020) 65:18–31. doi: 10.1016/j.bpobgyn.2019.11.006

6. Paluch-Shimon S, Pagani O, Partridge AH, Abulkhair O, Cardoso MJ, Dent RA, et al. ESO ESMO 3rd international consensus guidelines for breast cancer in young women (BCY3). *Breast* (2017) 35:203–17. doi: 10.1016/j.breast.2017.07.017

7. Boundouki G, Wilson R, Duxbury P, Henderson J, Ballance L, Wray J, et al. Patient and public priorities for breast cancer research: a qualitative study in the UK. *BMJ Open* (2021) 11(1):e036072. doi: 10.1136/bmjopen-2019-036072

8. Kim S, Han J, Lee MY, Jang MK. The experience of cancer-related fatigue, exercise and exercise adherence among women breast cancer survivors: Insights from focus group interviews. *J Clin Nurs.* (2020) 29(5-6):758–69. doi: 10.1111/jocn.15114

9. Liu L, Wu Y, Cong W, Hu M, Li X, Zhou C. Experience of women with breast cancer undergoing chemotherapy: a systematic review of qualitative research. *Qual Life Res* (2021) 30(5):1249–65. doi: 10.1007/s11136-020-02754-5

10. Ao L. The application of self-management mode based on empowerment theory in patients with postoperative chemotherapy for breast cancer. *Shanxi Med Univ* (2019).

11. Li JH, Li XY, Tan Y, Wei T. Application of the multidisciplinary-team management model in patients with breast cancer's chemotherapy-induced nausea and vomiting. *Chin Nurs Manage* (2018) 18(03):367–72. doi: 10.3969/j.issn.1672-1756.2018.03.018

12. Sun W, Chen Y. Application of 5S health education management model in health education for breast cancer patients. *J Nurs Administration* (2018) 18 (05):373–376+380. doi: 10.3969/j.issn.1671- 315x.2018.05.018

13. Jary J, Franklin L. The role of the specialist nurse in breast cancer. *Prof Nurse.* (1996) 11(10):664–5. doi: 10.1007/978-1-4419-6076-4_3

14. Chen YZ, Zhou YZ. The case managerment experience in Taipei veterans general hospital. *Chin Hosp Manag* (2010) 10(3):21–2.

15. Zhang LL. The development and future of tumor case managers. *J Cancer Care* (2010) 10(1):19.

16. Zhang LL. The current situation and prospect of case management in Taiwan//Training courses for cancer prevention professionals-role and function of tumor case manager. *Taichung: Affiliated Hosp China Med Univ* (2010) 70–75.

17. Giuliano KK, Poirier CE. Nursing case management: critical pathways to desirable outcomes. *Nurs Manage* (1991) 22(3):52–5. doi: 10.1097/00006247-199103000-00015

18. Dieterich M, Irving CB, Bergman H, Khokhar MA, Park B, Marshall M. Intensive case management for severe mental illness. *Cochrane Database Syst Rev* (2017) 1(1):CD007906. doi: 10.1002/14651858.CD007906.pub3

19. Reilly S, Miranda-Castillo C, Malouf R, Hoe J, Toot S, Challis D, et al. Case management approaches to home support for people with dementia. *Cochrane Database Syst Rev* (2015) 1(1):CD008345. doi: 10.1002/14651858.CD008345.pub2

20. Aubin M, Giguère A, Martin M, Verreault R, Fitch MI, Kazanjian A, et al. Interventions to improve continuity of care in the follow-up of patients with cancer. *Cochrane Database Syst Rev* (2012) 7:CD007672. doi: 10.1002/14651858.CD007672.pub2

21. Peng CE, Wang WH, Li Z, Chen YY, Chen XB, Cai X, et al. Influence of case management model on quality of life and psychosocial adaptation of patients with

breast cancer. *Nurs Res* (2015) 10(29):3541–5. doi: 10.3969/j.issn.1009-6493.2015.28.029

22. Gan L, Lin YH, Yang R. The development and present situation of nursing in Taiwan. *Nurs Res* (2014) 12(28):4491–3. doi: 10.3969/j.issn.10096493.2014.36.004

23. Chen YC, Chang YJ, Tsou YC, Chen MC, Pai YC. Effectiveness of nurse case management compared with usual care in cancer patients at a single medical center in Taiwan: a quasi-experimental study. *BMC Health Serv Res* (2013) 13:202. doi: 10.1186/1472-6963-13-202

24. Wulff CN, Vedsted P, Søndergaard J. A randomized controlled trial of hospital-based case management in cancer care: a general practitioner perspective. *Fam Pract* (2013) 30(1):5–13. doi: 10.1093/fampra/cms050

25. Hubbard G, Gray NM, Ayansina D, Evans JM, Kyle RG. Case management vocational rehabilitation for women with breast cancer after surgery: a feasibility study incorporating a pilot randomised controlled trial. *Trials.* (2013) 14:175. doi: 10.1186/1745-6215-14-175

26. Lantz PM, Keeton K, Romano L, Degroff A. Case management in public health screening programs: the experience of the national breast and cervical cancer early detection program. *J Public Health Manag Pract* (2004) 10(6):545–55. doi: 10.1097/00124784-200411000-00012

27. Wang H, Wang H. The factors influencing insured people seeking remote medical treatment– the suggestion for orderly seeking medical treatment. *Chin Heal Insur.* (2014) 7:122–7. doi: 10.369/j.issn.1674-3830.2014.7.4

28. Gallarza M, Gil S. Value dimensions perceived value, satisfaction and loyalty: an investigation of university students. *Tour Manag* (2004) 27(03):437–52. doi: 10.1016/j.tourman.2004.12.002

29. Zhang X, Sleeboom-Faulkner M. Tensions between medical professionals and patients in mainland China. *Camb Q Healthc Ethics.* (2011) 20(3):458–65. doi: 10.1017/S0963180111000144

30. Qian H, Lu W, Zhang D. Empirical investigation on the characteristics and perceived value of patients in medical treatment seeking: In-depth research in zhejiang province of China. *BioMed Res Int* (2021) 2021:5245041. doi: 10.1155/2021/5245041

31. Hu R, Chen HF, Xu WG. A case study on the formation mechanism of the patients perceived value in mobile medical system. *Manage Review.* (2017) 29 (03):261–72. doi: 10.3969/j.issn.1672-0334.2018.03.007

32. McPherson S, Reese C, Wendler MC. Methodology update: Delphi studies. *Nurs Res* (2018) 67(5):404–10. doi: 10.1097/NNR.0000000000000297

33. Keeney S, Hasson F, McKenna H. *The Delphi technique in nursing and health research*. West Sussex, UK: Wiley-Blackwell (2011).

34. Stitt-Gohdes WL, Crews R. The Delphi technique: A research strategy for career and technical education. *CTE J* (2004) 20:55–67. doi: 10.21061/jcte

35. McMillan SS, King M, Tully MP. How to use the nominal group and Delphi techniques. *Int J Clin Pharm* (2016) 38(3):655–62. doi: 10.1007/s11096-016-0257-x

36. Zeng G. *Modern epidemiological methods and applications*. China: Beijing Medical University, China Union Medical University Press (1994).

37. Macdonald EB, Ritchie KA, Murray KJ, Gilmour WH. Requirements for occupational medicine training in Europe: a Delphi study. *Occup Environ Med* (2000) 57(2):98–105. doi: 10.1136/oem.57.2.98

38. Agboola SO, Bates DW, Kvedar JC. Digital health and patient safety. *JAMA.* (2016) 315(16):1697–8. doi: 10.1001/jama.2016.2402

39. Armold S. Case management: An overview for nurses. *Nursing.* (2019) 49 (9):43–5. doi: 10.1097/01.NURSE.0000577708.49429.83

40. Buescher C, Thorenz A, Grochocka A, Koch U, Watzke B. Die Case-Management-basierte Betreuung von Brustkrebspatientinnen: Ergebnisse einer Befragung beteiligter ärztlicher und nichtärztlicher Netzwerkpartner [A case management programme for women with breast cancer: Results of a written survey of participating medical and non-medical, networking-partners. *Gesundheitswesen* (2011) 73(12):815–22. doi: 10.1055/s–0030–1262863

41. Wang ZJ, Lin ZJ, Ma HX. Application effect of specialized case management based on WeChat mobile platform in extended service of breast cancer patients. *Nurs Res* (2019) 33(3):524–7. doi: 10.12102/j.issn.1009-6493.2019.03.043

42. Bettencourt LA, Ulwick AW. The customer-centered innovation map. *Harv Bus Rev* (2008) 86(5):109–14, 130. doi: 10.12102/j.issn.1009-6493.2

frontiers | Frontiers in Oncology

TYPE Case Report
PUBLISHED 09 January 2023
DOI 10.3389/fonc.2022.1022913

OPEN ACCESS

EDITED BY
San-Gang Wu,
First Affiliated Hospital of Xiamen University, China

REVIEWED BY
Meghana V. Trivedi,
University of Houston, United States
Jürgen Geisler,
University of Oslo, Norway

*CORRESPONDENCE
Wenfeng Li
li_wenfeng@qdu.edu.cn

SPECIALTY SECTION
This article was submitted to Breast Cancer, a section of the journal Frontiers in Oncology

RECEIVED 19 August 2022
ACCEPTED 01 December 2022
PUBLISHED 09 January 2023

CITATION
Mao Y, Lv M, Wang Y, Cao W and Li W (2023) Hormone receptor-positive, HER2-negative, metastatic breast cancer responded well to abemaciclib and exemestane after palbociclib and fulvestrant failure: A case report and literature review.
Front. Oncol. 12:1022913.
doi: 10.3389/fonc.2022.1022913

Hormone receptor-positive, HER2-negative, metastatic breast cancer responded well to abemaciclib and exemestane after palbociclib and fulvestrant failure: A case report and literature review

Yan Mao, Meng Lv, Yongmei Wang, Weihong Cao and Wenfeng Li*

Breast Disease Center, The Affiliated Hospital of Qingdao University, Qingdao, Shandong, China

There is uncertainty regarding the usefulness of CDK4/6-inhibitor-based therapy for hormone receptor positive (HR+), human epidermal grow factor receptor 2 negative (HER2–), metastatic breast cancer (MBC), when CDK4/6 inhibitor treatment had previously failed. Furthermore, a biomarker for abemaciclib resistance has not been identified. Herein, we reported outcomes for an HR+/HER2– MBC patient diagnosed with multiple myeloma and treated with abemaciclib and exemestane, who had cancer progression after treatment with palbociclib and fulvestrant. Thalidomide was used in conjunction with all treatments. The patient had a good response to abemaciclib and exemestane, with progression-free survival much longer than previously reported. PIK3CA and TP53 mutations were identified after cancer progression following abemaciclib treatment. It is unclear whether thalidomide increased the effectiveness of abemaciclib. Whether benefit can be derived by the use of PI3K inhibitors, after cancer progression, requires further investigation, and this may be best accomplished by the use of next-generation sequencing.

KEYWORDS

CDK4/6 inhibitor, breast cancer, metastatic, abemaciclib, case report

Introduction

For hormone receptor-positive (HR+), human epidermal grow factor receptor 2-negative (HER2−), metastatic breast cancer (MBC) patients, endocrine therapy is the first line of treatment, except for patients in visceral crisis (1). Based on multiple trials of cyclin-dependent kinase 4 (CDK4) and CDK6 inhibitors, the combination of a CDK4/6 inhibitor with endocrine therapy has improved the survival and the quality of life for HR+/HER2− MBC patients, with outcomes far better than those with chemotherapy alone (2–8). Therefore, guidelines and consensus recommend a CDK4/6 inhibitor combined with endocrine therapy as the treatment of choice for HR+/HER2− MBC patients. There are three CDK4/6 inhibitors (palbociclib, abemaciclib, and ribociclib) that have been approved by the Food and Drug Administration (FDA) for MBC (2–8), with abemaciclib also approved for adjuvant therapy of HR+/HER2− high risk early breast cancer (9). This is good news for breast cancer patients, but a challenge for oncologists. For example, if an HR+/HER2− MBC patient chose a combination of a CDK4/6 inhibitor with endocrine therapy as a first-line treatment, what would be the best choice as a second line, chemotherapy or another CDK4/6 inhibitor? Which CDK4/6 inhibitor is the best choice? Limited data are available to address these questions. Professor Angela DeMichele provided three endocrine choices at the 2018 ASCO Annual Meeting: change treatment to another CDK4/6 inhibitor, use a different endocrine drug, or add another target drug (e.g., the mTOR inhibitor, everolimus). A retrospective multicenter study found abemaciclib to be well tolerated after prior treatment with palbociclib, with median progression-free survival (PFS) of 5.3 months. These results were similar to the results of the MONARCH-1 study (10). In that study, median PFS was similar for patients who received abemaciclib monotherapy or abemaciclib combined with endocrine therapy. The median PFS was longer (8.4 months, 95% CI, 4.1–NR) for patients who received sequential CDK4/6 inhibitor therapies than for patients who received non-sequential abemaciclib therapy (3.9 months, 95% CI, 2.9–5.7, p=0.0013) (10). As such, some patients may benefit from treatment with another CDK4/6 inhibitor. However, the question is which treatment regimen is the best choice for patients who progressed after prior CDK4/6 inhibitor treatment (i.e., chemotherapy, another CDK4/6 inhibitor, or alternative endocrine therapy)?

Herein, we reported outcomes for one HR+/HER2− MBC patient who was also diagnosed with multiple myeloma. The patient had a good response to non-sequential abemaciclib and exemestane after failure with palbociclib and fulvestrant. Next-generation sequencing (NGS) of circulating tumor DNA (ctDNA), after progression with abemaciclib, identified PIK3CA and TP53 mutations, which suggested that this patient may be sensitive to PI3K inhibitors. This case report provided new insight into a treatment strategy for HR+/HER2− MBC patients after prior failure of combined CDK4/6 inhibitor and endocrine therapy.

Case presentation

A 65-year-old woman underwent modified radical mastectomy on 17 November 2015. Her treatment is summarized in Figure 1. She was diagnosed with invasive ductal carcinoma (histological grade II, tumor size 1.4 × 1 × 1 cm), with 9 out of 18 axillary lymph nodes involved. Pathological stage was pT1cN2M0, stage IIIA. Immunohistochemical (IHC) results showed the following: ER (+++), 80%; PR (+++), 35%; CerbB-2 (0); Ki67 positive rate, 20%; and D2-40, vascular tumor thrombus (+). The patient received six cycles of TC regimen (docetaxel and cyclophosphamide), radiation therapy of the chest wall and regional nodes (50Gy in 25 fractions), and exemestane as adjuvant therapy. Although non-steroidal aromatase inhibitors are, in general, the first choice of adjuvant therapy, only

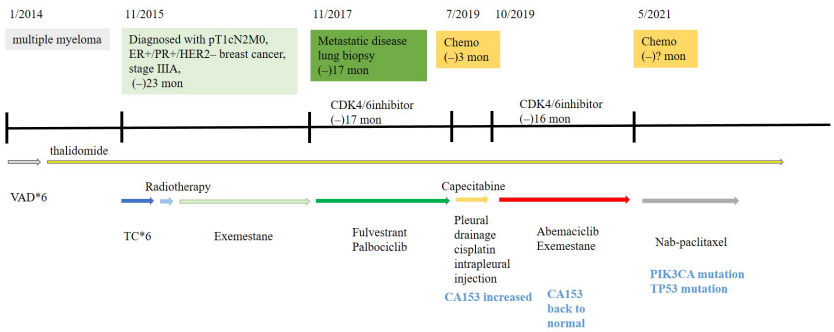

FIGURE 1
Treatment history of this HR+/HER2− breast cancer patient receiving abemaciclib combined with exemestane after prior progression on palbociclib and fulvestrant.

exemestane was reimbursed in our hospital. On 23 November 2017, PET-CT showed multiple small nodules in both lungs, with lung metastases suspected. There were no metastatic signs in other organs. CT-guided lung biopsy showed breast cancer lung metastasis. No further IHC examination was done due to a lack of biopsy tissue. Because disease-free survival (DFS) with endocrine therapy was only 16 months (<24 months) and because she had no visceral crisis, endocrine therapy was considered suitable for her treatment. Fulvestrant was an option. Based on the results of the PALOMA-3 trial, fulvestrant and palbociclib were given as her first line of treatment, and her disease remained stable until May 2019. PFS was 17 months. Grade 2 neutropenia occurred after 2 weeks of palbociclib, with adverse effects reversed after 7 days of palbociclib withdrawal. With re-occurrence of grade 2 neutropenia, she received a one dose reduction in palbociclib, with no more side effects observed. Seventeen months later, she developed chest tightness symptoms with increased serum carbohydrate antigen 153 (CA153) levels. Chest CT showed progression in both lungs, with left pleural effusion. Because she refused intravenous chemotherapy, she received capecitabine for 3 months. Unfortunately, left thoracic cavity effusion increased. Pleural drainage and intra-pleural injection of cisplatin improved symptoms. With the failure of capecitabine and refusal of chemotherapy, endocrine therapy was an option for treatment. With knowledge of the MONARCH-1 study, we administered abemaciclib and exemestane as her third line of treatment. After 1 month, CA153 levels decreased to normal (Figure 2), and lung lesions were stable. Although she was 71 years of age, second-line CDK4/6 inhibitor treatment toxicities were tolerable, and only grade 2 diarrhea occurred after 7 days of abemaciclib, which gradually improved after oral administration of Imogen and was normal after 40 days. Sixteen months (on 12-02-2021) later, she was short of breath, and chest CT scan showed progression of pulmonary lesions with liver metastatic lesions (Figure 3). Nab-paclitaxel (100 mg) was administered on days 1 and 8 with zoledronic acid for bone preservation. As of May 2022, she was in a stable condition.

She was also diagnosed with multiple myeloma in January 2014, when a thoracic vertebral fracture occurred. VAD (vindesine 1 mg, days 1–4; epirubicin 10 mg, days 1–4; dexamethasone 15 mg bid, days 1–14) chemotherapy regimen was given for a total of six cycles, and then, thalidomide, 100 mg, was given orally every night for 3 months followed by removal for 1 month. Thalidomide was tolerated with no side effects, and the myeloma was stable.

In order to find therapeutic targets for this patient, who progressed on abemaciclib after prior progression on palbociclib, we performed NGS of ctDNA (Geneseeq assay) derived from her blood. A PIK3CA p.E545K exon 9 missense mutation and a TP53 p.H214Lfs*33 frame shift mutation in exon 6 were found (Figure 1). The plasma tumor mutation burden (TMB) was 4.1 mutations/megabase [mut/Mb].

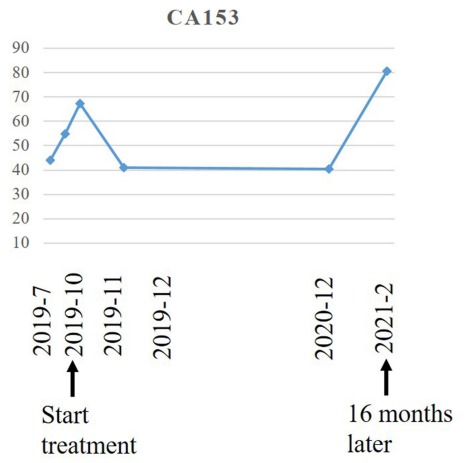

FIGURE 2
The changes in serum CA153 (U/ml) during the treatment of abemaciclib and exemestane.

Discussion

Recent studies have shown that the combination of a CDK4/6 inhibitor with hormone therapy was the first choice for treatment of HR+/HER2− MBC because this strategy improved survival (2–8). Palbociclib, abemaciclib, and ribociclib are all CDK4/6 inhibitors that provide similar survival data for MBC patients. Abemaciclib is the only effective monotherapy for HR+/HER2− MBC patients (11). Because of the FDA approval sequence, palbociclib was the first CDK4/6 inhibitor for MBC patients. The MONARCH E study showed abemaciclib to also be effective for high-risk early breast cancer patients (9). With the approval of these drugs, oncologists were challenged to determine the best treatment for HR+/HER2− MBC patients who had failed previous therapy with a CDK4/6 inhibitor.

In this study, we reported outcomes for a HR+/HER2- old MBC patient with a good response to non-sequential abemaciclib and exemestane after fulvestrant and palbociclib treatment failure. The PFS with abemaciclib and exemestane was 16 months for this patient, which was longer than previously reported (10). For MONARCH I and the retrospective multicenter experience, the median PFS for abemaciclib was <8.4 months (10, 11) and only 3.9 months (95% CI, 2.9–5.7, p=.0013) for those who received non-sequential CDK4/6 inhibitor therapy (10). There maybe two reasons. One is that this patient reported herein also had multiple myeloma and was given thalidomide. There are many studies that have shown thalidomide to be immunomodulatory, to have anti-angiogenic activities that may suppress tumor growth (12–14), and to play an important

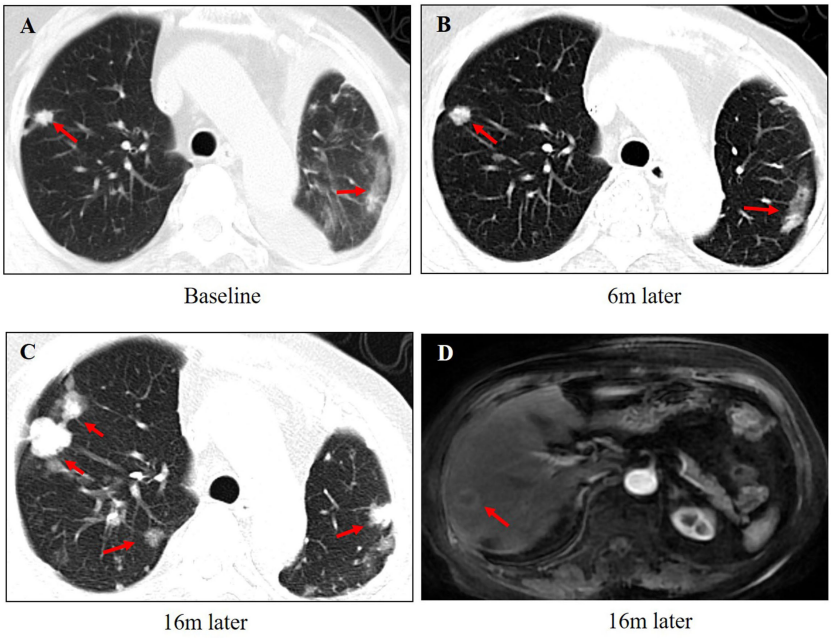

FIGURE 3
The changes in images during the treatment of abemaciclib and exemestane. **(A)** The baseline of lung metastasis at the beginning of abemaciclib and exemestane. **(B)** The lung lesions were stable after 6 months treatment. **(C)** The lung lesions progressed after 16 months of treatment. **(D)** Liver metastasis was found after 16 months of treatment.

role in cancer control. One recent study found that adding thalidomide to pyrotinib increased clinical benefit for advanced non-small-cell lung cancer (NSCLC) patients with HER2 exon 20 insertions, with reductions in the incidence of pyrotinib-related diarrhea (15). In a breast cancer murine model, Yang Jin et al. found that thalidomide inhibited breast tumor growth through inhibition of angiogenesis by reducing tumor-associated macrophage accumulation and infiltration and decreasing angiogenesis-related cytokine production (14). They also found that thalidomide increased tumor perfusion and decreased vascular leakiness, which may enhance the delivery and efficacy of chemotherapy (12). Meta-analysis showed that thalidomide reduced nausea and vomiting in delayed and overall phases (16), increasing treatment tolerance for older patients. Whether thalidomide can enhance the anti-tumor effect of CDK4/6 inhibitors requires further investigation. The other explanation that this patient had longer PFS may due to the combination of exemestane. Although her BMI was normal (BMI=21) and none of the three aromatase inhibitors (non-steroidal aromatase inhibitors: anastrozole, letrozole, and steroidal aromatase inhibitor exemestane) were superior to the others in terms of efficacy and safety, some studies still indicated that exemestane can significantly decrease serum levels of leptin while letrozole cannot (17). This hypothesis also needs to be further verified.

The patient reported herein was older, refused chemotherapy, and was satisfied with her two lines of endocrine therapy, which were well tolerated and provided lasting tumor control.

Previous studies found that the PIK3CA mutation, ERS1 mutation, cyclin E1 (CCNE1) amplification, and the CCND1 amplification contributed to endocrine resistance (18–23). The exploratory analysis of the PALOMA-3 study showed that high CCNE1 mRNA expression was associated with the poor anti-tumor activity of palbociclib (18). Lee et al. found that high TMB, the TP53 mutation, the PTEN loss of function mutation, and RB1 pathway alteration related to palbociclib resistance (19). Gene expression analysis of baseline tumor mRNA by the MONALEESA-7 study found survival benefit for patients treated with ribociclib who had high expression levels of CCND1, IGF1R, and ERBB3, and for patients with low expression levels of CCNE1 and MYC (21). A retrospective analysis found that RB1, ERBB2, and CCNE1 alterations contributed to rapid cancer progression with abemaciclib (10). There are barriers and limitations to the use of NGS for metastatic cancer patients. Many trials have used NGS to identify biomarkers and new drug targets for treatment of breast cancer patients (18, 21). Anna et al. found that for HR +/HER2− MBC patients with the BRCA mutation, a combination of PARP inhibitors, palbociclib, and letrozole was the most effective cancer treatment (24). Wang et al. found heavily pre-treated HR+/HER2− MBC patients with high TMB

to respond well to camrelizumab (25). These studies provide insight into new strategies by which to treat patients who were previously treated with many lines of endocrine and/or chemotherapy. In this case report, we used a new approach for the treatment of this patient. Because the patient denied biopsy of her new metastatic lesions, we collected a blood sample and, by NGS, found a PIK3CA p.E545K exon 9 missense mutation and a TP53 p.H214Lfs*33 frame shift mutation in exon 6. The TMB in plasma was 4.1 mutations/megabase (mut/Mb), which was quite low. Many studies have demonstrated the PIK3CA mutation to play an important role in endocrine resistance. PIK3CA-mutated HR+/HER2− MBC cells are less sensitive to chemotherapy (26), which may explain why this patient showed no response to capecitabine. Although the TP53 mutation is common in MBC patients, there are no target drugs for breast cancer patients. However, PIK3CA mutations have predictive value for treatment with the α-selective PI3K inhibitor, alpelisib, and the β-sparing PI3K inhibitor, taselisib (SANDPIPER trial), in an advanced situation (26, 27). Based on the NGS results, this patient may be sensitive to PI3K/AKT/mTOR pathway inhibitors. Considering drug accessibility and tolerance, she finally received nab-paclitaxel, 100 mg, on days 1 and 8 and was in a stable condition as of May 2022.

Conclusion

In conclusion, we reported an HR+/HER2− MBC patient, also diagnosed with multiple myeloma, who showed a good response to non-sequential abemaciclib and endocrine therapy after cancer progression following palbociclib therapy. The PFS of abemaciclib for this patient was longer than that reported previously. Furthermore, ctDNA plasma sequencing of this patient showed PIK3CA and TP53 mutations, which indicated that PI3K inhibitors may be one option for her future treatment. Overall, these findings suggested that some patients may benefit from continued CDK4/6-directed therapy, even though the utility of individual CDK4/6 inhibitors is unknown. Thus, additional, large-sample, prospective trials are necessary to evaluate the effectiveness of CDK4/6 inhibitors in such clinical situations.

Data availability statement

The datasets presented in this study can be found in online repositories. The names of the repository/repositories and accession number(s) can be found in the article/Supplementary material.

Ethics statement

The studies involving human participants were reviewed and approved by the ethics committee of the Affiliated Hospital of Qingdao University (QYFY WZLL 27231). The patients/participants provided their written informed consent to participate in this study.

Author contributions

YM contributed to the conception and writing of the manuscript. ML and YW were involved in explaining the data and doing the figures. WC interpreted the radiological images. WL contributed to the NGS test and reviewed the manuscript. All authors reviewed and approved the final version of this manuscript.

Funding

This study was supported by the National Natural Science Foundation of China (82102867), Natural Science Doctoral Funding of Shandong Province (ZR2021MH062, ZR2019BH013), and Beijing Medical Award Foundation (YXJL-2020-0941-0742).

Acknowledgments

The authors thank the patient and the patient's kin for the agreement to the publication of the report.

Conflict of interest

The authors declare that the research was conducted in the absence of any commercial or financial relationships that could be construed as a potential conflict of interest.

Publisher's note

References

1. Giuliano M, Schettini F, Rognoni C, Milani M, Jerusalem G, Bachelot T, et al. Endocrine treatment versus chemotherapy in postmenopausal women with hormone receptor-positive, HER2-negative, metastatic breast cancer: A systematic review and network meta-analysis. *Lancet Oncol* (2019) 20(10):1360–9. doi: 10.1016/S1470-2045(19)30420-6

2. Cardoso F, Paluch-Shimon S, Senkus E, Curigliano G, Aapro MS, Andrei F, et al. 5th ESO-ESMO international consensus guidelines for advanced breast cancer (ABC 5). *Ann Oncol* (2020) 31:1623–49. doi: 10.1016/j.annonc.2020.09.010

3. Finn RS, Martin M, Rugo HS, Jones S, Im SA, Gelmon K, et al. Palbociclib and letrozole in advanced breast cancer. *N Engl J Med* (2016) 375(20):1925–36. doi: 10.1056/NEJMoa1607303

4. Cristofanilli M, Turner NC, Bondarenko I, Ro J, Im SA, Masuda N, et al. Fulvestrant plus palbociclib versus fulvestrant plus placebo for treatment of hormone-Receptor-Positive, HER2-negative metastatic breast cancer that progressed on previous endocrine therapy (PALOMA-3): Final analysis of the multicentre, double-blind, phase 3 randomised controlled trial. *Lancet Oncol* (2016) 17:425–39. doi: 10.1016/S1470-2045(15)00613-0

5. Hortobagyi GN, Stemmer SM, Burris HA, Yap YS, Sonke GS, Paluch-Shimon S, et al. Updated results from MONALEESA-2, a phase III trial of first-line ribociclib plus letrozole versus placebo plus letrozole in hormone receptor-positive, HER2-negative advanced breast cancer. *Ann Oncol* (2018) 29:1541–7. doi: 10.1093/annonc/mdy155

6. Tripathy D, Im SA, Colleoni M, Franke F, Bardia A, Harbeck N, et al. Ribociclib plus endocrine therapy for premenopausal women with hormone-Receptor-Positive, advanced breast cancer (MONALEESA-7): A randomised phase 3 trial. *Lancet Oncol* (2018) 19(7):904–15. doi: 10.1016/S1470-2045(18)30292-4

7. Sledge GW, Toi M, Neven P, Sohn J, Inoue K, Pivot X, et al. MONARCH 2: Abemaciclib in combination with fulvestrant in women with HR+/HER2-advanced breast cancer who had progressed while receiving endocrine therapy. *J Clin Oncol* (2017) 35(32):2875–84. doi: 10.1200/JCO.2017.73.7585

8. Goetz MP, Toi M, Campone M, Trédan O, Bourayou N, Sohn J, et al. MONARCH 3: Abemaciclib as initial therapy for advanced breast cancer. *J Clin Oncol* (2017) 35(32):3638–46. doi: 10.1200/JCO.2017.75.6155

9. Johnston SRD, Harbeck N, Hegg R, Toi M, Martin M, Shao ZM, et al. Abemaciclib combined with endocrine therapy for the adjuvant treatment of HR+, HER2-, node-positive, high-risk, early breast cancer (monarchE). *J Clin Oncol* (2020) 38(34):3987–98. doi: 10.1200/JCO.20.02514

10. Wander SA, Han HS, Zangardi ML, Niemierko A, Mariotti V, Kim LSL, et al. Clinical outcomes with abemaciclib after prior CDK4/6 inhibitor progression in breast cancer: A multicenter experience. *J Natl Compr Canc Netw Act* (2021), 1–8. doi: 10.6004/jnccn.2020.7662

11. Dickler MN, Tolaney SM, Rugo HS, Cortés J, Diéras V, Patt D, et al. MONARCH 1, a phase II study of abemaciclib, a CDK4 and CDK6 inhibitor, as a single agent, in patients with refractory HR1/HER2– metastatic breast cancer. *Clin Cancer Res* (2017) 23(17):5218–24. doi: 10.1158/1078-0432.CCR-17-0754

12. Shen Y, Li S, Wang X, Wang M, Tian Qi, Yang J, et al. Tumor vasculature remolding by thalidomide increases delivery and efficacy of cisplatin. *J Exp Clin Cancer Res* (2019) 38(1):427. doi: 10.1186/s13046-019-1366-x

13. Iacopetta D, Carocci A, Sinicropi MS, Catalano A, Lentini G, Ceramella J, et al. Old drug scaffold, new activity: Thalidomide-correlated compounds exert different effects on breast cancer cell growth and progression. *Chem Med Chem* (2017) 12(5):381–9. doi: 10.1002/cmdc.201600629

14. Wang X, Shen Y, MengLv Li, Zhang X, Yang J, Wang F, et al. Thalidomide resses breast cancer tumor growth by inhibiting tumorassociated macrophage accumulation in breast tumor-bearing mice. *Eur J Pharm Sci* (2020) 151:105302. doi: 10.1016/j.ejps.2020.105302

15. Ai X, Song Z, Jian H, Zhou Z, Chen Z, Yu Y, et al. Pyrotinib combined with thalidomide in advanced non-small-cell lung cancer patients harboring HER2 exon 20 insertions (PRIDE): protocol of an open-label, single-arm phase II trial. *BMC Cancer* (2021) 21(1):1033. doi: 10.1186/s12885-021-08759-8

16. Wang N, Xu P, Liu Y, Zhao P, Ruan J, Zheng Y, et al. Efficacy and safety of thalidomide for chemotherapy-induced nausea and vomiting. *J Cancer* (2020) 11(15):4560–70. doi: 10.7150/jca.45678

17. Bahrami N, Jabeen S, Tahiri A, Sauer T, Ødegård HP, Geisler SB, et al. Lack of cross-resistance between non-steroidal and steroidal aromatase inhibitors in breast cancer patients: The potential role of the adipokine leptin. *Breast Cancer Res Treat* (2021) 190(3):435–49. doi: 10.1007/s10549-021-06399-x

18. Nanda R, Liu MC, Yau C, Shatsky R, Pusztai L, Wallace A, et al. Cyclin E1 expression and palbociclib efficacy in previously treated hormone receptor-positive metastatic breast cancer. *J Clin Oncol* (2019) 37(14):1169–78. doi: 10.1200/JCO.18.00925

19. Lee S, Park K, Kim GM, Jung KH, Kang SY, Park IH, et al. Exploratory analysis of biomarkers associated with clinical outcomes from the study of palbociclib plus endocrine therapy in premenopausal women with hormone receptor-positive, HER2-negative metastatic breast cancer. *Breast* (2022) 62:52–60. doi: 10.1016/j.breast.2022.01.014

20. Jeselsohn R, Buchwalter G, De Angelis C, Brown M, Schiff R. ESR1 mutations–a mechanism for acquired endocrine resistance in breast cancer. *Nat Rev Clin Oncol* (2015) 12(10):573–83. doi: 10.1038/nrclinonc.2015.117

21. Lu YS, Hurvitz SA, Su F, He W, Tripathy D, Gomez SC, et al. In-depth gene expression analysis of premenopausal patients with HR+/HER2 advanced breast cancer (ABC) treated with ribociclib-containing therapy in the phase III MONALEESA-7 trial. *J Clin Oncol* (2019) 37:1018. doi: 10.1200/JCO.2019.37.15_suppl.1018

22. Costa C, Wang Y, Ly A, Hosono Y, Murchie E, Walmsley CS, et al. PTEN loss mediates clinical cross-resistance to CDK4/6 and PI3Kα inhibitors in breast cancer. *Cancer Discovery* (2020) 10(1):72–85. doi: 10.1158/2159-8290.CD-18-0830

23. Mosele F, Stefanovska B, Lusque A, Tran Dien A, Garberis I, Droin N, et al. Outcome and molecular landscape of patients with PIK3CA-mutated metastatic breast cancer. *Ann Oncol* (2020) 31(3):377–86. doi: 10.1016/j.annonc.2019.11.006

24. Militello AM, Zielli T, Boggiani D, Michiara M, Naldi N, Bortesi B, et al. Mechanism of action and clinical efficacy of CDK4/6 inhibitors in BRCA-mutated, estrogen receptor-positive breast cancers: Case report and literature review. *Front Oncol* (2019) 9:759. doi: 10.3389/fonc.2019.00759

25. Wang R, Yang Y, Ye WW, Xiang J, Chen S, Zou WB, et al. Significant response to immune checkpoint inhibitor camrelizumab in a heavily pretreated advanced ER+/HER2- breast cancer patient with high tumor mutational burden. *Front Oncol* (2021) 10:588080. doi: 10.3389/fonc.2020.588080

26. Brandão M, Caparica R, Eiger D, de Azambuja E. Biomarkers of response and resistance to PI3K inhibitors in estrogen receptor-positive breast cancer patients and combination therapies involving PI3K inhibitors. *Ann Oncol* (2019) 30(Suppl_10):x27–42. doi: 10.1093/annonc/mdz280

27. André F, Ciruelos EM, Juric D, Loibl S, Campone M, Mayer IA, et al. Alpelisib plus fulvestrant for PIK3CA-mutated, hormone receptor-positive, human epidermal growth factor receptor-2-negative advanced breast cancer: Final overall survival results from SOLAR-1. *Ann Oncol* (2021) 32(2):208–17. doi: 10.1016/j.annonc.2020.11.011

frontiers | Frontiers in Oncology

TYPE Original Research
PUBLISHED 26 January 2023
DOI 10.3389/fonc.2023.1035645

OPEN ACCESS

EDITED BY
San-Gang Wu,
First Affiliated Hospital of Xiamen University, China

REVIEWED BY
Yutian Zou,
Sun Yat-sen University Cancer Center (SYSUCC), China
Jianghao Lu,
Shenzhen Second People's Hospital, China

*CORRESPONDENCE
Pin-tong Huang
huangpintong@zju.edu.cn

†These authors have contributed equally to this work

SPECIALTY SECTION
This article was submitted to Breast Cancer, a section of the journal Frontiers in Oncology

RECEIVED 03 September 2022
ACCEPTED 02 January 2023
PUBLISHED 26 January 2023

CITATION
Lin Z-m, Wang T-t, Zhu J-Y, Xu Y-y, Chen F and Huang P-t (2023) A nomogram based on combining clinical features and contrast enhanced ultrasound is not able to identify Her-2 over-expressing cancer from other breast cancers.
Front. Oncol. 13:1035645.
doi: 10.3389/fonc.2023.1035645

A nomogram based on combining clinical features and contrast enhanced ultrasound is not able to identify Her-2 over-expressing cancer from other breast cancers

Zi-mei Lin[1†], Ting-ting Wang[1†], Jun-Yan Zhu[2], Yong-yuan Xu[1], Fen Chen[2] and Pin-tong Huang[1*]

[1]Department of Ultrasound in Medicine, The Second Affiliated Hospital Zhejiang University School of Medicine, Hangzhou, China, [2]Department of Ultrasound, The First Affiliated Hospital of Zhejiang Chinese Medical University, Hangzhou, China

Objective: The aim of this study was to evaluate whether a predictive model based on a contrast enhanced ultrasound (CEUS)-based nomogram and clinical features (Clin) could differentiate Her-2-overexpressing breast cancers from other breast cancers.

Methods: A total of 152 pathology-proven breast cancers including 55 Her-2-overexpressing cancers and 97 other cancers from two units that underwent preoperative CEUS examination, were included and divided into training (n = 102) and validation cohorts (n = 50). Multivariate regression analysis was utilized to identify independent indicators for developing predictive nomogram models. The area under the receiver operating characteristic (AUC) curve was also calculated to establish the diagnostic performance of different predictive models. The corresponding sensitivities and specificities of different models at the cutoff nomogram value were compared.

Results: In the training cohort, 7 clinical features (menstruation, larger tumor size, higher CA153 level, BMI, diastolic pressure, heart rate and outer upper quarter (OUQ)) + enlargement in CEUS with $P < 0.2$ according to the univariate analysis were submitted to the multivariate analysis. By incorporating clinical information and enlargement on the CEUS pattern, independently significant indicators for Her-2-overexpression were used for further predictive modeling as follows: Model I, nomogram model based on clinical features (Clin); Model II, nomogram model combining enlargement (Clin + Enlargement); Model III, nomogram model based on typical clinical features combining enlargement (MC + BMI + diastolic pressure (DP) + outer upper quarter (OUQ) + Enlargement). Model II achieved an AUC value of 0.776 at nomogram cutoff score value of 190, which was higher than that of the other models in the training cohort without significant differences (all $P>0.05$). In the test cohort, the diagnostic efficiency of predictive model was poor (all AUC<0.6). In addition, the sensitivity and specificity were not significantly different between Models I and II (all $P>0.05$), in either the training or the test cohort. In addition, Clin exhibited an AUC similar to that of model III ($P=0.12$). Moreover, model III exhibited a higher sensitivity (70.0%) than the other models with similar AUC and specificity, only in the test cohort.

Conclusion: The main finding of the study was that the predictive model based on a CEUS-based nomogram and clinical features could not differentiate Her-2-overexpressing breast cancers from other breast cancers.

KEYWORDS

microbubbles, ultrasonography, breast cancer, biomarkers, nomogram

Introduction

Breast cancer is the most common cancer diagnosed and the fifth leading cause of cancer death among Chinese women (1). Recurrence and metastasis are the main causes of treatment failure and death in patients with breast cancer (2).

Numerous studies have concentrated on the molecular diagnosis and prognosis of breast cancer since the incidence rate and prognosis of breast diseases with different pathological types vary greatly (3–6). The human epidermal growth factor receptor 2 gene (Her-2) is a member of the HER family, which prevents apoptosis and promotes cell proliferation (7, 8). Breast cancers that overexpress Her-2 are aggressive, accounting for 25% of all breast cancer cases (1, 9). Patients with Her-2 positive breast cancer have a lower survival rate than those without Her-2 overexpression. Her-2 has been used as a predictive and prognostic biomarker for breast cancer (10–12). However, the results of immunohistochemistry are limited by tumor heterogeneity and volume. Many imaging techniques (e.g. ultrasound (US), mammography and magnetic resonance imaging (MRI)) can provide morphological information about breast tumors. BI-RADS-US is helpful for differentiating benign and malignant lesions. Mammography is the recommended screening test around the world. However, mammography has low sensitivity in patients with dense breasts, especially for Chinese women, which may cause delayed diagnosis and worse outcomes (13). Compared with MRI, US is a widely available, low-cost technique that is less time consuming. The American College of Radiology published Breast Imaging Reporting and Data System (BI-RADS) lexicon guidelines for breast cancer screening, to standardize image interpretation by radiologists and dictate management recommendations. Despite improved consistency, the interpretation of US features is operator-dependent and objective, which contributes to further interobserver variation (14). In addition, malignancies present overlapping US features between Her-2 overexpressing cancers and other malignancies (OMs) (15–17). Studies have evaluated the relationships between prognosis and preoperative demographic information and serum and cancer biomarkers, but they have reported contrasting findings (18, 19). Previous studies including our study found that the features on contrast enhanced ultrasound (CEUS) are significant tools for characterizing breast lesions (20–22). CEUS enables real-time scanning by injecting blood-pool agents and truly reflects the vascular condition within the tumor microenvironment with great convenience and cost-effectiveness. CEUS features [i.e., hyper-enhancement, sun-sign and enlargement] can be used as biosignatures for identifying aggressive biological behavior (20–22). However, the abovementioned studies were all carried out at a single center. Moreover, variable definitions of CEUS features in these studies inhibit their further clinical applications. To the best of our knowledge, studies have not yet evaluated the prognostic values of preoperative CEUS in estimating breast cancer classification. Hence, we aimed at to evaluate whether a predictive model based on a CEUS-based nomogram and clinical features (Clin) could differentiate Her-2-overexpressing breast cancers from OMs.

Abbreviations: CEUS, contrast-enhanced ultrasonography; US, ultrasound; SD, standard deviation; AUC, Area under the curve; MC, menstrual cycle; HR, heartrate; BMI, body mass index.

Methods

Patients

We retrospectively analyzed detailed clinical and pathological data from breast cancer patients. The requirement to obtain informed consent for study inclusion was waived. However, all patients undergoing CEUS, biopsy, or surgery signed informed consent forms for these examinations or procedures. All patients underwent a conventional US and CEUS before core biopsy and/or surgery. Patients with previously-diagnosed breast cancer or incomplete clinical information were excluded, and male patients were excluded as well. None of the patients had received preoperative chemotherapy or radiotherapy. Clinical information included several independent variables such as demographics (age, menstrual cycle [MC], family history of cancer, blood pressure, heartrate [HR], CA153, and body mass index [BMI]), histopathological features (histopathological type, pathologic stage of regional lymph node (pTN) stage, size of invasive component in millimeters, multifocality/multicentricity status, and lymph node status), and the expression of ER, PR, HER2, and Ki67. The ER, PR, HER2, Ki-67-labeling index and histological type were confirmed by surgery.

In total, 102 patients at the Second Affiliated Hospital Zhejiang University School of Medicine were included as the training set from January 2018 to June 2021. Another 50 patients from the Second Affiliated Hospital Zhejiang University School of Medicine and the First Affiliated Hospital of Zhejiang Chinese Medical University were prospectively included as the internal and external validation sets to validate the predictive model between July 2021 and July 2022.

US

US images of breast masses were obtained using a Resona 7/7S/9 scanner (Mindray, China), and MyLab TM Twice (Esaote, Italy) equipped with a 3- to 11-MHz linear probe and a 4- to 13-MHz linear probe by one of seven senior radiologists with 5–15 years of experience in conventional US and at least 2 years of experience in CEUS of the breast. The nodule size was defined by the maximal diameter on US. The number and location of the masses were also recorded. If multiple masses were present, the most suspicious (the higher BI-RADS category) or the largest mass was targeted. The machine settings were adjusted to obtain optimal US images, and the images were stored for further analysis.

CEUS and analysis

The same transducer as use with US equipped with contrast-specific, continuous-mode software was used for CEUS. Patients were instructed to breathe quietly during the entire process. A second-generation US contrast agent (sulfur hexafluoride, SonoVue; Bracco, Milan, Italy) was intravenously administered at a dose of 4.8 mL and was subsequently manually flushed with 5 mL of saline. Starting at the beginning of the saline injection, a 120-second-long clip was documented during the examination. We manually outlined the area most perfused within the mass as a selected ROI (≈5.0 mm^2), from which the following mean perfusion parameters were extrapolated: The plane with the most abundant vessels was selected as the CEUS target area. For lesions with no blood detected on color Doppler flow imaging (CDFI), the section with the most irregular shape was chose instead. The plane with maximal diameter was chosen as the last choice when a mass with a regular shape and no blood was detected. Then, time–intensity curves (TICs) using the local density random walk wash-in, wash-out (LDRW-WIWO) method was acquired using built-in software. Finally, we obtained the following parameters: (1) the enhancement echogenicity (hetero-enhancement or homo-enhancement); (2) the enhancement intensity (hyper-enhancement, hypo-enhancement, or iso-enhancement); (3) the enhancement shape (regular or irregular); (4) the enhancement border (well-defined or ill-defined border); (5) the enhancement size (larger than vs. equal to the US size); and (6) the crab-like sign (present or absent, defined as the nourishing vessels around the tumor). The features of hyperenhancement, enlarged, and crab-like sign in the contrast mode are related to malignant lesions, according to the findings of our earlier study and other studies (18–20). If the CEUS result was positive, the original BI-RADS score remained unchanged. If the CEUS result was negative, the original BI-RADS score was downgraded one level (e.g., BI- RADS 4A was downgraded to BI-RADS 3).

US and CEUS images and clips were assessed by two senior radiologists in consensus (1:15 years of experience in breast US and 8 years of experience in CEUS; 2:6 years of experience in breast US and 5 years of experience in CEUS). All radiologists were blinded to the patients' clinical data and pathology results.

Histopathological analysis and scoring

The histopathology results after surgery were used as the final diagnosis of the masses. Histopathological specimen assessments were carried out on formalin-fixed paraffin-embedded tissue sections selected to include representative sections of carcinomas and adjacent normal breast tissue. Tumor cell staining was compared with that of the surrounding normal breast epithelium, which was used as the negative control. The slides were scored according to the percentage of positive cells vs. total cell number, regardless of staining intensity for non-standardized biomarkers. The immunostaining scores for ER, PR, and Ki67 and the algorithm for HER2 scoring were determined according to the ASCO and CAP guidelines (23, 24). Cell proliferation (Ki67) was assessed by nuclear staining in at least 500 tumor cells using a mouse monoclonal antibody, clone MIB1 (Dako Denmark A/S, Glostrup, Denmark) at a 1/100 dilution. By convention, we considered the expression level of Ki-67 to be low if the percentage of nuclear staining was <20%, intermediate if between 21% and 60%, and high if ≥60%. The tissue sections were examined by two pathologists with 10 and 15 years of experience in histopathology who were blinded to the clinical information.

Statistical analysis

Continuous variables are expressed as the mean ± standard deviation while categorical variables are expressed as percentages according to normal distribution tests. Continuous data were compared by independent t tests while categorical data were compared using Chi-square tests or Fisher's tests if necessary. In the training cohort, significant parameters between Her-2-overexpressing and Her-2-negative patients with $P<0.2$ were enrolled in the multivariate regression model by the stepwise forward selection method. Then, independently significant indicators for Her-2 overexpressing were used for further predictive model establishment as follows: Model I, nomogram model based on clinical features (Clin); Model II, nomogram model combining enlargement (Clin + Enlargement); Model III, nomogram model based on typical clinical features combining enlargement (MC + BMI + diastolic pressure (DP) + outer upper quarter (OUQ) + Enlargement). The diagnostic performances of the predictive models were tested in both the training and test cohorts. The area under the receiver operating characteristics curve (AUC) was established to indicate the diagnostic performance of different predictive models. Comparisons of AUC were determined using the Delong test, both in the training and test cohorts. The sensitivities, specificities, positive predictive values (PPV) and negative predictive values (NPV) were compared by the chi-square test. Inter observer agreement was calculated by the intraclass coefficient (ICC) model. Statistical analyses were performed by the SPSS 23.0 software package (Chicago, USA) and Medcalc software (Mariakerke, Belgium). $P<0.05$ was taken as the threshold for statistical significance.

TABLE 1 Univariate analysis of Clinical, US and CEUS features for predicting Her-2 overexpressing in training cohort. .

	Level	Overall	OMs	Her-2+	*P*
n		102	67	35	
age (mean (SD))		55.96 (12.57)	56.25 (12.62)	55.40 (12.63)	0.746
Menstruation(0=no;1=yes)	0	31 (30.4)	17 (25.4)	14 (40.0)	0.174
	1	71 (69.6)	50 (74.6)	21 (60.0)	
BMI (median [IQR])		22.70 [21.23, 24.99]	22.31 [20.59, 24.88]	24.14 [21.89, 25.04]	0.049
BMI≥25	0	78 (76.5)	52 (77.6)	26 (74.3)	0.807
	1	24 (23.5)	15 (22.4)	9 (25.7)	
Systolic (mean (SD))		123.65 (15.78)	122.61 (14.69)	125.64 (17.75)	0.36
Systolic≥140	0	89 (87.3)	60 (89.6)	29 (82.9)	0.361
	1	13 (12.7)	7 (10.4)	6 (17.1)	
Diastolic (mean (SD))		75.53 (9.98)	74.32 (9.80)	77.83 (10.07)	0.092
Diastolic≥90	0	94 (92.2)	63 (94.0)	31 (88.6)	0.441
	1	8 (7.8)	4 (6.0)	4 (11.4)	
Diastolic≥80	0	69 (67.6)	48 (71.6)	21 (60.0)	0.269
	1	33 (32.4)	19 (28.4)	14 (40.0)	
Heart rate (mean (SD))		81.24 (14.27)	82.58 (14.82)	78.67 (12.98)	0.19
Heartrate≥100	0	93 (91.2)	59 (88.1)	34 (97.1)	0.159
	1	9 (8.8)	8 (11.9)	1 (2.9)	
CA153 (median [IQR])		9.00 [6.40, 11.78]	8.30 [6.40, 11.05]	9.10 [7.35, 13.15]	0.184
CA153≥14	0	87 (85.3)	59 (88.1)	28 (80.0)	0.377
	1	15 (14.7)	8 (11.9)	7 (20.0)	
CA153≥20	0	96 (94.1)	65 (97.0)	31 (88.6)	0.177
	1	6 (5.9)	2 (3.0)	4 (11.4)	
CA153≥25	0	98 (96.1)	66 (98.5)	32 (91.4)	0.116
	1	4 (3.9)	1 (1.5)	3 (8.6)	
Lesion location(1=left;2=right)	1	57 (55.9)	37 (55.2)	20 (57.1)	1
	2	45 (44.1)	30 (44.8)	15 (42.9)	
o'clock (0=areola)	0	19 (18.6)	16 (23.9)	3 (8.6)	0.306
	1	6 (5.9)	4 (6.0)	2 (5.7)	
	2	16 (15.7)	13 (19.4)	3 (8.6)	
	3	7 (6.9)	3 (4.5)	4 (11.4)	
	4	6 (5.9)	4 (6.0)	2 (5.7)	
	5	3 (2.9)	2 (3.0)	1 (2.9)	
	7	7 (6.9)	4 (6.0)	3 (8.6)	
	8	4 (3.9)	2 (3.0)	2 (5.7)	
	9	4 (3.9)	2 (3.0)	2 (5.7)	
	10	15 (14.7)	10 (14.9)	5 (14.3)	
	11	4 (3.9)	2 (3.0)	2 (5.7)	
	12	11 (10.8)	3 (4.5)	6 (17.1)	
Areola	0	83 (81.4)	51 (76.1)	32 (91.4)	0.067

(Continued)

10.3389/fonc.2023.1035645

TABLE 1 Continued

	Level	Overall	OMs	Her-2+	*P*
n		102	67	35	
	1	19 (18.6)	16 (23.9)	3 (8.6)	
OUQ	0	57 (55.9)	42 (62.7)	15 (42.9)	0.062
	1	45 (44.1)	25 (37.3)	20 (57.1)	
Size (median [IQR])		1.54 [1.13, 2.06]	1.52 [1.14, 1.93]	1.64 [1.13, 2.17]	0.617
Size≥2	0	74 (72.5)	52 (77.6)	22 (62.9)	0.16
	1	28 (27.5)	15 (22.4)	13 (37.1)	
Size≥2.5	0	86 (84.3)	57 (85.1)	29 (82.9)	0.78
	1	16 (15.7)	10 (14.9)	6 (17.1)	
Size≥3	0	93 (91.2)	62 (92.5)	31 (88.6)	0.489
	1	9 (8.8)	5 (7.5)	4 (11.4)	
BIRADS category	3	37 (36.3)	24 (35.8)	13 (37.1)	0.695
	4A	29 (28.4)	20 (29.9)	9 (25.7)	
	4B	33 (32.4)	22 (32.8)	11 (31.4)	
	4C	3 (2.9)	1 (1.5)	2 (5.7)	
BIRADS 4B	0	73 (71.6)	47 (70.1)	26 (74.3)	0.818
	1	29 (28.4)	20 (29.9)	9 (25.7)	
BIRADS 4C	0	69 (67.6)	45 (67.2)	24 (68.6)	1
	1	33 (32.4)	22 (32.8)	11 (31.4)	
BIRADS 5	0	99 (97.1)	66 (98.5)	33 (94.3)	0.27
	1	3 (2.9)	1 (1.5)	2 (5.7)	
Elastography	2	4 (3.9)	4 (6.0)	0 (0.0)	0.285
	3	50 (49.0)	34 (50.7)	16 (45.7)	
	4	39 (38.2)	25 (37.3)	14 (40.0)	
	5	9 (8.8)	4 (6.0)	5 (14.3)	
E3	0	52 (51.0)	33 (49.3)	19 (54.3)	0.68
	1	50 (49.0)	34 (50.7)	16 (45.7)	
E4	0	63 (61.8)	42 (62.7)	21 (60.0)	0.832
	1	39 (38.2)	25 (37.3)	14 (40.0)	
E5	0	93 (91.2)	63 (94.0)	30 (85.7)	0.268
	1	9 (8.8)	4 (6.0)	5 (14.3)	
CEUS BIRADS category	3	2 (2.0)	2 (3.0)	0 (0.0)	0.478
	4A	38 (37.3)	23 (34.3)	15 (42.9)	
	4B	27 (26.5)	20 (29.9)	7 (20.0)	
	4C	32 (31.4)	21 (31.3)	11 (31.4)	
	5	3 (2.9)	1 (1.5)	2 (5.7)	
4B	0	75 (73.5)	47 (70.1)	28 (80.0)	0.349
	1	27 (26.5)	20 (29.9)	7 (20.0)	
4C	0	70 (68.6)	46 (68.7)	24 (68.6)	1
	1	32 (31.4)	21 (31.3)	11 (31.4)	

(Continued)

TABLE 1 Continued

	Level	Overall	OMs	Her-2+	*P*
n		102	67	35	
5	0	99 (97.1)	66 (98.5)	33 (94.3)	0.27
	1	3 (2.9)	1 (1.5)	2 (5.7)	
Enhanced model					0.304
0	No-enhancement	1 (1.0)	0 (0.0)	1 (2.9)	
1	Hetro,hypoenhancement	5 (4.9)	3 (4.5)	2 (5.7)	
2	Homo,hypoenhancement	9 (8.8)	6 (9.0)	3 (8.6)	
3	Hetero,hyperenhancement	60 (58.8)	40 (59.7)	20 (57.1)	
4	Homo,hyperenhancement	25 (24.5)	18 (26.9)	7 (20.0)	
5	isoenhancement	2 (2.0)	0 (0.0)	2 (5.7)	
Model 3	0	42 (41.2)	27 (40.3)	15 (42.9)	0.835
	1	60 (58.8)	40 (59.7)	20 (57.1)	
Model 4	0	77 (75.5)	49 (73.1)	28 (80.0)	0.48
	1	25 (24.5)	18 (26.9)	7 (20.0)	
Model 5	0	100 (98.0)	67 (100.0)	33 (94.3)	0.116
	1	2 (2.0)	0 (0.0)	2 (5.7)	
Model 4/5	0	75 (73.5)	49 (73.1)	26 (74.3)	1
	1	27 (26.5)	18 (26.9)	9 (25.7)	
The enhancement size	Equal	33 (32.4)	25 (37.3)	8 (22.9)	0.182
	Enlarged	69 (67.6)	42 (62.7)	27 (77.1)	
Border	Well-defined	83 (81.4)	54 (80.6)	29 (82.9)	1
	Ill-defined	19 (18.6)	13 (19.4)	6 (17.1)	
Shape	Regular	12 (11.8)	10 (14.9)	2 (5.7)	0.211
	Irregular	90 (88.2)	57 (85.1)	33 (94.3)	
Wash-in	Obsent	22 (21.6)	13 (19.4)	9 (25.7)	0.46
	Present	80 (78.4)	54 (80.6)	26 (74.3)	
Wash-out	Obsent	100 (98.0)	65 (97.0)	35 (100.0)	0.545
	Present	2 (2.0)	2 (3.0)	0 (0.0)	
Crab-like sign	Obsent	53 (52.0)	37 (55.2)	16 (45.7)	0.408
	Present	49 (48.0)	30 (44.8)	19 (54.3)	

Results

Baseline characteristics

The incidences of Her-2-overexpressing breast cancers were 34.3% and 40.0% in the training and test cohorts, respectively. As shown in Supplemental Table 1, baseline parameters did not significantly differ between the training and test cohorts.

In univariate analysis (Table 1), elevated BMI levels were found in the Her-2-overexpressing group (P<0.05) of the training population. In contrast, there were no CEUS features that were significantly associated with Her-2 overexpressing (all P >0.05). For the test cohort, elevated systolic pressure levels were more prevalent in the Her-2-overexpressing population (P<0.05). Moreover, no CEUS features that were significantly associated with Her-2 overexpressing (all P >0.05) (Supplemental Table 2).

Nomogram model establishment

In the multivariate regression model I, OUQ was found to be the best predictor for Her-2 overexpressing with an odds ratio (OR) value of 2.52. For Model II, OUQ (OR=2.66) and an enlarged CEUS pattern (OR=1.51) were significant factors for predicting Her-2-overexpressing (Table 2). All nomogram figures are shown in Figure 1.

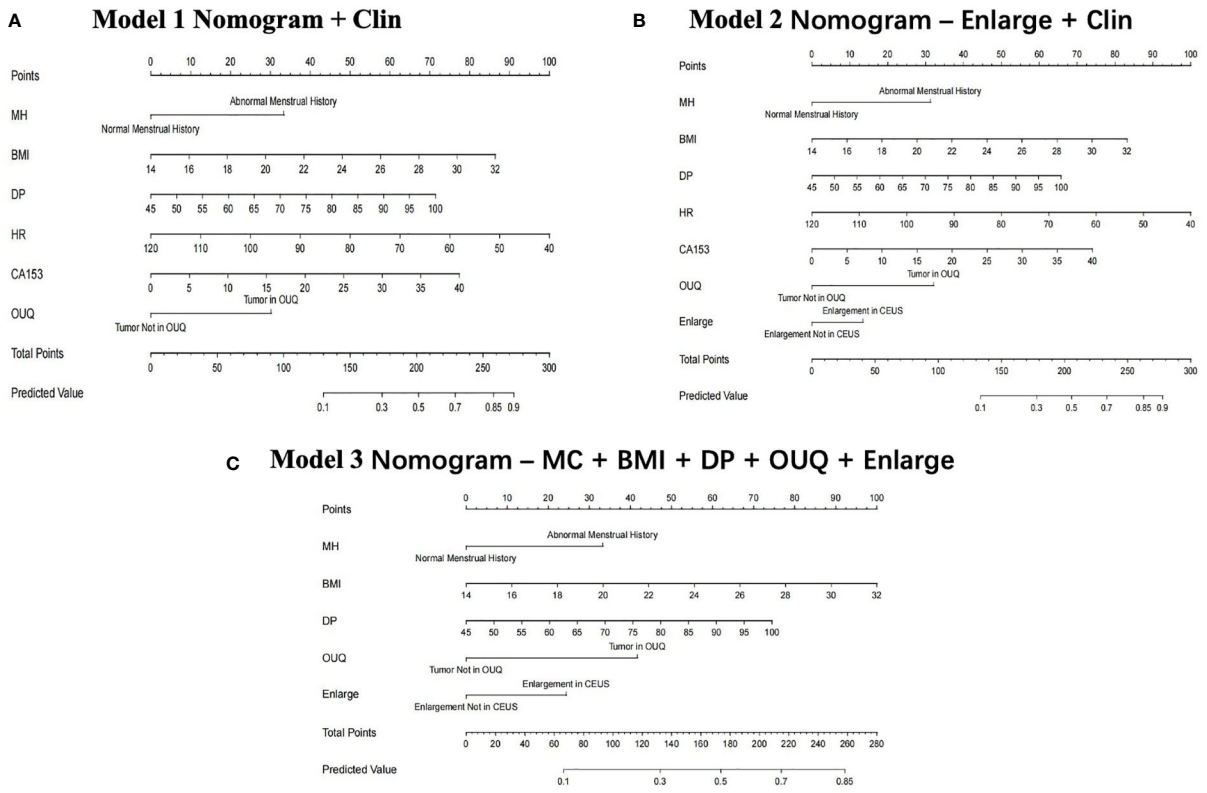

FIGURE 1
Clin, clinical features; MC, menstrual cycle; BMI, body mass index; DP, diastolic pressure; OUQ, outer upper quarter. Nomogram graphics of Clin model **(A)**, Enlarge + Clin model **(B)** and MC+BMI+ DP+ OUQ+ Enlarge model **(C)** for predicting Her-2 over-expression patients.

Diagnostic performance of different models

Model II achieved an AUC value of 0.776 at nomogram cutoff score value of 190, higher than that of the other models in the training cohort, but without significant differences. In the test cohort, model II achieved a higher AUC value when compared to that of model I without significant differences (P=0.94) (Table 3 and Figure 2).

In addition, the sensitivity and specificity were not significantly different between Models I and II (all $P>0.05$), in either the training or the test cohort. Moreover, model III exhibited a higher sensitivity (70.0%) than those of other models with similar AUC and specificity, only in the test cohort.

Inter-reader agreement

The results showed that interobserver agreement on CEUS BI-RADS category was good.

Discussion

The application of nomograms combined with multiple imaging modalities and clinical information is becoming increasingly popular in breast cancer research. It is not only used to identify malignancies and differentiate tumor grades, but also used to predict prognostic factors (23–25). Many studies have shown that nomograms can accurately discriminate breast cancer (23–26). The prognosis of Her-2-overexpressing cancers may be worse, however, patients with Her-2 overexpressing cancers could be effectively treated by targeted therapies, which are personalized and effective treatments (27, 28). The identification of positive Her-2 expression from the features extracted from medical information is an important issue in the clinical decision-making of breast cancer. In this study, we proposed a novel nomogram based on clinical, pathologic and CEUS features to predict Her-2 overexpression in OMs. The nomogram incorporated 9 possible predictors including MC, BMI, DP, HR, CA153 level, tumor size (maximum diameter), location (areola, OUQ), and enlargement. Our results showed the nomogram did not have good discrimination ability in either the training dataset or the validation dataset.

This study found that the clinical model contained several cardiovascular-related variables including BMI, DP, and HR. Several studies have proven that patients with breast cancer, especially those specific demographic characteristics, an elevated risk of developing cardiovascular diseases including hypertension heart failure, ischemic heart disease, cerebrovascular disease, peripheral vascular disease, and atrial fibrillation (29–31). However, neither the previous studies nor our study found a relationship among clinical features, cardiovascular diseases and the classification of breast cancer. Many factors are associated with cardiovascular disease, including age, lifestyle, metabolism, genetics, BMI, ovarian function, and emotional health. With large database studies including breast cancer subgroup classification, we hope that the relationship between breast cancer and cardiovascular disease may be explained more clearly.

TABLE 2 Multivariate analysis of clinical and CEUS features for predicting Her-2 overexpressing in training cohort.

	OR (95% CI)	β value	*P* value
Clin			
MC	0.36(0.12,0.99)	-1.02	0.052
BMI	1.16(1.00,1.36)	0.15	0.053
DP	1.04(0.99,1.09)	0.04	0.099
HR	0.96(0.93,1.00)	-0.04	0.041
CA153	1.06(0.98,1.15)	0.06	0.139
OUQ	2.52(1.02,6.48)	0.93	0.048
Clin+Enlarge			
MC	0.39(0.13,1.08)	-0.95	0.074
BMI	1.15(0.99,1.35)	0.14	0.067
DP	1.04(0.99,1.09)	0.04	0.138
HR	0.96(0.93,1.00)	-0.04	0.044
CA153	1.06(0.98,1.15)	0.06	0.165
OUQ	2.66(1.06,6.99)	0.98	0.040
Enlarge	1.51(0.53,4.57)	0.41	0.453
MC+BMI+DP+OUQ+Enlarge			
MC	0.51(0.19,1.30)	-0.68	0.157
BMI	1.12(0.98,1.29)	0.11	0.099
DP	1.03(0.98,1.08)	0.03	0.228
OUQ	2.35(0.98,5.79)	0.85	0.058
Enlarge	1.65(0.62,4.69)	0.50	0.330

Clin, clinical features; MC, menstrual cycle; BMI, body mass index; DP, diastolic pressure; HR, heart rate; OUQ, outer upper quarter.

For many years, tumor size has been used to evaluate the prognosis and determining the appropriate treatment strategy (32–34). In the present study, tumor sizes larger than 20 mm were found to be predictors for predicting Her-2 overexpression, but this correlation was not significant (OR=2.05, *P*=0.12) in the univariate regression analysis, which agrees with previous results (35). Invasive growth is one of the typical characteristics of all breast cancers, and size did not significantly different types. Similarly, Her-2 positivity was more frequently found in the OUQ than in other quadrants in this study (OR=2.24, *P*=0.06), which was consistent with past findings. Breast cancer is thought to most likely to occur in the OUQ, which is the quadrant with the highest breast area and a dense area (36). However,

TABLE 3 Diagnostic performance of different models for predicting Her-2 overexpressing in training and test cohort.

Model		Cut-off value	AUC	SEN	SPE	PPV	NPV
1	Clin	185					
	Training cohort		0.771	0.657	0.836	0.676	0.824
	Test cohort		0.472	0.75	0.367	0.441	0.688
2	Clin+Enlarge	190					
	Training cohort		0.776	0.629	0.851	0.688	0.814
	Test cohort		0.458	0.7	0.4	0.438	0.667
3	MC+BMI+DP+OUQ+Enlarge	138					
	Training cohort		0.736	0.771	0.657	0.54	0.846
	Test cohort		0.43	0.9	0.2	0.429	0.75

Clin, clinical features; MC, menstrual cycle; BMI, body mass index; DP, diastolic pressure; HR, heart rate; OUQ, outer upper quarter; AUC, area under the receiver operating characteristic; SEN, sensitivity; SPE, specificity; PPV, positive predictive values; NPV, negative predictive values.

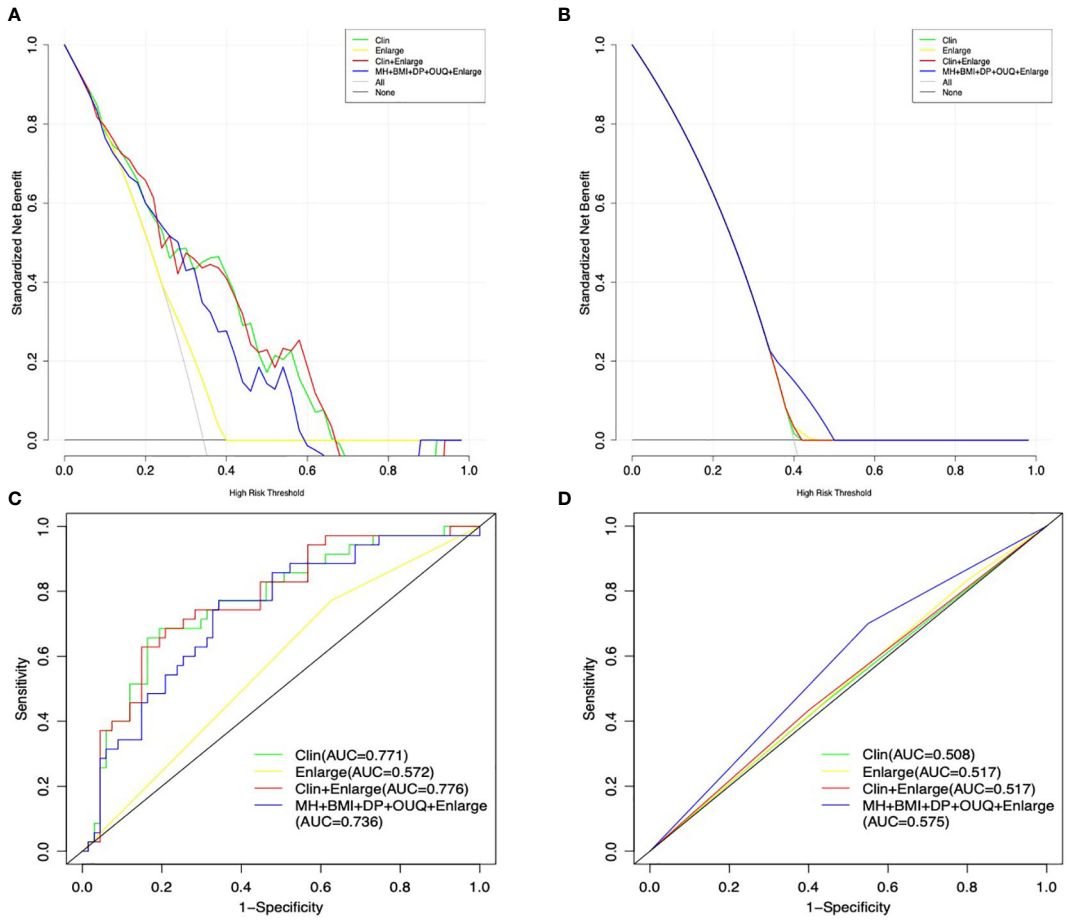

FIGURE 2
Decision curve graphics of all models for predicting Her-2 over-expression patients in the training **(A)** and test cohort **(B)**. AUC graphics of all models for predicting Her-2 positive patients in the training **(C)** and test cohort **(D)**.

the incorporation of these features in a combined Clin model resulted in a poor diagnostic performance in predicting Her-2-overexpression (AUC=0.47, sensitivity=75.0%, and specificity=36.7%) in the test cohort. The proportion of dense breasts in Chinese women may be a contributing factor. Future study with the factor of breasts density is needed.

Her-2 overexpression increases vascular endothelial growth factor (VEGF) synthesis, which could increase angiogenesis in breast cancer. Angiogenesis, which differs among the various molecular types of breast cancer, is essential to the growth and metastasis of breast tumors since they are vascular-dependent. Clinical research, including our own, has concluded that hyper-enhancement, enlargement and crab-like sign on the CEUS pattern is more common in malignant breast lesions than in benign lesions (20–22). Previous study showed that Her-2 over-expression subtype contrast enhancement pattern was more frequently present with centripetal enhancement with a perfusion defect (37). However, no currently existing study has yet reported the effectiveness of the combination of clinical information and CEUS features in predicting breast cancer subtypes. In the era of personalized or precision medicine, the integration of nomograms based on clinical, and CEUS features may increase the possibility for clinicians to plan patient-centered treatments. The Her-2 over-expression subtype expresses VEGF in high levels, which can stimulate tumor angiogenesis from the tumor's periphery to its core. As a result, the heterogeneity of VEGF expression within the tumor is greater than that of the tumor mass itself, and this distinguishes the Her-2 over-expression subtype's contrast enhancement pattern from that of other cancers. Unfortunately, in the current study, the combination of clinical and CEUS features showed no significant diagnostic performance in predicting Her-2-overexpression compared with the clinical model alone. We also established a model based on several types of clinical information that could enhance the efficacy of the "enlargement" sign. However, the result was not satisfactory. This lack of effect may be affected by factors such as the size of the included lesions and the sample size. Also, the quantitative analysis of CEUS was not included in the study. In this respect, further studies from larger trials will be necessary to achieve prediction of Her-2 through preoperative information.

This study had some limitations. First, the retrospective nature of the training set may have led to unavoidable selection bias. Therefore, a prospective study is required to achieve the predictive model. Second, the sample size was relatively small, especially in the test cohort. Third, different US machines were used to collect CEUS data at the two centers, which may result in image variability. The limited number of Her-2-overexpressing breast cancer patients in the test cohort inhibits

subgroup evaluation of US-machine-derived inconsistencies. This problem could be solved by conducting a prospective multicenter study of a large sample. Finally, a quantitative analysis of interpreting CEUS features would be much better and required to address the inconsistency associated with naked-eye observation. Further research will need to be conducted in the future.

Conclusions

In summary, the nomogram is based on clinical and CEUS features that can be obtained in a preoperative setting. The proposed nomogram could not be used to individually predict Her-2-overexpression in breast cancer patients. The results may indicate the need for a deep study to obtain more meaningful results for clinical application.

Data availability statement

The raw data supporting the conclusions of this article will be made available by the authors, without undue reservation.

Ethics statement

The studies involving human participants were reviewed and approved by The Second Affiliated Hospital Zhejiang University School of Medicine and The First Affiliated Hospital of Zhejiang Chinese Medical University. The patients/participants provided their written informed consent to participate in this study.

Author contributions

All authors contributed to the conception and design of the study. The entire study was chaired by PTH. ZML and TTW contributed significantly to the analysis and manuscript preparation and wrote the manuscript, and they contributed equally to this study. ZML, TTW, JYZ, YYX helped perform the analysis with constructive discussions. All authors contributed to the article and approved the submitted version.

Funding

This study has received funding from the Medical Scientific Research Foundation of Zhejiang Province, China (Grant No. 2022480391).

Conflict of interest

The authors declare that the research was conducted in the absence of any commercial or financial relationships that could be construed as a potential conflict of interest.

Publisher's note

Supplementary material

The Supplementary Material for this article can be found online at: https://www.frontiersin.org/articles/10.3389/fonc.2023.1035645/full#supplementary-material

References

1. Sung H, Ferlay J, Siegel RL, Laversanne M, Soerjomataram I, Jemal A, et al. Global cancer statistics 2020: GLOBOCAN estimates of incidence and mortality worldwide for 36 cancers in 185 Countries. *CA Cancer J Clin* (2021) 71(3):209–49. doi: 10.3322/caac.21660

2. Chen W, Zheng R, Baade PD, Zhang S, Zeng H, Bray F, et al. Cancer statistics in China, 2015. *CA Cancer J Clin* (2016) 66(2):115–32. doi: 10.3322/caac.21338

3. Siegel RL, Miller KD, Jemal A. Cancer statistics. *CA: A Cancer J Clin* (2019) 69(1):7–34. doi: 10.3322/caac.21551

4. Al-Thoubaity FK. Molecular classification of breast cancer: A retrospective cohort study. *Ann Med Surg (Lond).* (2019) 49:44–8. doi: 10.1016/j.amsu.2019.11.021

5. Xie X, Wang J, Shi D, Zou Y, Xiong Z, Li X, et al. Identification of a 4-mRNA metastasis-related prognostic signature for patients with breast cancer. *J Cell Mol Med* (2019) 23(2):1439–47. doi: 10.1111/jcmm.14049

6. Xie J, Tian W, Tang Y, Zou Y, Zheng S, Wu L, et al. Establishment of a cell necroptosis index to predict prognosis and drug sensitivity for patients with triple-negative breast cancer. *Front Mol Biosci* (2022) 9:834593. doi: 10.3389/fmolb.2022.834593

7. Strauss B. Best hope or last hope: access to phase III clinical trials of HER-2/neu for advanced stage breast cancer patients. *J Adv Nurs* (2000) 31:259–66. doi: 10.1046/j.1365-2648.2000.01302.x

8. Kaufmann R, Muller P, Hildenbrand G, Hausmann M, Cremer C. Analysis of Her2/neu membrane protein clusters in different types of breast cancer cells using localization microscopy. *J Microscopy* (2011) 242:46–54. doi: 10.1111/j.1365-2818.2010.03436.x

9. Petit T, Borel C, Ghnassia JP, Rodier JF, Escande A, Mors R, et al. Chemotherapy response of breast cancer depends on HER-2 status and anthracycline dose intensity in the neoadjuvant setting. *Clin Cancer Res* (2001) 7:1577–81.

10. Arteaga CL, Sliwkowski MX, Osborne CK, Perez EA, Puglisi F, Gianni L, et al. Treatment of HER2-positive breast cancer: current status and future perspectives. *Nat Rev Clin Oncol* (2012) 9:16–32. doi: 10.1038/nrclinonc.2011.177

11. Slamon DJ, Leyland-Jones B, Shak S, Fuchs H, Paton V, Bajamonde A, et al. Use of chemotherapy plus a mono- clonal antibody against HER2 for metastatic breast cancer that overexpresses HER2. *N Eng J Med* (2001) 344:783–92. doi: 10.1056/NEJM200103153441101

12. Ding L, Zhang Z, Xu Y, Zhang Y. Comparative study of her-2, p53, ki-67 expression and clinicopathological characteristics of breast cancer in a cohort of northern China female patients. *Bioengineered.* (2017) 8(4):383–92. doi: 10.1080/21655979.2016.1235101

13. Bakker MF, de Lange SV, Pijnappel RM, Mann RM, Peeters PHM, Monninkhof EM, et al. Supplemental MRI screening for women with extremely dense breast tissue. *N Engl J Med* (2019) 381(22):2091–102. doi: 10.1056/NEJMoa1903986

14. Gilbert FJ, Pinker-Domenig K. Diagnosis and staging of breast cancer: When and how to use mammography, tomosynthesis, ultrasound, contrast-enhanced mammography, and magnetic resonance imaging. In: Hodler J, Kubik-Huch RA, von Schulthess GK, editors. *Diseases of the chest, breast, heart and vessels 2019-2022: Diagnostic and interventional imaging*. Cham (CH: Springer (2019).

15. Guo Q, Dong Z, Zhang L, Ning C, Li Z, Wang D, et al. Ultrasound features of breast cancer for predicting axillary lymph node metastasis. *J Ultrasound Med* (2018) 37 (6):1354–3. doi: 10.1002/jum.14469

16. Huang Y, Zheng S, Lin Y, Miao H. Breast cancer classification prediction based on ultrasonic image feature recognition. *J Healthc Eng.* (2021) 2021:4025597. doi: 10.1155/2021/4025597

17. Wang Y, Choi EJ, Choi Y, Zhang H, Jin GY, Ko SB. Breast cancer classification in automated breast ultrasound using multiview convolutional neural network with transfer learning. *Ultrasound Med Biol* (2020) 46(5):1119–32. doi: 10.1016/j.ultrasmedbio.2020.01.001

18. Misek DE, Kim EH. Protein biomarkers for the early detection of breast cancer. *Int J Proteomics* (2011) 2011:343582. doi: 10.1155/2011/343582

19. Strauss B. Best hope or last hope: access to phase III clinical trials of HER-2/neu for advanced stage breast cancer patients. *J Adv Nurs* (2000) 31:259–66. doi: 10.1046/j.1365-2648.2000.01302.x

20. Li Q, Hu M, Chen Z, Zhang X, Song Y, Xiang F. Meta-analysis: Contrast-enhanced ultrasound versus conventional ultrasound for differentiation of benign and malignant breast Lesions[J]. *Ultrasound Med Biol* (2018) 44(5):919–29. doi: 10.1016/j.ultrasmedbio.2018.01.022

21. Liang YC, Jia CM, Xue Y, Lü Q, Chen F, Wang JJ. Diagnostic value of contrast-enhanced ultrasound in breast lesions of BI-RADS 4. *Zhonghua Yi Xue Za Zhi* (2018) 98 (19):1498–502. doi: 10.3760/cma.j.issn.0376-2491.2018.19.009

22. Lin ZM, Chen JF, Xu FT, Liu CM, Chen JS, Wang Y, et al. Principal component regression-based contrast-enhanced ultrasound evaluation system for the management of BI-RADS US 4A breast masses: objective assistance for radiologists. *Ultrasound Med Biol* (2021) 47(7):1737–46. doi: 10.1016/j.ultrasmedbio.2021.02.027

23. Liu Z, Mi M, Li X, Wu G, Zhang L. A lncRNA prognostic signature associated with immune infiltration and tumour mutation burden in breast cancer. *J Cell Mol Med* (2020) 24(21):12444–56. doi: 10.1111/jcmm.15762

24. Yan S, Wang W, Zhu B, Pan X, Wu X, Tao W. Construction of nomograms for predicting pathological complete response and tumor shrinkage size in breast cancer. *Cancer Manag Res* (2020) 10(12):8313–8323. doi: 10.2147/CMAR.S270687

25. Yang Y, Hu Y, Shen S, Jiang X, Gu R, Wang H, et al. A new nomogram for predicting the malignant diagnosis of breast imaging reporting and data system (BI-RADS) ultrasonography category 4A lesions in women with dense breast tissue in the diagnostic setting. *Quant Imaging Med Surg* (2021) 11(7):3005–17. doi: 10.21037/qims-20-1203

26. Cui X, Zhu H, Huang J. Nomogram for predicting lymph node involvement in triple-negative breast cancer. *Front Oncol* (2020) 10:608334. doi: 10.3389/fonc.2020.608334

27. Guarneri V, Dieci MV, Bisagni G, Frassoldati A, Bianchi GV, De Salvo GL, et al. De-escalated therapy for HR+/HER2+ breast cancer patients with Ki67 response after 2-week letrozole: results of the PerELISA neoadjuvant study. *Ann Oncol* (2019) 30(6):921–6. doi: 10.1093/annonc/mdz055

28. Zou Y, Zheng S, Xie X, Ye F, Hu X, Tian Z, et al. N6-methyladenosine regulated FGFR4 attenuates ferroptotic cell death in recalcitrant HER2-positive breast cancer. *Nat Commun* (2022) 13(1):2672. doi: 10.1038/s41467-022-30217-7

29. Guo S, Wong S. Cardiovascular toxicities from systemic breast cancer therapy. *Front Oncol* (2014) 4:346. doi: 10.3389/fonc.2014.00346

30. Hershman DL, Till C, Shen S, Wright JD, Ramsey SD, Barlow WE, et al. Association of cardiovascular risk factors with cardiac events and survival outcomes among patients with breast cancer enrolled in SWOG clinical trials. *J Clin Oncol* (2018) 36 (26):2710–7. doi: 10.1200/JCO.2017.77.4414

31. Jones LW, Habel LA, Weltzien E, Castillo A, Gupta D, Kroenke CH, et al. Exercise and risk of cardiovascular events in women with nonmetastatic breast cancer. *J Clin Oncol* (2016) 34(23):2743–9. doi: 10.1200/JCO.2015.65.6603

32. Autier P, Boniol M, Middleton R, Doré JF, Héry C, Zheng T, et al. Advanced breast cancer incidence following population-based mammographic screening. *Ann Oncol* (2011) 22(8):1726–35. doi: 10.1016/j.ultrasmedbio.2021.02.027

33. Coates AS, Winer EP, Goldhirsch A, Gelber RD, Gnant M, Piccart-Gebhart M, et al. American Society of clinical oncology; college of American pathologists. tailoring therapies—improving the management of early breast cancer: St gallen international expert consensus on the primary therapy of early breast cancer 2015. *Ann Oncol* (2015) 26 (8):1533–46. doi: 10.1093/annonc/mdv221

34. Fan L, Strasser-Weippl K, Li JJ, St Louis J, Finkelstein DM, Yu KD, et al. Breast cancer in China. *Lancet Oncol* (2014) 15:e279–89. doi: 10.1016/S1470-2045(13)70567-9

35. Li J, Zhang K, Shi Z, Zhang X, Xie J, Liu JY, et al. Triple-negative invasive breast carcinoma: the association between the sonographic appearances with clinicopathological feature. *Sci Rep* (2018) 8(1):9040. doi: 10.1038/s41598-018-27222-6

36. Chan S, Chen JH, Li S, Chang R, Yeh DC, Chang RF, et al. Evaluation of the association between quantitative mammographic density and breast cancer occurred in different quadrants. *BMC Cancer.* (2017) 17(1):274. doi: 10.1186/s12885-017-3270-0

37. Liang X, Li Z, Zhang L, Wang D, Tian J. Application of contrast-enhanced ultrasound in the differential diagnosis of different molecular subtypes of breast cancer. *Ultrason Imaging.* (2020) 42(6):261–70. doi: 10.1177/0161734620959780

Frontiers in Oncology

Advances knowledge of carcinogenesis and tumor progression for better treatment and management

The third most-cited oncology journal, which highlights research in carcinogenesis and tumor progression, bridging the gap between basic research and applications to imrpove diagnosis, therapeutics and management strategies.

Discover the latest Research Topics

See more →

Frontiers

Avenue du Tribunal-Fédéral 34
1005 Lausanne, Switzerland
frontiersin.org

Contact us

+41 (0)21 510 17 00
frontiersin.org/about/contact